

ULTRASONIC METAL WELDING:  
THE WELDABILITY OF STAINLESS STEEL, TITANIUM, AND NICKEL-BASED  
SUPERALLOYS

A Thesis

Presented in Partial Fulfillment of the Requirements for  
the Degree Master of Science in the  
Graduate School of The Ohio State University

By

Matthew Carlton Bloss, B.S.

\* \* \* \* \*

The Ohio State University  
2008

Master's Examination Committee:

Dr. Karl Graff, Advisor

Dr. Charles Albright

Approved by

---

Adviser  
Graduate Program in Welding Engineering



## ABSTRACT

Ultrasonic metal welding (UMW) is a solid-state joining process in which materials are held together under moderate forces while applying localized high frequency shear vibrations. The result is a true metallurgical bond that occurs well below the melting temperature of the workpieces.

While ultrasonics has been applied extensively to joining soft materials, such as copper and aluminum, for applications ranging from electronics to aerospace and automotive, applications for joining more advanced materials are limited. With the increased use of more advanced alloys, such as titanium, stainless steels, advanced high strength steels and nickel-base superalloys in critical applications, there exists a corresponding demand for capable welding processes. UMW has generally been thought of as not being viable for these advanced materials due to poor tooling life and inadequate ultrasonic power levels. In a relatively short period of time, significant developments in UMW equipment, along with the development of potential tool materials, may allow UMW to be applied to these more advanced metals.

Using commercially-available ultrasonic spot welding equipment, the ultrasonic weldability of type 304 and 410 stainless steel, commercially pure and 6Al-4V titanium, and Nickel-base superalloys 625 and 718 was investigated. The titanium alloys were clearly the most weldable. C.P. Ti welds achieved tensile strengths above 800-lbf. Ti 6Al-4V welds had the greatest strengths in the experiment, exceeding 1250-lbf. SS 410 appears to be slightly more weldable than SS 304, but the statistical analysis is not good enough to do so with a high level of confidence. SS 410 welds strengths exceeded 800-lbf tensile and SS 304 welds exceeding 700-lbf

tensile. These stainless steel weld trials required high energy, and low clamping forces due to equipment limitations. Nickel 625 and 718 were the most challenging materials to weld in this investigation and were detrimental to the tooling. Nickel alloy 625 reached almost 800-lbf tensile and Nickel alloy 718 reached almost 600-lbf peak tensile at high energy and high clamping forces.

Tool materials developed for friction-stir weld tooling were used to develop new ultrasonic tools. Tool textures and designs were also evaluated. The materials evaluated for ultrasonic tools include: AISI M2 high speed steel, AISI grade 18Ni (350M) Maraging steel, molybdenum TZM, CMW Elkon 100W tungsten, a higher-quality wrought tungsten, tungsten-25% rhenium, and a proprietary tungsten-lanthanum alloy. The tool materials had mixed performance due to the variety of welding materials, parameters, and cycles.

The weldability of a material is influenced by the yield strength of a material and the tenacity of the oxide layer. Titanium is an excellent material for UMW; titanium has a thin oxide that is easily removed by the ultrasonic process and is very reactive at elevated temperature, possibly promoting the interaction at the weld interface. Nickel-based alloys, as well as stainless steels, have a tenacious chromium oxide layer that needs to be removed in order to initiate the weld. During many of the weld trials, the interface was observed to glow red-hot, effectively increasing the weldability by lowering the yield strength. Nickel-based alloys, however, have excellent high temperature strengths, making them more difficult to weld.

## ACKNOWLEDGMENTS

I would like to thank my advisor, Professor Karl Graff for his guidance and support of my thesis work.

I would also like to thank the Edison Welding Institute for funding this research, and the staff for their assistance. A research effort with such broad scope as the work herein absolutely requires the knowledge and assistance of a team of qualified experts. Matt Short and Tim Frech provided much needed consultation of the ultrasonic welding process. Jerry Gould provided insight into the metallurgical and material consultation.

I would like to express my appreciation toward many graduate and undergraduate students at the Ohio State University for a variety of assistance throughout the project, especially those studying within the Welding Engineering department. Some of the equipment and laboratories used in this study were made available by the Ohio State University Welding Engineering department.

Branson ultrasonics graciously provided ultrasonic welding equipment for this investigation. Without the generous corporate support, the materials and equipment that were used in this investigation may not have been attainable.

Finally, I wish to thank my parents Richard and Pamela Bloss for their support throughout my studies.

## VITA

May 6, 1983.....	Born – Newark, New York
2006.....	B.S. Welding Engineering, Ohio State University
2006-2007.....	Graduate Fellow, Ultrasonics, Edison Welding Institute, Inc, Columbus, Ohio

## FIELDS OF STUDY

Major Field: Welding Engineering

## TABLE OF CONTENTS

	Page
Abstract .....	ii
Acknowledgments .....	iv
Vita.....	v
List of Tables .....	ix
List of Figures.....	x
 Chapters:	
1. Introduction.....	1
1.1 Ultrasonic Spot Welding Equipment .....	2
1.1.1 Lateral-drive Ultrasonic Welding System .....	3
1.1.2 Wedge-reed Ultrasonic Welding System.....	6
1.1.3 Related Ultrasonic Welding Technologies .....	6
1.2 Process Variables .....	7
1.2.1 Frequency .....	7
1.2.2 Amplitude .....	8
1.2.3 Clamping Force .....	9
1.2.4 Power, Energy, and Time .....	9
1.2.5 Materials .....	10
1.2.6 Tooling.....	12
1.3 Weldability .....	13
1.4 Project Outline .....	14
2. Literature Review .....	16
2.1 Solid- State Bonding Mechanism .....	16
2.2 UMW Advanced Alloys .....	20
2.3 Tool Materials.....	26
2.3.1 Refractory Metals .....	27
2.3.2 High Speed Steels .....	28
2.3.3 Cladding or Coatings .....	29
2.3.4 Composites and Ceramics.....	30
2.3.5 Other Materials .....	31
2.3.6 Conclusions.....	31
3. Equipment and Materials .....	33
3.1 Equipment.....	33

3.1.1	Welding Equipment.....	33
3.1.2	Equipment for Tool Development.....	35
3.1.3	Mechanical Testing Equipment.....	39
3.2	Materials.....	40
3.3	Tool Materials.....	44
3.4	Brazing Filler Metals.....	47
3.5	Metallurgical sectioning.....	48
4.	Ultrasonic Tooling.....	50
4.1	Tool Design and Function.....	50
4.2	Tool Mass.....	58
4.3	Development of Tools.....	60
4.4	Brazing UMW Tooling.....	62
4.5	Laser Machining.....	66
4.6	Tool Performance.....	70
4.6.1	AISI Grade 18Ni Maraging Steel, AISI M2 High Speed Steel.....	71
4.6.2	Wrought-Tungsten.....	74
4.6.3	Tungsten-25% Rhenium.....	80
4.6.4	Tungsten-Lanthanum.....	84
4.6.5	Molybdenum TZM.....	86
4.6.6	Tool Wear Summary.....	88
5.	Weld Trials.....	91
5.1	Coupon Length.....	91
5.2	Hardness Testing.....	94
5.3	Experiment Design.....	96
5.4	Type 304 Stainless Steel.....	100
5.5	Type 410 Stainless Steel.....	103
5.6	C.P. Titanium.....	107
5.7	Titanium 6Al-4V.....	109
5.8	Nickel 625.....	112
5.9	Nickel 718.....	113
5.10	Summary.....	115
6.	Metallurgy and Fractography.....	117
6.1	Metallurgy.....	118
6.1.1	Type 304 Stainless Steel.....	120
6.1.2	Type 410 Stainless Steel.....	125
6.1.3	C.P. Titanium.....	133
6.1.4	Titanium 6Al-4V.....	140
6.1.5	Nickel 625.....	146
6.1.6	Nickel 718.....	148
6.2	Fractography.....	151
6.2.1	Type 304 Stainless Steel.....	153
6.2.2	Type 410 Stainless Steel.....	154
6.2.3	C.P. Titanium.....	156
6.2.4	Titanium 6Al-4V.....	158

6.2.5	Nickel Alloy 625.....	160
6.2.6	Nickel Alloy 718.....	161
6.3	Summary.....	162
7.	Conclusions.....	163
8.	Future Work.....	166
	Bibliography.....	168
Appendices:		
A.	Weld Data Tables.....	171
B.	Pictures of Tool Wear.....	200
B.1	C. P. Titanium Weld Trials.....	202
B.2	Titanium 6Al-4V Weld Trials.....	206
B.3	SS 304 Weld Trials.....	210
B.4	SS 410 Weld Trials.....	218
B.5	Nickel 718 Weld Trials.....	225
B.6	Nickel 625 Weld Trials.....	229
C.	Tool Drawings.....	233
C.1	Tip Design.....	234
C.2	Anvil Design.....	236
D.	Minitab Regression Analysis.....	237
D.1	Type 304 Stainless Steel DOE.....	238
D.2	Type 410 Stainless Steel DOE.....	241
D.3	C. P. Titanium DOE.....	243
D.4	Titanium 6Al-4V DOE.....	246

## LIST OF TABLES

Table	Page
Table 1: Summary of mechanical test results from N. E. Weare and R. E. Monroe .....	23
Table 2: Basic material properties .....	43
Table 3: Tool material properties and description .....	46
Table 4: Pictures of UMW tool geometries and textures.....	52
Table 5: Pictures of weld surfaces using different tool designs and textures .....	56
Table 6: Power vs. Time characteristic plots due to variations in tooling .....	57
Table 7: Laser Machining Parameters .....	68
Table 8: Summary of Tool Material Performance .....	89
Table 9: Summary of welding parameters for sectioned welds .....	119
Table 10: Welding parameters for SEM fracture surfaces.....	151
Table 11: Complete welding parameters from all trials.....	198
Table 12: Terms and abbreviations used throughout Table 11.....	199

## LIST OF FIGURES

Figure	Page
Figure 1: Ultrasonic Spot Welding Systems; A – Lateral-drive; B – Wedge-reed .....	3
Figure 2: Lateral-Drive Ultrasonic Welding System; A - Components; B - Ultrasonic "Stack" .....	5
Figure 3: Weld Power Curve .....	10
Figure 4: AWS Ultrasonic Weldability Chart.....	12
Figure 5: Strength vs. Coupon Extension .....	20
Figure 6: AmTech Ultraweld 20 Lateral-drive Ultrasonic Spot Welder.....	34
Figure 7: AmTech Ultraweld 20; A – Detachable-Tip Horn; B – Welding Tip; C – Coupon Fixture; D - Anvil .....	35
Figure 8: A – 3in Lindberg 1200°C Vacuum Tube Furnace; B – Inside 3in Lindberg Vacuum Tube Furnace during Braze-cycle at 1100°C; C – Method of applying force to braze joints; D – Torit Comco Micro blasting System .....	36
Figure 9: Laser Machining System; A – Laser-machining setup; B – Power supply/ Controller; C – Galvo-scanner software screen cap; D – CCTV Monitor; E – Precision Axis .....	38
Figure 10: A - Instron Tensile Tester; B - Microhardness tester .....	39
Figure 11: A – Zeiss scanning electron microscope, B – Olympus stereo microscope, C – Nikon microscope .....	49
Figure 12: Diagram of tensile testing weldments .....	55
Figure 13: Weld and interface image diagram.....	55
Figure 14: Comparison of weld strengths using different tip designs .....	57
Figure 15: Comparison of power levels for welding trials using different tip designs .....	58
Figure 16: Overview of Anvil and Tip designs.....	61

Figure 17: A – W-25Re Tips, Braze Foil Squares, and Ground M2 Tool; B – Assembled Pre-Brazing; C – Brazed Assembly; D –Braze Joint viewed through Stereoscope .....	63
Figure 18: Furnace cycles for several braze alloys .....	64
Figure 19: A – W-La tip brazed with Incusil ABA foil before SS410 weld trial 5001; B – W-La tip brazed with Incusil ABA foil after SS410 weld trial 5008; C – Incusil ABA braze joint fracture surfaces; D – W-La tip brazed with Nicrobraz 150 (BNi-9) glowing red-hot during SS410 trial 5101 .....	66
Figure 20: Laser Machining Weld Tips; A – After several passes on monitor, B – Laser machining in progress; C – W-25Re tip face after machining; D – W-25Re tip texture profile; E – 350M tip before laser machining; F – 350M tip after laser machining .....	69
Figure 21: Tool-steel anvils with machined knurl pattern: A - AISI M2 High Speed Steel (left), AISI Grade 18Ni (350M) Maraging Steel (right); B - Macrograph of knurl pattern; C - 350M anvil installed in anvil fixture.....	71
Figure 22: 350M anvil wear during C.P. Titanium weld trials 2000-2084.....	73
Figure 23: 350M anvil wear during Ni 625 weld trial 7000 .....	74
Figure 24: CMW Elkon 100W Anvil: A - Ground to size; B - Laser-machining knurl pattern; C - Installed in anvil fixture .....	75
Figure 25: Stereoscope pictures of the anvil interface from weld trials 1022 and 1024.....	76
Figure 26: Stereoscope pictures of CMW Elkon 100W anvil wear.....	77
Figure 27: Wrought-tungsten brazed anvil: A – Ground braze joint in M2 anvil and tungsten insert; B – Assembled components with braze paste; C – Furnace brazing; D – Surface-ground assembly face; E – Laser machining anvil knurl; F – Finished assembly; G – Installed in anvil fixture.....	78
Figure 28: Wrought-tungsten anvil wear during Ti 6-4 weld trials 3000-3066.....	79
Figure 29: Titanium 6Al-4V weld anvil interface pictures from weld trials 3000, 3038, and 3066.....	80
Figure 30: Brazed W-25Re Anvil: A – Brazed Assembly; B – Braze Joints ground; C – Laser-machined knurl, first direction; D – Finished anvil; E – Knurl profile; F – CTE mismatch fracture; G – Installed in anvil fixture; H – Fractured braze joint, W-side.....	81
Figure 31: W-25Re anvil wear during weld trials 4000-4085, anvil surface fractured and re-brazed during trials .....	82
Figure 32: SS 304 weld trial 4000, 4011, and 4085 anvil interface pictures .....	83

Figure 33: Solid W-La anvil with laser-machined texture: A – Surface-ground face before laser-machining; B – First direction laser-machining; C – Second direction laser-machining; D – Installed in anvil fixture.....	84
Figure 34: Stereoscope pictures of W-La anvil face during SS 410 weld trials 5000-5101 .....	85
Figure 35: Anvil-side interfaces of SS 410 weld trials 5000 and 5101 .....	86
Figure 36: Molybdenum TZM anvil build: A – Furnace brazing; B – Brazed assembly; C – Laser-machining knurl; D – Finished anvil assembly; E – Installed in anvil fixture .....	87
Figure 37: TZM anvil wear during C.P. Ti welds 1099-1100 and SS 304 welds 4086-4091.....	88
Figure 38: A – Welded lap-shear coupons of different lengths; B – Coupon length/extension diagram .....	92
Figure 39: Strength vs. coupon length .....	93
Figure 40: Minimum energy required for ultrasonic welding.....	94
Figure 41: Average Microhardness Measurements of Materials using a LECO M-400-H1 Hardness Testing Machine.....	95
Figure 42: Ultrasonic Energy Curves .....	97
Figure 43: Scatter plot of Tensile Force vs. Energy, Clamping Force for SS 304.....	102
Figure 44: Scatter plot of Tensile Force vs. Energy, Clamping Force for SS 304 with Regression Trendlines.....	103
Figure 45: Power vs. Time plot for weld cycle with failed braze joint, Trial No. 5004 .....	104
Figure 46: Scatter plot of Tensile Force vs. Energy, Clamping Force for SS 410.....	106
Figure 47: Scatter plot of Tensile Force vs. Energy, Clamping Force for SS 410 with Regression Trendlines.....	107
Figure 48: Scatter plot of Tensile Force vs. Energy, Clamping Force for C.P. Titanium.....	108
Figure 49: Scatter plot of Tensile Force vs. Energy, Clamping Force for C.P. Titanium with Regression Trendlines.....	109
Figure 50: Scatter plot of Tensile Force vs. Energy, Clamping Force for Titanium 6Al-4V .....	111
Figure 51: Scatter plot of Tensile Force vs. Energy, Clamping Force for Titanium 6Al-4V with Regression Trendlines.....	112
Figure 52: Ni 718 weld trial 6013: A – 350M Tip sticking to work; B – 350M tip cut-off while bonded to work, then sectioned for metallurgy .....	114

Figure 53: Trendlines developed from Regression Equations; Plot of Tensile vs. Energy, Clamping Force .....	116
Figure 54: Cross-section of SS304 Trial No. 4057 .....	121
Figure 55: SS304 Trial No. 4057 weld centerline; A – 20X, B – 40X, C – 100X.....	122
Figure 56: Cross-section of SS304 Trial No. 4061 .....	122
Figure 57: SS304 Trial No. 4061 weld centerline; A – 20X, B – 40X, C – 100X.....	123
Figure 58: Cross-section of SS304 Trial No. 4064.....	123
Figure 59: SS304 Trial No. 4064 weld centerline; A – 20X, B – 40X, C – 100X.....	124
Figure 60: Cross-section of SS304 Trial No. 4066.....	124
Figure 61: SS304 Trial No. 4066 weld centerline; A – 20X, B – 40X, C – 100X, D – Fracture at 10X.....	125
Figure 62: Cross-section of SS410 Trial No. 5054.....	126
Figure 63: SS410 Trial No. 5054 weld centerline; A – 20X, B – 40X, C – 100X.....	127
Figure 64: Cross-section of SS410 Trial No. 5075 at 5X .....	127
Figure 65: SS410 Trial No. 5075 weld centerline; A – 20X, B – 40X, C – 100X.....	128
Figure 66: Cross-section of SS410 Trial No. 5081 at 5X .....	128
Figure 67: SS410 Trial No. 5081 weld centerline; A – 20X, B – 40X, C – 100X, Tip deformation; D - Left side at 10X, E - Right side at 20X .....	129
Figure 68: Cross-section of SS410 Trial No. 5091 at 5X .....	130
Figure 69: SS410 Trial No. 5091 weld centerline; A – 20X, B – 40X, C – 100X.....	130
Figure 70: Cross-section of SS410 trial No. 5094 at 5X .....	131
Figure 71: SS410 Trial No. 5094 weld centerline; A – 20X, B – 40X, C – 100X; Tip Deformation at 20X.....	131
Figure 72: Cross-section of SS410 Trial No. 5099 .....	132
Figure 73: SS410 Trial No. 5099 weld centerline; A – 20X, B – 40X, C – 100X.....	132
Figure 74: Cross-section of C.P. Ti Weld Trial No. 2057 .....	133
Figure 75: C.P. Ti Trial No. 2057 weld centerline; A – 20X, B – 40X, C – 100X.....	134
Figure 76: Cross-section of C.P. Ti Weld trial No. 2060.....	134

Figure 77: C.P. Ti Trial No. 2060 left side at 20X, weld centerline; A – 20X, B – 40X, C – 100X.....	135
Figure 78: Cross-section of C.P. Ti Weld Trial No. 2063 .....	135
Figure 79: C.P. Ti Trial No. 2063 weld centerline; A – 10X, B – 20X, C – 40X, D – 100X.....	136
Figure 80: Cross-section of C.P. Ti Weld Trial No. 2067 .....	136
Figure 81: C.P. Ti Trial No. 2067 weld centerline: A – 10X; B – 20X; C – 40X; D – 100X, E – left side at 10X.....	137
Figure 82: Cross-section of C.P. Ti Weld Trial No. 2080. ....	138
Figure 83: C.P. Ti Trial No. 2080 weld centerline: A – 20X; B – 40X; C – 100X. ....	138
Figure 84: Cross-section of C.P. Ti Weld Trial No. 2081 .....	139
Figure 85: C.P. Ti Trial No. 2081 weld centerline: A – 20X; B – 40X; C – 100X. ....	139
Figure 86: Cross-section of Ti 6Al-4V Weld Trial No. 3023 .....	140
Figure 87: Ti 6-4 Trial No. 3023 weld centerline: A – 10X; B – 20X; C – 40X; D – 100X. ....	141
Figure 88: Cross-section of Ti 6Al-4V Weld Trial No. 3025 .....	141
Figure 89: Ti 6-4 Trial No. 3025 weld centerline: A – 20X; B – 40X; C – 100X.....	142
Figure 90: Cross-section of Ti 6Al-4V Weld Trial No. 3026.....	142
Figure 91: Ti 6-4 Trial No. 3026 weld centerline: A – 10X; B – 20X; C – 40X; D – 100X. ....	143
Figure 92: Cross-section of Ti 6Al-4V Weld Trial No. 3027 .....	143
Figure 93: Ti 6-4 Trial No. 3027 weld centerline: A – 10X; B – 20X; C – 40X; D – 100X, anvil interface: E – center at 20X; F – left side at 10X, G – left side tip interface at 10X. ....	144
Figure 94: Cross-section of Ti 6Al-4V Weld Trial No. 3029.....	145
Figure 95: Ti 6-4 Trial No. 3029 weld centerline: A – 20X; B – 40X; C – 100X, D – left side weld at 20X.....	145
Figure 96: Cross-section of Ni 625 Weld Trial No. 7000.....	146
Figure 97: Ni 625 Trial No. 7000 weld centerline: A – 20X; B – 40X; C – 100X.....	147
Figure 98: Cross-section of Ni 625 Weld Trial No. 7003.....	147
Figure 99: Ni 625 Trial No. 7003 weld centerline: A – 20X; B – 40X; C – 100X.....	148

Figure 100: Cross-section of Ni 718 Weld Trial No. 6013.....	149
Figure 101: Ni 718 Trial No. 6013 weld centerline: A – 10X; B – 20X; C – 40X; D – 100X, right side tip interface: E – 10X; F – 20X. ....	150
Figure 102: Fracture surfaces for SEM, anvil/ lower coupon side of interface .....	152
Figure 103: SEM Fracture surface from SS304 trial 4062, location 1.....	153
Figure 104: SEM Fracture surface from SS304 trial 4062, location 2.....	154
Figure 105: SEM Fracture surface from SS410 trial 5086 .....	155
Figure 106: SEM Fracture surface from CP Ti trial 2070, locations 1 & 3 .....	157
Figure 107: SEM Fracture surface from CP Ti trial 2070, location 2.....	158
Figure 108: Titanium 6Al-4V SEM Weld Fracture Surface Pictures .....	159
Figure 109: Nickel 625 SEM Weld Fracture Surface Pictures .....	160
Figure 110: Nickel 718 SEM Weld Fracture Surface Pictures .....	161
Figure 111: 350M weld tip during C.P. titanium weld trials 2000-2025 .....	202
Figure 112: 350M weld tip after C.P. titanium weld trials 2026-2084 .....	203
Figure 113: 350M anvil after C.P. titanium weld trials 2000-2038 .....	204
Figure 114: 350M anvil after C.P. titanium weld trials 2039-2084 .....	205
Figure 115: Wrought-tungsten tip during Titanium 6Al-4V weld trials 3000-3008.....	206
Figure 116: Wrought-tungsten tip after Titanium 6Al-4V weld trials 3008-3066.....	207
Figure 117: Wrought-tungsten anvil during Titanium 6Al-4V weld trials 3000-3054.....	208
Figure 118: Wrought-tungsten anvil after Titanium 6Al-4V weld trials 3055-3066.....	209
Figure 119: W-25Re tip after SS 304 weld trials 4000-4025.....	210
Figure 120: W-25Re tip during SS 304 weld trials 4033-4041 .....	211
Figure 121: W-25Re tip after SS 304 weld trials 4042-4054.....	212
Figure 122: W-25Re tip during SS 304 weld trials 4055-4091 .....	213
Figure 123: W-25Re tip braze joint failure after SS 304 weld trial 4091 .....	214
Figure 124: W-25Re anvil during SS 304 weld trials 4000-4012.....	214

Figure 125: W-25Re anvil during SS 304 weld trials 4025-4034.....	215
Figure 126: W-25Re anvil after SS 304 weld trials 4040-4085.....	216
Figure 127: TZM anvil after SS 304 weld trials 4086-4091.....	217
Figure 128: W-La tip after SS 410 weld trials 5000-5008.....	218
Figure 129: W-La tip after SS 410 weld trials 5008-5011.....	219
Figure 130: 350M tip before SS 410 weld trials 5012-5014.....	220
Figure 131: W-La tip during SS 410 weld trials 5024-5056.....	221
Figure 132: W-La tip after SS 410 weld trials 5057-5101.....	222
Figure 133: W-La anvil after SS 410 weld trials 5000-5056.....	223
Figure 134: W-La anvil after SS 410 weld trials 5057-5101.....	224
Figure 135: 350M tip during Ni 718 weld trials 6000-6010.....	225
Figure 136: 350M tip after Ni 718 weld trials 6010-6013.....	226
Figure 137: 350M anvil after Ni 718 weld trials 6000-6010.....	227
Figure 138: 350M anvil after Ni 718 weld trials 6011-6013.....	228
Figure 139: 350M tip during Ni 625 weld trials 7000-7002.....	229
Figure 140: 350M tip after Ni 625 weld trials 7002-7003.....	230
Figure 141: 350M anvil after Ni 625 weld trials 7000-7002.....	231
Figure 142: 350M anvil after Ni 625 weld trial 7003.....	232
Figure 143: W-25Re brazed to M2 UMW Tip Drawing.....	234
Figure 144: Solid tool-steel spherical weld tip.....	235
Figure 145: UMW Machined Anvil.....	236
Figure 146: SS 304 Residual Plots for Tensile Force.....	240
Figure 147: SS 410 Residual Plots for Tensile Force.....	242
Figure 148: C.P. Ti Residual Plots for Tensile Force.....	245
Figure 149: Ti 6Al-4V Residual Plots for Tensile Force.....	248

## CHAPTER 1

### INTRODUCTION

Ultrasonic metal welding (UMW) is a solid-state welding process in which materials are held together under moderate forces while applying localized high frequency shear vibrations. This action removes contaminants and oxides, and creates shearing and plastic deformation of asperities at the weld interface, to allow intimate contact to occur, forming a true metallurgical bond. While ultrasonics has been applied extensively to joining soft materials, such as copper and aluminum, for applications ranging from electronics to aerospace and automotive, applications for joining more advanced materials have been limited. With the increased use of more advanced alloys, such as titanium, high-strength steels (HSS), and nickel-base superalloys in critical applications, a growing need for capable welding processes has arisen. Solid-state welding processes for these advanced alloys are in demand because conventional welding processes often require melting and diffusion, resulting in excessive heat input and exposure to atmospheric contamination, with deterioration in joint properties. A number of alloys that are considered unweldable by resistance-spot welding have recently been proven ultrasonically weldable [1]. Although nearly all metals can be welded using ultrasonics, standardized weldability information is not available [2]. UMW is generally thought of as not being viable for these advanced materials due to poor tooling life and historically inadequate power levels. In recent years, significant developments in UMW equipment, along with the development of potential tool materials, may allow UMW to be applied to more metals. This study was initiated to investigate the ultrasonic

weldability of several advanced alloys, as well as to develop the appropriate tooling that is required for welding these materials.

UMW dates back to the 1940s when AeroProjects (now Sonobond Corporation) applied ultrasonics to a resistance welder in an attempt to decrease the contact resistance of aluminum, making it easier to weld. It was discovered that ultrasonics alone could produce a bond. Since this discovery, a variety of investigations have been conducted to investigate UMW of different materials and applications. Unfortunately, standards and weldability practices have not yet been established for UMW. It is difficult to compare the results of prior studies because of the wide range of equipment, non-standardized welding practices, and an overall lack of detail that would be required to develop a comprehensive understanding of the ultrasonic weldability of metals.

## 1.1 ULTRASONIC SPOT WELDING EQUIPMENT

UMW, unlike its relative, ultrasonic plastic welding, applies the ultrasonic vibration laterally in a “scrubbing” motion. While there are a variety of UMW systems; spot, seam, and torsion, this study will focus on spot welding. Spot welders generally fall into two categories: lateral-drive and wedge-reed [Figure 1]. The difference between these systems is in the application of the ultrasonics, however, the vibration mechanics at the weld remain the same.

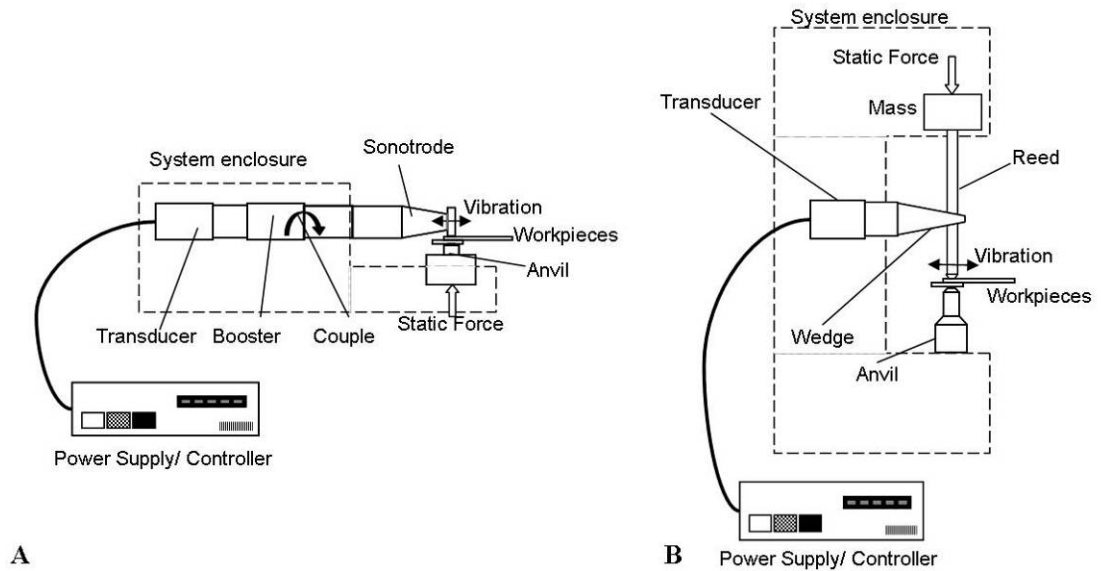


**Figure 1: Ultrasonic Spot Welding Systems; A – Lateral-drive; B – Wedge-reed [2]**

All UMW systems have similar components: a power supply and a system to deliver the ultrasonic energy to the weld. The power supply and a frequency converter generate a high frequency voltage. Most modern power supplies have the weld parameter controls built-in. For the purpose of this discussion, the components will be discussed as they apply to the different system configurations.

### 1.1.1 LATERAL-DRIVE ULTRASONIC WELDING SYSTEM

The lateral-drive system consists of a transducer, booster, and sonotrode assembly. The transducer, also known as the converter, consists of a stack of piezo-electric disks, most commonly made from Lead Zirconate Titanate (PbZTi) [3]. When a voltage potential is applied across the piezo-electric crystals, a small mechanical displacement occurs. When the voltage is

applied at high frequencies, the transducer produces a corresponding high-frequency mechanical displacement. The booster then modifies the vibration amplitude (amount depends on the gain) produced by the transducer. The sonotrode can further modify the amplitude of the vibration to meet the weld requirements. Some sonotrodes allow for replaceable tips, others are a solid, one-piece design to reduce the extra interface and corresponding energy losses. The length of the booster and sonotrode individually are equal to  $\frac{1}{2}$  the ultrasonic wavelength. This allows the interfaces of the components to be placed at locations in which they resonant at nodes with minimal vibration amplitude. Boosters and sonotrodes are commonly machined from aluminum and titanium alloys. The clamping mechanism applies force to the transducer/ booster/ sonotrode stack through the use of diaphragm springs and a polar shell around the booster. A rigid enclosure houses the ultrasonic stack and clamping mechanism. The anvil is bolted to the enclosure, and is considered a rigid element. During the weld cycle, the clamping mechanism lowers the ultrasonic stack so that the welding tip is in contact with the upper weld coupon. On the opposite face, the anvil rigidly supports the lower weld coupon. When the sonics are applied, the texture on the tool surfaces grips the coupons, allowing the ultrasonic energy to be effectively transferred to the interface with the lowest friction, the weld interface. The lateral-drive ultrasonic welding system components are illustrated in Figure 2.

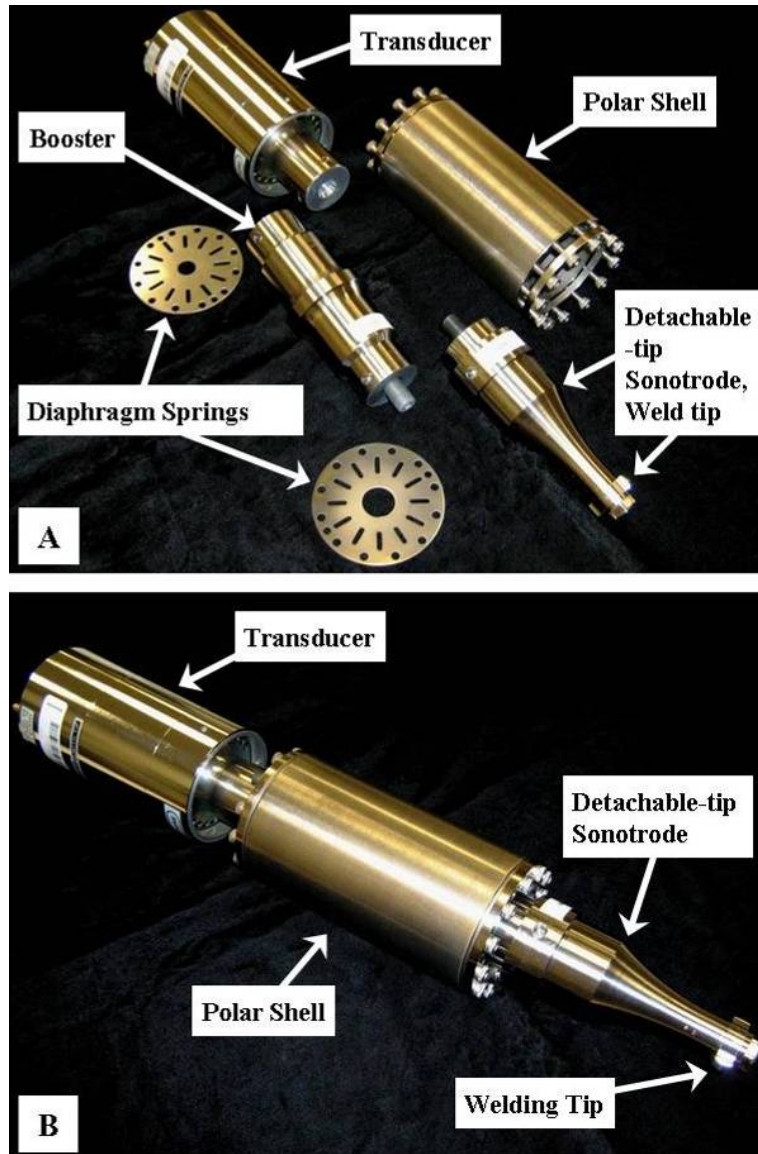


Figure 2: Lateral-Drive Ultrasonic Welding System; A - Components; B - Ultrasonic "Stack"

### 1.1.2 WEDGE-REED ULTRASONIC WELDING SYSTEM

In the wedge-reed system, the “wedge” has the same function as the booster of the lateral-drive system. The wedge is connected to a reed. The ultrasonic energy is transferred from the transducer, through the wedge, into the reed. The reed vibrates in a bending mode, like a guitar string, creating transverse oscillations at the weld tip, as with the lateral-drive system [2]. Clamping force is applied along the longitudinal axis of the reed. Unlike the lateral-drive system, the anvil is often a vibrating member, resonating out-of phase to increase the overall motion across the interface [2]. It is for these reasons that the wedge-reed system may be more capable of welding higher-strength alloys. The ultrasonic transducer does not receive resistance directly from the parts (as with the lateral-drive setup); the transducer only drives the reed, which in-turn drives the welding tip. However, this configuration does not allow accurate control of the parameters at the weld interface. The lateral-drive system can measure the weld parameters at the transducer. This cannot be done with the wedge-reed system because of the bending mode. To perform a weldability study, it is important to be able to accurately monitor and control the weld process. For this reason the lateral-drive system is used in this study.

### 1.1.3 RELATED ULTRASONIC WELDING TECHNOLOGIES

Aside from the standard spot-welding equipment, ultrasonics have been applied to a number of related welding processes including: wire bonding, torsion welding, seam welding, and ultrasonic additive manufacturing (UAM).

Wire bonding, more specifically ultrasonic wedge bonding, is a small-scale ultrasonic spot weld system used for electronic interconnects. Torsion welding is also similar to spot welding, but in this case the transducers are arranged so that the tool rotates torsionally instead of

laterally about the work. The torsional weld is therefore circular in nature, and well-suited for applications such as welding copper and aluminum container lids on cylindrical containers. Seam welding uses the same technology as lateral-drive spot welding, but the tool is a solid wheel, which translates across a joint surface. Hermetic sealing of foil bags is a common application of this technology. A new technology, UAM, is a variant of the seam welding process. UAM welds layers of foil onto themselves, one at a time, to build-up a solid structure. This rapid-prototyping process also incorporates a CNC mill to machine features in situ. Applications include plastic injection molds, metal composite armor, and corrosion repair of aerospace structures.

## 1.2 PROCESS VARIABLES

The parameters and variables for most ultrasonic welding systems include: vibration frequency, vibration amplitude, clamping force, power, energy, time, materials, and tooling. A brief discussion of these parameters, as relevant to this study, is appropriate. Several of these parameters are dependent on one another, and the relationship of these parameters depends on the specific welding system.

### 1.2.1 FREQUENCY

The frequency of ultrasonic welders is fixed. While there is no known critical frequency, higher frequencies have the potential for shorter weld times. The frequency oscillation is generated in the power supply. Most ultrasonic welding equipment uses frequencies in the range of 15 to 75KHz. The dimensions and materials of the ultrasonic assembly are selected to allow the system to resonant at the operating frequency. A small shift from this operating frequency will

cause a significant decrease in vibration amplitude [2]. This shift can be due to a change in temperature or welding load on the assembly, tool wear, or variation between different welding components. Systems have to compensate for these variations to allow the system to operate at its operating frequency. This is one of the most notable operational differences between the lateral-drive and the wedge-reed systems. With the lateral-drive system, the sonotrodes and/ or welding tips need to be designed within a certain tolerance, after which the system's controls incorporate real-time feedback circuitry to monitor the transducer frequency and make adjustments, as necessary, to compensate for any frequency shifts. The wedge-reed system requires the operator to adjust the level of impedance until it the system transfers power most efficiently. This is necessary because the ultrasonic energy is transmitted through the reed, and the transducer cannot directly monitor the frequency transmitted to the weld tip. Even with advance ultrasonic controls, both the lateral-drive and wedge-reed systems require some level of experimental trial and error.

### 1.2.2 AMPLITUDE

The amplitude of vibration is related to the system's power and the gain developed by the booster and/or sonotrode. For most current welding applications, vibration amplitude is usually the most significant variable. Lateral-drive systems are calibrated so that the desired amplitude can be controlled by the operator. By modifying the amplitude, the operator is actually modifying the current through the transducers. When the system is set to 100% amplitude, the power supply will provide 100% of the system's power, if the load on the system is great enough. As previously discussed, wedge-reed systems transmit ultrasonic oscillations through a reed, and therefore amplitude cannot be controlled by the user. Under the same principle as the lateral-drive system, the amplitude is controlled by the power level. Common amplitudes range from 20 to 80 microns.

### 1.2.3 CLAMPING FORCE

Clamping forces are static and usually controlled with pneumatic air pressure cylinders. The pressure applied to the weld zone is dependent on both clamping force and tip geometry. A threshold pressure within the weld is essential for achieving intimate contact across the interface, a requirement of the solid-state weld mechanism. Excessive forces cause sample deformation and require high power levels, while insufficient forces can promote tip slipping or sticking to the weldment, resulting in tooling damage and excessive heating of the weldment [4].

### 1.2.4 POWER, ENERGY, & TIME

The electrical power level is dynamic. A weld-to-energy mode is often used to regulate weld quality by compensating for part-to-part variances. For each weld cycle, a peak power level is selected to drive the sonics. A closed-loop feedback system monitors the amount of power required to keep the ultrasonic stack in motion during the weld cycle. The system controls' change the weld time in order to meet the specified energy. When the desired energy level is reached, the weld cycle is completed. Therefore, weld time is primarily determined by the power and energy levels. Certain UMW systems can provide a power vs. time curve for each weld cycle. Figure 3 is an example of a power curve, with time represented along the x-axis and percent of total available power along the y-axis. The weld energy is represented by the shaded region under the curve.

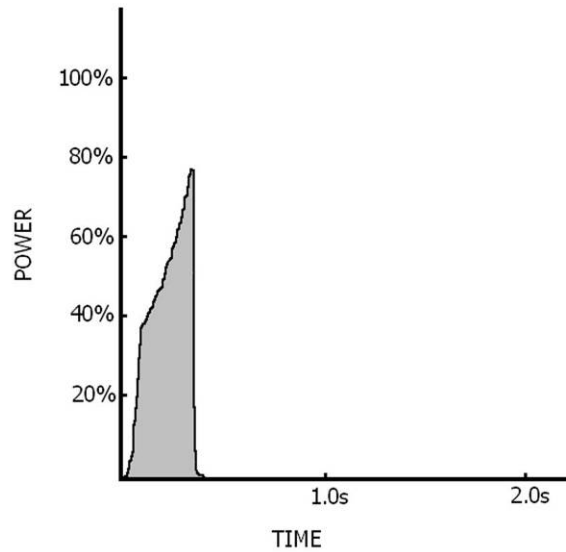


**Figure 3: Weld Power Curve**

Typical ultrasonic welds in aluminum and copper alloy sheets have a weld time of less than 0.5 seconds. Excessive weld times may indicate a need for higher-powered welding equipment. The American Welding Society (AWS) Handbook [5] suggests that the longer weld times “cause poor surface appearance, internal heating, and internal cracks.”

### 1.2.5 MATERIALS

Ultrasonic spot welding allows the joining of a variety of similar and dissimilar materials in relatively small gauges. Dissimilar thickness and multiple-layer joints are a common application of ultrasonics. Material properties are especially significant with ultrasonic welding. Generally, the harder the material, the more difficult it is to weld [2]. Softer metals, such as aluminum, copper, gold, and silver are very easily welded. Harder materials, such as the refractory alloys tungsten and molybdenum, are much more difficult to weld; however, even

these materials have been welded with ultrasonics. In addition to hardness, the material surface condition also significantly influences weld quality. Surface conditions include roughness, oxides, coatings, and contaminants. In each case, ultrasonic energy has to be consumed to remove these different surface conditions to allow for intimate contact. The relative differences in hardness and oxide properties influence the ability to join dissimilar materials. Metals with an oxide layer that is significantly harder than the base metal are sometimes easier to weld than metals that have a similar oxide and base metal hardness. For example, aluminum has a very hard oxide layer that is easily broken-up at the weld interface, whereas copper has an oxide layer that is more similar to the base metal hardness, requiring more energy to disperse.

Pre-heating the materials or the use of a foil interlayer has been employed to weld difficult material combinations including metal to glass or ceramic joints. AWS has published a chart [Figure 4] of metal combinations that can be welded [5]. The black dots are supposed to represent combinations that can be welded, and the blank spaces are supposed to indicate combinations that are either not weldable or have not yet been attempted. Unfortunately, the chart is unsubstantiated and was most likely developed using data from a variety of experiments, where the classification for weldability was inconsistent. In addition, the chart implies that all the weldable combinations are considered equally weldable, which is not the case.

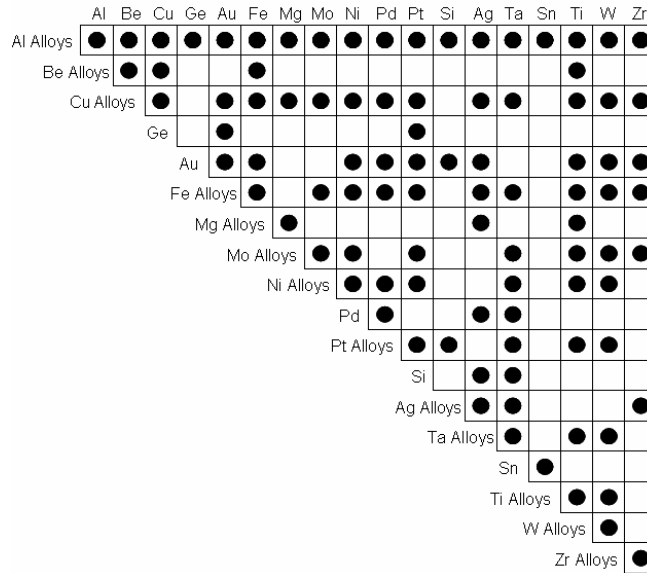


**Figure 4: AWS Ultrasonic Weldability Chart [5]**

Other than the material properties, the material dimensions are also important. Most ultrasonic welds are of the lap-joint configuration. Ultrasonic energy has to transfer through the thickness of the part to make the weld; the thicker the material, the more energy required. The maximum thickness depends on the material, the tool geometry, and the equipment power. In addition to part thickness, the overall dimensions of the part are an important consideration. For larger parts (any multiple of the ultrasonic wavelength), there may exist critical length and width dimensions in which the vibrations resonate through the part and influence the weld quality. Resonant problems can be avoided with clamping or part modifications [2].

### 1.2.6 TOOLING

One of the last parameters, in which a significant portion of this study is focused, is the tooling. The tools are the components of the equipment that are in contact with the parts to be

welded. After the application of the clamping force, ultrasonic energy is applied by the coupling of the welding tip and the respective (top) part. The anvil rigidly holds the lower part, or the substrate, so that the ultrasonic energy is concentrated at the interface between the two parts. The tool materials have extreme requirements; they need to be very strong to effectively transmit the ultrasonic energy under the applied clamping forces, through repetitive weld cycles. Specifically, tooling requires a high hardness to avoid deformation, good toughness to avoid fracturing, and good high-temperature strengths. It should be noted that although ultrasonic welding is a low-heat input process and the materials are not melted, the weld can ‘glow’ red-hot during the weld cycle when welding high-strength metals [1]. The tool material needs to be considered regarding its ability to resist bonding to the work, as sticking between the tooling and the work is traditionally a major problem.

### 1.3 WELDABILITY

AWS [5] defines weldability as “the capacity of a material to be welded under fabrication conditions imposed onto a specific suitably designed structure and to perform satisfactorily in the intended service.” Without an intended service (or a suitably designed structure, for that matter), it could be argued that the weldability of materials cannot be determined. However, it would be unreasonable to consider a welding process for an intended service without first having knowledge of the process capabilities. With that in mind, the so-called weldability of a material can be evaluated using standard welding and testing procedures to define the process capabilities for a range of relevant process parameters. Ultrasonic weldability can be based on the following criteria:

1. The ability to produce sound welds with tensile strengths that are near base-material strength levels.

2. The ability to produce repeatable welds under similar welding conditions.
3. The ability to create consecutive welds on the same set of tooling without excessive sticking or tool wear.

While not inclusive, this summarizes the basic criteria for determining the ultrasonic weldability of materials.

#### 1.4 PROJECT OUTLINE

With the background of ultrasonic welding, including the process, the parameters, and the weldability of materials completed, an overview of some of the material presented in the following sections is appropriate. As stated previously, this investigation will focus on ultrasonic spot welding of advanced alloys.

Equipment and selection of materials are discussed in Chapter 2. A literature review of publications focused on ultrasonic metal welding of advanced alloys is presented in Chapter 3. The review is broken-up into two sections: ultrasonic weldability experiments and tooling.

The design and development of the tooling for the welding trials are addressed in Chapter 4. Conclusions from a tool geometry and texture experiment are reviewed. Using the conclusions drawn from the tool material review, and the tool geometry experiments, new tools were manufactured. A number of additional experiments were required to develop the processes for manufacturing these new tools. A limited number of screening trials evaluated the performance and wear characteristics of these tools while welding these advanced alloys. In addition, the window for designed experiments was determined. Tool wear during the course of the designed experiments is documented and discussed in Chapter 5.

Designed welding experiments were followed with each advanced alloy. The procedures and results of the weld trials and mechanical testing are presented in Chapter 5. Regression plots

were drawn for the weld trials of each material. During the preliminary weld trials, nickel-based alloys significantly wore the tooling, and so the experimentation was much more limited. Experiments revealed not only material characteristics, but the operational windows of the equipment.

Selected welds were repeated from the weld trials for metallurgical evaluation. Cross-sections are presented in Chapter 6, along with a brief explanation of the results. Weld fracture surfaces from each alloy were observed with a scanning electron microscope. An overall discussion of the experiments is presented. The conclusions developed through the course of this experiment are documented in Chapter 7.

Supplementary data is presented in the Appendix. This includes the full data set from the weld trials, pictures of tool wear during the experiments, drawings of the tooling, and detailed regression analysis.

## CHAPTER 2

### LITERATURE REVIEW

The focus of this chapter is to provide a review of the published research relevant to the topic of ultrasonic metal welding of advanced alloys. This review will be divided into three sections: the solid-state bonding mechanism, ultrasonic weldability of advanced alloys, and ultrasonic tools.

#### 2.1 SOLID- STATE BONDING MECHANISM

The ultrasonic weldability of metals is known to vary with hardness, crystal structure, critical shear stress, and oxide layers [5-10]. Since UMW is a solid-state process, a brief review of the solid-state bonding mechanism is in order. The basic mechanism of the solid-state bond has been detailed by Tylecote [11] and Gould [12]. To summarize, the solid state bond formation is dependent on:

- Threshold levels of temperature, pressure, and deformation
- Conditions for intimate contact
- Asperities on the surfaces are collapsed
- Removal, dispersion, or fragmentation of oxides and surface contaminants
- Crystallographic matching across boundaries must occur, grains re-orient [12]

- Local bondline stresses are relieved by thermal energy

Greitmann, M. et al. [6] attributes the formation of the ultrasonic joint to frictional heat and abrasion. The ultrasonic weldability of a metal is primarily dependent on hardness and crystal structure. Generally, as hardness increases, the weldability of a material decreases. Metals are also ranked by their crystal structure. Metals with a face-centered cubic (FCC) crystal structure, such as Al, Cu, Ag, Au, Pd, and Pt are most weldable. Metals with a hexagonal close-packed (HCP) crystal structure, such as Mg, Ti, Zn, and Zr have limited weldability. Metals with a body-centered cubic (BCC) crystal structure, such as Cr, Fe, Mo, Ta, and W, have weldability somewhere between FCC and HCP materials. The weldability of HCP structured-materials can be improved by preheating or insertion of a filler material. The ability to join glasses and ceramics with “high precision and reproducibility” is discussed. The bond between a ceramic and a metal is measured at 2 to 10-nm wide with a transmission electron microscope, and is therefore concluded to be due to the intermolecular interaction of the joint materials. For more challenging applications, consistent joint surface preparation is stressed.

An explanation on the role of crystal structure relative to the weldability will require a review of slip systems. In short, the strength of a metal is based on the lattice structure and the atomic bonding energy between atoms within that structure. The lattice structure is the arrangement of atoms in a repeating three-dimensional pattern (single crystals). The ability for a single metal crystal to plastically deform (slip) depends on the number of slip planes and directions (slip system). Slip occurs on the most favorably oriented slip system when the resolved shear stress reaches a critical level (critical resolved shear stress). Most metals consist of one of three crystal structures, and each requires different levels of shear stress to induce deformation. FCC and BCC crystal structures have a relatively large number of slip systems (at least 12). When stress is applied to a single crystal, slip may eventually begin on a second slip system and so forth. These crystal structures exhibit ductile behavior because extensive plastic deformation is

possible. HCP crystal structures have only a few active slip systems (2). If the stress is applied perpendicular to the slip direction or parallel to the slip plane (also depends on lattice parameters), the critical resolved shear stress will be zero, causing brittle fracture. [13]

Real lattice structures, however, include defects and dislocations that influence the mechanical behavior of a metal. Defects are irregularities in the crystal lattice structure, whether it is a point defect, such as a vacancy, interstitial or impurity atom, or a line defect such as an edge or a screw dislocation [14]. All real metals have some amount of impurities. These impurities are often intentionally added, for example, to increase the yield strength of a material. Dislocations also have varying effect on the different crystal structures. This is a broad topic known as dislocation theory. The goal of this discussion is to point out that while weldability can understandably be organized by crystal structure and that the influence of such things as processing and alloying additions to create defects in a metal structure significantly modifies mechanical properties.

To further categorize ultrasonic weldability, one can also consider the atomic energy between atoms in a unit cell. The atomic energy is the force or energy required to separate atoms within a unit cell. It can then be concluded that lattice structure and atomic energy can be used to organize the ultrasonic weldability of metals. However, one must also take into other factors, such as the presence of and properties of oxide layers.

Recent studies have included TEM [15], stress measurements [16], and a variety of modeling approaches [7, 17, 18] in an attempt to further the UMW mechanism and the influence of a variety of factors. deVries [7] developed a mechanics-based model to calculate interfacial forces and correlate them with weld quality. A Sonobond wedge-reed system fitted with a flat, heavy-knurl tip and anvil was used to weld 1mm Al 6061 T-6 coupons. Interfacial forces were measured at the anvil with a shear force sensor. The weld strength increased with increasing power and shear force. Shear force proved to be a very good indication of weld strength. This

may be true because the power was measured at the transducer, and is not necessarily a precise measurement of the power put into the weld (for the wedge-reed system). The shear force sensor, however, was directly beneath the weld coupon, allowing an accurate reading of the interfacial forces. Maximum weld strengths of 2000N were recorded with a power level of 600W and 2700N measured shear force. FEA models were developed to predict the heat generation at the interface, and the results correlated with experimentation. Temperature measurements were possible by creating welds at the edge of a sample and viewing the thermal signature with an infrared camera. The maximum weld temperatures recorded by the camera were around 350°C. The maximum tensile strengths were recorded with the samples that achieved the highest temperatures. Critical part dimensions were predicted in which the anti-resonance vibrations would significantly influence the weld, and it was proven that under those conditions no weld could be produced. Figure 5 is a plot of the tensile strengths for welds made, varying only the size (extension) of the coupons. The models developed were in agreement with the experimental results, but are in need of further development before they can be applied in production environments.

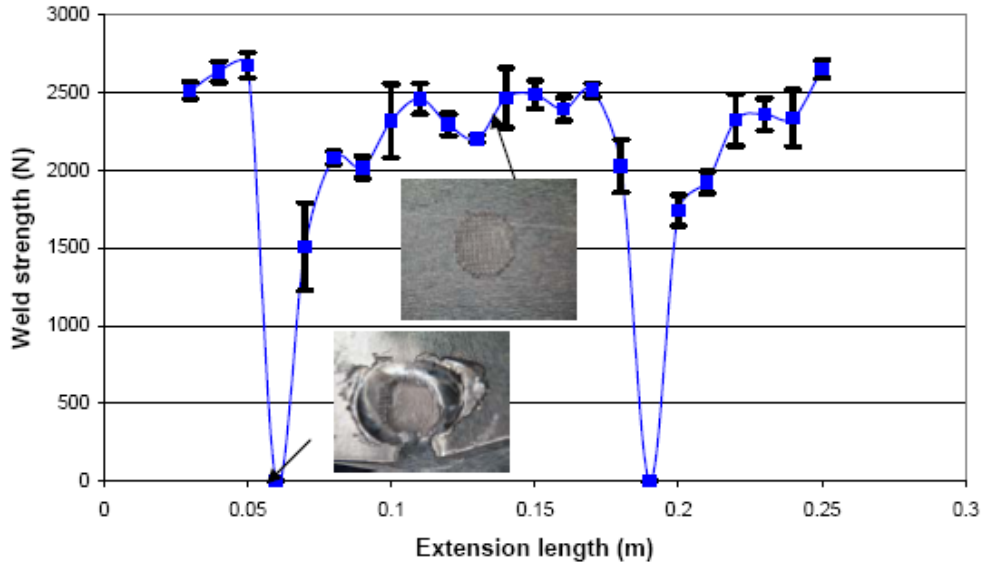


**Figure 5: Strength vs. Coupon Extension [7]**

## 2.2 UMW ADVANCED ALLOYS

Numerous publications involve a variety of UMW technologies, including: spot welding, seam welding, torsion welding, additive manufacturing, and even wire bonding. In the dissertation by deVries [7], an extensive recent literature review is presented. The focus of this present work is spot welding of thicker gauge, higher-strength alloys. When considering UMW of advanced alloys, the number of relevant publications significantly decreases. For a number of reasons, UMW has not been widely used for welding of advanced materials in production. With the development of higher-power ultrasonic systems, and a better understanding of the process mechanism, UMW is now becoming applicable for welding these alloys.

Gencsoy, Adams, and Shin [19] performed a factorial designed experiment to investigate welding of low-carbon steel, stainless steel, and zirconium foils in dissimilar combinations. They developed curves to relate clamping force, power level, and weld strength. While they proved

feasibility, they ended up using an aluminum foil interlayer due to low strengths, inconsistent quality, and cracking (without the foil). The average shear stress of welds was estimated at 13ksi, which is a fraction of the strength of the metals in which they were welding. Tooling was manufactured from drill rod for good wear properties. Sticking was reported as one of the largest difficulties encountered. Personal experience suggests that the 150-W lateral-drive welding unit may have been significantly under-powered for these metals. Quality welds in 1-mm thick aluminum alloys require more than 1000-W. Higher-strength materials require significantly higher ultrasonic power levels.

Lewis et. al [20] studied a combination of similar and dissimilar welds in heat resistant alloys. C-110M titanium, AISI Type 316 SS, Niobium, Inconel, and Mo-0.5Ti were welded with a 2.2-kW system, fitted with a Type 7 Monel spherical-radius tip, and a hard-face coated mild steel anvil. Materials ranged from 0.015 to 0.018-in thick. Clamping force and weld time were varied from 200 to 300-lbf and 0.5 to 1.5-sec, respectively. The weld quality was determined by tensile-shear testing and metallurgical evaluation. Tip-sticking was observed when welding the stainless steel, niobium, Inconel, and Monel, but not C-110M titanium. With C-110M, weld times above 1.0-sec promoted cracking and decreased the weld strength. Metallurgical evaluation indicated that the interface temperature exceeded 760°C in the C-110 titanium welds. No satisfactory shear strengths were achieved with Molybdenum. “Severe” tip sticking suggested energy losses at the tip/ weldment interface. Different tip materials were experimented with by brazing molybdenum, titanium, and stainless steel to the Monel tip, but the braze interface was reported to be ineffective at transferring the energy to the joint surface. Although any interface will influence the transmission of ultrasonic energy, it believed that a small cross-section, high-quality, braze joint would not significantly influence the weld quality. Welds in all materials were observed to have cracking in different degrees and locations. The interface was found to have high hardness levels as compared to the unaffected base metal.

In what seems to be a continuation of the study by Lewis et. al., Weare and Monroe [21] investigated similar and dissimilar welding of titanium, AISI Type 316 SS, molybdenum, niobium, iron, and Inconel in thicknesses ranging from 0.015 to 0.020-in. A purpose-built 2.4-kW lateral-drive system was fitted with Monel weld tips and mild steel or drill rod anvils for this study. The tips had a 0.3125 or 3-in radius, while the anvil had a 3-in radius. Weld coupons measured 0.5 x 1-in. Significant cracking was reported to occur at the edge of some of the welds, possibly due to “high-concentrated cyclic stresses.” Relationships for the weld strength, tip displacement, clamping force, and weld time were created. In titanium and stainless weldments, welds with the 3-in tip radius were reported to have less cracking than welds made with the 0.3125-in radius. Cracking in the titanium was reported to be due to hydrogen embrittlement. In some welds, material was reported to extrude out of the bond interface. The acicular microstructure near the interface indicates that the interface reached temperatures above 900°C. A weld time of 4.0-sec is considered excessive for any application, and may have caused the cracking. In titanium to titanium weld trials, the same second-phase acicular structure was observed. Tensile strengths of 440-lbf were achieved, pulling a nugget out of both coupons. To weld stainless steel and niobium, a 0.005-in thick buffer (interlayer) of iron was used to achieve increased weld strengths. As shown in Table 1, Welds in Inconel, molybdenum, and niobium had low strengths.

**Table 3 - Summary of Tensile-Shear and Cross-tension Strengths of Welds Made During This Investigation**

Weldment <sup>a</sup>	For weldments produced at same condition			
	Tensile-shear load at failure, lb	Cross-tension load at failure, lb	Ratio cross-tension load, tensile-shear load	Maximum tensile-shear load obtained, lb
Aluminum to aluminum (1100-H18, 0.040 in. thick)	445	85	0.191	500 <sup>e</sup>
Gold to gold	175 <sup>b</sup>	...	...	175 <sup>b</sup>
Titanium to AISI 316 stainless steel	200	20	0.1	350
Titanium to titanium	440 <sup>c</sup>	105 <sup>c</sup>	0.24	440 <sup>c</sup>
Molybdenum to molybdenum	60	Nil	Nil	60
Molybdenum to AISI 316 stainless steel	120	10	0.0834	190
Columbium to AISI 316 stainless steel	90	5	0.056	100
Columbium to iron to AISI 316 stainless steel	175 <sup>d</sup>	50 <sup>d</sup>	0.286	175 <sup>d</sup>
Columbium to Inconel	125	10	0.08	145

<sup>a</sup> All material was 0.015-0.20 in. thick except as noted.

<sup>b</sup> Failed by tearing of gold sheet adjacent to the bond.

<sup>c</sup> Failed by shearing the nugget from both sheets of titanium.

<sup>d</sup> Iron was pulled out on both the niobium and stainless steel.

<sup>e</sup> No failure; this was the limit of the testing machine used.

**Table 1: Summary of mechanical test results from N. E. Weare and R. E. Monroe [21]**

Metallographic investigations revealed that the amount of cracking was dependent on the displacement of the tip and the weld time. It is suggested that higher powers and clamping forces than those used in this study may decrease or eliminate cracking. With dissimilar weld joints, there is a possibility for the formation of brittle intermetallic compounds. In all the welds examined, no intermetallic compounds were formed.

In a follow-up study, N. E. Weare, J. N. Antonevich, and R. E. Monroe [22] used a modified version of the lateral-drive setup used in the previous studies to further study the bonding mechanism and determine the effects of various parameters and materials. A spherical Monel weld tip with a 3 or 6-in radius was intentionally welded directly to a flat copper plate, effectively isolating the interface to be studied. They placed a thermocouple directly within the interface to record the temperatures during the weld. While this presents itself as a straight-

forward method of recording the temperatures at the interface, the thermocouple is likely to be destroyed during the weld cycle. They recorded a linear temperature increase with time, at which it leveled-off near 230°C. They later concluded that the temperatures exceeded 520°C due to the presence of hot spots. Increasing the amount of displacement of the tip into the work, with a spherical tip, created an increase in weld area and an increase in joint strength. Excessive tip displacement can significantly deform the sample and decrease the joint strength. Interestingly, no difference of weld strength was found for using a 3 or 6-in spherical tip. It was noted that in previous investigations using various tip radii discovered 3in to be optimum. They also investigated carbon steel, mild steel, alumina, glass, and Lavite for tip or anvil materials, but they all fell short in performance. The steel tips created low strength welds, attributed to poor energy coupling. The glass and alumina tips had short life cycles due to high wear. They suggest that welding tips be made of material with low conductivity and high shear-strength at elevated temperatures. In contrast, a number of RSW studies have found that high-conductivity electrodes had less wear as compared with low-conductivity electrodes.

To study the effect of oxide films, Al 1100 H-18 sheet was welded under several conditions. Welds made with the oxide-film chemically removed were clean and circular. Welds without oxide-removal were annular in shape, and bonding only took place at the periphery. A black residue was observed surrounding the weld, most likely consisting of aluminum oxide due to fretting during the initial stages of the weld. Welding gold achieved good strengths with little tip displacement and weld time. Because the mechanical properties of gold and aluminum 1100 are similar, the difference in weldability was attributed to the lack of an oxide film on the surface of the gold; gold and platinum are the only metals or alloys that do not form an oxide or film coating. When welding aluminum of various thicknesses, it was found that less tip displacement was required for equivalent strength welds in thinner sections. This was attributed to thicker cross-sections having more energy loss, and therefore less energy transmitted to the weld

interface. Also significant, they noted that for thicker cross-sections, the clamping pressure becomes distributed over a larger area, thereby requiring higher forces and power levels to create an ultrasonic weld. While investigating welding of several different tempers of aluminum alloys, using constant welding parameters, the extent of turbulence at the interface was increased with increasing prior cold work. Theoretical analysis of the sphere-plate interface was also performed. The use of preheating to “alter material properties” and eliminate cracking was recommended.

R. Jahn, R. Cooper, and D. Wilkosz [23] investigated the effect of anvil geometry and energy on 0.9-mm Al 6111-T4 ultrasonic welds. The approximate energy to create these welds, 600-J, is compared to the 50 or 100-kJ required in resistance spot welding. It is reported that UMW is strongly affected by the tip knurl pattern. (Note that the same tip and anvil design will be utilized in experiments in Chapter 4, but is discarded due to insufficient weld strengths, poor repeatability, and non-uniform interfacial stresses.) Using a wedge-reed welding system, the following parameters were constant: 2500-W power, 8-impedance setting, and 525-lbf clamping force. Using three anvil designs with varied knurl dimensions and surface areas, welds were made with 100 to 1000-J of energy. The weld strength increased with increasing energy, up to 500-J, where strength appeared to level-out. Welds made at 500-J or higher generally pulled buttons during tensile testing whereas lower-energy welds had interfacial failure modes. The difference in weld strength with anvil geometry variations was negligible at lower energies, but there was a definitive difference in weld strength at energy levels above 500-J. The anvil with the largest area produced the highest strengths, and the anvil with the smallest area produced the lowest strengths, each separated by about 10% in relative strength. This was attributed to higher stress levels and increased deformation created in the welds made with the smaller-area anvil. Unfortunately, the anvils varied not only in area, but in knurl design, so it is difficult to isolate the influence of each design characteristic. In addition, it would have been more useful if the geometry differences were heavily exaggerated to better study the differences. A significant microstructural study was

conducted as part of this investigation. There are several observations worth noting. A characteristic “wavy” interface was observed, and it is attributed to the pressure gradient formed from the anvil and tip knurl pattern and geometry. The size and length of weld area increased with increasing energy.

A review of ultrasonic metal welding literature confirms that investigations have been completed in the weldability of more advanced alloys. Inadequate power levels, inadequate tooling life, and frequent tip-sticking have led many of the previous investigations to conclude that UMW of advanced alloys is not feasible for production applications. With significant advancements in ultrasonic welding equipment, and improved tool materials, it is appropriate to reconsider the weldability of these advanced alloys.

### 2.3 TOOL MATERIALS

Special demands are placed on the tool necessary for transmitting the ultrasonic energy in regard to fatigue, wear resistance, and resistance to welding to the work. The welding tip, the portion of the sonotrode that contacts the work, needs to be made of a material with high hardness, good wear resistance, and good fatigue strength. The material cannot readily bond with the workpiece material, an occurrence known as tip sticking or prewelding [4]. The tools and work must not be soluble or otherwise have a strong affinity for each other. Grietmann et al. [6] discussed the relevance of the sonotrode texture when welding aluminum to avoid tip sticking. The requirements of tool materials when welding higher-strength materials are considered. These materials can create “considerable thermal and mechanical stresses on the working surfaces of the sonotrode” [6].

A dome-shaped tip is utilized in many UMW investigations. The tip radius needs to be 50 to 100 times the coupon thickness [5], because the distribution of tangential forces in the contact

zone become more uniform with increasing tip radius [4]. However, a spherical-radius tip has several disadvantages; increased deformation of the weldment is to be expected, and increased clamping forces will result with a larger area in contact with the tip, producing decreased stress levels at the interface [4]. Because critical stress levels are a requirement of the ultrasonic weld process, interpreting the results of welds with increasing pressure, using a spherical-radius tip, is more complicated. To transfer the ultrasonic energy to the work, the tools need a texture to prevent slippage at the tip-work interface and promote movement at the weld interface. Although the tool textures are not well documented for welds in more advanced alloys in thicker gauges, a knurl pattern of approximately  $\frac{1}{2}$  the material thickness has been found to be appropriate in a variety of projects. The anvil, much like the tip, has similar requirements. The function of the anvils is to rigidly support the substrate. The anvil is not ultrasonically-driven and generally has less wear than the tip. Due to the larger surface area of the anvil, a less aggressive knurl pattern can be utilized. Generally, the anvil is made of the same material as the welding tip [5].

Friction-stir welding (FSW) is a solid-state welding technology that has had significant research and development over the past decade. The material properties required for the tooling in this welding technology may apply to UMW. In a series of discussions with several FSW engineers at Edison Welding Institute, Inc. (EWI) [24], several potential materials were suggested to evaluate for ultrasonic tooling. These materials can be broken down into four general classes: Tungsten-based, Tool-steels, Cladding/ Coatings, and Composites/ Ceramics.

### 2.3.1 REFRACTORY METALS

Tungsten alloys have significant potential for use in ultrasonic tools. They offer very good wear resistance and strength. In the EWI project, “Ultrasonic Welding Development for Aluminum Automotive Structures” [25], tip sticking and tool requirements were addressed. A tip

consisting of a piece of wrought tungsten brazed to a conventional tool steel provided over 5,000 welds in Aluminum 5754 without any sign of wear or tip-sticking. Although this is significant for UMW of harder aluminum alloys, pure tungsten has poor ductility at room temperature. The following refractory-based alloys were suggested for consideration:

1. W-25%Re – Stronger than pure tungsten, ductile-to-brittle transition temperature (DBTT) below room temperature
2. W-4%Re – Similar to W-25%Re, but very limited availability
3. W-1%La<sub>2</sub>O<sub>3</sub> – Also known as Plansee WL-10
4. WVM – Potassium doped tungsten
5. W – Pure wrought tungsten
6. CW75 – Tungsten-25% Copper, RWMA Class 11 Electrode

Tungsten- 25% Rhenium was determined to be the most potentially-useful tool material from this class due to its improved ductility and strength over pure tungsten. Tungsten-based alloys have proven to have good fracture toughness in FSW of high temperature materials [26]. Tungsten-based materials are predicted to be very promising for ultrasonic tooling tips.

### 2.3.2 HIGH SPEED STEELS

Tool steels, or high speed steels (HSS), are currently the most common materials used for ultrasonic tools; specifically AISI M2 because of its high hardness and good wear resistance. When UMW is applied to advanced materials, M2 tools wear quickly and readily bond to some of the materials. In addition, it was found that the vanadium component in M2 readily forms compounds with aluminum substrates thus promoting tip-sticking [25]. FSW has found some success with tools made of AISI Grade 18Ni Maraging steel, commonly known as 350M, for welding aluminum alloys. UMW tips constructed of 350M had improved life and wear resistance

over M2 while welding AHSS and UHSS [1]. T1 tool steel was also tested, but its performance fell short of the 350M tool steel tips. Improved wear resistance was also observed during some prior unpublished work on UMW of Titanium 6Al-4V sheet. Tool steels can be machined using conventional techniques and can be heat-treated for specific properties. In addition, tool steels are relatively available and inexpensive. If a tool steel is found to be acceptable for an UMW application, its use should be investigated for cost purposes.

### 2.3.3 CLADDING OR COATINGS

A variety of coatings have been applied to ultrasonic tooling with limited success. The thought being that conventional HSS can be used to fabricate tooling and then a thin coating of a hard, wear and adhesion-resistant material can be applied to the contact surfaces. A previous project at EWI also experimented with several coatings to reduce the occurrence of tip-sticking when welding aluminum alloys [25]. An artificial oxidation layer was applied to a standard M2 sonotrode using an oxy-acetylene torch, but the coating wore off in ten welds. Additional M2 sonotrodes had two-micron-thick Rhodium and Tungsten coatings applied, but they too wore off quickly. The bond quality between the coatings and the sonotrodes was questioned. Tungsten-carbide was spark-alloyed to a M2 sonotrode, but the finish was too rough, and actually promoted sticking. EWI's FSW engineers [24] suggested cladding tools with special filler rods using a low-dilution TIG welding practice. The list of possible coatings is as follows:

1. Rene 41 – Nickel superalloy
2. Stellite 6 – Cobalt superalloy
3. Coast metal 63/ 64 – TIG filler rod
4. Waspaloy – Nickel superalloy
5. Inconel 718 – Nickel superalloy

Coatings are best applied either manually with the assistance of a skilled TIG welder or using the Laser Engineered Net Shaping (LENS) process. Assuming low enough dilution, and a good bond to the base tool material, these coatings could be very promising for some applications. A coating thickness of 0.020” is recommended [24]. Maintaining a uniform coating thickness and dilution, as well as the fact that the coatings are similar, if not the same, as some of the materials that are being welded in this study, puts their potential relatively low on the candidate list for these advanced alloys. At the same time, coatings should not be ruled out for welding high-strength aluminum and copper alloys.

#### 2.3.4 COMPOSITES AND CERAMICS

The last class of candidate tool materials is composites and ceramics. Ceramics have very high hardness, but poor toughness. Composites often combine materials so that beneficial properties of more than one alloy can be utilized. An experiment with a piece of alumina brazed to a M2 sonotrode initially worked well, but it fractured due to the low toughness [25]. The difference in properties between the alumina and the M2 could result in a brittle braze joint. To benefit from ceramics, this class of materials must be thoroughly investigated. Composites like TC50, Tungsten with 50% Tungsten carbide, or WC-Co, Tungsten carbide in a cobalt matrix could be investigated. Superabrasives, like polycrystalline diamond (PCD) and polycrystalline cubic boron nitride (PCBN) are another class of tool material that is being tested for use with titanium alloys, a variety of steels, and nickel-based alloys. Both materials consist of small ultrahard crystals in a skeletal matrix [26]. These materials were not evaluated at this time because of inconsistent FSW trial results, poor availability, and poor machinability. An entire UMW tool made from these materials would not only be difficult to manufacture, but may not be tough enough to transmit the ultrasonic energy into the substrate effectively. Therefore, most of

the materials in this category, much like the refractory metals, would need to be brazed to standard HSS tools to work effectively. The differences between the ceramic or composite tip and the HSS tool make this a challenging braze joint. Ultimately, it remains that the material would still have poor toughness, and is not appropriate for UMW of advanced materials.

### 2.3.5 OTHER MATERIALS

The materials suggested in the groups above certainly do not include all the potential ultrasonic tool materials. Other materials that could be considered include copper-base alloys, such as Beryllium-Copper, as well as Graphite-impregnated alloys, such as Graphmoly and Howegraph. Copper-based materials could best be used with a resistive-heating hybrid ultrasonic welding process. The copper alloys can be alloyed and treated to have mechanical properties that are similar to steel. If RSW electrodes are of any relation to UMW tools, electrodes with higher-conductivity are known for decreased tip-sticking. Graphite-impregnated materials could reduce tip-sticking. TZM, a molybdenum alloy, has been investigated at EWI for FSW. It has improved properties over pure Molybdenum, but it is still lower in strength to many of the other alloys discussed. These alloys may find application-specific use.

### 2.3.6 CONCLUSIONS

In the search for the next generation of ultrasonic tool materials, it is necessary to choose materials which are, by and large, insoluble with the substrate. Currently, it is believed that Tungsten alloys and high speed steels have the most potential for UMW tools. Tungsten's proven UMW and FSW performance make it an obvious choice. Tungsten alloys cannot be machined

using conventional processes, so the tooling must be manufactured using ‘unconventional’ machining processes like Electro-Discharge Machining (EDM), grinding, or laser processing. 350M steel has good performance with FSW of softer alloys, and more recently promising results with UMW. Because it can be machined using conventional techniques, then hardened to specifications, tool steels such as 350M should be used when possible. Some of the tungsten-based alloys are met with high cost and low availability. Many of these materials proposed in this document require advanced machining, joining, and otherwise complex processing operations. It is apparent that they may be significantly more expensive to produce than conventional tooling. The benefits of these tungsten-based tools may be improved adhesion-resistance, wear-resistance (life), and ultimately repeatable weld quality.

## CHAPTER 3

### EQUIPMENT AND MATERIALS

#### 3.1 EQUIPMENT

This section reviews the equipment that was significant to this study. This review is divided into four sections: welding equipment, equipment for tool development, mechanical testing equipment, and equipment used for metallurgical evaluation. Much of the machining was outsourced, and a review of equipment and procedures will not be included.

##### 3.1.1 WELDING EQUIPMENT

A 20-kHz, 3.6-kW, AmTech Ultraweld 20 lateral-drive ultrasonic spot welder was used for this study. When using the ‘weld-to-energy’ mode, the system has three main process variables: vibration amplitude, clamping force, and energy. Figure 6 is a picture of the actual welding system. The system was fitted with a 1:1 gain booster. Due to the high power levels required to bond the materials in this study, the amplitude was kept constant at 100%, or 58- $\mu\text{m}$  displacement. This setting enabled the system to apply the maximum power levels. The two remaining variables for this study, therefore, are clamping force and weld energy.



**Figure 6: AmTech Ultraweld 20 Lateral-drive Ultrasonic Spot Welder**

The system components have already been reviewed, but it is useful to note that the breakdown of this system's components is shown in Figure 2. A detachable-tip sonotrode was used to expedite weld tip changes. Custom welding tips and anvils were designed and manufactured for this study. Details of the tools are described in later sections of this document. Detailed drawings of the tools are included in APPENDIX C. To promote weld repeatability, a steel fixture was bolted to the anvil assembly to locate the coupons. Figure 7 illustrates the location of the horn, welding tip, coupon fixture, and anvil.

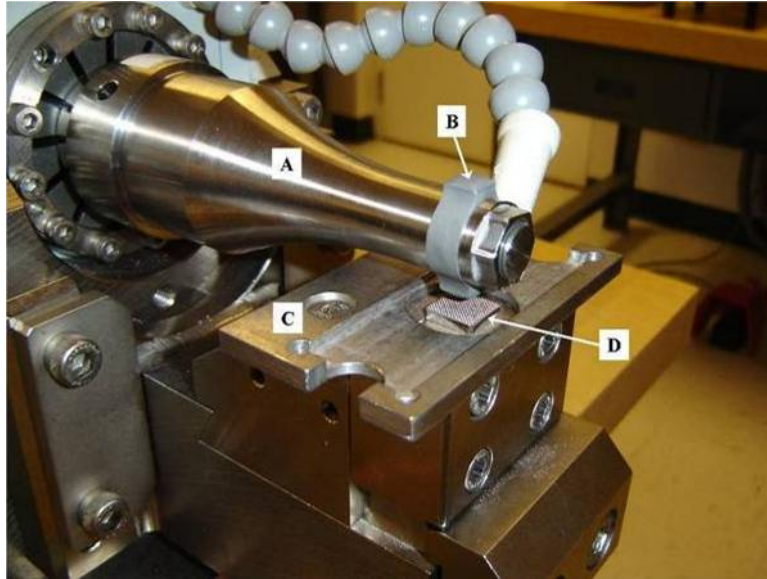


**Figure 7: AmTech Ultraweld 20; A – Detachable-Tip Horn; B – Welding Tip; C – Coupon Fixture; D - Anvil**

### 3.1.2 EQUIPMENT FOR TOOL DEVELOPMENT

For the tools consisting of refractory-alloy wear-surfaces, brazing operations required a vacuum furnace. In addition, several local machine-shops were contracted for services ranging from CNC-grinding to wire-EDM cutting. To finish the tools, complex knurl patterns were applied with a laser-machining system.

A 3-in Lindberg furnace tube furnace was utilized for brazing and heat-treatment of the weld tips and anvils. The furnace in Figure 8 – A is capable of temperatures up to 1200°C, and vacuum levels lower than  $1.0 \times 10^{-7}$ -torr. All furnace runs were carried-out in a high-vacuum atmosphere. Figure 8 – B is a picture of the inside of the tube furnace during a braze-cycle at 1100°C. Labtech Notebook Pro Build-Time software was used to acquire data from the furnace runs; K-type thermocouples were spot-welded either directly to or nearby the parts. Several plots from the furnace cycles are available in the Appendix. Figure 8 – C is a picture of one of the

braze joints setup to illustrate the method of applying force; a stainless steel weight was carefully balanced on top. Figure 8 – D is a picture of the Comco Torit micro blaster used to prepare the joint surfaces for brazing. The parameters used for the micro blaster included a 50- $\mu\text{m}$  Silicon-carbide abrasive powder with 40-50% powder flow and 40-80-psi pressure. A Branson 2510 ultrasonic bath was used to clean parts immediately prior to brazing. The bath was in combination with acetone and methanol.

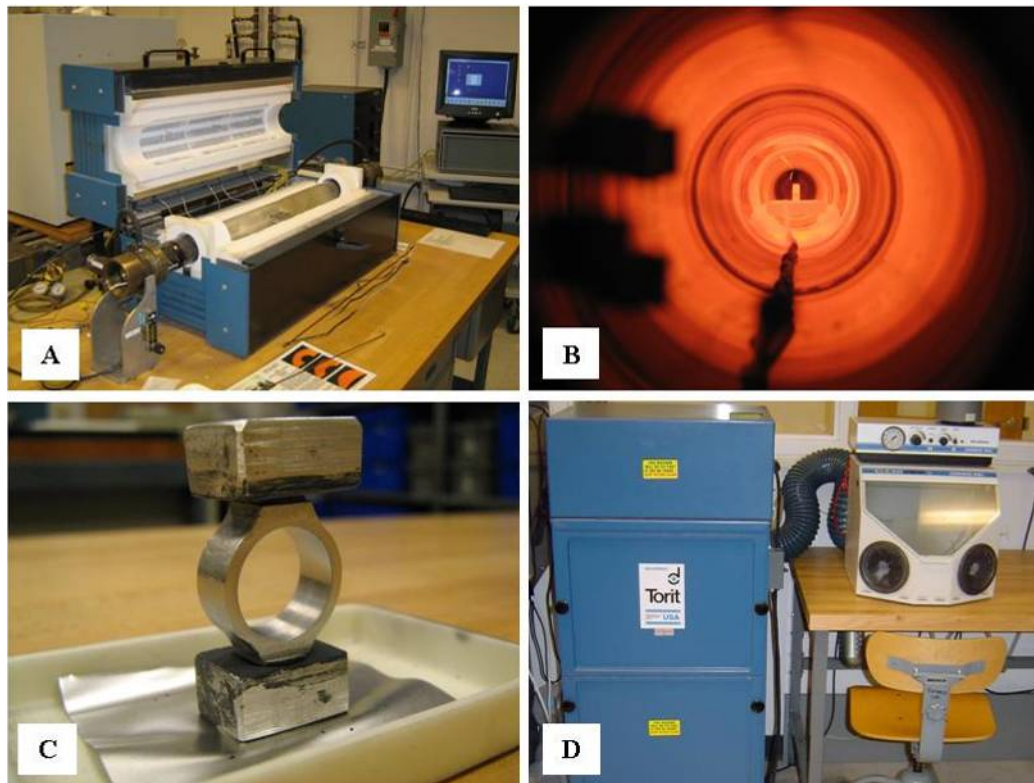


**Figure 8: A – 3in Lindberg 1200°C Vacuum Tube Furnace; B – Inside 3in Lindberg Vacuum Tube Furnace during Braze-cycle at 1100°C; C – Method of applying force to braze joints; D – Torit Comco Micro blasting System**

After the tools were brazed and/or machined, the surface texture was applied with a laser-machining system. A picture of the entire setup is shown in Figure 9 – A with all the major

components called out. This system consists of an Nd: YAG Diode laser and a galvo scanner. The laser is a Stiletto Model 3335 CW Diode-pumped Nd: YAG rod by Cutting-Edge Optronics (CEO). The laser is powered with a CEO model 2800 laser controller/ driver. Figure 9 – B is a picture of the controller. The galvo scanner consisted of a two-axis Scanlab AG SK1020 digital scan-head controlled by Alase technologies' WinLase Editor 3.0 software. Figure 9 – C is an image of the captured software display. The setup uses a CCTV camera and monitor with digital cross-hairs to allow the alignment of the beam relative to the part. Figure 9 – D is a picture of the monitor during laser-machining of a weld tip. The workpieces were set up below the galvo scanner on a precision axis [Figure 9 – E] controlled by an analog micrometer drive system. The scanner would only scribe one line at a time, and the part would then be advanced for the next scribe manually.

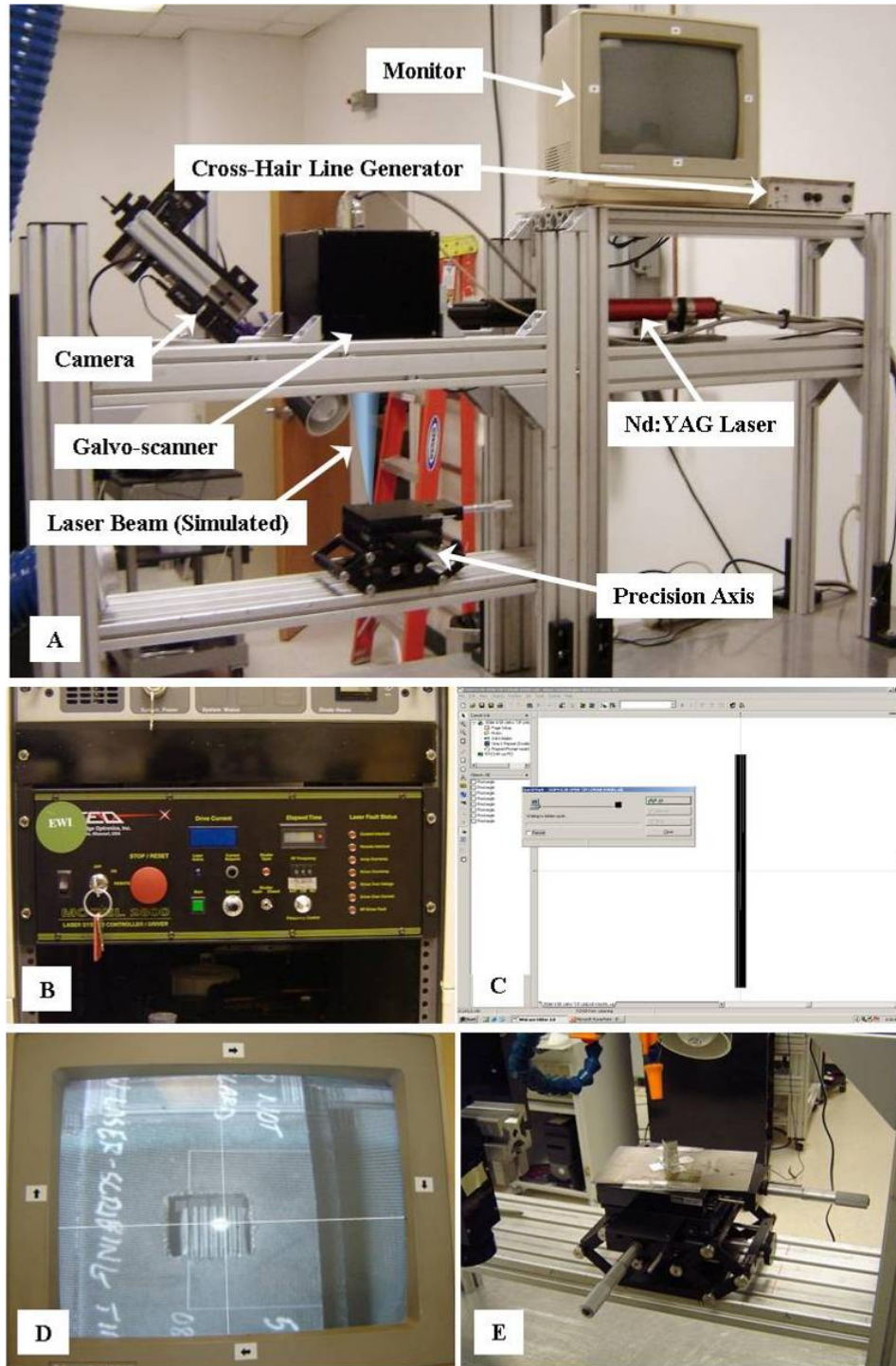


**Figure 9: Laser Machining System; A – Laser-machining setup; B – Power supply/ Controller; C – Galvo-scanner software screen cap; D – CCTV Monitor; E – Precision Axis**

### 3.1.3 MECHANICAL TESTING EQUIPMENT

Weld performance was quantified by mechanical testing. Tensile testing was performed using an MTS Instron with a 10,000-lb load cell and a 0.010-in/sec cross-head travel speed. No attempt was made to brace the joint and minimize any bending moment. Hardness testing of the materials and the tooling was performed using a LECO M-400-H1 microhardness testing machine. The load was varied depending on the material tested. In accordance with the ASTM hardness standard E384-06, the surfaces were polished with at least 600-grit paper before microhardness measurements were taken. Figure 10 illustrates the microhardness tester and the tensile tester used for this study.

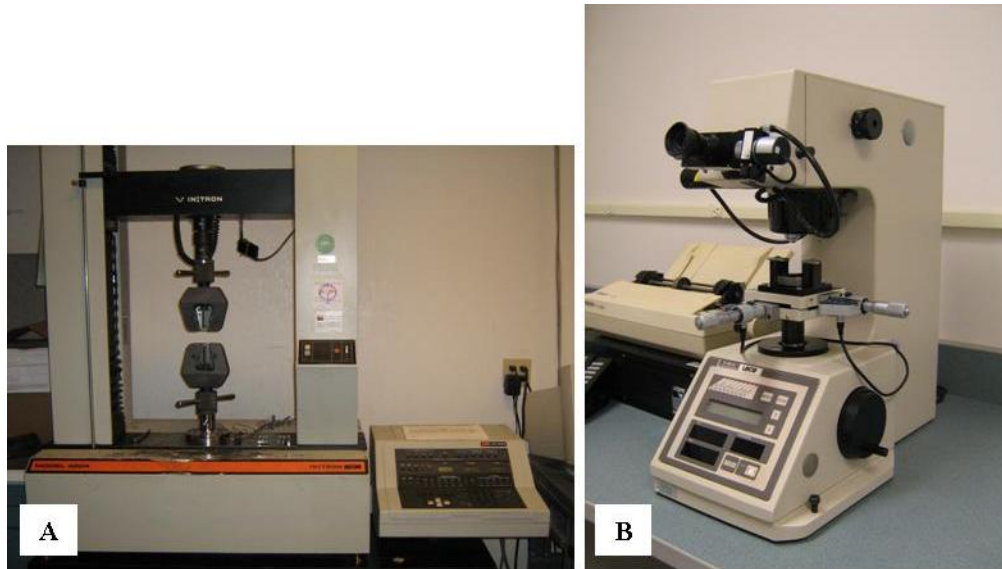


**Figure 10: A - Instron Tensile Tester; B - Microhardness tester**

## 3.2 MATERIALS

The increased use of advanced alloys for a variety of applications brings with it a corresponding need for joining processes that can maintain the original properties of the parent metal(s). In addition, dissimilar combinations are becoming increasingly popular as a cost reduction initiative so that the advanced, more-expensive alloys can be used only where needed, and joined to more less costly materials elsewhere. Solid-state welding processes are becoming increasingly popular because of their known capabilities in these challenging applications. The aerospace, automotive, and medical industries have particularly strong interest in ultrasonic welding for the aforementioned reasons. The commercial turbine engine, for example, incorporates welding applications including of a variety of advanced alloys with very high-temperature strengths.

For this project, a number of market-leaders and senior engineers at EWI were consulted to review the materials that are being actively investigated for a board range of industries and welding technologies. Generally speaking, the joining of stainless steel, titanium, and nickel-base alloys were found to be under active investigation. In addition, a variety of UMW projects have given similar guidance as to the industries' needs and interests for weldability knowledge. The following materials will be evaluated in this study:

1. Stainless Steel
  - a. AISI Type 304 Stainless Steel 2B – Austenitic 18Cr-8Ni-2Mn stainless steel with a face-centered cubic structure. Most widely-used stainless steel alloy because of good corrosion resistance, high-temperature strength, and high ductility.
  - b. AISI Type 410 Stainless Steel 2D – 12.5Cr-0.15C stainless steel with a body-centered cubic crystal structure. General-purpose martensitic stainless steel has mild corrosion resistance due to decreased chromium content.

## 2. Titanium

- a. ASTM Grade 5 Titanium – The two-phase alpha-beta titanium alloy 6Al-4V is the most widely-used titanium alloy. It has a high specific strength and good corrosion resistance.
- b. ASTM Grade 2 Titanium – Ultra corrosion-resistant, commercially-pure (C.P.), alpha-phase (hexagonal close-packed structure) titanium has relatively low strength and good toughness and ductility.

## 3. Nickel-base

- a. Nickel Alloy 625 –Nickel-chromium-molybdenum has increased resistance to crevice corrosion cracking and pitting.
- b. Nickel Alloy 718 – Precipitation-hardenable nickel-chromium alloy has corrosion resistance and high strength.

A discussion is necessary in regard to the material properties which may influence ultrasonic weldability. Increased amounts of alloying additions in nickel-base superalloys allow their use in corrosive, high temperature, and high-stress environments. Increasing nickel content improves fatigue strength, high-temperature strength, and increases corrosion resistance in reducing environments [27]. The addition of chromium to stainless steel promotes the formation of a continuous passive film, spontaneously and immediately, in the presence of oxygen for corrosion protection. More than likely, both stainless steel and nickel-base alloys form a similar chromium-oxide film. Titanium is very reactive, and forms a thin, conductive, oxide film instantly and spontaneously when exposed to oxygen. Considering the oxide exists at a much lower energy level than the metal itself, there is an obvious driving force for the (oxide) formation. Therefore, nickel-base and stainless steels form a chromium-oxide film, and titanium-alloys form a titanium-oxide. The titanium alloys have a low elastic modulus, and titanium 6Al-4V has the highest strength and hardness of the materials tested. The C.P. titanium has the lowest

ultimate tensile strength and hardness of the materials tested. The nickel-base alloys both have similar mechanical properties in all categories. The yield tensile strength of 304 SS is approximately half that of the SS 410, otherwise the hardness and ultimate tensile strengths are similar. Some of the more-relevant properties of these materials are summarized in Table 2.

While it is suggested that hardness is the main indication of the amount of energy required to ultrasonically weld a material [5], it is more likely that a combination of material properties influence its ultrasonic weldability.

Unless indicated otherwise, all the materials were obtained in the annealed condition. The hardness values were measured experimentally, and are presented in Figure 41 for both the welding materials and the tooling materials. Excluding 304 SS and C.P. Ti, the compositions were obtained from the material test reports provided with the materials. The remaining properties were obtained from ASM Handbooks [27] and MatWeb [28].

Abbrev.	Common Name, UNS	Thickness (mm)	Hardness (HV)	Elastic Modulus (GPa)	Tensile Strength (MPa)		Typical Applications	Composition
					Yield	Ultimate		
<b>304 SS</b>	AISI Type 304 Stainless Steel 2B, UNS S30400	0.4572	161.4	193 - 200	215	505	Chemical and food processing equipment, cryogenic vessels	(Bal)Fe, 0.08C, 2.00Mn, 1.00Si, 9Ni, 0.045P, 0.03S
<b>410 SS</b>	AISI Type 410 Stainless Steel 2D, UNS S41000	0.508	177.1	200	409-422	570	Rifle barrels, cutlery, jet engine parts	(Bal)Fe, 0.142C, 0.420Mn, 0.42Si, 11.86Cr, 0.59Ni, 0.024P, 0.001S, 0.10Mo, 0.13Cu, 0.040Co, 0.012N, 0.001Al, 0.001Ti, 0.012Sn
<b>CP Ti</b>	ASTM Grade 2 Titanium, UNS R50400	0.508	155.7	102	275-410	343	Aircraft and missiles, corrosion resistance for marine and chemical-processing	(Bal)Ti, 0.10C, <0.015H, 0.25O, 0.03N, 0.30Fe
<b>Ti 6Al-4V</b>	ASTM Grade 5 Titanium, UNS R56400	0.508	333.2	105-120	938-965	1020-1041	Aircraft gas turbine disks and blades, aircraft structural, prosthetic implants, chemical-processing	(Bal)Ti, 6.47Al, 3.86V, 0.10N, 0.020C, 0.0090H, 0.190Fe, 0.130O, <0.0050Y
<b>Ni 625</b>	Inconel 625, UNS N06625	0.508	256.4	208	503	930	Chemical processing, aerospace and marine, pollution-control, nuclear reactors	61.79Ni, 22.03Cr, 2.92Fe, 0.07Co, 0.01C, 3.46Nb, <0.01Ta, 0.13Mn, 0.06Si, 0.22Ti, 0.27Al, 9.02Mg, 0.013N, 0.006P, 0.001S,
<b>Ni 718</b>	Inconel 718, UNS N07718	0.5334	235	211	537	907	Gas turbines, rocket motors, spacecraft, nuclear reactors, pumps, and tooling	53.86Ni, 18.39Cr, 17.81Fe, 0.15Co, 3.01Mo, 4.95Nb, <0.01Ta, 1.00Ti, 0.54Al, 0.03C, 0.09Mn, 0.06Si, 0.002B, 0.08Cu, 0.010P, 0.0002S

**Table 2: Basic material properties [27, 28]**

The minimum thickness of the materials in this study was  $0.508 \pm 0.05\text{mm}$ . Equipment power limitations dictate the maximum weldable sheet thicknesses. The weld strength is known to rapidly decrease with increasing material thickness due to frictional energy losses (internal damping) and energy spreading in the through-thickness direction [4]. It would be insightful to perform welding trials on a range of thicknesses for each alloy, but this would create a very large number of trials with this combination of materials. The materials were cut into 25.4mm by 50.8mm coupons. This coupon size minimizes material waste, but is large enough to be easily handled and tested with standard tensile-tester grips. Additionally, the coupon length was verified experimentally (Chapter 5) to be void of any critical dimensions in which overwelding or a no-weld condition occurs. The materials were cut with a hydraulic shear, and then cleaned with acetone followed by methanol. The surface finish was as provided (as rolled), and was not tested. Although surface finish is important in ultrasonic welding, it is believed to be less critical in very high-power welds.

### 3.3 TOOL MATERIALS

Solid, one-piece tools were machined from high-speed tool steels. Refractory-alloy tools consisted of a small piece of the (refractory alloy) brazed to a standard AISI M2 high-speed steel tool. From the literature review, tungsten-alloys appeared to be most promising for welding of advanced alloys. The materials used to develop tooling for this project include:

1. AISI M2 High Speed Steel – Tool steel composed of 5Mo-6W-2V, with good machinability, toughness, wear resistance, and compressive strength.
2. AISI grade 18Ni (350) Maraging Steel – A precipitation-hardened tool steel composed of 18Ni-12Co-4.8Mo.

3. Molybdenum TZM – The addition of 0.5 weight percent Ti and 0.1 weight percent Zr increases the high temperature strength over pure Molybdenum.
4. CMW Elkon 100W – Pure tungsten powder ingots are pressed and sintered followed by rolling and swaging. Commonly called Wolfram, it is described as “pure wrought tungsten.”
5. Wrought Tungsten – Pure wrought tungsten with improved strength and ductility over 100W because of increased deformation and mechanical working.
6. Tungsten-25Rhenium – The addition of 25 weight percent Rhenium lowers the ductile-to-brittle transition temperature below room temperature. Known for its extreme strength and corrosion resistance.
7. Tungsten-Lanthanum – A promising FSW tool material, the exact composition is proprietary.

Some of the relevant material properties, as well as standard applications, of the tool materials are listed in Table 3. The hardness was determined experimentally. The remaining properties were obtained from ASM Handbooks [27] and MatWeb [28]. Blank cells indicate the data was not available.

Abbrev.	Common Name	UNS	Hardness (HV)	Elastic Modulus (GPa)	CTE, linear ( $\mu\text{m}/\text{m}\cdot^{\circ}\text{C}$ )	Yield Tensile Strength (MPa)	Ultimate Tensile Strength (MPa)	Typical Applications
<b>M2</b>	AISI M2 High Speed Steel	T11302	926	179-228	12.4-13 (250°C)			Cold work applications, tools for punching, forming, and pressing, very wide use for all cutting tools
<b>350M</b>	AISI grade 18Ni (350) Maraging Steel	K92810	778	200	11.3 (500°C)	827	1140	Bearings, recoil springs, missile cases, aerospace drive shafts, cold forming dies, plastic molding dies, pins, punches
<b>TZM</b>	Molybdenum TZM	R03640	313.1	315	6.0 (500°C)	860	965	Heat engines, heat exchangers, nuclear reactors, radiation shields, extrusion dies, boring bars, high-stress furnace parts, hot pressing dies, x-ray tube anodes
<b>100W</b>	CMW Elkon 100W Tungsten		431.7	406	4.43 (100°C)	450	475	Low-arc erosion contacts, automotive horn, magneto ignition, motor speed governor contacts, RSW electrodes
<b>Wrought W</b>	Pure Wrought Tungsten		355.8		4.43 (100°C)			Low-arc erosion contacts, automotive horn, magneto ignition, motor speed governor contacts, RSW electrodes
<b>W-25Re</b>	Tungsten-25% Rhenium		509	430	4.48 (500°C)		1370	High-temperature furnace elements, lighting, electronics, FSW welding tools
<b>W-La</b>	Tungsten-Lanthanum Alloy		439.6					FSW weld tools

**Table 3: Tool material properties and description [27, 28]**

### 3.4 BRAZING FILLER METALS

A number of braze alloys were tested to join the refractory-alloy wear surfaces to the tools. Due to the CTE mismatch between the refractory alloys and the steels, the joint would have some level of inherent stress before being used to create welds. The braze alloys were selected based on manufacturer recommendations for the dissimilar combinations, predicted temperature and strength requirements. The foil form was preferred because any interface is subject to ultrasonic energy losses and the thicker the joint or more porosity, the worse the situation. The braze alloys used in the study include:

1. Incusil ABA – Wesgo Metals' Incusil ABA, or active braze alloy, has the following composition (in weight percent): 59Ag-27.25Cu-12.5In-1.25Ti, and a yield strength of 338MPa [29]. It has a 715°C liquidus, and so most braze cycles were brought up to 750°C for several minutes. It was used in a 0.0508mm thick foil, cut to size for the particular joint.
2. AWS BNi-9 – NICROBRAZ 150 is a nickel-based powder with the composition: 81.5Ni-15Cr-3.5B-0.05C. It has a liquidus of 1060°C and a suggested brazing temperature of 1120°C [30]. It is applied as a paste by mixing in NICROBRAZ 'S' binder until an 88 wt% powder, 12wt% binder is achieved. It is suggested to be able to produce joints with 50-100% more strength than those created with the Incusil ABA foil [31].
3. AWS BNi-2 – A nickel-based braze alloy with the composition: 82.35Ni-7Cr-3.1B-4.5Si-3Fe-0.05C. It was used in both paste and foil forms:
  - a. NICROBRAZ L.M. – A nickel-based powder applied as a paste by mixing in NICROBRAZ 'S' binder until an 88 wt% powder, 12wt% binder is achieved. It has a liquidus of 1000°C and a suggested brazing temperature range from

1010-1175°C [30], allowing it to be used in a “step” brazing operation with a pre-existing BNi-9 braze joint. It should achieve joint strengths slightly lower than with BNi-9.

- b. MBF-20 – An amorphous nickel-based braze foil by Metglas, Inc. It was used in a 0.0508mm thick foil, cut to size for the particular joint. Potentially increased joint strengths because of less chance for porosity and contamination from the binder.

### 3.5 METALLURGICAL SECTIONING

Sample cross-sections were cut with a Buehler Abrasimet “2” abrasive saw with light pressure and heavy coolant flow. Sections were mounted in Buehler Epomet molding compound using plastic specimen support clips in a Buehler Metaserv Pneumet II hot mounting press with the following parameters: 50psi mold pressure, 16min heating time, and 5min cooling time. Sections were polished using a Struers Abramin automatic polisher with 20N downward force, 150RPM velocity, and a 6min cycle time. Sections were wet ground with silicon carbide paper using to at least 800-grit, followed by polishing with Struers OP-S 0.5 $\mu$ m SiO<sub>2</sub> suspension on a black velvet cloth. The samples were etched to bring out the weld bondline and microstructural features. The etchant used differed for each alloy; Stainless Steel and Nickel-based alloys were etched with an Oxalic acid solution, commercially-pure titanium with Keller’s reagent, and titanium 6Al-4V with Kroll’s reagent.

Macrographs were taken with an Olympus SZ1145 stereo microscope. Some macrographs were taken with either a 1/64<sup>th</sup> increment scale or a digital scale was later added to the image. Micrographs were taken of the sections with a Nikon Optiphot microscope fitted with a 2-megapixel PAXcam digital camera. PAXit software was used to adjust and edit the images.

Fracture surfaces were examined using a Zeiss EVO 60XVP scanning-electron microscope (SEM). Figure 11 A-C includes images of the SEM, stereo microscope, and optical microscope. The amount of magnification of micrographs and SEM images is indicated by the scale on the image.

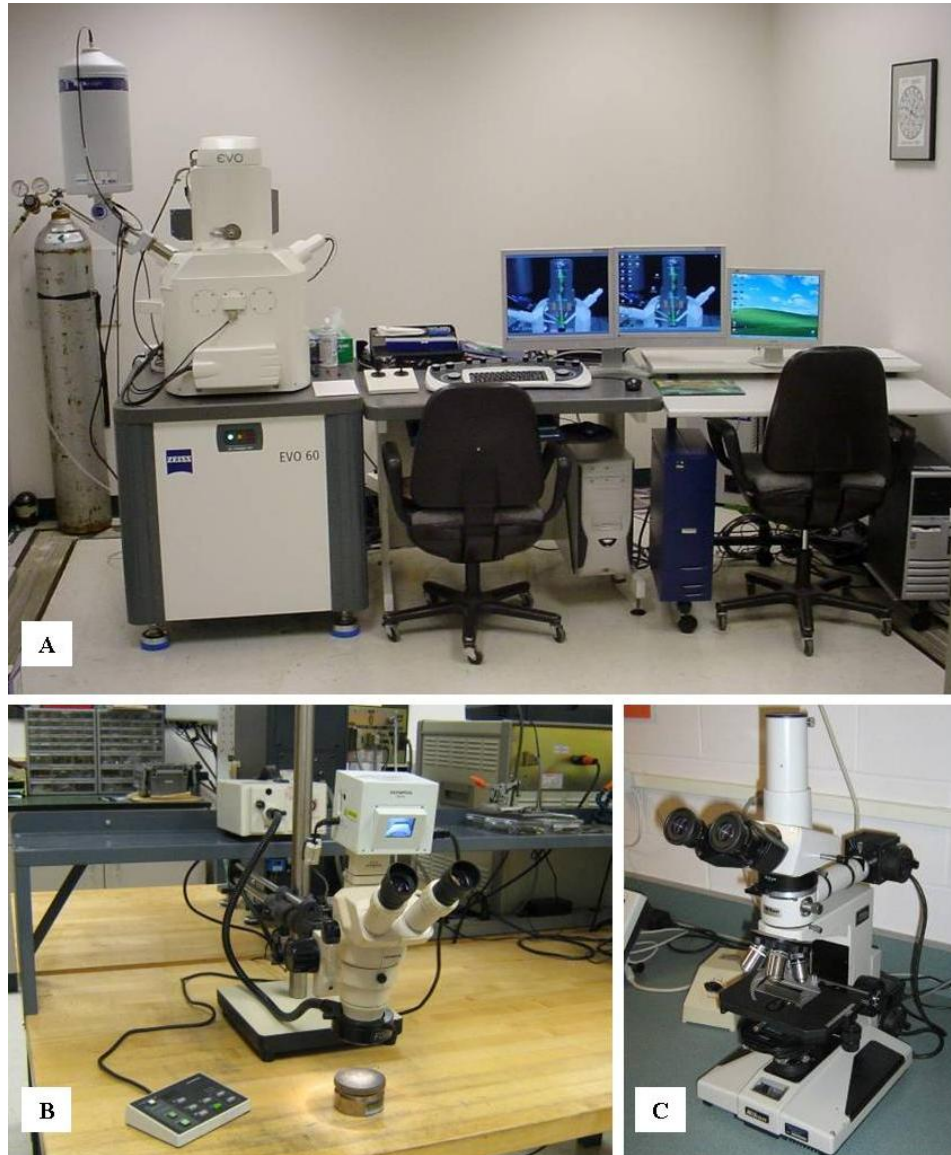


**Figure 11: A – Zeiss scanning electron microscope, B – Olympus stereo microscope, C – Nikon microscope**

## CHAPTER 4

### ULTRASONIC TOOLING

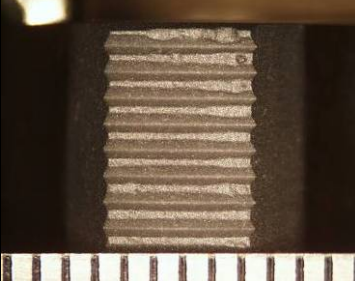
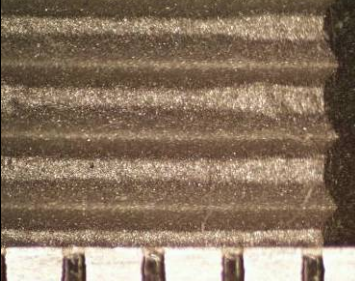
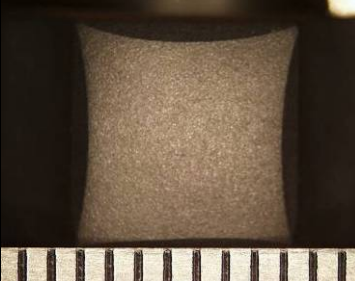
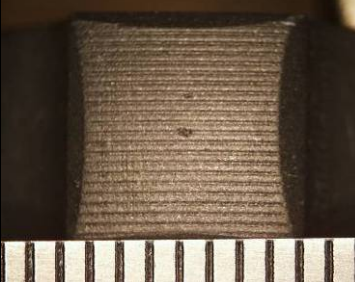
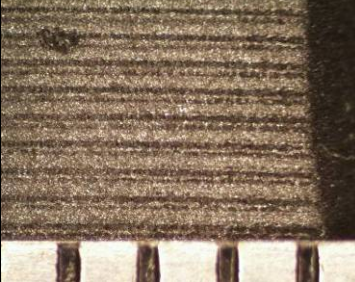
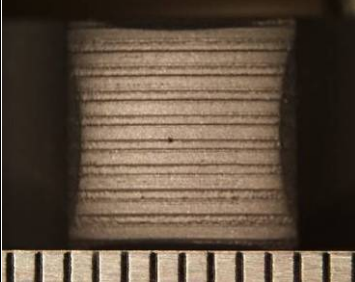
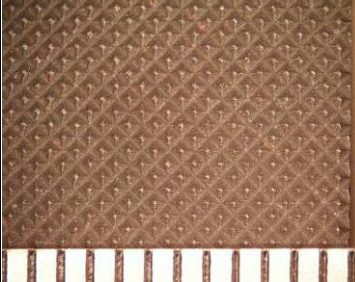
The ultrasonic tooling consists of the anvil and the tip. Ultrasonic vibration is applied to the welding tip. The anvil is static. When force is applied to the tip, the texture of the tooling grips the weld specimens, effectively isolating the relative motion to the joint interface. With the proper tool texture and geometry, weld process parameters aside, a weld is formed.

This study investigated the geometry, texture, and material of the tooling in order to weld advanced alloys. In cooperation with an OSU Capstone Project [32], preliminary weld trials evaluated tool geometry and texture. The results of these initial investigations were applied to the tool design used for this study. A number of materials were evaluated for use as tool materials. Some of the tool materials required brazing operations and non-traditional machining.

#### 4.1 TOOL DESIGN AND FUNCTION

In cooperation with an OSU Welding Engineering Capstone Project [32], it was found that for difficult-to-weld materials, a spherical radius tip with a knurl pattern produced the highest strength welds with the lowest deviation. The investigations used 0.51mm aluminum alloy 7075 to evaluate the weld quality for different tip designs and textures by making a series of repeated welds using the same welding parameters for each tip. A 3.6kW AmTech UW20 lateral-drive ultrasonic spot welder was used with detachable-tips to allow expedient changing of different

tools. All the tips were made with heat-treated AISI M2 high speed steel. The anvils were also made from M2 steel, all featuring a 6.35mm x 2.54mm x 45° machined knurl pattern. Table 4 illustrates the different tip designs and textures evaluated.

<p>Tip #1, Flat Rectangular Weld Tip with FWF- Style Heavy Knurl (following Weld Trials and Micro-grit blasting)</p>		
<p>Tip #2, Micro-grit-blasted 12.7-mm radius Spherical Spot Welding Tip</p>		
<p>Tip #3, 12.7-mm radius Spherical Spot Welding Tip, Laser Machined and Micro-grit-blasted 1, Less Aggressive Pattern</p>		
<p>Tip #4, 12.7-mm radius Spherical Spot Welding Tip, Laser Machined and Micro-grit-blasted 2, More Aggressive Pattern</p>		
<p>Heavy- Knurl Anvil, Micro-grit blasted, 6.35-mm Pitch X 2.54-mm Depth X 45°</p>		

**Table 4: Stereoscope pictures of UMW tool geometries and textures (Note: Scale is in mm) [32]**

The difference in weld quality is shown by both images of the weld surfaces, Table 5, and typical power characteristic curves, Table 6, from weld trials conducted with the different tip designs. Figure 12 demonstrates the orientation of each of the pictures of the weld surfaces shown in Table 5. Figure 14 is a plot of the weld strengths vs. run order while Figure 15 is a plot of the weld power vs. the run order for this study.

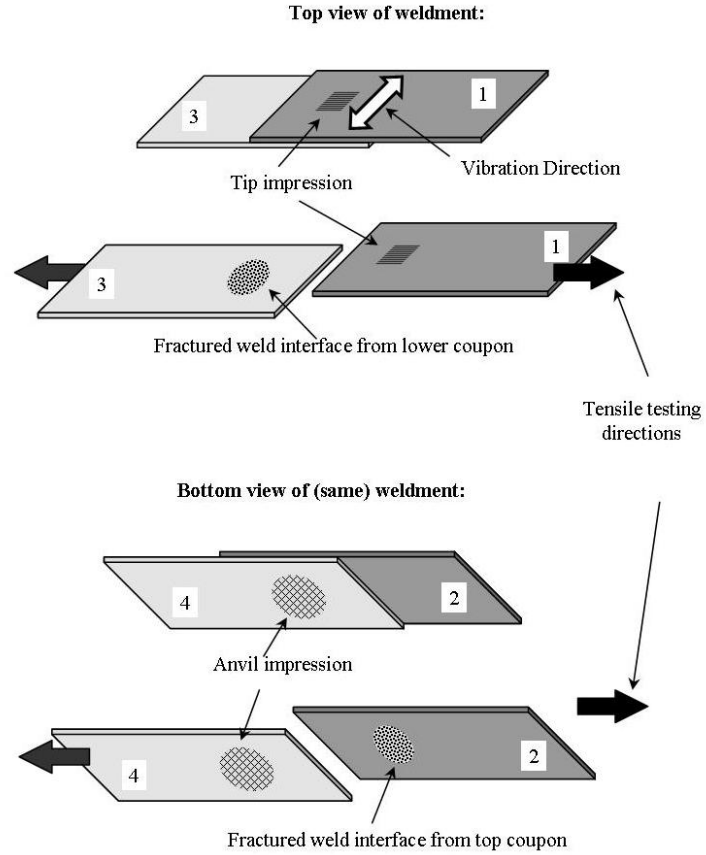
Small differences in the knurl have been observed to have significant effects on the resultant weld. The spherical tip reduces perimeter stress concentrations normally associated with flat, rectangular weld tips, and may allow the weld area to be more easily measured following testing. The spherical-radius tip also initiates the weld at the center, growing radially with time, whereas the flat tip has to weld the entire surface area simultaneously. The flat tip requires very high power levels for advanced materials, which may not be currently available from the ultrasonic welding equipment.

The flat tip, in general, produced the lowest weld strengths and required relatively high power levels. The repeatability was reasonable; the first weld appears to have been an outlier. No variations of knurl pattern or surface area were evaluated. Although all the fracture surfaces were of interfacial failure modes after tensile testing, the welds created with the flat tip had the lowest bond area density and therefore were of the lowest quality. High-powered ultrasonic equipment may be able to produce higher-quality bonds with this tip design. The contact area of the flat tip was much greater than with the spherical tips, and therefore a lower power density was applied during the trials with the flat welding tip. Variations in surface area for the flat welding tip were not evaluated.

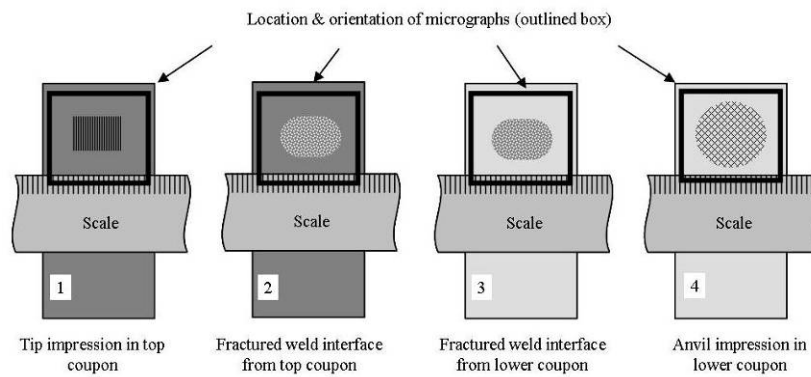
A 12.7-mm spherical-radius tip was evaluated with several different textures. A light grit-blast finish was applied to all the tips. Of the two tips with laser-machined textures, the second tip had a much more aggressive knurl pattern. The “plain” tip with only the light grit-blasting had the highest deviation of tensile strengths all the trials, and required the lowest power levels. The

pictures of the tip interfaces may be evidence that the tip was inadequate at properly gripping the weld coupons; there appears to be some degree of sliding between the tip and the top coupon. This would explain the low power draw and the variation in weld strengths. The second spherical-radius tip had a light laser-machined texture applied. The light-knurl spherical tip achieved similar average strengths as compared to the previous, non-knurled tip, but with much smaller deviation. It required higher-power levels than the non-knurled tip, but still less than the flat tip. The final tip featured a coarse laser-machined knurl pattern applied to the same spherical-radius tip. The welds had the highest tensile strengths and good repeatability. The power levels surpassed even the flat-knurl welding tip. All the welds made with the spherical-radius tips failed in an interfacial mode during tensile testing and have similar weld areas. The stress supported by the three different welds, therefore, increases with increasing tensile strengths.

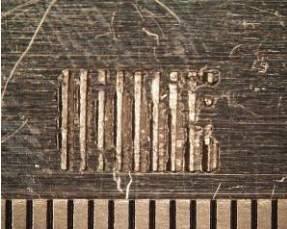
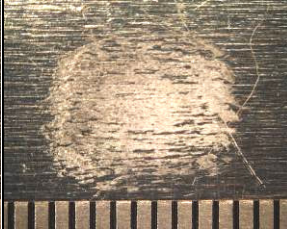
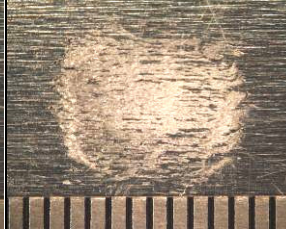
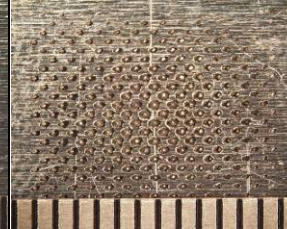
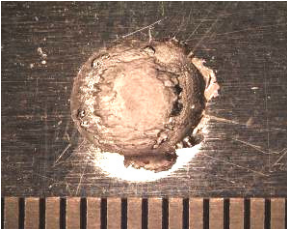
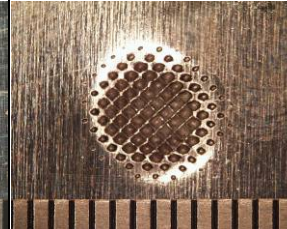
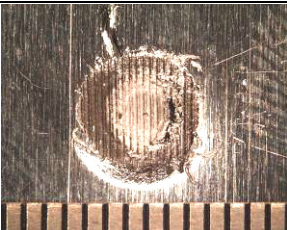
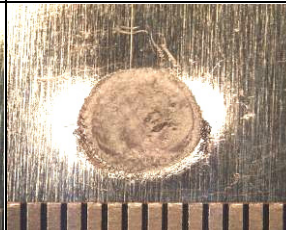
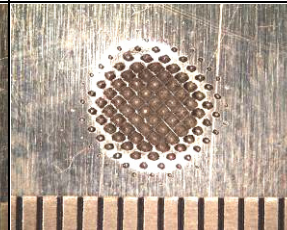
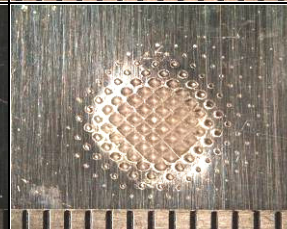
With such a limited number of weld trials, the amount of statistical value that can be drawn from this data is limited. Fortunately, the results were more than adequate to suggest the appropriate tip design and texture for the next series of weld trials in more advanced alloys. This experiment design was excellent for providing a basic comparison of weld quality due to tool variations. In conclusion, a spherical radius tool with a laser machined texture was used for the remaining experiments.



**Figure 12: Diagram of tensile testing weldments**



**Figure 13: Weld and interface image diagram**

	Tool Impression	Weld Interface – Tip Side	Weld Interface – Anvil Side	Anvil Impression
Tip #1, Trial #101				
Tip #2, Trial #213				
Tip #3, Trial #400				
Tip #4, Trial #500				

**Table 5: Stereoscope pictures of weld surfaces using different tool designs and geometries (Note: Scale is in mm) [32]**

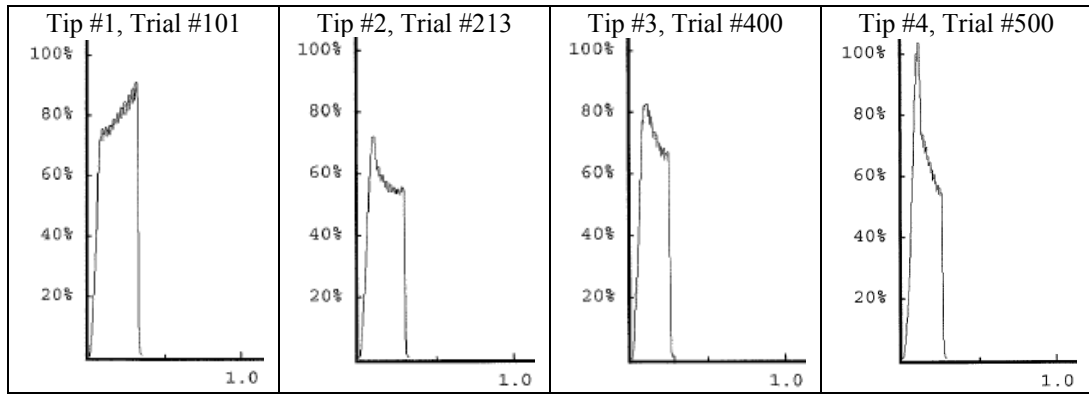


**Table 6: Power vs. Time characteristic plots due to variations in tooling [32]**

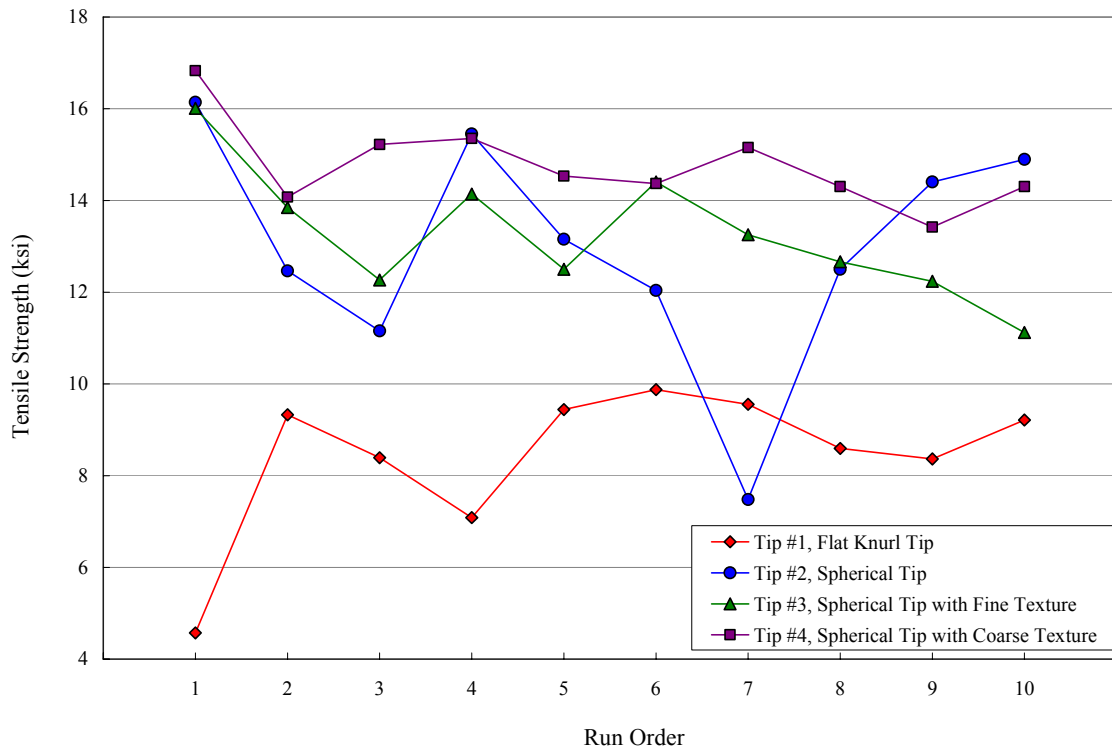


**Figure 14: Comparison of weld strengths using different tip designs [32]**

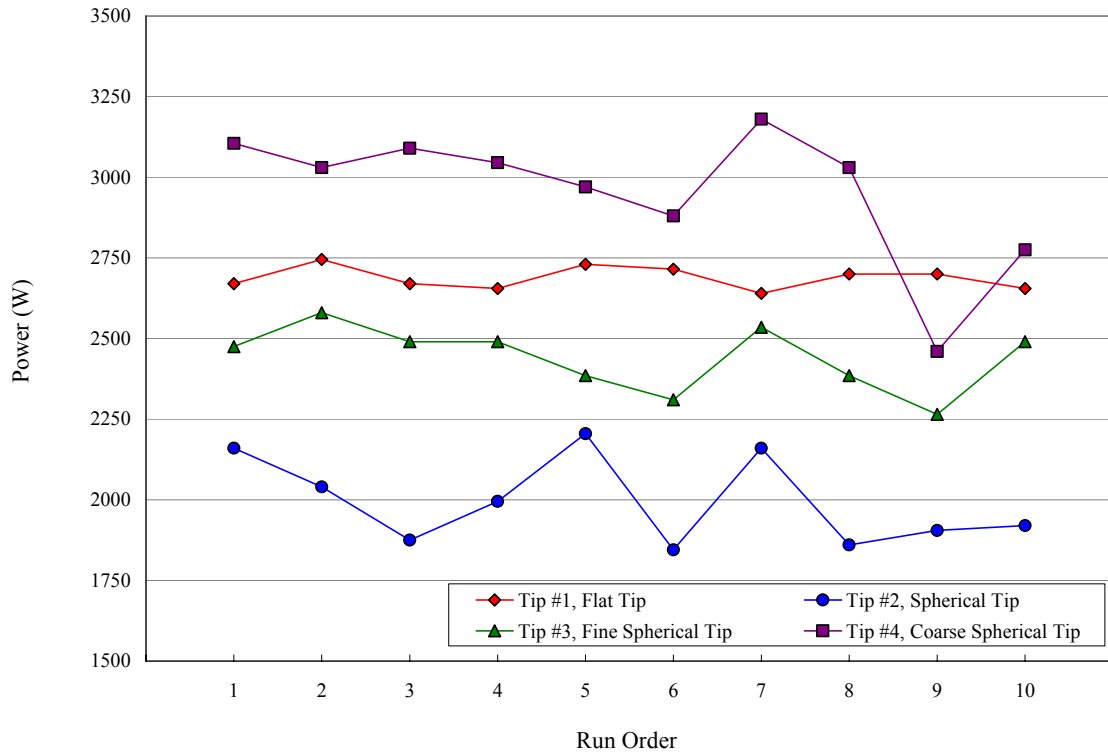


**Figure 15: Comparison of power levels for welding trials using different tip designs [32]**

## 4.2 TOOL MASS

The allowable detachable-tip tool dimensions have been established from past experience, although the limitations are not well defined. The tools must efficiently transmit the ultrasonic energy to the weld, as well as be resistant to wear and sticking (to the weld coupon). M2 tool steel is well-established for ultrasonic spot weld tooling because of its fatigue and wear resistance for traditional UMW applications involving softer materials, such as aluminum and copper. When welding harder materials, like those proposed in this study, the wear resistance is inadequate. Significant wear and/or tip sticking have been observed while welding a wide range of steels [1]. In addition to investigating other tool steels with improved properties, refractory

alloys are also being investigated due to their high temperature strength and wear-resistance. Machining solid tips out of refractory alloys is not appropriate for the following reasons: they may be too brittle to transmit the ultrasonic energy, they cannot easily be machined with conventional machining operations, and they can be relatively expensive. In addition, there is concern that the refractory alloy tips have significantly more mass than conventional tips and the equipment may not operate efficiently. Therefore, wear-resistant materials were brazed onto ground M2 welding tip blanks.

To find the operational window for tool mass, several cylindrical weld tips of varying mass were fitted to the detachable-tip sonotrode and the sonics were activated. As previously discussed, frequency-shifting circuitry enables ultrasonic system to operate continuously with varying resistance. Using several tips of incrementally increasing mass, the allowable operational window was found to be between 6.3847-g (min.) and 16.1703-g (max.) for the lateral-drive 3.6-kW system with a 1:1 booster. The total mass of the tips need to fall within this window. The 3-D CAD software SolidWorks 2007 SP4.0 was used to design the ultrasonic tooling. The software allows the user to specify the materials and/or density of the parts, so the mass of the tooling can be modified during the design phase before any parts are machined. This was a useful feature, because the brazed assemblies had complex geometries that otherwise would have been developed using volumetric approximations and the “guess and test” method. Drawings of the tools are provided in the appendix section, Figure 143 – Figure 145.

With the main intent of the experiment to evaluate the weldability of several alloys, it was not desired to perform a large tool life study at the time. Several potential tool materials will be evaluated during screening experiments. The most promising tool materials will be used for the course of the remaining weld trials.

### 4.3 DEVELOPMENT OF TOOLS

Several tool materials were investigated as a part of this study, consisting of refractory-based alloys and heat-treated tool steels. The tool materials were created from both conventional machining processes followed by heat treating for the M2 and 18Ni materials and unconventional machining processes including wire-EDM cutting and CNC grinding for the refractory-based alloys. The refractory-alloys were only used for the weld tip contact surfaces due to their expense, difficulties in machining, and relatively low toughness. Illustrations of the different anvil and tip designs used in this experiment are presented in Figure 16.

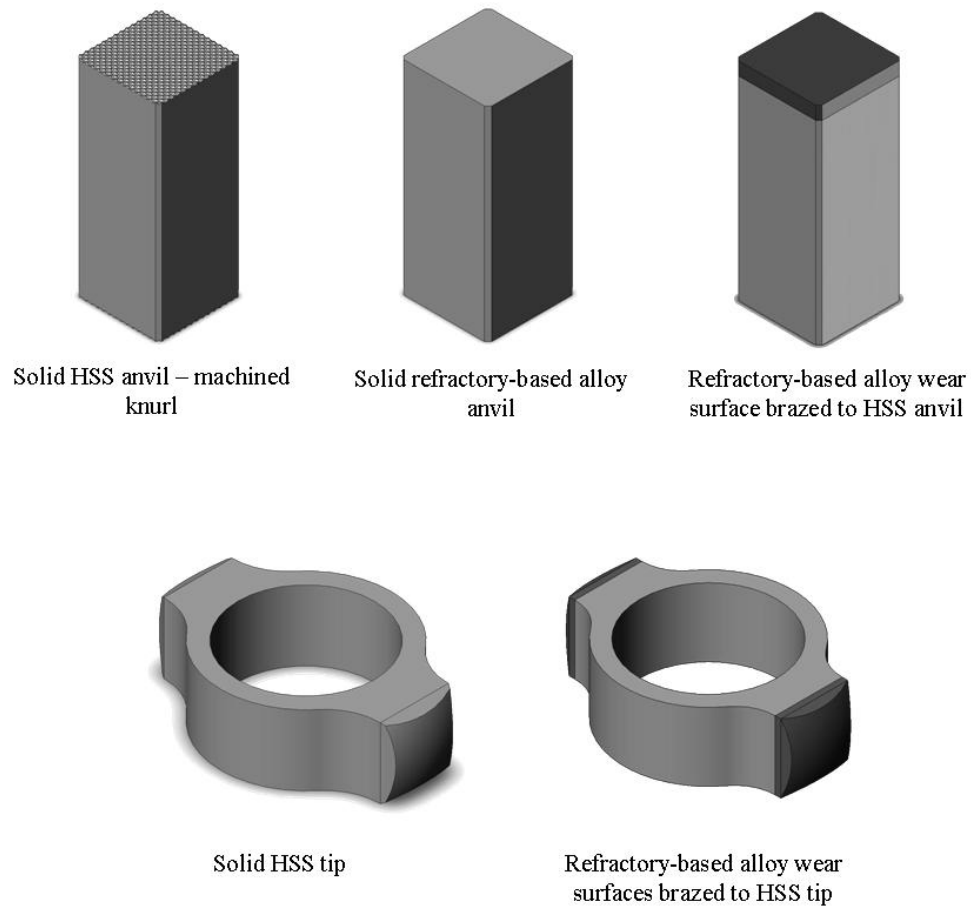


**Figure 16: Overview of Anvil and Tip designs (not drawn to scale)**

Solid weld tips and anvils were machined from AISI Grade M2 high speed steel and hardened to 60-65  $R_C$  by quenching from 1200°C. They were not tempered. Similarly, solid weld tips and anvils were machined from AISI Grade 18Ni Maraging (350M) tool steel. They were subsequently precipitation-hardened at 500°C for 8-12 hours.

Refractory-based alloys were used as solid or brazed assemblies for the anvils and as brazed assemblies for the weld tips only. Refractory-based alloy wear surfaces were brazed onto M2 tool steel tips. Since M2 tool steel has proven performance for transmitting ultrasonic energy

and solid refractory-based tips are not feasible, taking advantage of the properties of both using a welding or brazing operation is a logical solution.. Anvils are not ultrasonically driven so the concern for mass and density is not significant. Solid refractory anvils were used when possible. Refractory-alloy wear surfaces were brazed to standard M2 anvils in such cases where the supply of material was limited.

The (brazed) welding tips consisted of Molybdenum TZM, wrought-tungsten, tungsten-25% rhenium, and tungsten- lanthanum wear-surfaces brazed to AISI M2 steel tips. The Molybdenum TZM tips were brazed with Metglas BNi-2, and failed after a limited number of weld cycles. It is thought that the thick oxide layer on molybdenum may have prevented the braze from fully wetting the surface. For the tungsten-based tips, the nickel-based braze joints were much more reliable than the Incusil ABA braze joints.

After brazing, the tips were machined to size. A CNC grinding operation machined the parts symmetric with a spherical radius according to the drawing in Appendix A, Figure 143. The braze joints were ground smooth to avoid any stress risers. After machining, a laser was used to apply texture to the tools.

Solid CMW Elkon 100W and W-La alloy anvils were wire-EDM cut. Molybdenum TZM, wrought-tungsten, and tungsten- 25% rhenium were successfully brazed to standard AISI M2 anvils using both active braze alloys and nickel-based braze alloys.

#### 4.4 BRAZING UMW TOOLING

Initially, Incusil ABA braze foil was selected to join the tungsten-based alloys to the tools according to both the AWS Brazing Handbook and Wesgo Metals Alloy Selection Table [29, 33]. The 0.002-in thick foil was cut to size and lightly sanded with 600-grit paper on both sides to lightly remove any oxides or contaminants. All the components to be brazed were lightly grit-

blasted, and cleaned with Methanol. Figure 17 – A shows the components before assembly. The parts were loaded onto a small ceramic tray, along with a thermocouple, and loaded into a 3-in Lindberg vacuum tube furnace. Figure 17 – B shows the parts prior to inserting into the furnace. The furnace was pumped down to  $5.0 \times 10^{-7}$  TORR prior to starting the heating cycle. Figure 18 is a temperature-time plot of the brazing cycles for several different braze alloys. The furnace was programmed to ramp up a temperature just below the solidus (of the braze alloy), dwell to allow all the parts reach temperature, ramp up to a temperature above the liquidus (of the braze alloy) for several minutes, and then slow cool down. Once cool, the furnace was vented to atmosphere, and the parts were removed. Figure 17 – C & D shows the assembly following the brazing cycle.

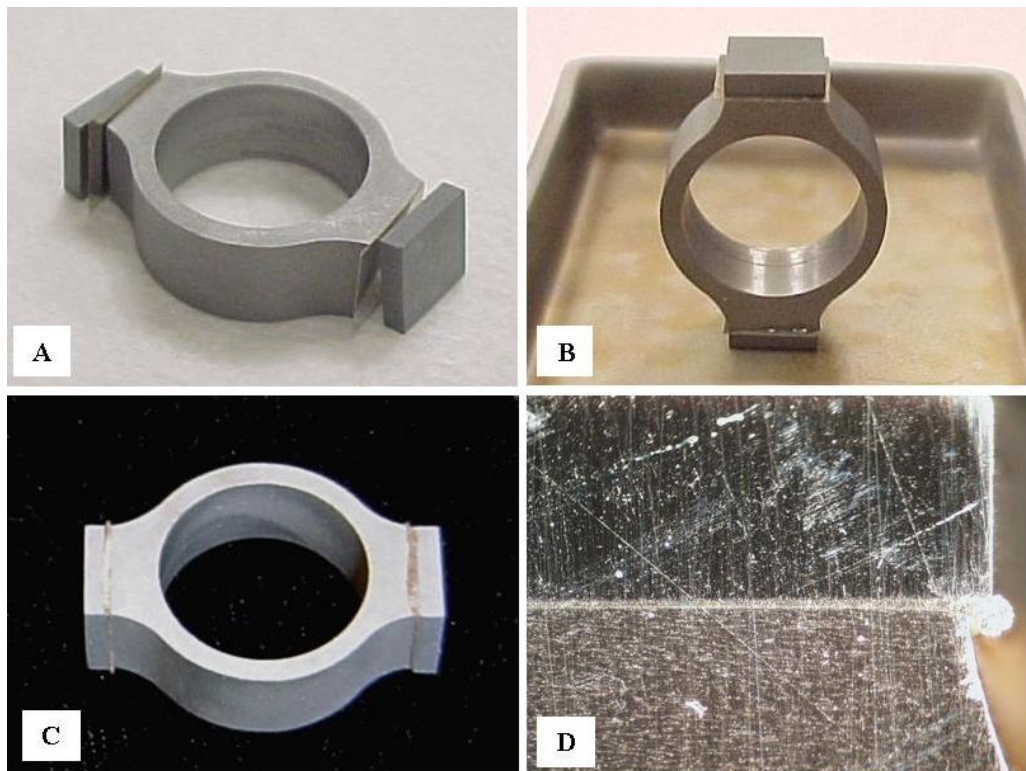


**Figure 17: A – W-25Re Tips, Braze Foil Squares, and Ground M2 Tool; B – Assembled Pre-Brazing; C – Brazed Assembly; D –Braze Joint viewed through Stereoscope**

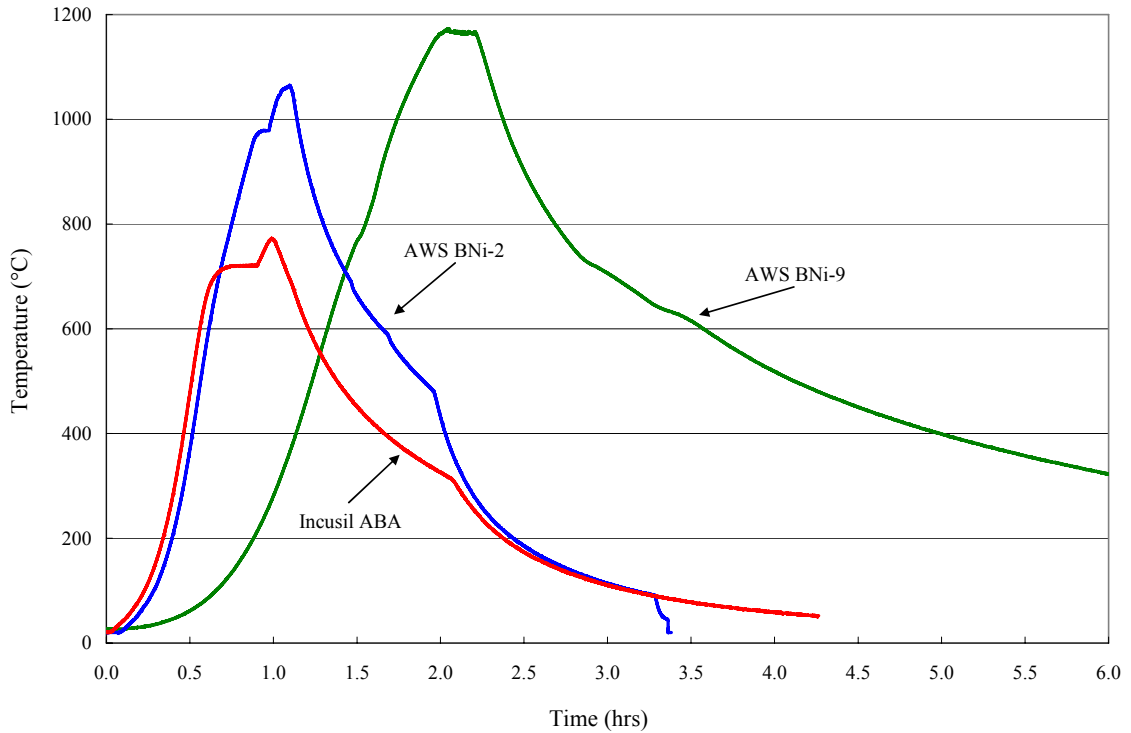


**Figure 18: Furnace cycles for several braze alloys**

It was later determined that some weld cycles generated enough heat to melt the Incusil braze foil. Figure 19 – A is a macrograph of a W-La tip brazed to a M2 tool using Incusil ABA braze foil before weld trial 5001. Figure 19 – B is a macrograph of the same tip after weld trial 5008. During the weld cycle, the temperature exceeded the melting temperature of the braze foil allowing the tip to move and re-solidify in a new location. Several weld cycles later, the braze joint completely fractured. Figure 19 – C is a picture of the corresponding fracture surfaces. If the braze joint was melting during the weld cycle, the ultrasonic motion would be concentrated at the braze joint instead of the weld interface, and the weld would be expected to be very weak, if any weld was formed at all.

It was apparent that a higher-strength, higher-temperature braze alloy was necessary. EWI brazing expert Dan Hauser and Met-Glass brazing expert Anatol Rabinkin, were consulted for suggestions on higher-strength braze alloys. Nickel braze alloys AWS BNi-2, AWS BNi-3, and AWS BNi-9 were concluded as possibilities. All of these alloys should promote a joint strength of roughly 40ksi when used with tool steel, as compared to the 20-30ksi strength from the Incusil ABA [31]. However, the ability to get these strengths with Tungsten is unclear; the formation of brittle Tungsten Borides are possible. The AWS brazing handbook recommends short brazing cycles with minimal brazing temperatures to minimize the formation of these constituents [33]. For the most part, nickel-based braze pastes were used. The joints were prepared by grit-blasting and cleaning with methanol, as done previously. 88wt% Microbraz 150 (AWS BNi-9) or Microbraz LM (AWS BNi-2) braze powder and 12wt% Microbraz S binder were measured, mixed, and applied generously to the joint surfaces. The components were immediately assembled, excess braze paste was wiped off, and brazed in a vacuum tube furnace. Although the paste required more effort to prepare, it had several advantages: joints did not have to be perfectly parallel (as compared to braze foil), and a fillet could be applied to sharp edges to minimize stress concentrations. Unfortunately, braze paste could introduce porosity, and generally produce joints with thicker cross-sections, both of which would decrease the joint efficiency to transfer ultrasonic energy.

An amorphous nickel-based braze foil, Metglas MBF 20 (AWS BNi-2), was also used on a limited basis. It did not work well with a Molybdenum TZM to AISI M2 joint, but more than likely this is indicative of an incompatible braze alloy or a flaw in the joint preparation or the brazing cycle itself. The braze foil should be chosen when possible to minimize ultrasonic energy loss across the interface.

The performance of the braze alloys is also summarized by the pictures of the tooling throughout the weld trials in APPENDIX B. Figure 19 – D is a picture of a SS 410 weld in which the BNi-9 brazed tip is glowing red-hot and did not fail.

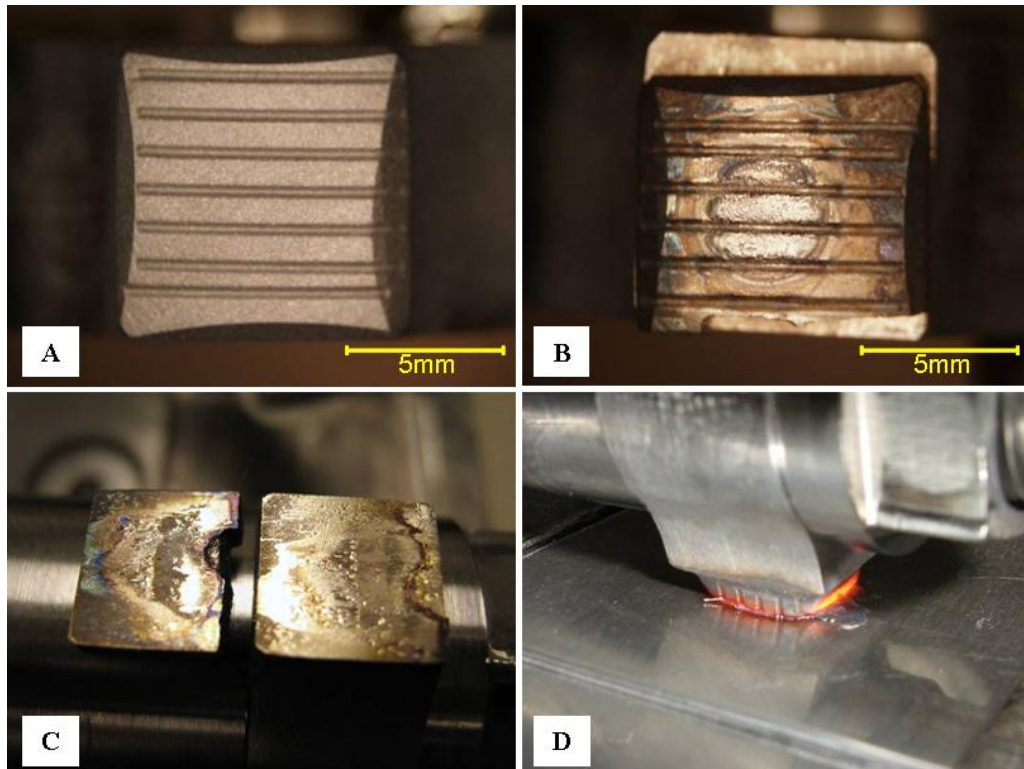


**Figure 19: A – W-La tip brazed with Incusil ABA foil before SS410 weld trial 5001; B – W-La tip brazed with Incusil ABA foil after SS410 weld trial 5008; C – Incusil ABA braze joint fracture surfaces; D – W-La tip brazed with Microbraz 150 (BNi-9) glowing red-hot during SS410 trial 5101**

#### 4.5 LASER MACHINING

Texture was applied to the tool surfaces with a Nd:YAG Diode laser. After several practice runs with a scrap piece of tungsten, the parameters to scribe a “V” shaped groove with a small radius at the bottom were found. The laser machining process parameters for laser-

machining refractory-based alloy and tool steel textures are listed in Table 7. Pictures of the laser machining process for welding tips are found in Figure 20, and anvils in Chapter 4.6. Each notch was approximately 0.014" wide and 0.006" deep. The lines were separated 0.040-in center-to-center for the tips, and 0.035-in for the anvils.

Parameters	Refractory-based Alloy	Tool Steel
Laser	Cutting-Edge Optronics' Stiletto model 3335 CW Diode-pumped Nd:YAG Rod, serial no. 99242, 50W power, 1064nm wavelength, >50nsec pulsewidth, 0-50kHz PRF	
Power Supply	Cutting-Edge Optronics model 2800 Laser Controller/ Driver	
Galvo Scanner	SCANALB AG model SK1020 two-axis digital scan head, serial no. 10807, 200mm focal length, for 10.6 $\mu$ m wavelength	
Software	Alase Technologies WinLase Editor 3.0	
Pulse Frequency	4000Hz	
Pulse Width	5 $\mu$ s	
Jump Speed	500in/s	
Jump Delay	100 $\mu$ s	
Pattern	Parallel Lines, each made from 8 sequentially narrower Rectangles using "Mark Fill" to create a "V-shaped" notch	Parallel Lines, each made from 6 sequentially narrower Rectangles using "Mark Fill" to create a "V-shaped" notch
Pattern Spacing	0.040in center-to-center	0.040in center-to-center
Number of Passes	1 <sup>st</sup> rectangle- 0.013in wide w/ 6 passes; 2 <sup>nd</sup> rectangle- 0.012in wide w/ 6 passes; 3 <sup>rd</sup> rectangle- 0.011in wide w/ 6 passes; 4 <sup>th</sup> rectangle- 0.010in wide w/ 6 passes; 5 <sup>th</sup> rectangle- 0.009in wide w/ 6 passes; 6 <sup>th</sup> rectangle- 0.008in wide w/ 6 passes; 7 <sup>th</sup> rectangle- 0.007in wide w/ 6 passes; 8 <sup>th</sup> rectangle- 0.006in wide w/ 6 passes	1 <sup>st</sup> rectangle- 0.013in wide w/ 5 passes; 2 <sup>nd</sup> rectangle- 0.012in wide w/ 5 passes; 3 <sup>rd</sup> rectangle- 0.011in wide w/ 5 passes; 4 <sup>th</sup> rectangle- 0.010in wide w/ 5 passes; 5 <sup>th</sup> rectangle- 0.009in wide w/ 5 passes; 6 <sup>th</sup> rectangle- 0.008in wide w/ 5 passes;
Peak Voltage	10.77V	10.77V
Current	40.8A	40.8A
Average Power	~30-35W (Estimated)	~30-35W (Estimated)
Travel (Max) Speed	1.2in/sec	1.2in/sec

**Table 7: Laser Machining Parameters**

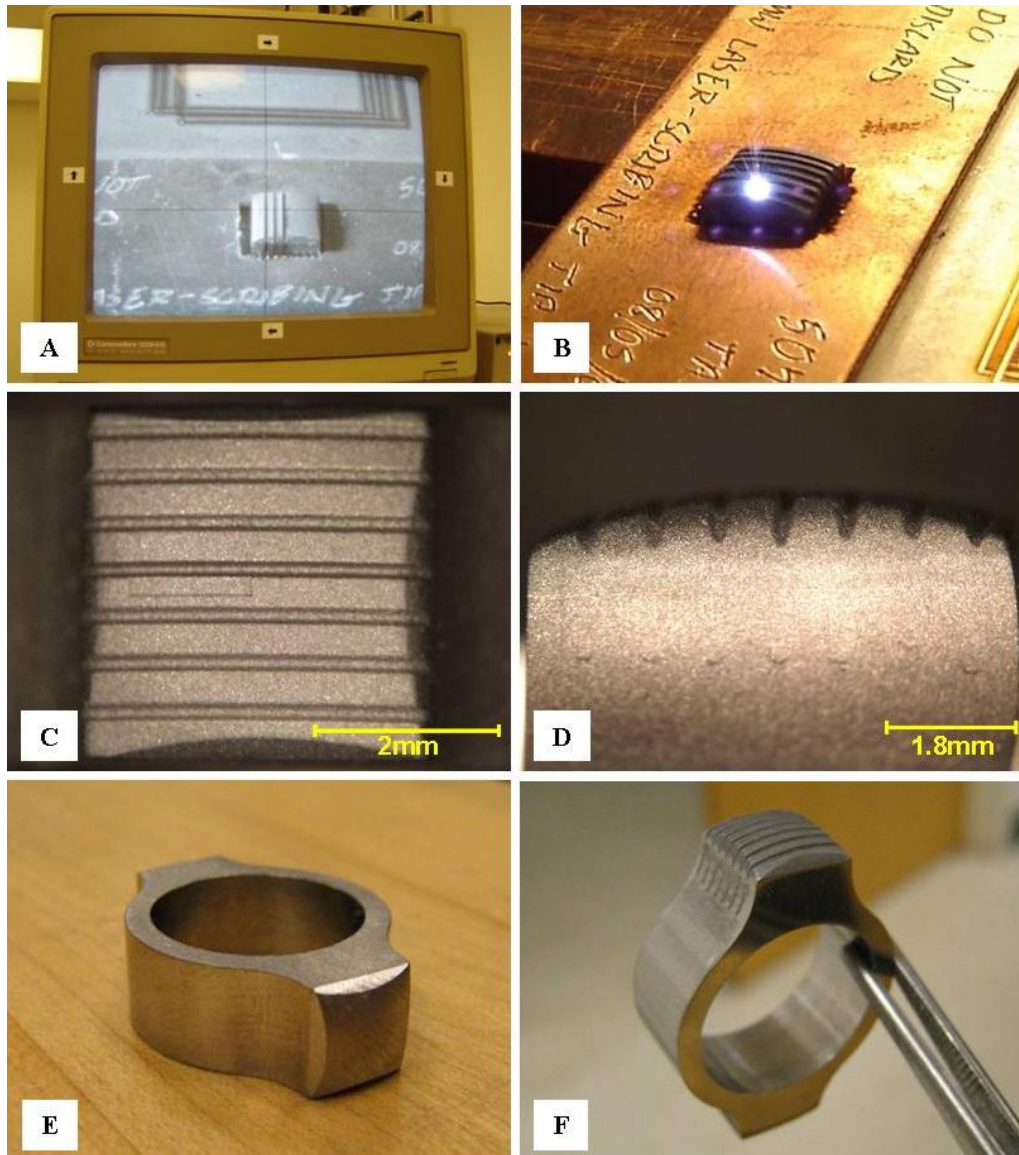


**Figure 20: Laser Machining Weld Tips; A – After several passes on monitor, B – Laser machining in progress; C – W-25Re tip face after machining; D – W-25Re tip texture profile; E – 350M tip before laser machining; F – 350M tip after laser machining**

## 4.6 TOOL PERFORMANCE

The tools were tested in a variety of combinations in the preliminary weld trials. The performance was evaluated based on visual inspection of the wear. Tools were then selected for use in the designed experiments. Unless otherwise noted, the welding tip and the anvil were of the same material.

Pictures of the tooling were periodically taken during the weld trials. These are included in APPENDIX B. A condensed version of the tool wear pictures are presented in this chapter. The build process, and comments about the overall performance during the trials is also included. Excessive wear and braze joint failures complicate the review of the welding tips. To simplify the tool evaluation, only the anvil performance will be reviewed in this chapter, although pictures of the weld tips are also in APPENDIX B, and comments about the welding tips are added when necessary. For the designed experiments, the tools used in the preliminary trials were either reconditioned or duplicates were manufactured.

M2 worked well when welding softer materials, such as copper and aluminum. However, when welding high-strength aluminum 7075 T-6 and stainless steel 304, the weld specimens readily bonded to the M2 anvils and tips [32]. In some cases, the tools fractured.

The tungsten-based tools all had similar performance, but it is difficult to compare them directly because of non-uniform parameters and each was subject to a different number of cycles with different materials.

#### 4.6.1 AISI GRADE 18NI (350M) MARAGING STEEL, AISI M2 HIGH SPEED STEEL ANVILS

After several AISI M2 anvil failures in small number of weld trials, several 350M anvils were machined. A 6.35mm x 2.54mm x 45° cross-hatch knurl pattern was machined into the anvils before heat-treatment. A small radius was added to the bottom of the knurl to improve fatigue properties. The anvils were heat-treated and tested with all the alloys.

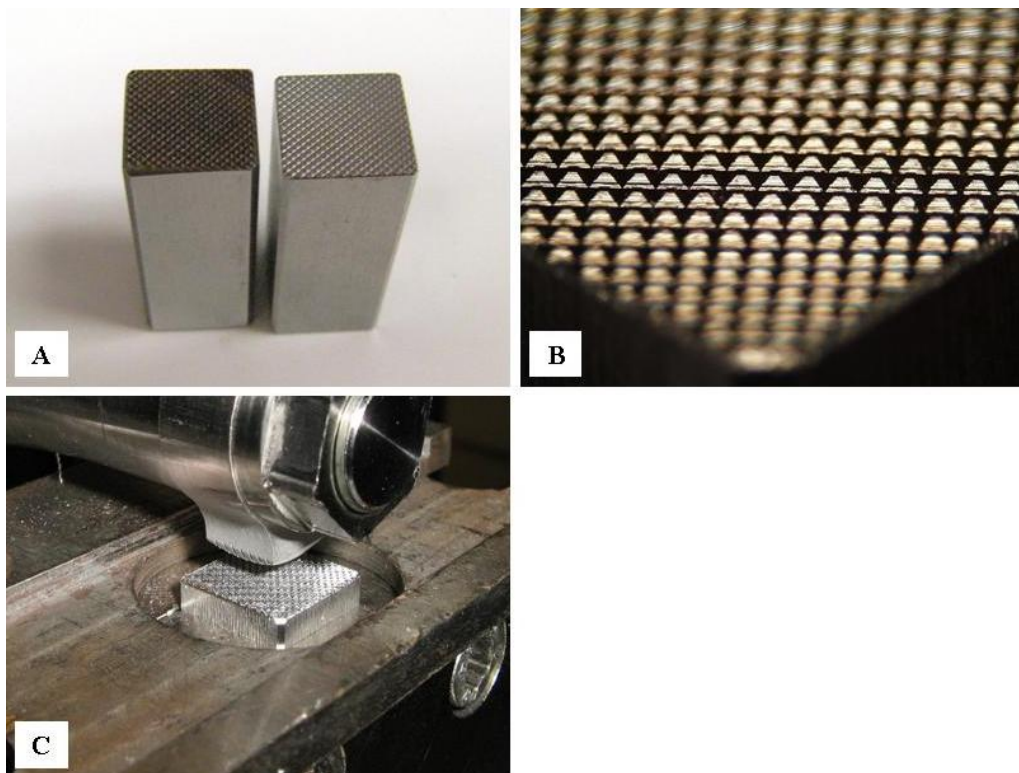


**Figure 21: Tool-steel anvils with machined knurl pattern: A - AISI M2 High Speed Steel (left), AISI Grade 18Ni (350M) Maraging Steel (right); B - Macrograph of knurl pattern; C - 350M anvil installed in anvil fixture**

350M anvils were used with the C.P. Titanium designed experiments and the nickel-based trials. Excluding the commercially-pure titanium, 350M anvils wore excessively and

readily bonded to the weldments in many of the preliminary trials. C.P. Ti is a much softer alloy than many of the others in this experiment, and the 350M tools performed well in the preliminary trials. Figure 22 has pictures of the 350M anvil surface wear after 85 C.P. Titanium weld trials. While the anvil wear appears excessive, the incremental pictures demonstrate that the wear was gradual and ductile. Many of the weld trials involved the samples glowing red-hot. This was not a concern with the tungsten-based anvils because of their excellent high temperature strength. The strength of the heat-treated tool steels, however, drops-off much faster with increased temperature. In addition, the repeated thermal cycles would be expected to modify the heat treatment; a substantial decrease in hardness may be expected near the anvil surface. Improved cooling may offset some of these concerns (air cooling is only applied to the welding tip after the weld cycle).

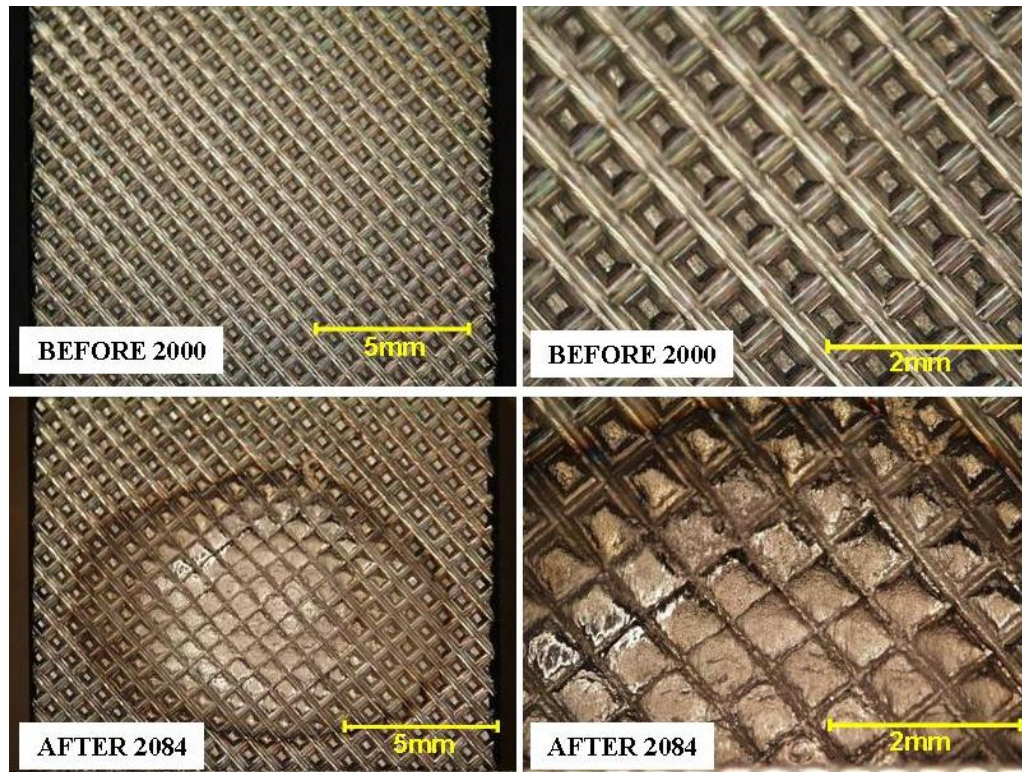


**Figure 22: 350M anvil wear during C.P. Titanium weld trials 2000-2084**

For the nickel-based weld trials, 350M was also utilized. During preliminary experiments, the tungsten-based alloy tools did out-perform the 350M tools, but the wear was greater than that experienced with any other materials. The nickel-based alloys had a relatively high-hardness, so the 350M, with a much greater hardness, was determined appropriate for the limited number of trials. Excessive wear and sticking to the work was expected, so the tools were artificially oxidized with an oxyacetylene torch prior to the welds. Both Ni 625 and Ni 718 were successfully welded using the 350M anvils, but excessive wear was experienced with only a single weld trial. Pictures of the anvil faces before and after Ni 625 weld trial 7000 are in Figure 23. Due to the high strength and hardness, the knurl was removed from the anvil after one weld.

Welds with the oxidized tools did not stick (to the tools), but welds without needed great force to be separated from the anvil.

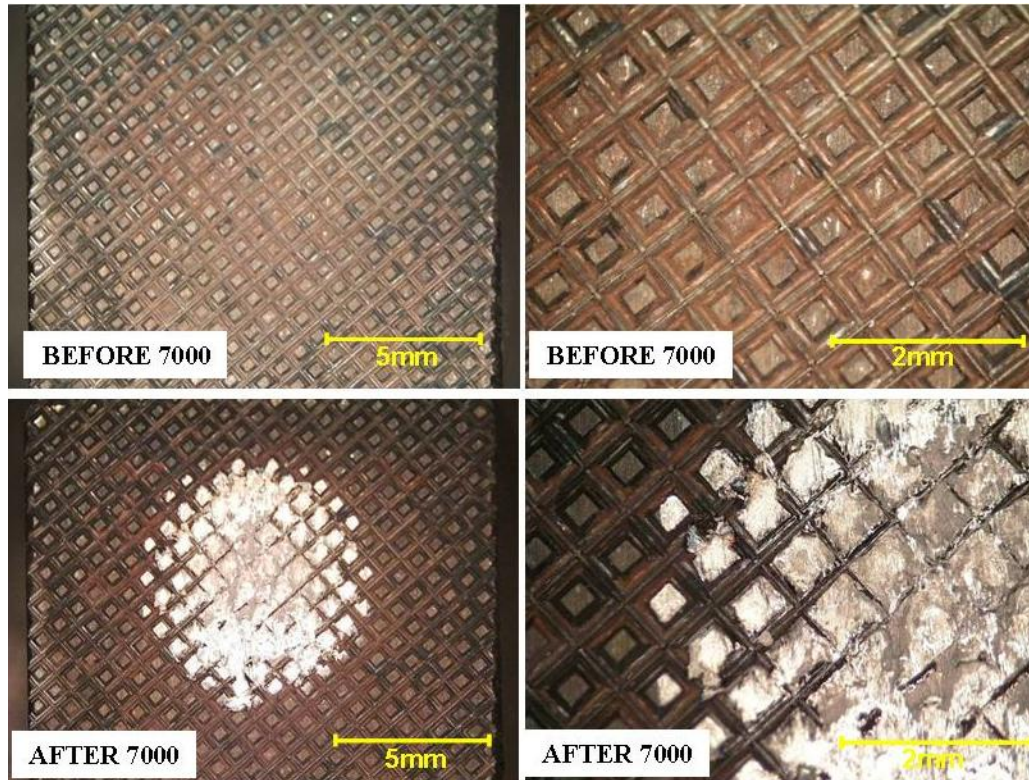


**Figure 23: 350M anvil wear during Ni 625 weld trial 7000**

#### 4.6.2 WROUGHT-TUNGSTEN ANVILS

Two wrought-tungsten alloys were tested. The first Elkon 100W, by CMW, is a popular RSW electrode material. It will be referred to by the manufacturer's name to avoid confusion with the other (non-branded) wrought tungsten alloy. Elkon 100W was ground to size, and a knurl pattern was applied via laser machining. Pictures of this process are included in Figure 24.

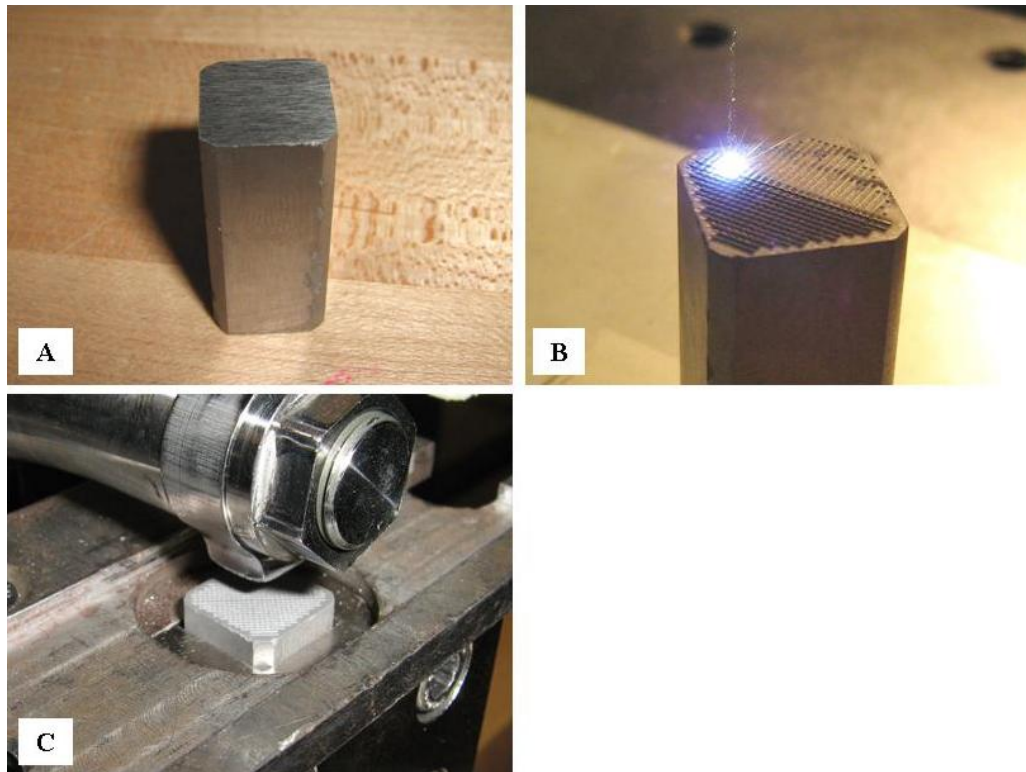


**Figure 24: CMW Elkon 100W Anvil: A - Ground to size; B - Laser-machining knurl pattern; C - Installed in anvil fixture**

The anvil was tested, in conjunction with a W-25Re welding tip, in weld trials 1022 through 1024. The first weld was a SS 410 coupon, and the weld strength approached 770-lbf. When viewing the anvil-side surface of the coupon, pieces of tungsten were visible. Two more weld trials were attempted with Ni 718 and Ni 625, but no welds were formed. Pictures of the anvil-side interfaces are included in Figure 25. The anvil was then observed [Figure 26], and the tungsten that had been removed from the anvil, and stuck to the coupon was visible. The tungsten alloy was breaking apart, and not capable of gripping the coupons as needed.

The tungsten alloy is formed from pressed and sintered powder, followed by rolling and swaging. Although this is a wrought-tungsten by definition, it is clearly a pressed and sintered powdered-metallurgy alloy with less working and swaging than the other wrought-tungsten alloy.

The strength of the bond between the tungsten particles was not sufficient for this application. Because of these results, the Elkon 100W material was not used for any additional weld trials.

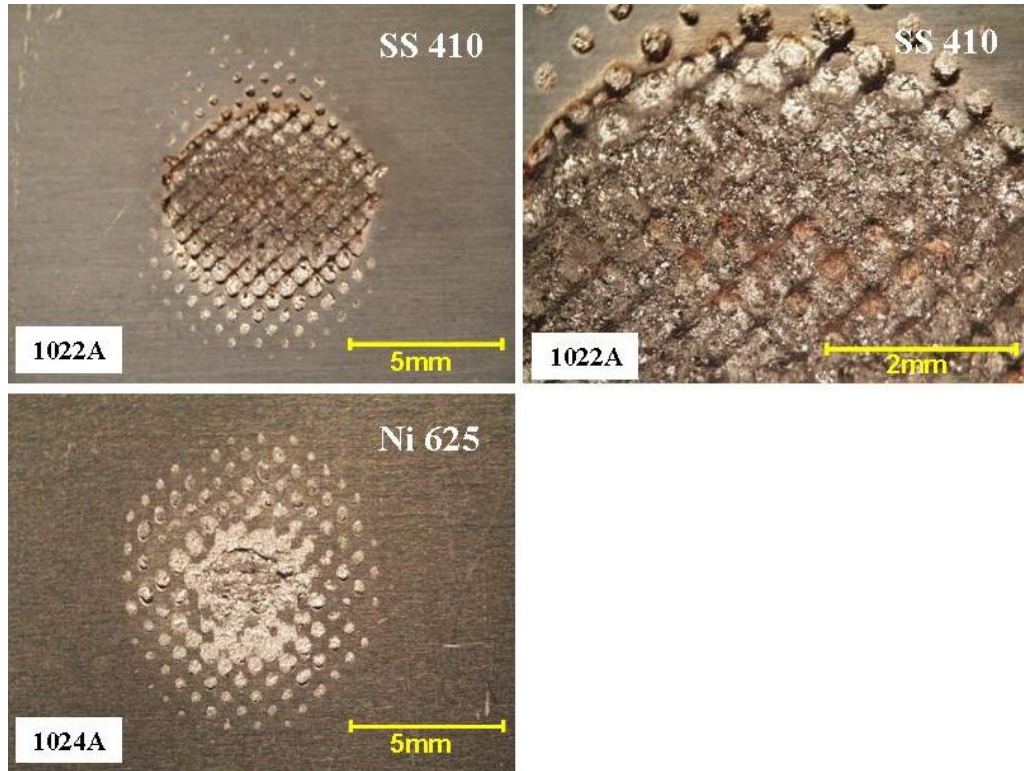


**Figure 25: Stereoscope pictures of the anvil interface from weld trials 1022 and 1024**

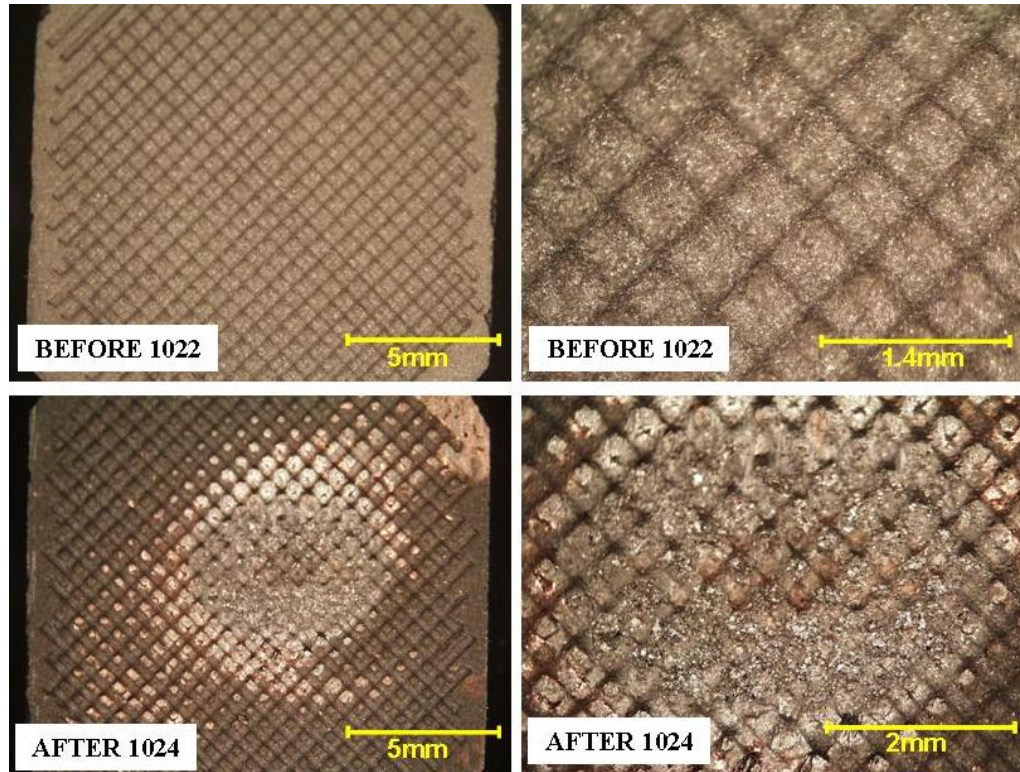


**Figure 26: Stereoscope pictures of CMW Elkon 100W anvil wear**

After the Elkon 100W tungsten was tested, another wrought-tungsten alloy, manufactured for use in high-quality electrical contacts, was obtained. The available quantity of this material was much more limited, so a piece was cut and brazed to a standard AISI M2 anvil. The material was only available in thin cross-sections, about 9-mm wide. The width of the available material did not cover the entire tool face. Two pieces could have been brazed adjacent to each other, but there was concern for the effect of the joint in the center of the anvil face. In other words, it is possible that during the weld trials, material would be forced into the joint, pushing the pieces apart and fracturing the braze joints. A single piece could also be brazed directly on top of the tool face, but again there was concern that this would modify the stress fields within the weld, or even more fundamental, provide less surface area to grip the sample. The solution was to grind

out a slightly oversized notch into the M2 anvil face, and braze it flush within. Microbraz LM (AWS BNi-2) paste was used to join the components. The paste effectively filled the voids at the joints. After brazing, the part was surface-ground so that the face was truly flush. Only the tungsten-insert was laser-machined; the laser parameters used for the tungsten would ruin the tool steel. The texture and braze joint quality was good. The braze joint did not fail during the weld trials. Pictures of the brazing, machining, and finish anvil are shown in Figure 27.

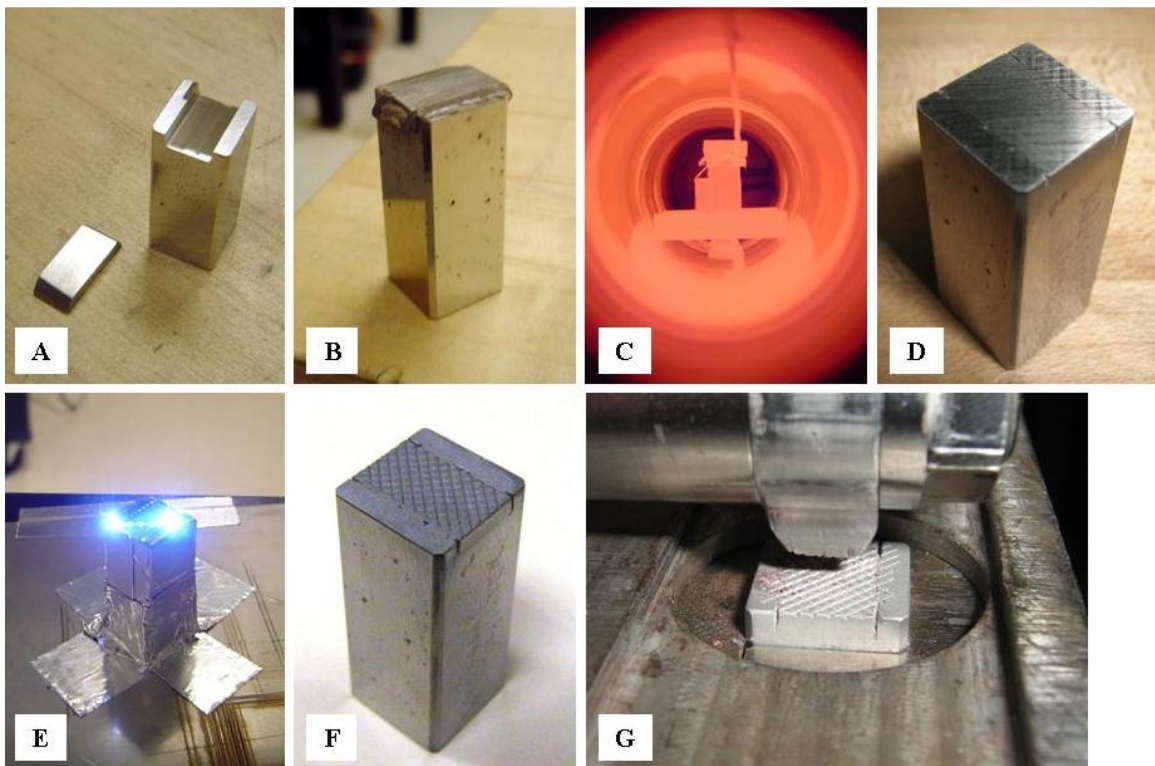


**Figure 27: Wrought-tungsten brazed anvil: A – Ground braze joint in M2 anvil and tungsten insert; B – Assembled components with braze paste; C – Furnace brazing; D – Surface-ground assembly face; E – Laser machining anvil knurl; F – Finished assembly; G – Installed in anvil fixture**

The anvil tested well with all the materials in the preliminary trials. The decision was made to use this anvil with the titanium 6Al-4V alloy for the designed experiments. The anvil

was refaced, and used for trials 3000-3066. The wear of the tooling is summarized by the stereoscope pictures in Figure 28. While the anvil wore significantly during the 67 trials, the wear was gradual and predictable. The wear was more ductile than with the Elkon 100W anvil. Again, pieces of the tungsten broke-off the anvil and stuck to the weld coupons. Stereoscope pictures of several titanium 6Al-4V anvil- side interfaces are shown in Figure 29. Sticking to the anvil was common, but the amount of force required to separate the weld and the anvil was minimal. The difference in performance over the Elkon 100W was most-likely due to an increase in the amount of forging and swaging.

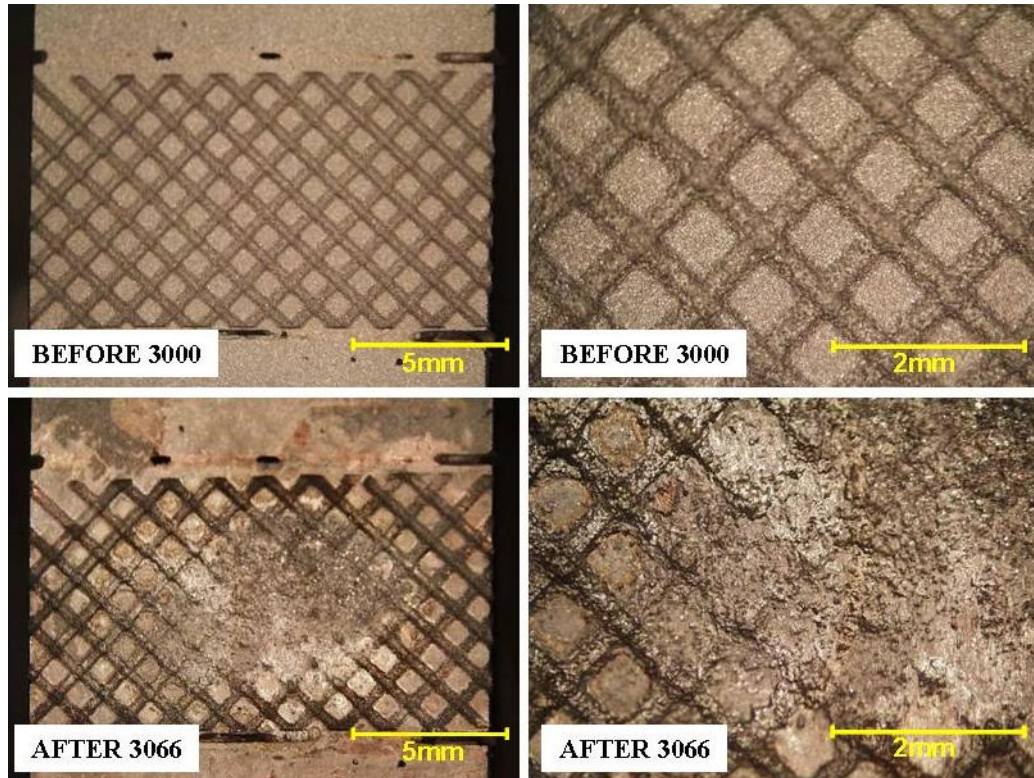


**Figure 28: Wrought-tungsten anvil wear during Ti 6-4 weld trials 3000-3066**

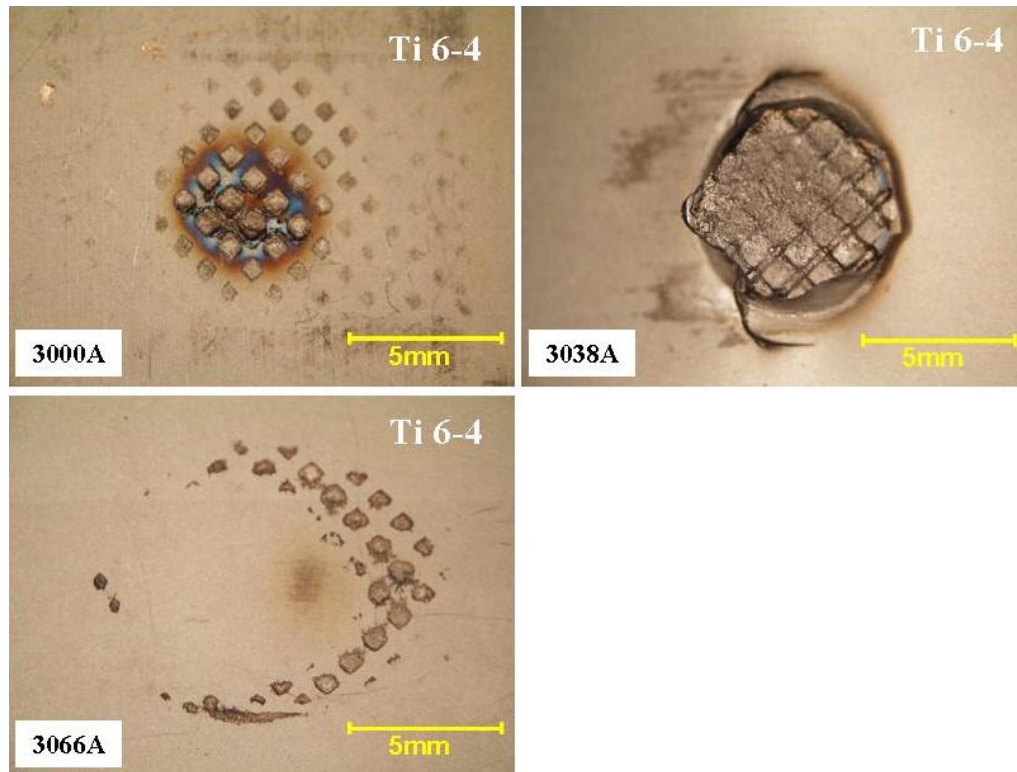


**Figure 29: Titanium 6Al-4V weld anvil interface pictures from weld trials 3000, 3038, and 3066**

#### 4.6.3 TUNGSTEN-25% RHENIUM ANVIL

Due to cost and availability, a piece of W-25%Re was brazed to a standard M2 anvil with Incusil ABA braze foil. A knurl pattern was applied with a laser machining system. A crack that traveled through the center of the W-25Re piece was noticed. It is believed to be a result of a coefficient of thermal expansion (CTE) mismatch between the tungsten and the tool steel following the braze cycle. Pictures of the W-25Re anvil manufacture, including brazing and laser-machining, as well as the CTE crack, are in Figure 30.

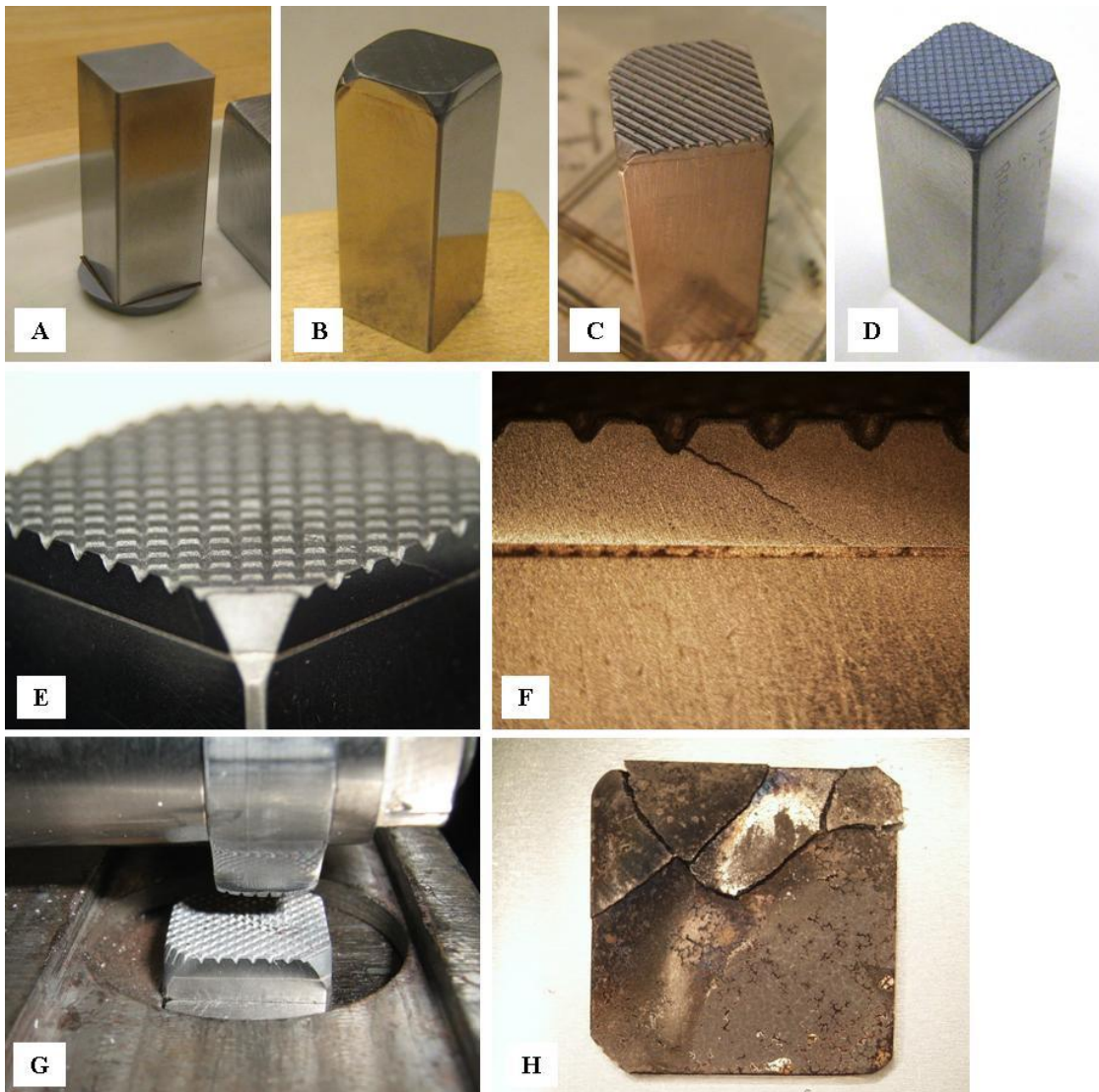


**Figure 30: Brazed W-25Re Anvil: A – Brazed Assembly; B – Braze Joints ground; C – Laser-machined knurl, first direction; D – Finished anvil; E – Knurl profile; F – CTE mismatch fracture; G – Installed in anvil fixture; H – Fractured braze joint, W-side**

Preliminary weld trials with a variety of materials were promising. W-25Re tools were used with the SS 304 designed experiments. The tool wear was documented incrementally during the 86 weld trials. The anvil fractured along the CTE crack during the trials, and was re-brazed to allow the trials to be continued with the same surface. The amount of wear was greater than that observed with the wrought-tungsten anvil, but this anvil was subject to more weld cycles and a different material. The anvil wear was reported as being more ductile than that experienced with the wrought-tungsten, but not as ductile as the W-La. Pictures of the anvil wear during the weld trials are shown in Figure 31.



**Figure 31: W-25Re anvil wear during weld trials 4000-4085, anvil surface fractured and re-brazed during trials**

Many of the SS 304 weld trials did stick to the anvil, but they were removed from the anvil without excessive force. Stereoscope pictures of several SS 304 weld anvil interfaces are in Figure 32 . Tungsten was found deposited on a majority of the anvil interfaces. It appears that the bond between the tungsten and the 304 SS was greater than the bond holding the tungsten to itself.

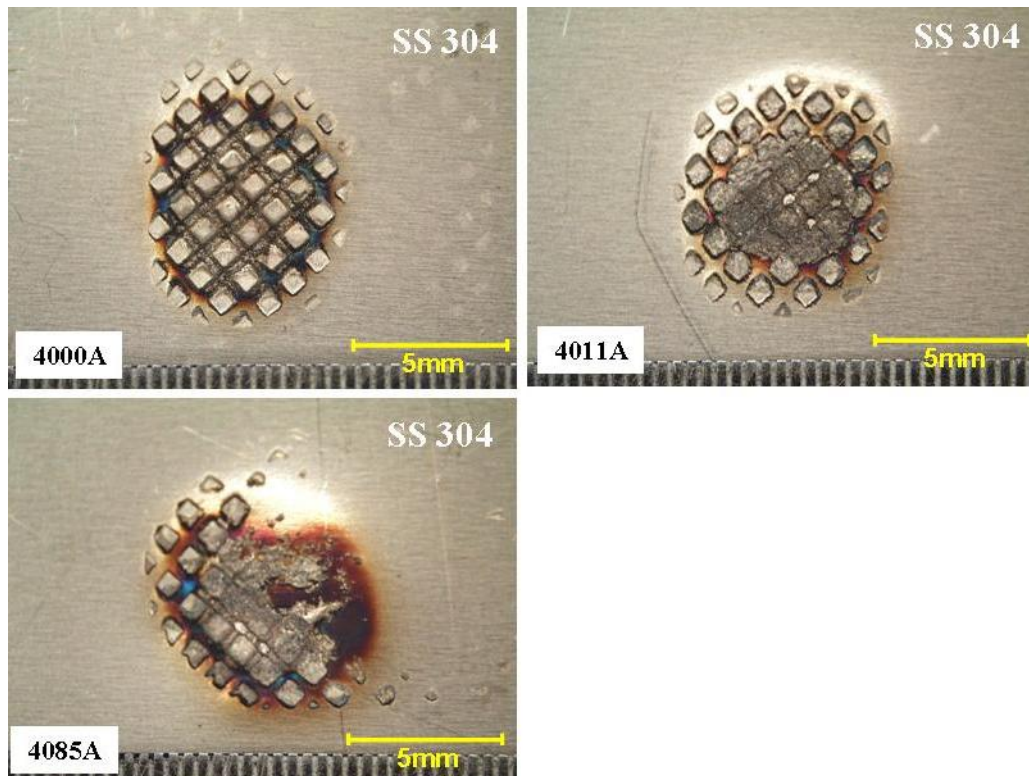
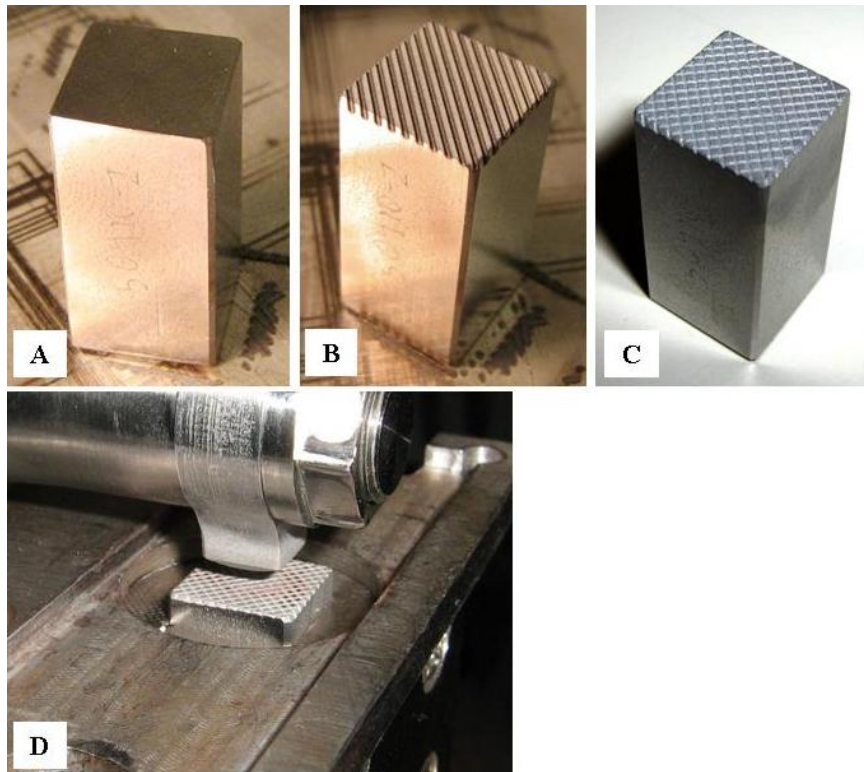


Figure 32: SS 304 weld trial 4000, 4011, and 4085 anvil interface pictures

#### 4.6.4 TUNGSTEN-LANTHANUM ANVIL

A solid tungsten-lanthanum anvil was wire-EDM to the required dimensions. The faces were surface-ground and a laser-machined texture applied. Pictures of the anvil are shown in Figure 33



**Figure 33: Solid W-La anvil with laser-machined texture: A – Surface-ground face before laser-machining; B – First direction laser-machining; C – Second direction laser-machining; D – Installed in anvil fixture**

After over 100 SS 410 weld trials, the anvil performed very well. Stereoscope pictures of the anvil face before trial 5000 and after 5101 are shown in Figure 34. Even after 100 welds with the ferritic stainless steel, the knurl pattern is still clearly visible. Compared with some of the

other tungsten-alloy anvils, the wear is more ductile, and the tungsten did not disintegrate into small pieces. Pictures of the corresponding coupon interfaces from these trials are included in Figure 35. The anvil is worn, and the anvil impression in trial 5101 is not as sharp as that in trial 5000. Trial 5101 was made with more than twice the energy (2000-J) as trial 5000. The heat marks surrounding the weld from trial 5101 are more significant than those from trial 5000. Trial 5000 has a weld strength of just over 600-lbf, while the strength from trials similar to 5101 is near 780-lbf.. The SS 410 trials did not stick to the anvil.

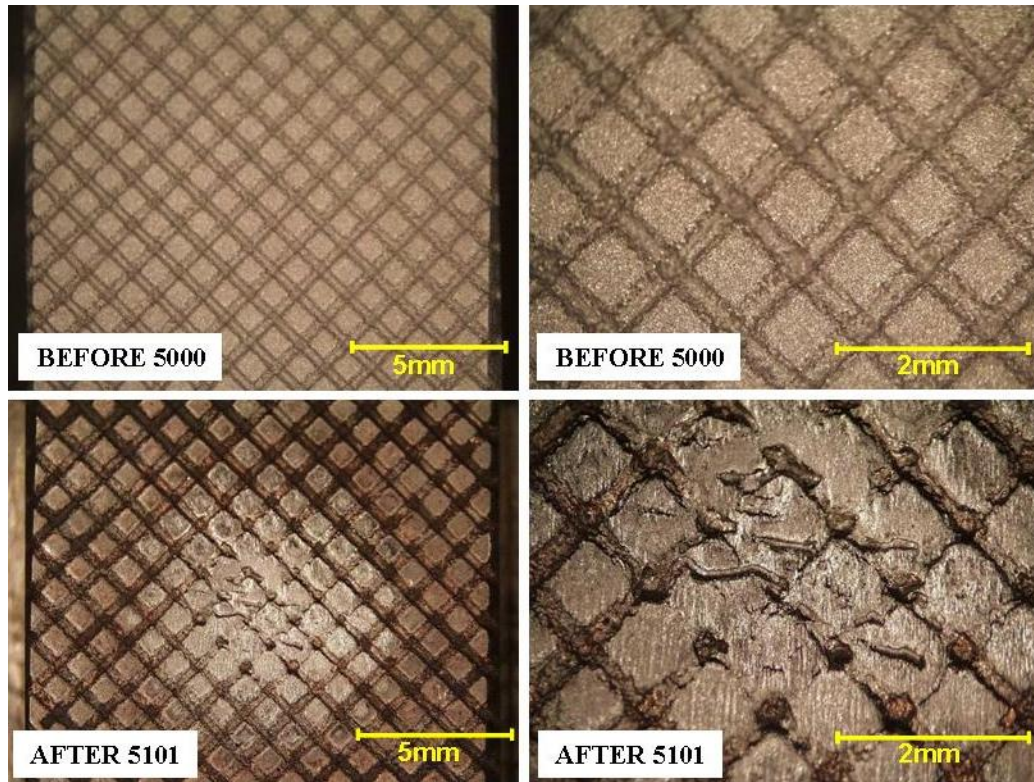


**Figure 34: Stereoscope pictures of W-La anvil face during SS 410 weld trials 5000-5101**

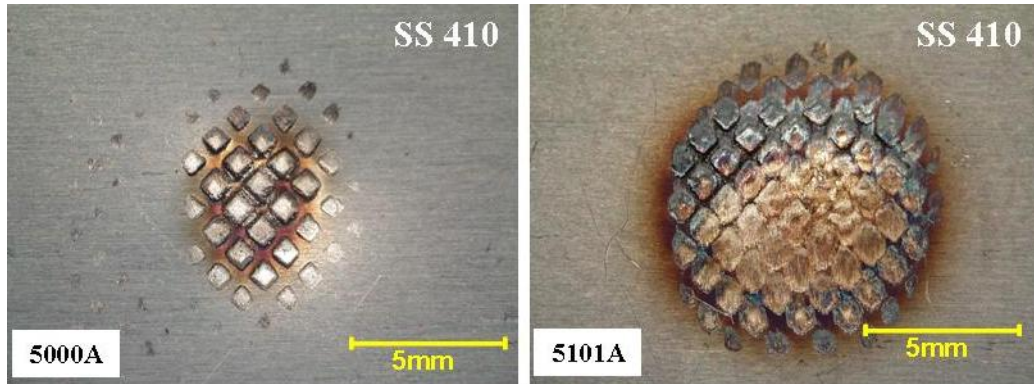


**Figure 35: Anvil-side interfaces of SS 410 weld trials 5000 and 5101**

The W-La anvil performed very well, possibly the best in this investigation. It was only evaluated with the 410 SS, so it is hard to predict whether it would out-perform the other tungsten alloys with the other weld materials. The solid anvil worked much better than the brazed anvils, because of some of the problems experienced with the braze joints in other configurations. The exact composition and processing methods are proprietary, but it appears to have improved ductility due to the alloying elements and increased forging and swaging.

#### 4.6.5 MOLYBDENUM TZM ANVIL

A molybdenum TZM anvil wear-surface was brazed to a standard AISI M2 anvil using 0.002-in thick Metglas MBF 20 (AWS BNi-2) brazing foil. The braze joint did not fail during the limited number of weld trials. Pictures of the brazing and laser machining of the TZM anvil are included in Figure 36.

It was used for C.P. Ti weld trials 1099 and 1100, as well as SS 304 trials 4086 through 4091. The welds had comparable strengths with welds made with other anvils at similar

parameters. No sticking to the anvil was reported for both C.P. Ti and SS 304. Figure 37 has stereoscope pictures of the anvil face before and after the weld trials.

The anvil was used for a total of 8 weld trials, and has wear similar to the W-La anvil after more than 100 weld trials with harder material. Its wear was similar to the W-La anvil in that it was more ductile than many of the pressed and sintered tungsten alloy anvils. A Molybdenum TZM tip had very poor performance and braze joint problems. That, combined with the relatively poor performance when compared with W-La, prevented the TZM anvil from being investigated further.

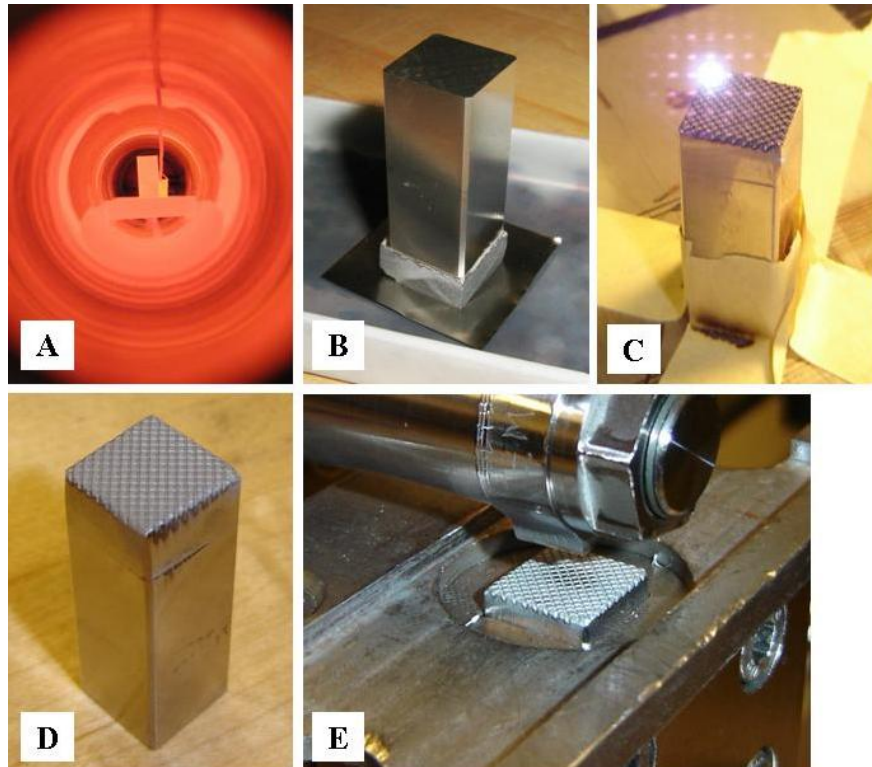


**Figure 36: Molybdenum TZM anvil build: A – Furnace brazing; B – Brazed assembly; C – Laser-machining knurl; D – Finished anvil assembly; E – Installed in anvil fixture**

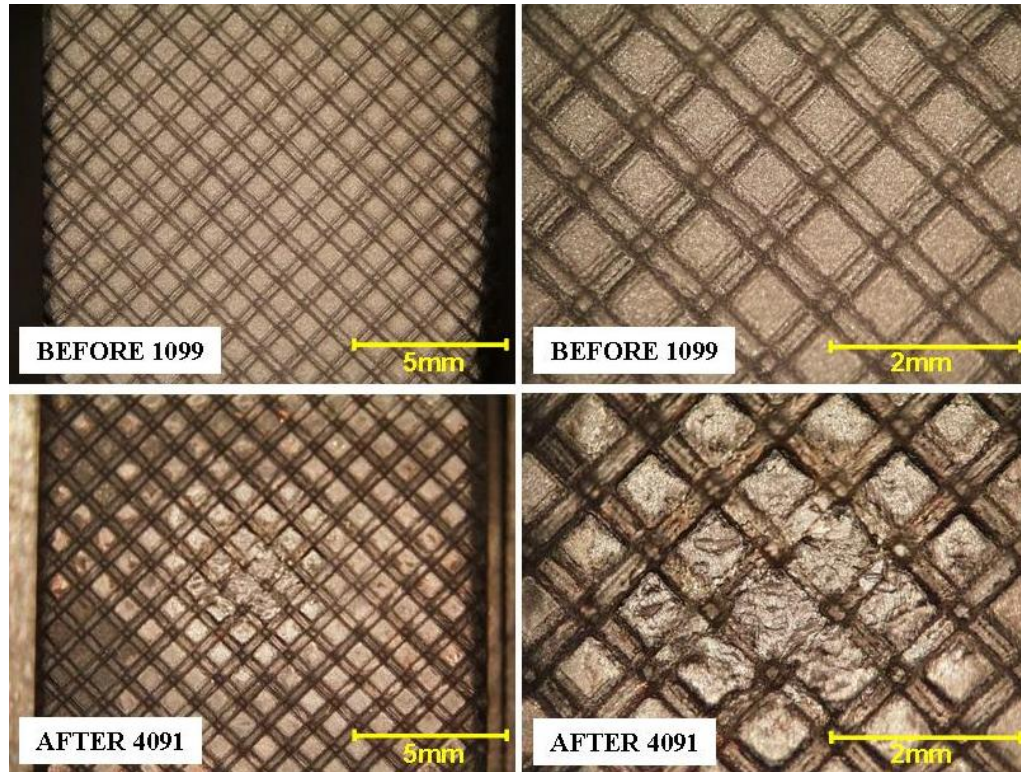


**Figure 37: TQM anvil wear during C.P. Ti welds 1099-1100 and SS 304 welds 4086-4091**

#### 4.6.6 TOOL WEAR SUMMARY

The wear of the anvil surfaces experienced during the weld trials has been reviewed. It is difficult to compare the performance of the tools because of the different materials they were used to weld, the different welding parameters used during the trials, and an inconsistent number of weld cycles applied to each tool. A full-matrix comparison of each tool material with each alloy under the same conditions and cycles was not feasible. However, a general understanding of the performance of each tool material has been established.

The tool steels, particularly 350M, performed well with the lower-strength metals. In addition, a consistent knurl pattern could be machined. The Molybdenum TQM anvil fared well,

but a Molybdenum TZM tip failed after several weld cycles. The TZM anvil had a more ductile wear pattern than the tungsten-alloys. The tungsten alloys performed to varied degrees. The wrought-tungsten and W-25Re wore heavily during the trials, but the wear was gradual and consistent. Elkon 100W was too brittle for use as ultrasonic tooling. The wrought-tungsten and the W-25Re wore by fracturing-off small particles, which could be seen bonded to the weld coupon anvil interfaces. The W-La seemed to perform even better, with a more ductile wear than the other tungsten alloys. Table 8 is an objective summary of the tool performance. Since the tool materials were evaluated with different materials, different welding conditions, and different total cycles, it is difficult to draw these conclusions with a high level of confidence. It is important to keep in mind that many of the tool materials originated from FSW technologies, where the tool is expected to wear during the weld.

M2		350M		Elkon 100W		Wrought-W		W-25Re		W-La		TZM	
Al 7075	good	Al 7075	good	SS 410	fair	C.P. Ti	fair	SS 304	fair	SS 410	good	C.P. Ti	fair
SS 304	bad	C.P. Ti	good	Ni 718	poor	Ti 6-4	fair	SS 410	fair			SS 304	poor
C.P. Ti	fair	Ni 625	poor	Ni 625	poor	SS 304	fair						
Ti 6-4	fair	Ni 718	bad			SS 410	fair						
Ni 625	bad	SS 304	poor			Ni 718	poor						
		SS 410	poor			Ni 625	poor						
		Ti 6-4	bad										

**Table 8: Summary of Tool Material Performance**

It may be possible to use a non-knurled tool in situations where high clamping forces are possible. Then, the wear could be better controlled and the tip could be periodically reground as is common in the RSW industry. In addition, as the tungsten-based materials wore, the surfaces had a distinctly rough texture, which may increased the efficiency of these weld tools.

Many of the tools wore excessively during the trials, but did not prevent continued, high-strength welds. Braze joint failure was also problematic, and created many setbacks. Braze joints should be avoided in close-proximity to the interface if possible. Many of the welds were only possible at low clamping forces due to equipment limitations. Low clamping force, especially with high energy, accelerates the tool wear by preventing adequate friction between the tool and the work. It is believed that higher-powered ultrasonic welding equipment may be able to produce these welds at higher clamping forces, which should significantly decrease the wear experienced during these weld trials.

## CHAPTER 5

### WELD TRIALS

In this chapter, mechanical testing of welds and base materials are evaluated. A standard coupon size and preparation method was established. Hardness testing of both weld materials and tool materials were performed. Preliminary weld trials established welding parameters, promising tool materials and development procedures. Welds quality was measured by tensile testing. A range of parameters was established for the highest-strength welds. Using the results of these trials, designed experiments were developed and evaluated using MiniTab 15 software.

Much of the mechanical (shear-tensile) testing results are recorded in peak force (lbf), and have not been converted to stress values (psi). Calculating the weld stress requires dividing the peak force by the measured weld area. While this is generally an appreciated practice because it normalizes the weld strength data, the experiments in this study had mixed failure modes and relatively complicated fracture areas. Measuring the fracture areas also introduces an entirely new source of error. Therefore, it was determined to report the weld strengths as peak force instead of stress.

#### 5.1 COUPON LENGTH

As previously discussed, the dimensions of the coupon size significantly affect the weld quality. The influence of the coupon size on weld tensile strength was verified experimentally.

Figure 39 is a plot of 1-mm thick, 25.4-mm deep aluminum 1100 H-18 spot weld strengths and power levels for increasing coupon lengths at the same weld parameters. The experiment was non-randomized using 25.4-mm width lap-shear samples with a 25.4-mm overlap. Figure 38-A illustrates the various-length coupon sizes, and Figure 38-B is a diagram illustrating both the coupon length and the coupon extension. Coupon lengths were varied for this experiment, and later converted to coupon extension lengths to allow a direct comparison with similar experiments by deVries [7]. Welds were created with a 2.5-kW AmTech 20-KHz lateral-drive ultrasonic welder fitted with a solid-sonotrode featuring a flat, “FWF” heavy-knurl weld tip. The data points in the plot are the average of 5 or more welds at the same coupon extension length. Standard deviation bars have been added to these data points. Because of the limited number of data points, trends cannot be developed.

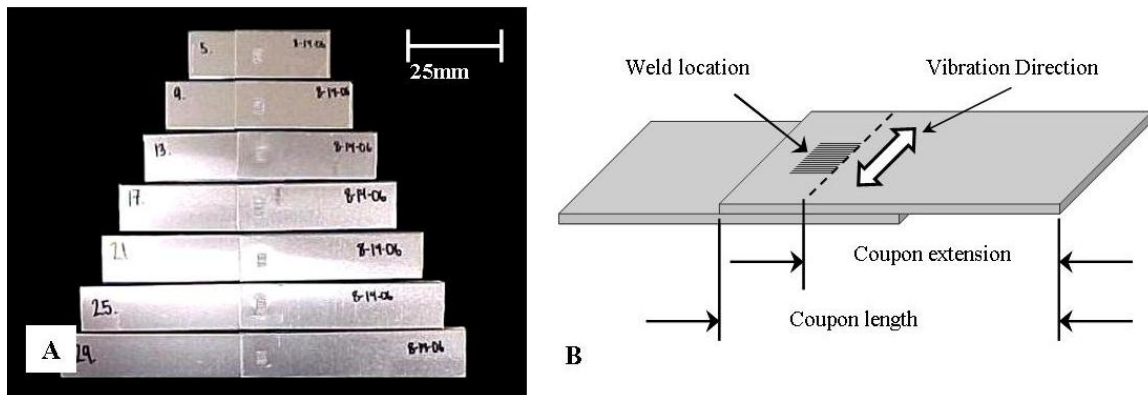


**Figure 38: A – Welded lap-shear coupons of different lengths; B – Coupon length/ extension diagram**

The results are in agreement with deVries [7], even though he used a 2.5-kW Sonobond wedge-reed system and 1-mm thick, 12.7-mm depth aluminum 6061 T-6. It is believed that if smaller increments of extension lengths were experimented with, the “no weld” locations that

deVries determined would also be recorded. For this reason, a trend line has not been added to Figure 39. It can be seen that for the 50.4-mm coupon lengths (outlined box in plot), high-strength welds were created with moderate power levels. This coupon length also minimizes the amount of material consumed during the course of the weld trials. It can be concluded that the coupon extension length affects the weld strength.

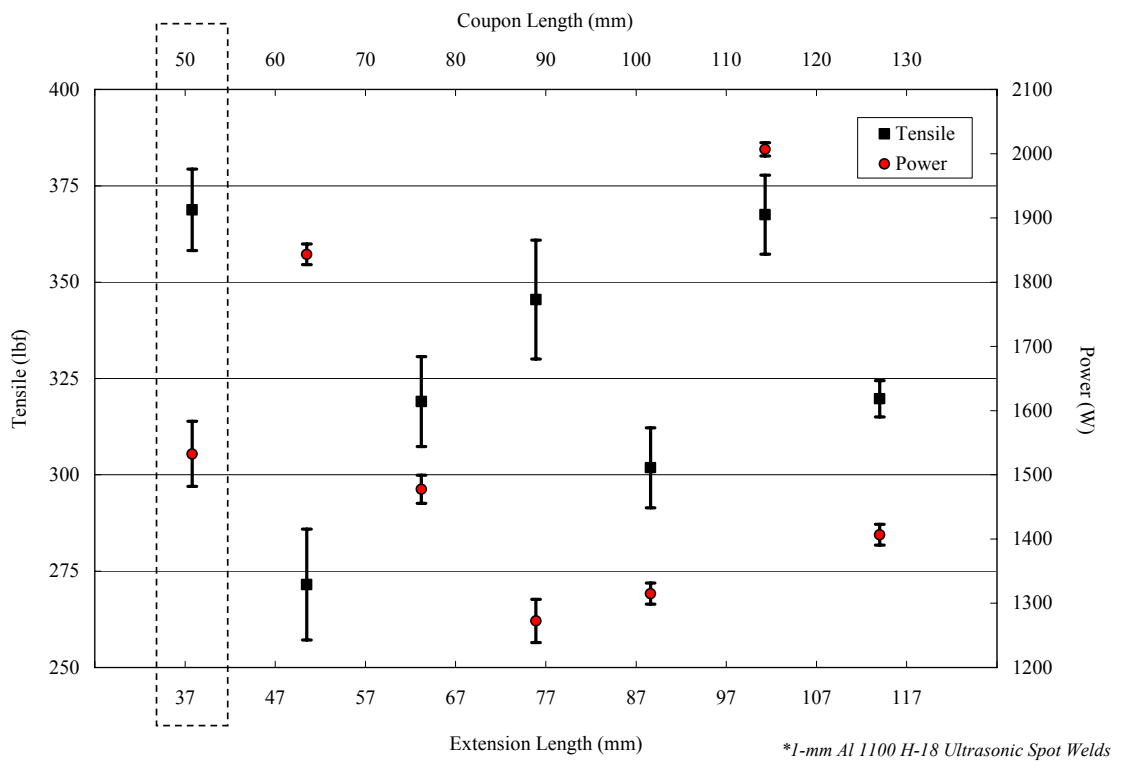


**Figure 39: Strength vs. coupon length**

## 5.2 HARDNESS TESTING

Hardness is, in most simplistic terms, is a materials resistance to deformation. While hardness is not a fundamental material property, it can be related to the ultimate tensile strength of a material. A Vicker's microhardness tester was used because it has a very wide scale, can be used on finished parts without concern for damage, is considered one of the few universal hardness testing methods, and has good accuracy and repeatability.

It is suggest that the ultrasonic weldability is related to the hardness of a material [5]. Figure 40 is a plot of the minimum energy level required to ultrasonically weld different hardness and thickness materials. The chart was developed with lower-powered equipment than that which is available today and it is possible that the higher-powered equipment is capable of producing ultrasonic welds with lower energy levels.

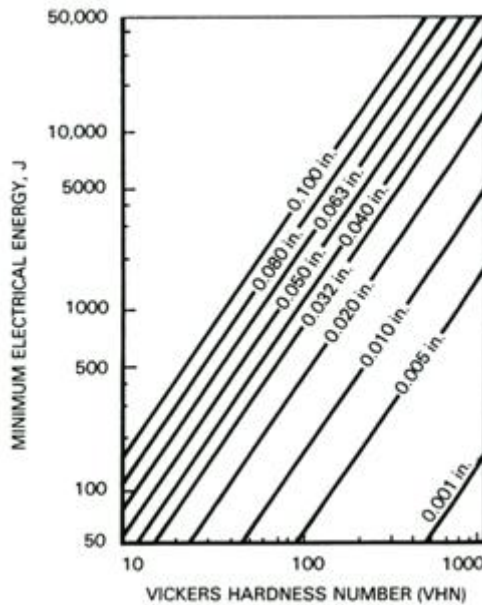


**Figure 40: Minimum energy required for ultrasonic welding [5]**

Microhardness testing of the welding materials and the tooling materials (prior to brazing cycles) was conducted. The results are organized in Figure 41. Each value shown is the average of 5 indents at different locations. Standard deviation bars have been omitted because of low deviations.

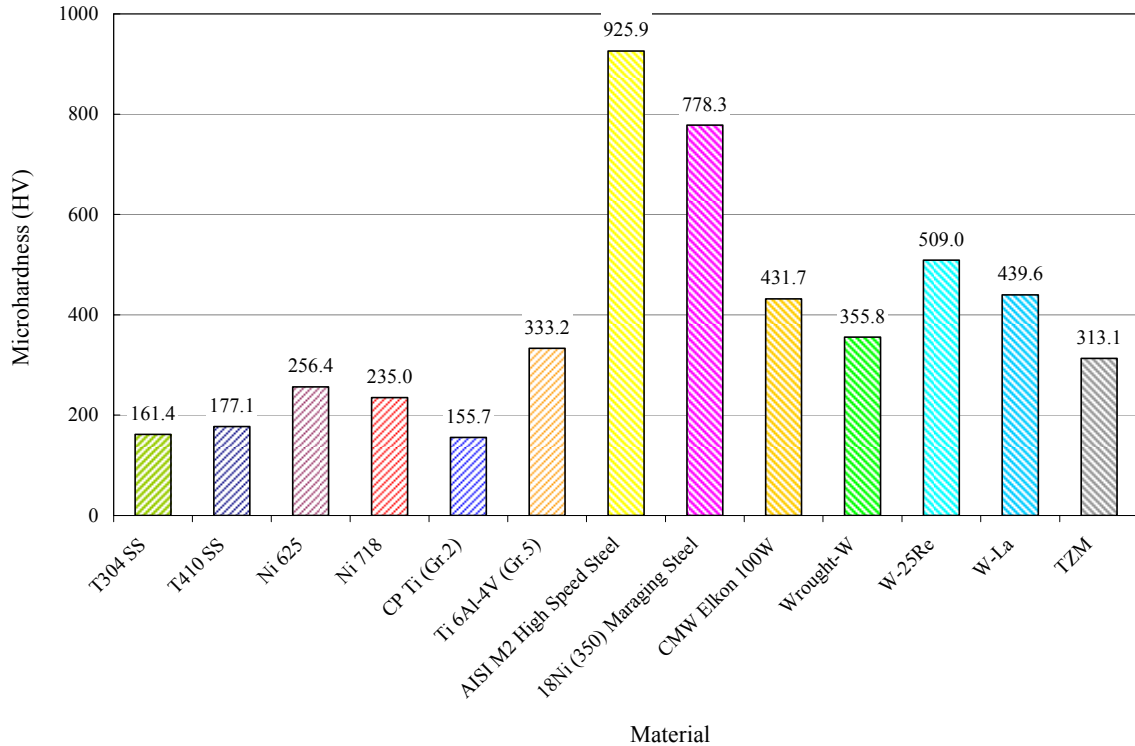


**Figure 41: Average Microhardness Measurements of Materials using a LECO M-400-H1 Hardness Testing Machine**

Heat-treated tool steels have significantly higher hardness than any of the other materials. Following a furnace brazing cycle, the hardness would decrease by 50 to 75%. The tungsten-based tool materials all had hardness values between 350 and 500 Vickers, which is still higher than any of the welding materials. The molybdenum alloy, TZM, had a slightly lower hardness.

The majority of the tools were much harder than the tool steels they were welded with, excluding the titanium 6Al-4V trials with the wrought-tungsten tooling.

The materials for the weld trials were purchased in the annealed condition when available. The commercially-pure titanium was the most ductile with a 155 Vickers hardness measured. The T-304 and T-410 stainless steels measured slightly higher at 160 and 177, respectively. Nickel alloy 625 measured 256 Vickers, while the nickel alloy 718 measured about 20-HV lower. The titanium 6Al-4V was 30 to 50% higher in hardness than all other welding alloys. In reference to the chart in Figure 40, it can be said that the weldability of these materials can be organized according to hardness. For the materials in this investigation, the weldability (based on Figure 40) is as follows: C.P. Ti (most weldable), 304 S.S., 410 S.S., Ni 718, Ni 625, and Ti 6-4 (least weldable). During the welding trials in this investigation, it will be shown that this is not exactly true.

The relationship of the required tooling hardness to the welding material hardness is not well defined.

### 5.3 EXPERIMENT DESIGN

In welding more common ultrasonic materials, such as thin gauge copper and aluminum, at constant clamping force, an energy curve can be developed. Starting at low energy levels, welds made at increasing energy levels will tend to show an increase in strength up to a point, at which the strength will level-off. This is commonly where the weld strength exceeds the base material strength and a small increase in energy yields no net gain in weld strength. Further increasing the welding energy can eventually lead to an overwelding condition, where the tip excessively drives into the material or otherwise causes a decrease in strength. An example of this tendency is shown in Figure 42. This investigation will attempt to generate energy curves in order

to best describe the parameters that generate the optimal weld strengths with the advanced materials.

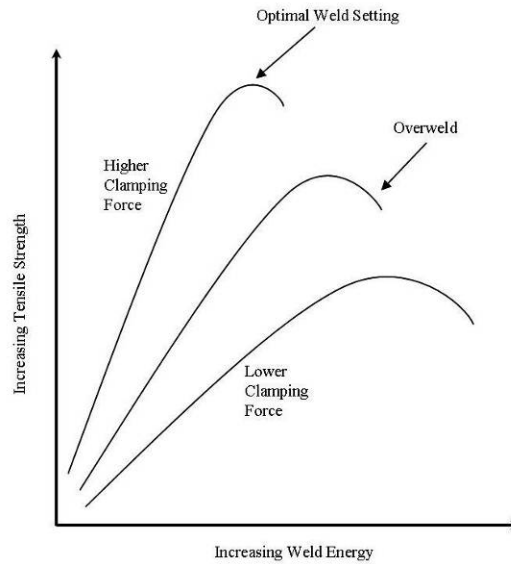


**Figure 42: Ultrasonic Energy Curves**

The preliminary trials did not follow a designed screening experiment. Different alloys were welded varying the energy and the pressure. Different tools were simultaneously evaluated. Some of the tools wore rapidly or even fractured. In addition, braze joints failed on some of the tools. Welds made with different tools, even with nearly identical designs, had significantly different qualities. Welds were evaluated by tensile testing. Using the results from a limited number of preliminary trials, contour plots of the variables energy and pressure were established. Because of the simultaneous evaluation of tool materials, design, and construction, the contour plots for each material did not provide clear parameter windows. Nevertheless, parameter windows were selected using these contour plots to define designed experimentation.

In the preliminary trials, it appeared that the nickel-base alloys wore the tungsten-based tooling and readily bonded to the tool steel tooling. A decision was made to limit the trials of the nickel-base alloys, and focus the experimental efforts on the titanium and stainless-steel alloys. A limited number of nickel-base welds were still made, tensile tested, cross-sectioned, and studied with the SEM.

Minitab software will be used to design the experiment and interpret results. Due to the strength and thickness of the materials, it was determined that the maximum amplitude produces the highest possible weld strengths. Using the results of the initial experiments, a central composite experiment was designed for each material. The run order was randomized. The experiment included three replicates, blocked by replicate, and two variables (energy and pressure). At the end of a block or a short series of weld trials, the tools were removed and pictures were taken with a stereoscope to allow observation of the wear. After taking pictures, the tooling was re-installed. At the end of each replicate, the samples were tensile tested. These optimization experiments help define the best weld parameters, and the nature of the curvature.

The original intent was to make three replicates at each setting, however; this was not always possible. Several times, after the first replicate was completed and the welds were tensile tested, it became evident that the parameter window did not contain the maximum strength welds. Therefore, the experiment was re-designed using a larger parameter window. During the course of some of the trials, the tool either had significant wear, fractured, had material adhered to tip, or the braze joint failed. In order to continue the experiment, the tool was either repaired or replaced. In any case, the tool would have to be modified, altering the results. In addition, when the tooling was removed for pictures, the alignment was modified, again with some influence on the weld quality. From the tooling standpoint alone, it is clear the results may have significant scatter and poor repeatability.

The equipment also influenced the quality of the results. Often, a “cycle alarm” occurred following the weld cycle. Cycle alarms occur after a weld does not fall within predetermined quality limits. This was most common for power, although a time alarm can also occur. System Protection Monitoring is a safety feature in which ultrasonics are stopped when the power supply is overloaded. The power supply had a maximum rating of 3600-W, therefore, welds requiring more power would activate the cycle alarm. A weld overload is the point or limit at which the amount of power in watts, required to keep the ultrasonic stack in motion, exceeds the available power from the power supply. Many of the trials in this experiment were at or near the peak power level of the equipment.

It was known from the beginning of this experiment that welding these alloys may be at the edge of or beyond the equipment’s capabilities. In fact, personal experience suggests that high amplitude (100%), high clamping force (500-lbf), and moderate energy (500-J) is required for challenging applications. When applying these parameters, a weld overload or similar fault occurs, stopping the weld cycle short. Initially, when a weld cycle begins, the interface between the coupons is clean and relatively smooth. As the cycle continues, and the weld begins to form, a significant amount of resistance to the motion of the ultrasonic stack is generated. Sometimes the amount of resistance during the weld exceeds the equipment power level, and the weld cycle stops prematurely. The full data set, by trial number, is included in Appendix #. Columns are included for a number of variables, responses, and comments. There are in fact two columns for energy. The first is labeled “Input Energy”, and the second “Actual Energy.” For some of the trials, these values are significantly different. This is more common for higher clamping forces. At lower clamping forces there is less resistance on the power supply, and higher energy levels are achievable. The drawback with low clamping force is that the tip may slip at the interface with the top coupon. This generates significant heat and expedites tool wear. Low clamping forces appear to generate high weld strengths in some of the trials. It is proposed that the

excessive heat generation lowered the yield stresses, allowing the formation of a strong bond. A higher-powered ultrasonic welder would be necessary to weld these alloys at higher clamping forces. In fact, clamping forces above the equipment limitations (i.e. greater than 570-lbf) may be necessary to achieve the local deformation required to weld thicker, high-strength materials.

The results of the weld trials are provided in plots of tensile strength vs. energy, for a number of clamping forces. Problems with tooling wear and equipment limitations limit the statistical quality of the results. Detailed statistical analysis will not be provided. A basic regression analysis for each material is provided in APPENDIX D. The regression equations were used to develop trendlines and were included with the original data points for comparison. Then, the regression trendlines for each material were applied to a single plot for a direct comparison of the welding characteristics of each material. Welds of the nickel-base alloys were much more limited and regression analysis was not possible.

#### 5.4 TYPE 304 STAINLESS STEEL

Preliminary trials with T-304 stainless steel found that AISI M2 and 18Ni Maraging Steel tooling was not acceptable. The stainless steel readily bonded to the tip and the anvil. The weld specimen needed to be pried apart from the tooling, damaging both the weld and the tooling. Tungsten-based tools discouraged adhesion and had much-improved wear properties. Several different tungsten-based tools were tested in the preliminary trials with all the alloys. It was difficult to differentiate the performance of the different tungsten alloys, especially because the shape and mass of each tool varied slightly. It was decided to select a separate tungsten-based alloy for welding each alloy that so required. W-25Re tips and anvils were used with the T-304 weld trials.

Preliminary weld trials suggested an energy range of 350 to 650-J and a pressure range of 20 to 80-psi for further study. An experiment was designed, and during the course of the first set of replicates, most of the weld cycles overloaded the system. The pressure was then lowered to 20 to 40-psi, and energy modified to 450 to 650-J. A single replicate experiment was evaluated with these new settings, and less weld overload situations occurred. The weld strengths at this set of parameters, along with the strengths recorded from the first set of parameters, showed little evidence of curvature. Next, the effect of very high and low energy at the same 20 to 40-psi window was studied. Maximum weld strengths (up to 700-lbf peak tensile) were measured at 16 to 20-psi, and 1000 to 1200-J energy. This was not expected. During these trials, the anvil fractured along a crack generated following the brazing cycle, most likely due to a strong CTE mismatch. It was repaired, and welding continued. Also, overwelding led to multiple tip failures. When welding at higher energy, the sample was over-welded, and the weld button was left deposited on the tip. Higher pressures simply overloaded the system, and could not be evaluated. Due to the inconsistencies in the tooling used, and the different DOE parameters, the results have significant scatter. Figure 43 is a plot of the tensile force vs. energy for different clamping forces. Figure 44 is the same plot, but with regression trendlines added. Clamping force and energy both effect the tensile strength, but the scatter observed limits further analysis.

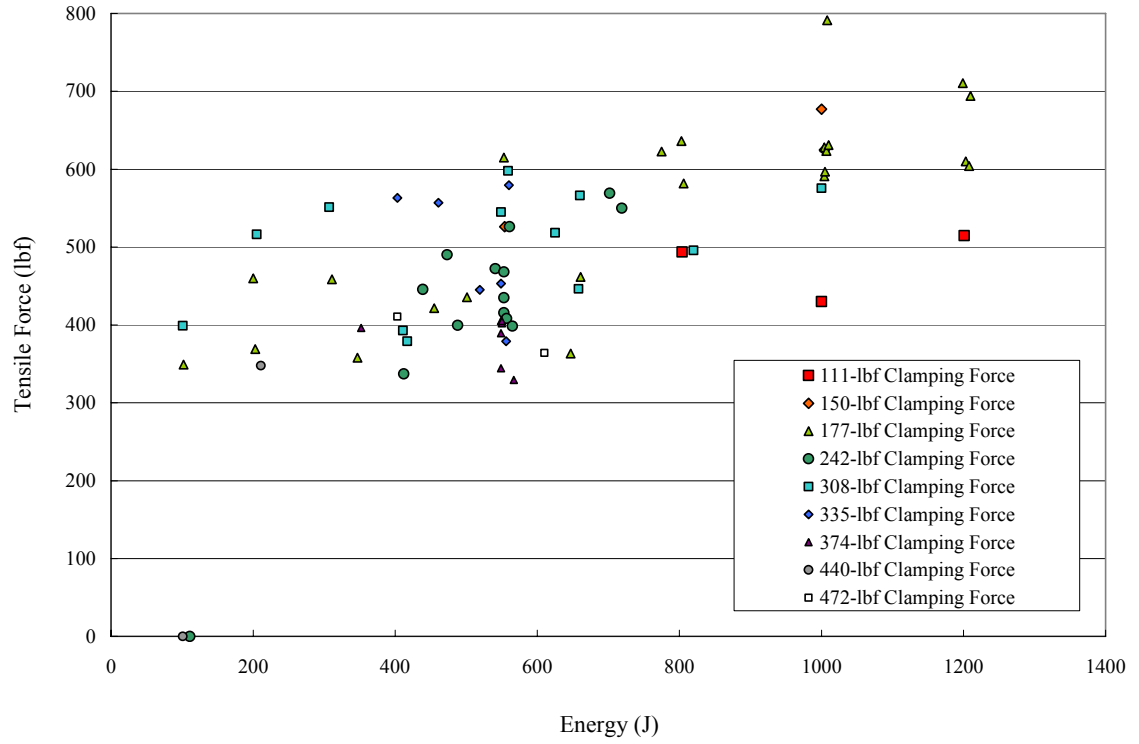


**Figure 43: Scatter plot of Tensile Force vs. Energy, Clamping Force for SS 304**

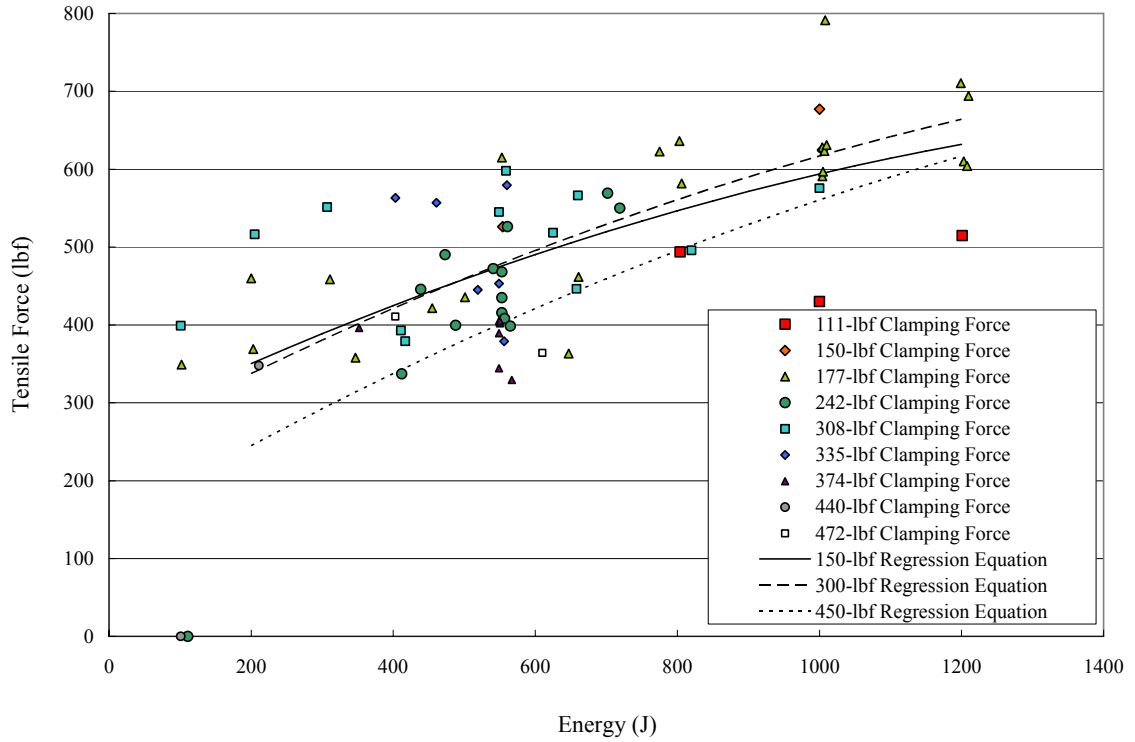


**Figure 44: Scatter plot of Tensile Force vs. Energy, Clamping Force for SS 304 with Regression Trendlines**

## 5.5 TYPE 410 STAINLESS STEEL

The preliminary weld trials suggested a range of 350 to 650-J and 30 to 70-psi for the designed experiments. W-La tooling was used for the T-410 stainless steel trials. Based on the results from the T-304 trials, it was decided to try a few more parameters before starting a designed experiment. Several welds at 1000-J and 10 to 60-psi were tested, and again indicated high strengths at low clamping force and high energy. After a weld was made with the clamping force lowered to 110-lbf, the tip braze joint failed. Pictures of this tip failure are shown in Figure 19. The braze joint failure is also evident on the power vs. time plot of Figure 45. The first 0.5-sec of the weld cycle is as normal, but a dramatic drop in resistance occurs, and the amount of

power required to continue the weld cycle dropped from 2800 to 700-W, indicating the failure of the braze joint. This was not immediately obvious because the braze resolidified at the end of the weld cycle. The next few cycles at similar setting achieved no or very low strengths due to the compromised integrity of the braze joint. It later broke off completely. The tip was then rotated, and the other (good) end was aligned for continued weld trials. During the next few weld cycles, no welds were created. It was determined that the missing piece of tungsten on the opposite end of the tip made the system unbalanced; 70% of the systems total power was required to fire the ultrasonics in free air, leaving little power for the weld cycle itself. The tip was originally brazed with Incusil ABA braze foil. Therefore, a higher-temperature, higher-strength braze alloy, BNi-9 was used to repair the tip.

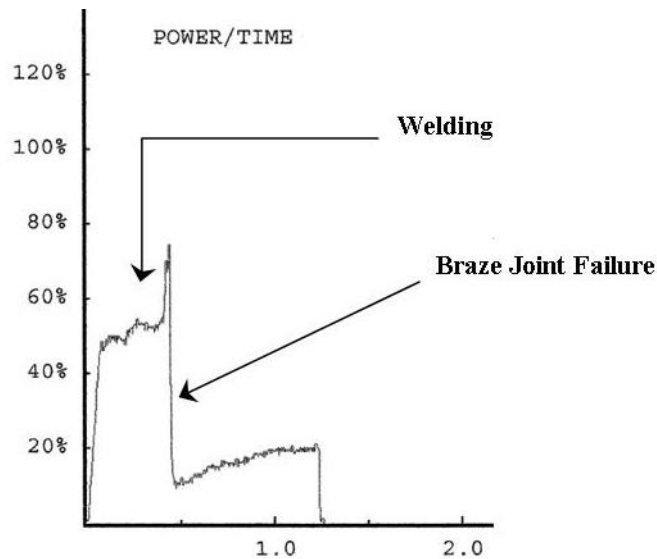


**Figure 45: Power vs. Time plot for weld cycle with failed braze joint, Trial No. 5004**

After the tip was repaired with a nickel-based braze alloy, several cycles were repeated, and reasonable weld strengths were recorded. An experiment was designed with the following parameters: 300 to 800-J energy and 20 to 40-psi pressure. Almost half the welds overloaded the system. The results were again demonstrating the machine characteristic, not the metal characteristic. To avoid overloading the system, another experiment was designed with the same pressure levels and 200 to 400-J energy. Additional welds were created for testing and metallurgy.

As with the T-304 trials, the repair and replacement of the welding tip produced significant scatter with the weld strengths. Because of the use of the nickel-based braze alloy, the investigation was able to include energy levels up to 2000-J. The range of parameters allowed the evidence of curvature to be more obvious. Figure 46 is a plot of the tensile force vs. energy for different clamping forces. Figure 47 is the same plot, but with regression trendlines added. Based on the experiments, the trendlines suggest weld strengths above 1000-lbf are possible with high energy and a clamping force of 225 to 300-lbf. This may not be reasonable, because welds with much lower strengths (600 to 700-lbf) pulled buttons. At the same time, 800-lbf tensile was recorded with interfacial failures. Therefore, the buttons may have been overwelded samples. It would be ideal to test welds at high energy and high clamping force, but again this is not possible due to equipment limitations.

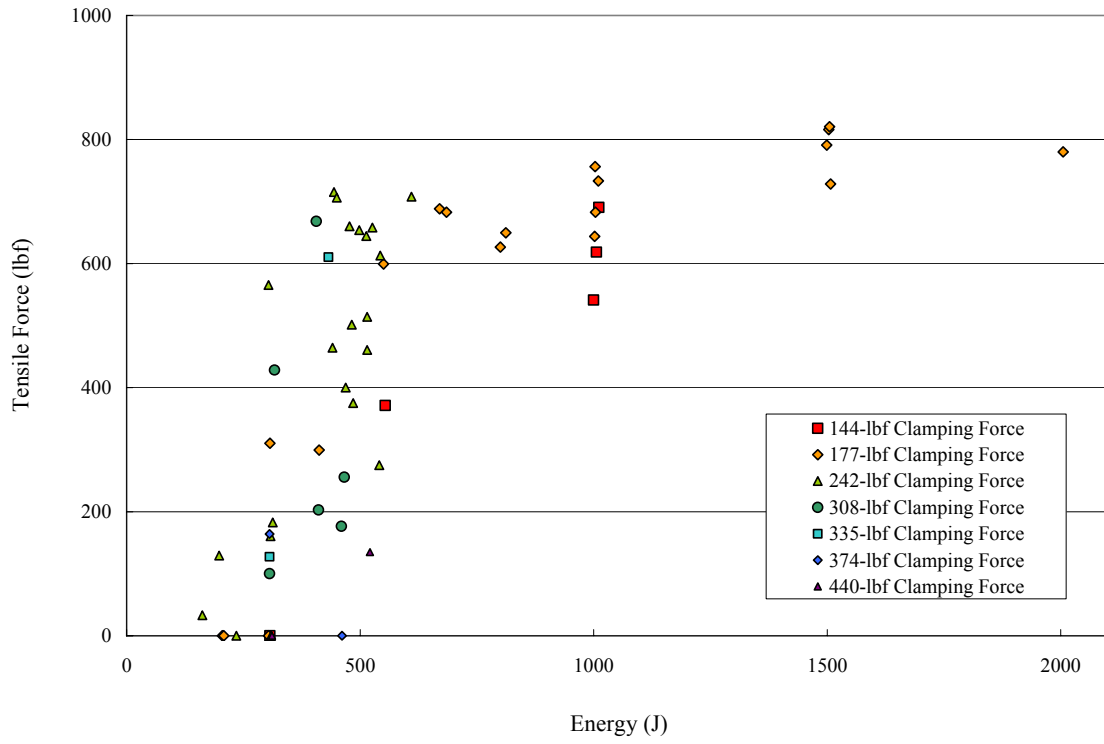


**Figure 46: Scatter plot of Tensile Force vs. Energy, Clamping Force for SS 410**

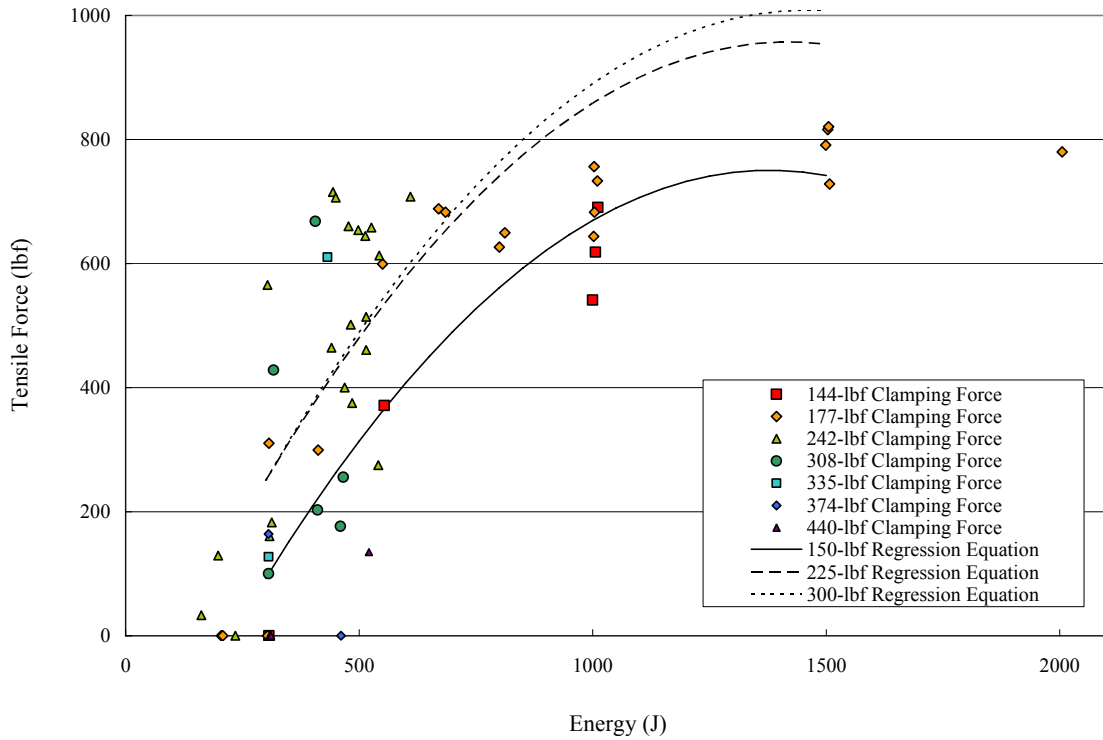


**Figure 47: Scatter plot of Tensile Force vs. Energy, Clamping Force for SS 410 with Regression Trendlines**

## 5.6 COMMERCIALY-PURE TITANIUM

Commercially-pure titanium was found to be weldable using 350M tooling in the preliminary trials. A three-replicate experiment design varying energy from 200 to 500-J and pressure from 35 to 65-psi was possible. The only significant tool wear was at the anvil, where the knurl appeared to be rounded-off by the end of the trials. The titanium did stick to the tooling, but it was no greater than the amount of sticking that is experienced with UMW of aluminum. It may have been promoted by the tip knurl pattern. The welds would break-free from the tip without depositing material. No overload conditions occurred. The peak weld strengths occurred at the maximum energy and pressure conditions, suggesting the parameter window was too small.



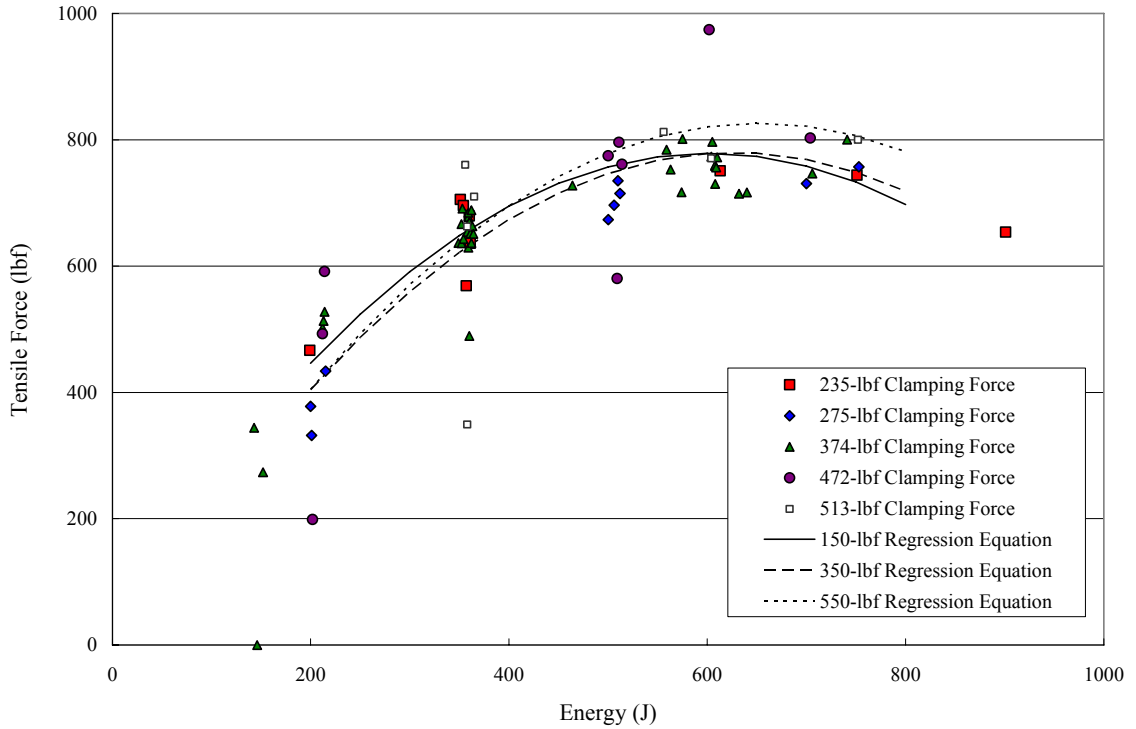


**Figure 49: Scatter plot of Tensile Force vs. Energy, Clamping Force for C.P. Titanium with Regression Trendlines**

## 5.7 TITANIUM 6AL-4V

Wrought-tungsten tooling was used for the titanium 6Al-4V trials. Preliminary trials experimented with 350M and tungsten-based tooling materials. 350M did not produce welds, and threw a shower of white sparks from the tip/ top coupon interface even at high clamping forces. Wrought-tungsten tooling worked well in the preliminary trials, so it was selected for the Titanium 6-4 designed experiments. A two-replicate design of experiment varying pressure from 20 to 40-psi and energy from 300 to 800-J was carried-out. Additional welds for testing and metallurgy were created following the DOE. Peak tensile forces above 1300-lbf were recorded for

40 to 60-psi and 500-J energy. Additionally, tensile forces above 1000-lbf were recorded at 60-psi clamping force and energy levels as low as 200-J.

The tip and weld area were observed to glow red-hot during the weld cycle for higher input energy levels. White sparks from the tip/ top coupon interface were observed with lower clamping forces. Most of the tensile tests pulled a button, so the data appears to somewhat level-out with increasing energy. Sticking to the tip or the anvil was common. The titanium welds sometimes required a good deal of force to separate it from the anvil, especially with higher pressures. Small particles of tungsten were found on the titanium weldments. With that being said, the tool wear was slow and predictable without any major failures, even though this tool was brazed with the lower-strength Incusil ABA braze foil. The tip was rotated after the DOE trials to take advantage of the less-worn tip face.

Figure 50 is a plot of the tensile force vs. energy for different clamping forces. Figure 51 is the same plot, but with regression trendlines added. Again, the data has significant scatter, most likely due to the removal and re-installation of the tooling and the wear of the tooling. The trendlines show a characteristic plot of UMW strength for increasing energy, at increasing pressures.

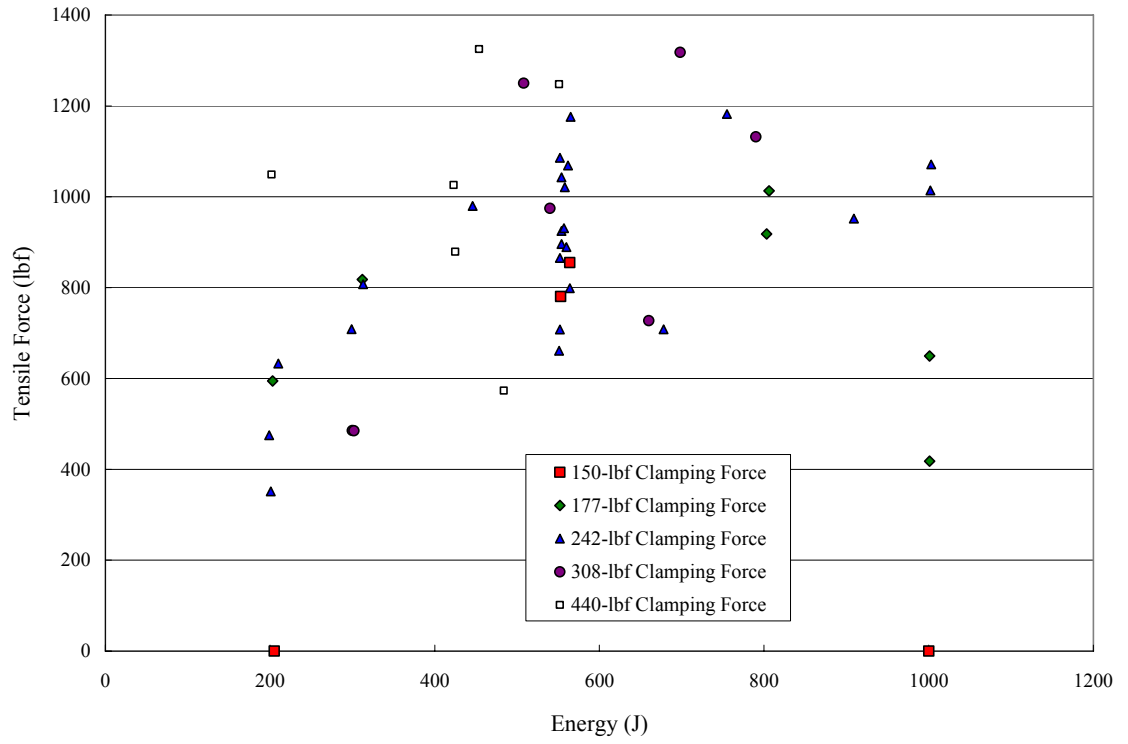


**Figure 50: Scatter plot of Tensile Force vs. Energy, Clamping Force for Titanium 6Al-4V**

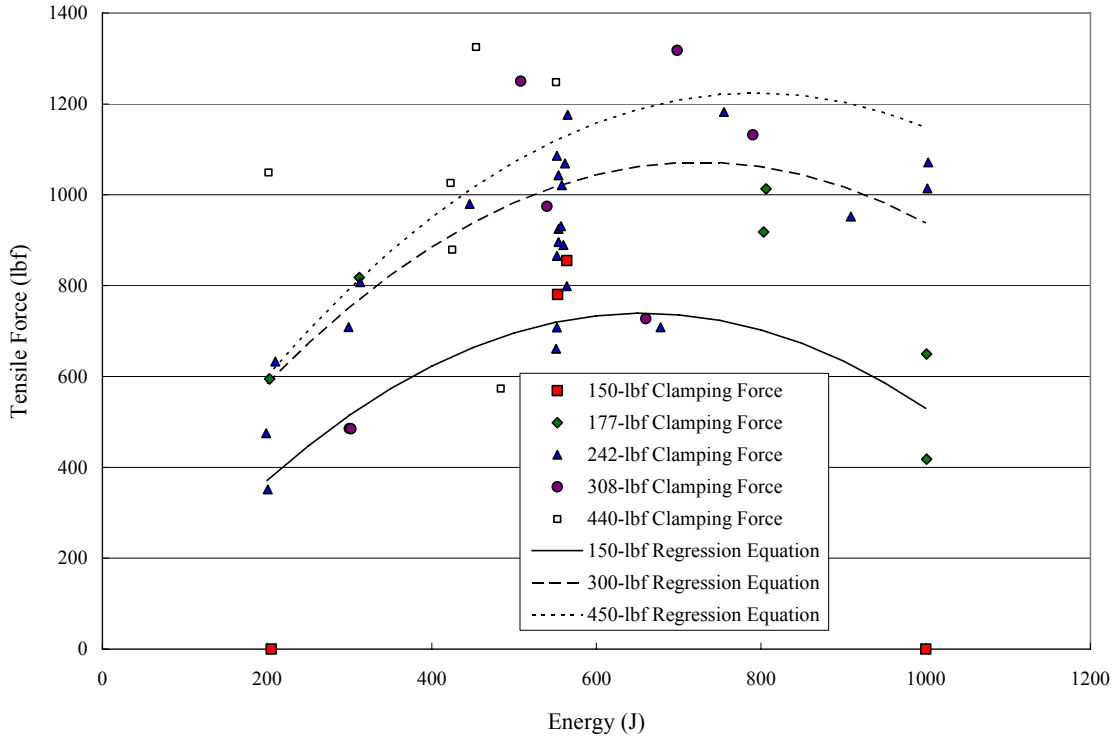


**Figure 51: Scatter plot of Tensile Force vs. Energy, Clamping Force for Titanium 6Al-4V with Regression Trendlines**

## 5.8 NICKEL 625

Nickel-base weld trials were limited. A W-25Re tip was first used with a number of anvil materials. An AISI M2 tool steel anvil fractured after one weld cycle at 600-J and 60-psi, in which no weld was produced. A CMW Elkon 100W tungsten anvil did not have the strength required to grip the weldment, and broke apart into small fragments during a weld cycle. At 400-J and 60-psi, no weld was formed. Using a wrought-tungsten tip and anvil, at 400-J and 40-psi, no weld was formed, and the wear was much greater than was observed with the titanium and stainless steel welds. Due to these initial findings, it was decided to limit the scope of the nickel-based weld trials.

Grade 18Ni Maraging Steel (350M) tooling was selected to be used for both the Ni 625 and 718 weld trials. 350M was selected because there was no concern for braze joint failures, even though it was anticipated to stick to the work or fracture. The surfaces of the tools were artificially oxidized with an oxy-acetylene torch before each trial to help avoid sticking. Although the oxide layer only lasted one weld, it significantly reduced sticking. Without the oxide layer, the system overloaded and the weld coupons stuck to the tip and anvil so much that they had to be pried-off with pliers. Weld settings ranged from 1000 to 1500-J and 60 to 80-psi. On the trial when the system overloaded (No. 7001), the actual energy was only 530-J, and no weld was formed. With the oxide layer, there was no sticking to the anvil, and the sticking to the tip was strong, but the weld coupon could be separated without damage to the tip or anvil. The weld area was observed to glow red-hot during the weld cycle. Weld trial No. 7002, at 1000-J and 80-psi, recorded a peak tensile load of 789-lbf. It had an interfacial failure mode, and the weld area appears to only have been around the circumference of the tip impression. This data point has been added to the plot in Figure 53.

## 5.9 NICKEL 718

Nickel alloy 718 was similar to the Ni 625 weld trials in that accelerated tool wear limited the number of experiments. With a W25Re tip and a 350M anvil, trials 1020 and 1021 used 400-J energy. The first weld (at 40-psi) stuck to the anvil so strongly that it needed to be pried-off with a pair of pliers, heavily deforming the weld coupon and destroying the anvil knurl. It was tensile tested to 294.2-lbf, and had a interfacial fracture. The second weld (at 60-psi) again stuck to the anvil, and needed to be removed with pliers, but this time the weld nugget was permanently bonded to the anvil. A CMW Elkon 100W tungsten anvil was used for trial no. 1073. With the welding parameters 400-J and 40-psi, no weld was formed. A wrought-tungsten

tip and anvil were used at 400-J and 40-psi for trial no. 1073. Although increased tip and anvil wear were observed, a peak tensile force of 327.5-lbf was measured. The fracture was interfacial. 350M tooling was artificially oxidized with an oxy-acetylene torch before each trial to help avoid sticking. Trial 6010, at 40-psi and 600-J, was observed glowing red-hot. It did not stick to the anvil, but it did stick to the tip. The weld broke while removing from the tip. Without re-oxidizing the tooling, the next trial (no. 6011) used the same parameters. Again the sample was observed glowing red-hot, did not stick to the anvil, but stuck to the tip. While trying to separate from the tip, the weld nugget was left deposited on the tip. For trial 6012, the tip was rotated to expose a new, oxidized surface. With the same 600-J energy and a higher pressure, 60-psi, the weld stuck to the tip. This time, the tip was cut-off and left bonded to the work for tensile testing and fractography. A peak tensile force of 588.2-lbf was recorded with an interfacial fracture surface along the weld circumference only. Another 350M tip and anvil was oxidized, and the parameters were increased to 80-psi and 1000-J. Again, the tip was cut-off and left bonded to the work for a cross-section. Pictures of the tip sticking and sectioning are shown in Figure 52. The data point from trial 6012 has been added to the plot in Figure 53.

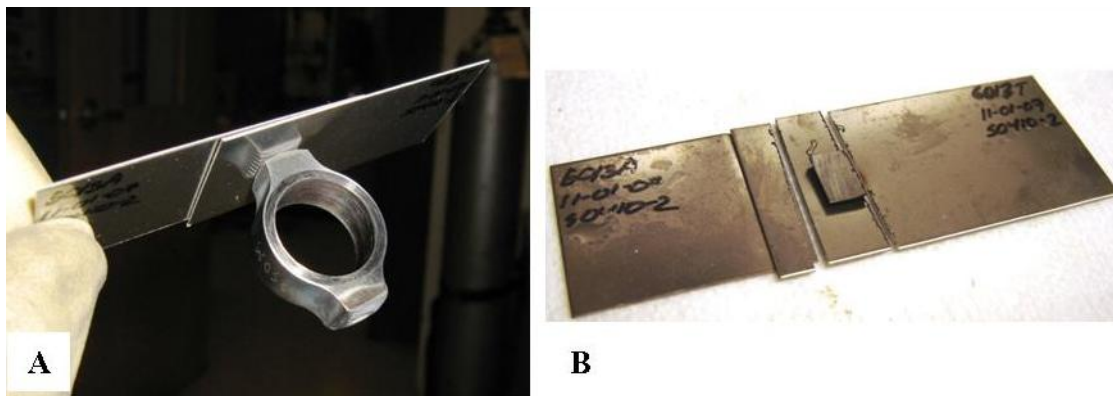


**Figure 52: Ni 718 weld trial 6013: A – 350M Tip sticking to work; B – 350M tip cut-off while bonded to work, then sectioned for metallurgy**

## 5.10 SUMMARY

The regression trendlines for several clamping forces for the stainless steel and titanium alloy weld trials, as well as the data points from the nickel-based weld trials have been added to the plot in Figure 53. Excessive tool wear, braze joint failures, difference in tool alignment, and equipment limitations introduced significant scatter into the experimental results, so a detailed analysis of the statistical results was not considered appropriate. The titanium weld trials produced trends with strong curvature. Stainless steel trendlines are more linear, showing little evidence of overwelding. It is difficult to verify the effect of higher clamping forces at higher energy levels because of equipment limitations. Higher-powered equipment is required to perform welds under these conditions. Higher clamping forces may have less tool wear and higher efficiency. This is compared to low-clamping force welds in these trials, where the tip/ top coupon interface did not have enough friction to prevent slipping and maximize the energy transfer to the interface. At low clamping forces and high energy, the tool wear was accelerated and the braze joints failed prematurely, causing poor repeatability. At the same time, these welding conditions generated significant amounts of heat, effectively lowering the yield strength of the material, and allowing a high-strength bond to form, nevertheless.

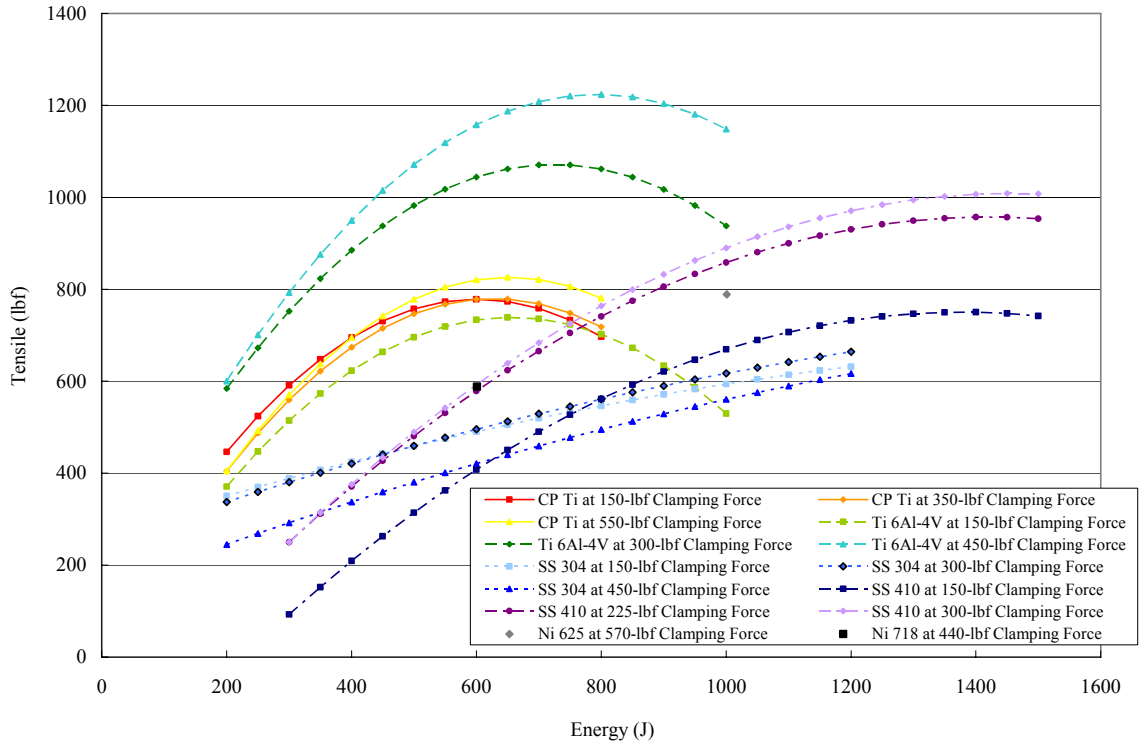


**Figure 53: Trendlines developed from Regression Equations; Plot of Tensile vs. Energy, Clamping Force**

## CHAPTER 6

### METALLURGY & FRACTOGRAPHY

Select welds were chosen for metallurgy and fractography. Welds were sectioned, mounted, ground, polished, and etched to view the bondline and microstructure. Several lower-resolution micrographs (50x total) were taken along each cross-section and spliced together to produce a continuous high-quality picture of the bondline. Additional micrographs were also taken at high resolution (20x, 40x, and 100x). The discussion will focus on the physical characteristics of the bond, and how they relate to the mechanical testing and visual appearance of similar welds. Supporting metallurgical discussion is also provided.

Six samples were tensile tested, trimmed to size, cleaned in an ultrasonic bath with acetone and methanol, and then dried in a low-temperature oven for an hour. Within several hours of tensile testing, the fracture surfaces were loaded into the SEM chamber and pumped down under vacuum. One interfacial fracture surface of each alloy was observed. The fracture surfaces observed are not necessarily from the highest strength or otherwise best quality welds. Higher-strength welds in several of the alloys often failed outside of the welds in the base material without provide a weld fracture surface for observation. A low-resolution picture (12 to 13x) was first taken of each fracture surface, with the locations of the higher-resolution images indicated. The high-resolution images for each alloy were between 1000 and 10000x. In some cases, 10000x did not provide a clear image, so the highest-resolution may have been limited to 1000 or 5000x. A discussion of the characteristics of the observed surfaces is provided.

## 6.1 METALLURGY

Several cross-sections for each of the stainless-steel and titanium alloys have been evaluated. A very limited number of nickel-based weld trials were conducted, and so the number of cross-sections is limited. Table 9 summarizes the welding parameters of the cross-sections.

Material	Trial	Actual Energy (J)	Clamping Force (lbf)	Time (s)	Power (W)	Tensile Force (lbf) <sup>1</sup>	Tensile Force (lbf) <sup>2</sup>	Tooling Material	Comments
SS 304	4057	665	308	0.26	3540	500	516	W-25Re	Fast, reset light on power supply
	4061	550	335	0.22	3600	455	467		Reset light on power supply, stronger sticking-to-anvil
	4064	216	177	0.12	3540	370	360		Fast, sticking-to-tip
	4066	1400	177	0.52	3570	530	674		Long, lots of heat input, strong sticking-to-tip, high deformation
SS 410	5054	311	242	0.15	3465	170	278	W-La	Sticking-to-tip, weaker
	5075	454	242	0.19	3630	700	447		Cycle alarm: power, sticking-to-tip, glow red-hot
	5081	1000	177	0.39	3600	700	755		Glow red-hot, long weld, sticking-to-tip
	5091	611	210	0.23	3600	700	567		WO, short glow, stronger sticking-to-tip
	5094	1002	144	0.41	3330	580	648		Glow red-hot, long weld
	5099	2006	177	0.82	3585	780	629		Long weld, lots of glow-orange, sticking-to-tip, threw sparks from tip-coupon interface
C.P. Ti	2057	601	374	0.26	3630	745	781	350M	Cycle alarm: power, sticking-to-anvil
	2060	363	374	0.19	3630	655	636		Cycle alarm: power, less sticking-to-anvil
	2063	908	374	0.36	3630	800	624		Cycle alarm: power, red-hot during weld
	2067	903	235	0.42	3105	650	599		Glow red-hot during weld, strong weld, heat marks, CS
	2080	609	235	0.32	3120	750	774		Sticking-to-anvil & sticking-to-tip, heat marks
	2081	599	513	0.25	3615	770	809		WO, Sticking-to-anvil
Ti 6-4	3023	736	308	0.29	3540	1300	1085	Wrought-W	Repeated welds for additional testing and metallurgy, weld overload, sticking-to-tip, good appearance
	3025	306	242	0.18	3060	1170	693		Fast, small diameter weld, sticking-to-tip
	3026	559	242	0.26	3540	1000	931		Sticking-to-tip, okay
	3027	801	177	0.35	3555	920	781		Reset light on PS, coupon around tip glow red-hot, sticking-to-tip
	3029	567	335	0.25	3615	700	1070		Cycle alarm: power, sticking-to-tip
Ni 625	7000	1000	440	1.46	1560	790	NA	350M	New 350M tip and anvil oxidized w/ an oxy-acetylene torch prior to weld, long weld, glow red-hot, sticking-to-tip, no sticking-to-anvil
	7003	1309	571	2.01	2250	790	NA		Re-oxidized worn 350M tip and anvil from Trial 7002, long weld, no sticking-to-anvil, strong sticking-to-tip, pry-off, similar appearance to Trial 7002
Ni 718	6013	1002	571	1.04	2940	590	NA	350M	Re-oxidized worn 350M tip and anvil from Trial 7003, glow red-hot, long weld, no sticking-to-anvil, strong sticking-to-tip, tip cut-off in order to further evaluate weld

<sup>1,3</sup>Estimated from welds with similar parameters, power characteristic curves, and tooling

<sup>2</sup>Estimated using regression equations developed from tensile testing

**Table 9: Summary of welding parameters for sectioned welds**

All the cross-sections are shown after etching. Unetched ultrasonic cross-sections are featureless. The concern with etching an ultrasonic cross section is that the etchant will attack the areas of microstructure with the highest levels of strain, the weld centerline. Therefore, many of the etched sections appear as if there is no evidence of a bond across the weld centerline. There are other features, such as grains that have grown across the interface, grain boundaries that are aligned across the interface, and twin boundaries that provide evidence of the bond quality.

#### 6.1.1 TYPE 304 STAINLESS STEEL

Four type 304 stainless steel welds were selected for cross-sections: trials 4057, 4061, 4064, and 4066. During sectioning, the edges of the cut were rough, and splinters can be seen in some of the sections isolated from the edge of coupon. These should be ignored.

Figure 54 and Figure 56 are of weld trials 4057 and 4061, respectively. The etched interface of both sections revealed a characteristic “wavy” ultrasonic interface. Both welds were made using just over 300-lbf clamping force. The weld trial 4057 was made with 17% higher energy, resulting in a slightly longer weld time and slightly more deformation to the coupon. The increased energy is predicted to yield a 10% increase in tensile force. Both sections represent a good quality ultrasonic weld.

The cross section in Figure 58 is from weld trial 4064. It is the result of low energy (216-J) and clamping force (177-lbf). The sample is much less deformed than that in trial 4057 and 4061. Comparable welds had relatively low tensile strengths due to the featureless interface. The black spot on the lower left side is the result of a mechanical gash during the sectioning process and should not be related to the weld quality.

Using the same low clamping force as in trial 4064, Figure 60 is the result of weld trial 4066. This time, however, the energy level was increased by almost 700% to 1400-J. The weld

time was over ½ second. Due to the low clamping force, much of the energy was consumed at the top coupon/ welding tip interface. This is apparent by the high levels of deformation and recrystallization. The interface itself appears similar to that of trials 4057 and 4061. The high energy not only thinned the sample, but it created a large crack on the top-right side of the coupon. The influence of the crack on the weld strength depends on the direction of loading. The combination of low clamping force and high energy causes excessive heat input and premature tool failure.

Banding can be seen in the base metal in Figure 54 and Figure 56 due to variations in chrome and nickel content during casting. Figure 55 and Figure 57 are a collection of higher-magnification micrographs at the weld centerline. Annealing twins are visible in the microstructures as parallel, straight lines (boundaries) within grains. Twin boundaries are a type of grain boundary in which atoms across a boundary align at mirror-image positions of one another. Specifically, annealing twins are formed during an annealing thermal cycle following deformation [13].

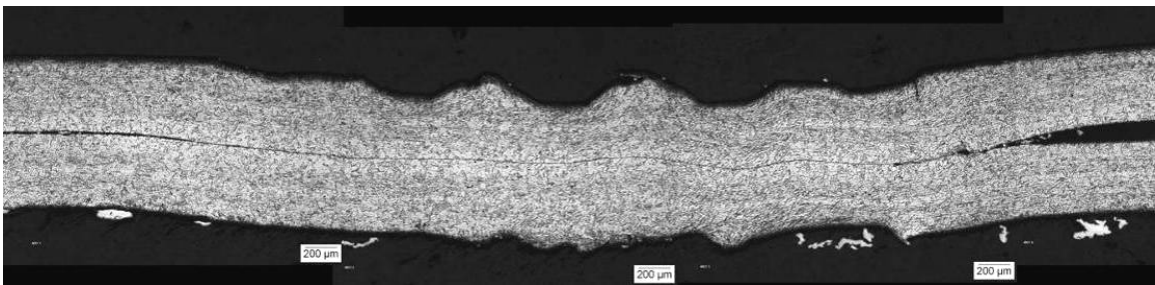


**Figure 54: Cross-section of SS304 Trial No. 4057**

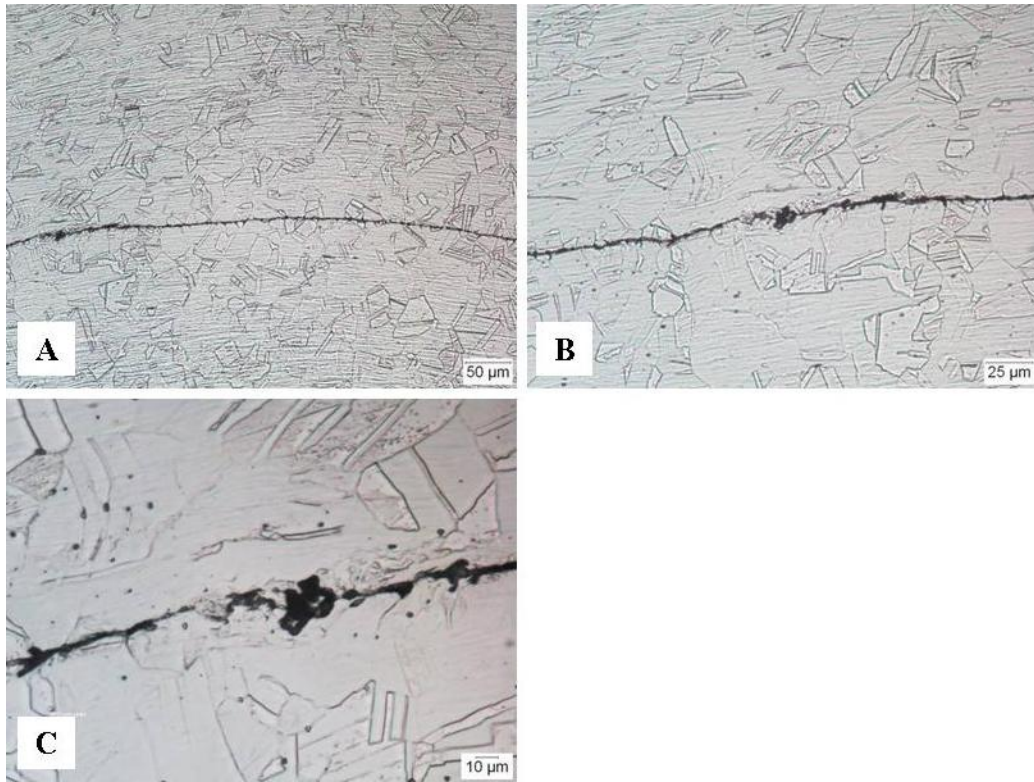


**Figure 55: SS304 Trial No. 4057 weld centerline; A – 20X, B – 40X, C – 100X.**

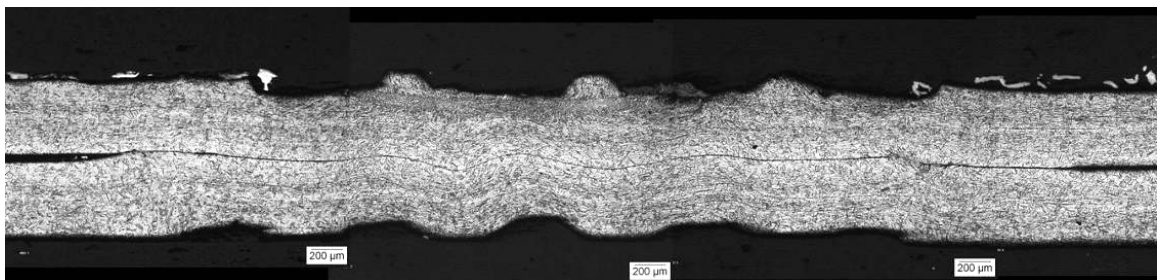


**Figure 56: Cross-section of SS304 Trial No. 4061**

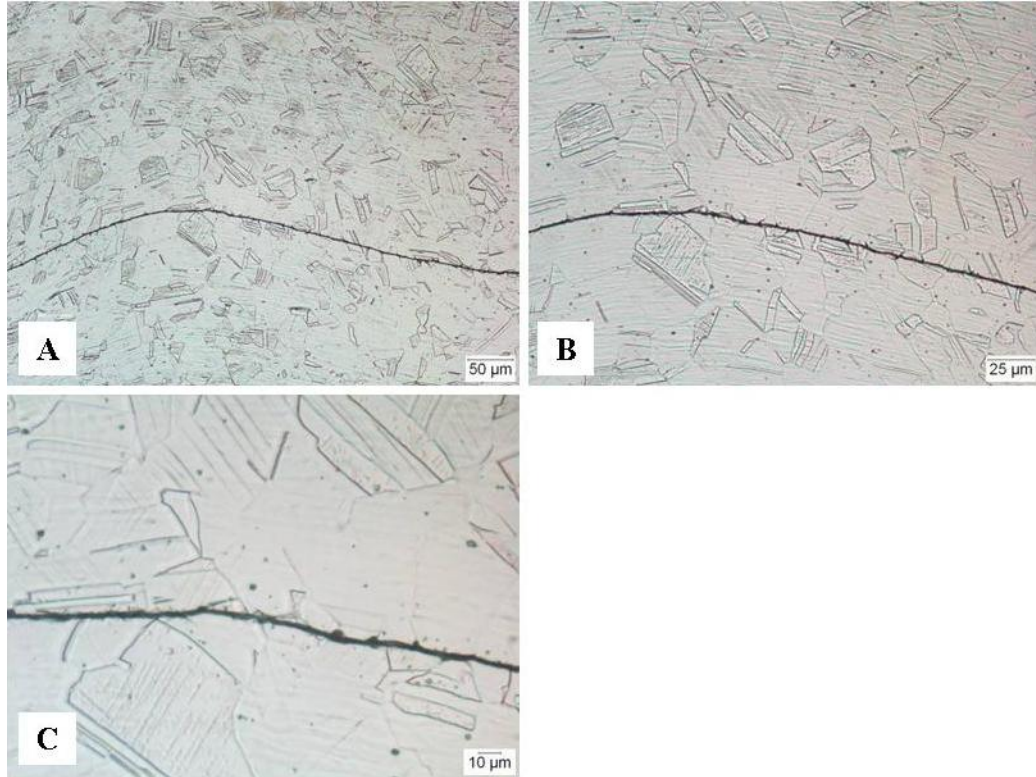


**Figure 57: SS304 Trial No. 4061 weld centerline; A – 20X, B – 40X, C – 100X.**

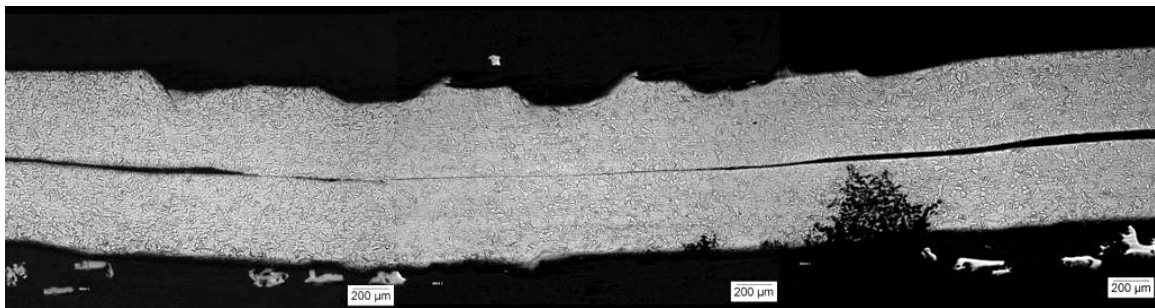


**Figure 58: Cross-section of SS304 Trial No. 4064**

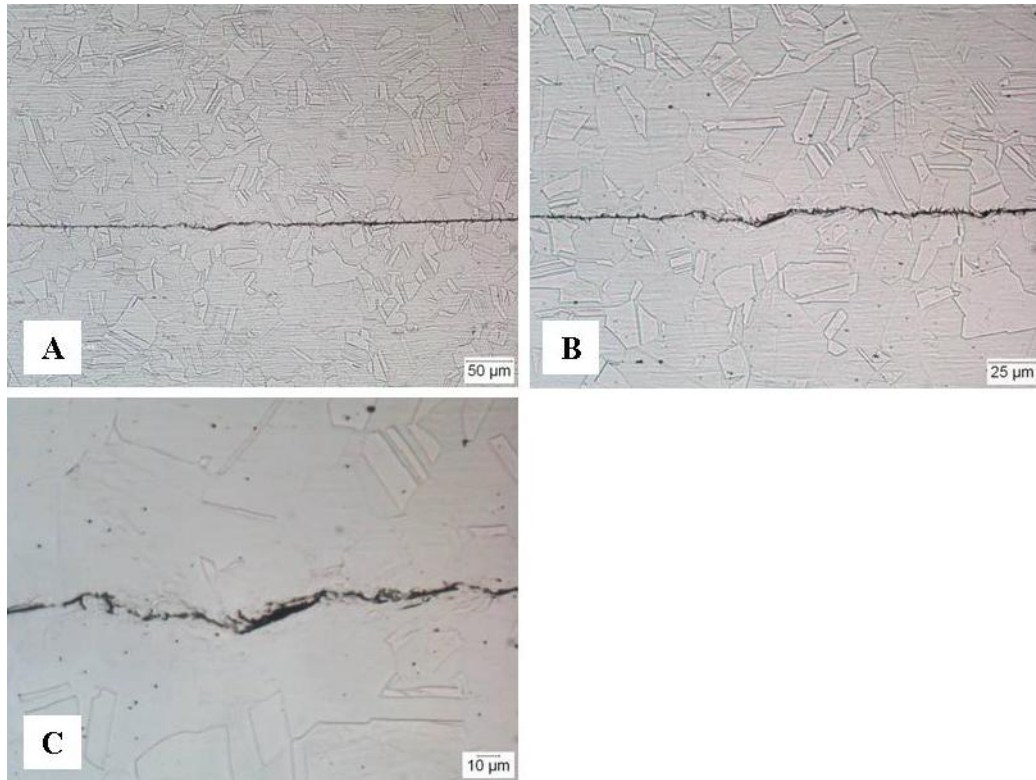


**Figure 59: SS304 Trial No. 4064 weld centerline; A – 20X, B – 40X, C – 100X.**

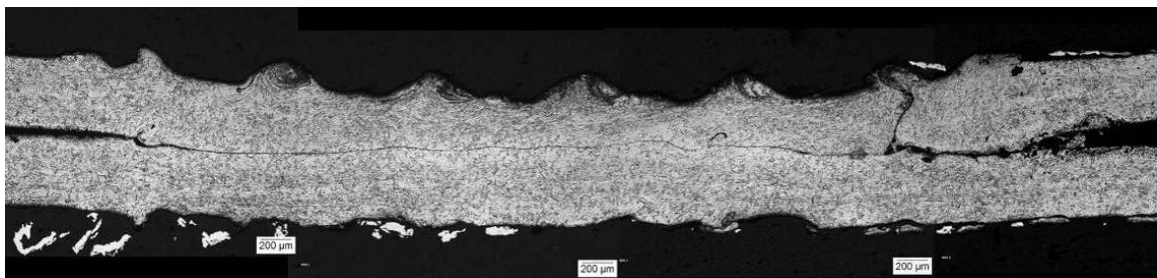


**Figure 60: Cross-section of SS304 Trial No. 4066**

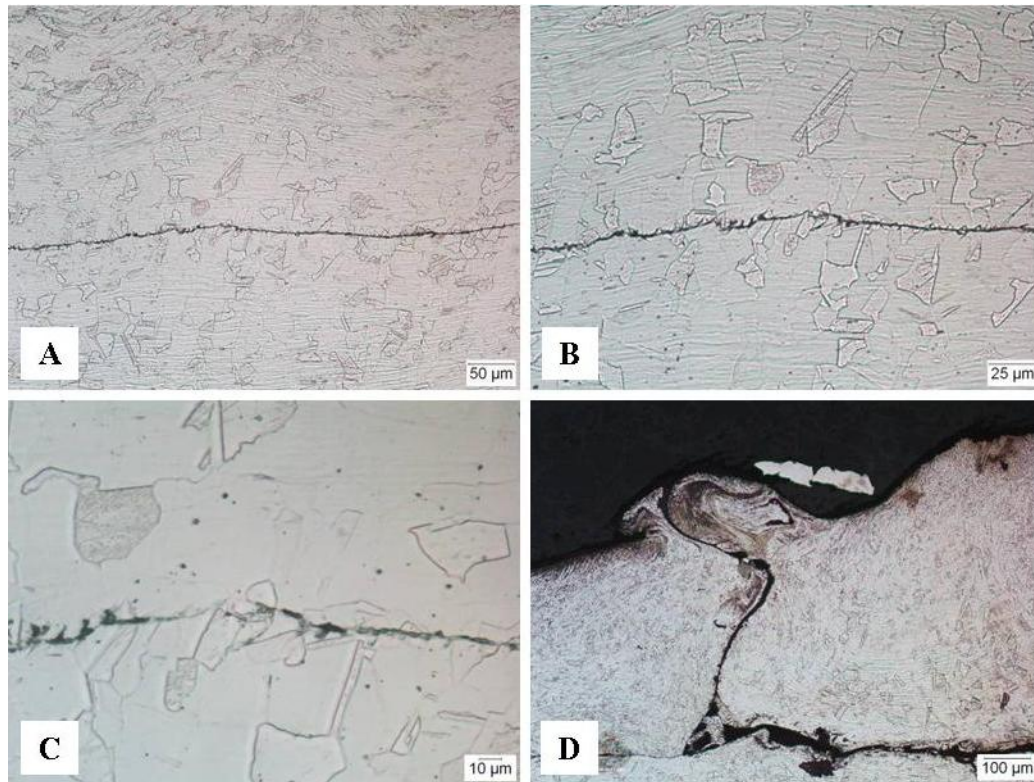


**Figure 61: SS304 Trial No. 4066 weld centerline; A – 20X, B – 40X, C – 100X, D – Fracture at 10X**

### 6.1.2 TYPE 410 STAINLESS STEEL

Six type 410 stainless steel welds were sectioned, trials: 5054, 5075, 5081, 5091, 5094, and 5099. Most of these welds were generated near the end of the 410 SS weld trials, and the tip was worn. Because of the wear of the tip, the quality of the tip imprint into the top coupon is not as great as some of the earlier trials.

Weld trial 5054 and 5075, Figure 62 and Figure 64, respectively, were both generated using 242-lbf of clamping force. Trial 5075 was created with 30% higher energy. Trial 5054 has little deformation at the tip interface and the weld interface. The tensile strength of welds with similar parameters was low. Trial 5075, however, has significantly greater bonding at the

interface. In addition, large amounts of deformation and recrystallization are present at the top coupon/ tip interface for trial 5075. This is also noticeable for the remaining SS 410 weld sections. The interface is difficult to observe in some of the sections, so arrows have been added to indicate its location.

Figure 66 is a cross-section of trial 5081. At 1000-J energy and 177-lbf clamping force, a direct comparison with the influence of clamping force and energy is possible with sections of weld trials 5094 and 5099.

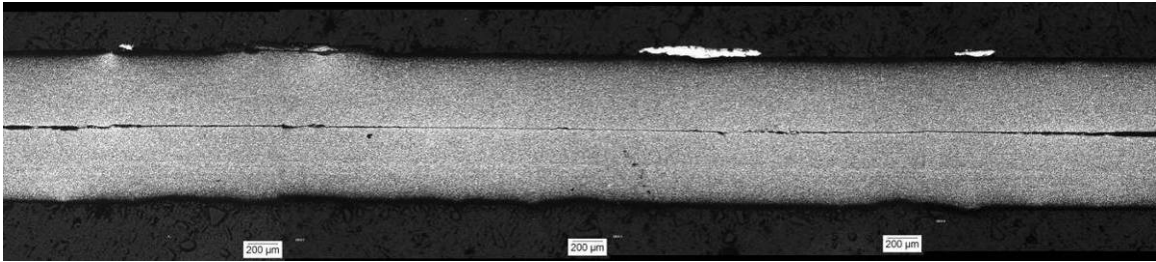


**Figure 62: Cross-section of SS410 Trial No. 5054**

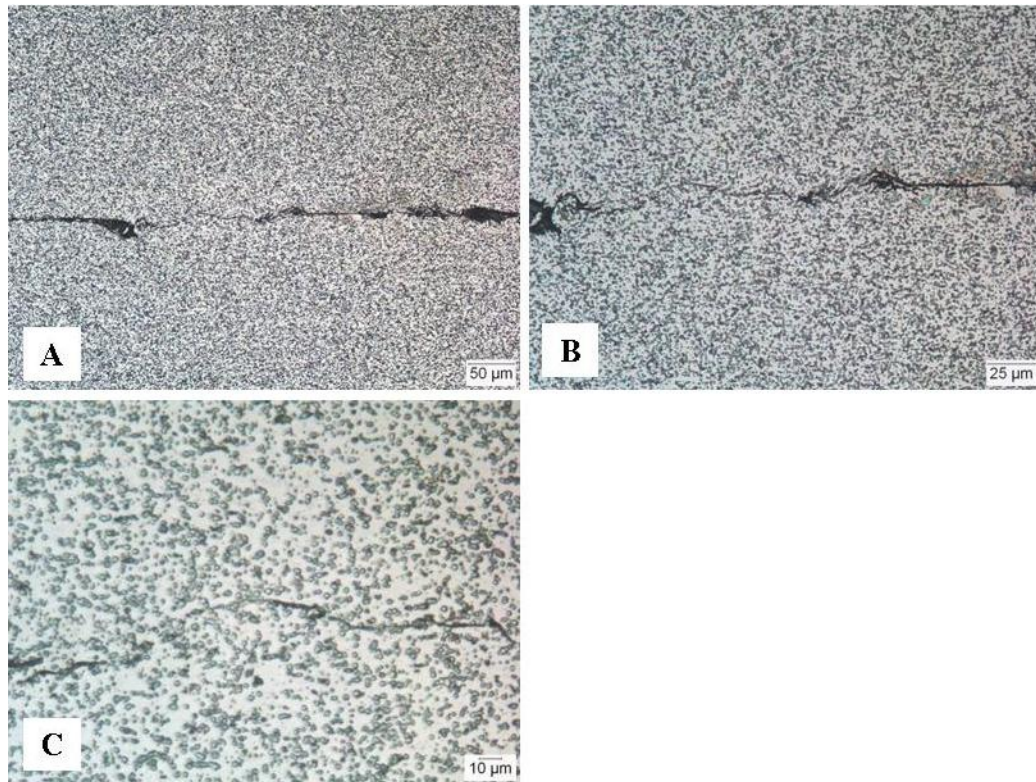


**Figure 63: SS410 Trial No. 5054 weld centerline; A – 20X, B – 40X, C – 100X**

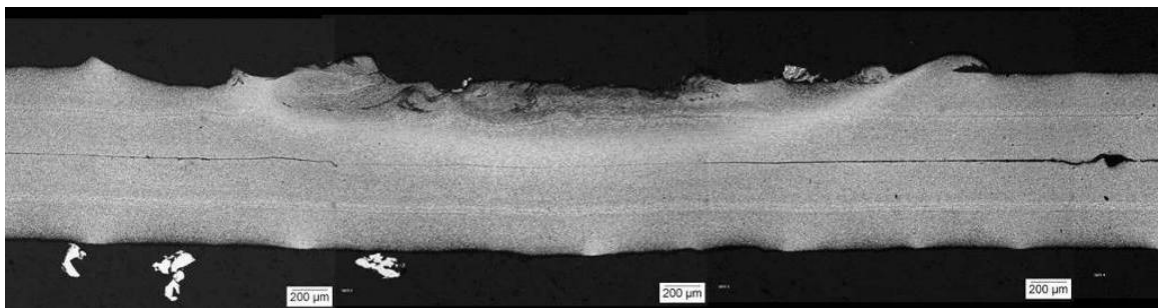


**Figure 64: Cross-section of SS410 Trial No. 5075 at 5X**

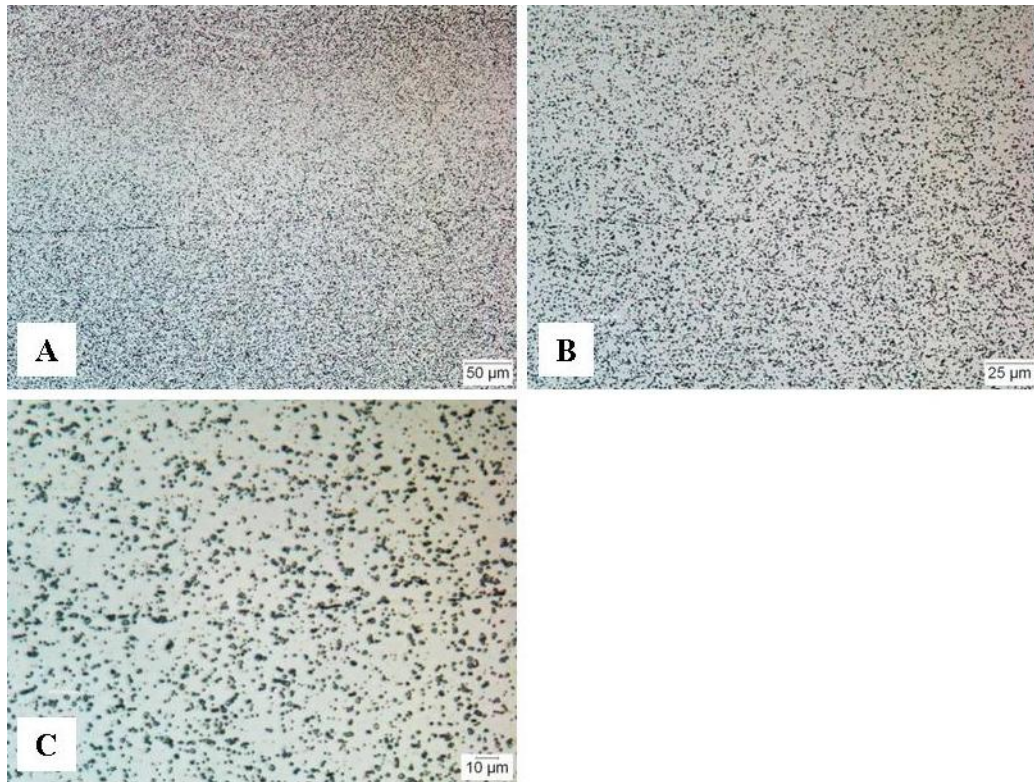


**Figure 65: SS410 Trial No. 5075 weld centerline; A – 20X, B – 40X, C – 100X**



**Figure 66: Cross-section of SS410 Trial No. 5081 at 5X**

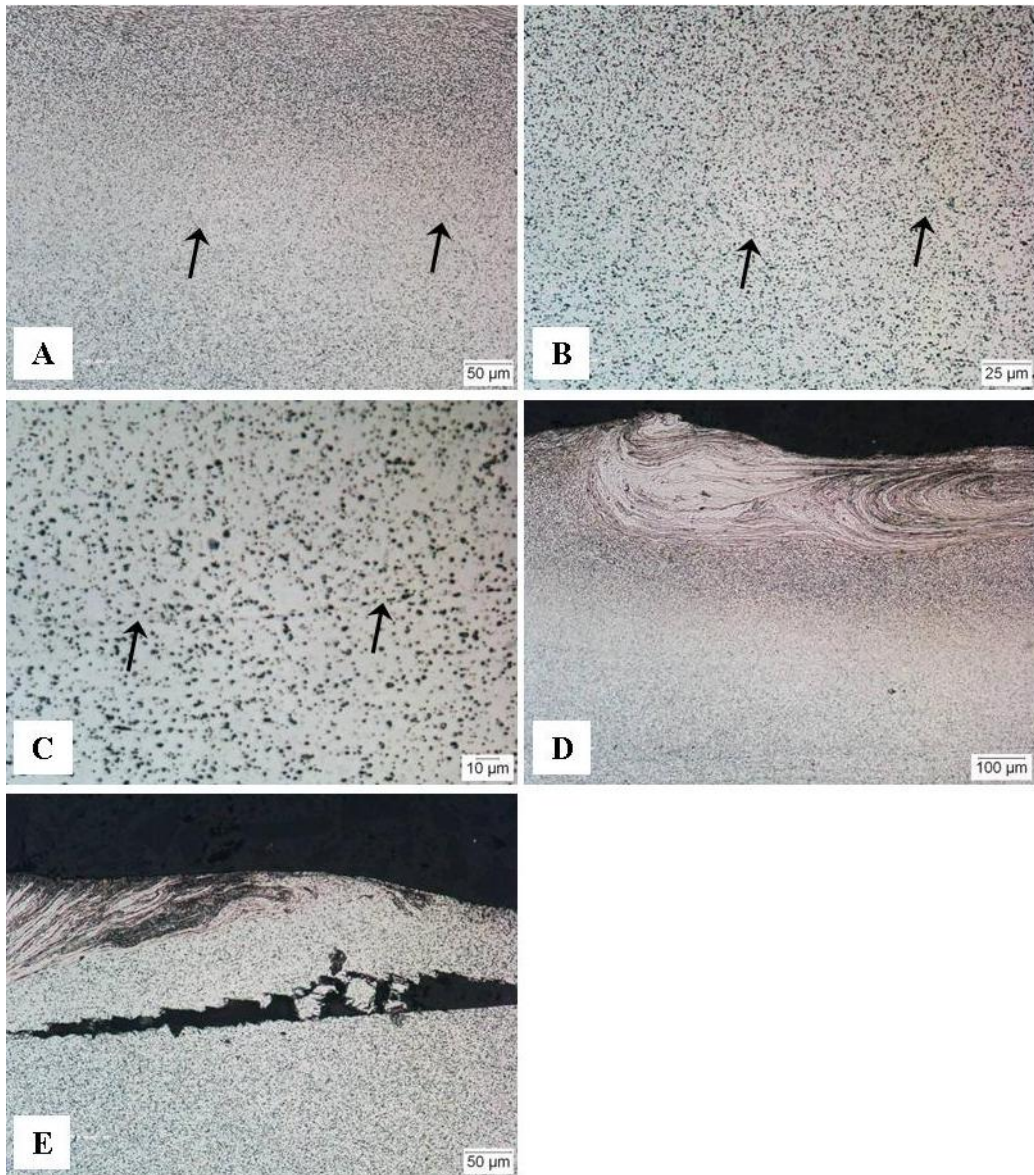


**Figure 67: SS410 Trial No. 5081 weld centerline; A – 20X, B – 40X, C – 100X, Tip deformation; D - Left side at 10X, E - Right side at 20X**

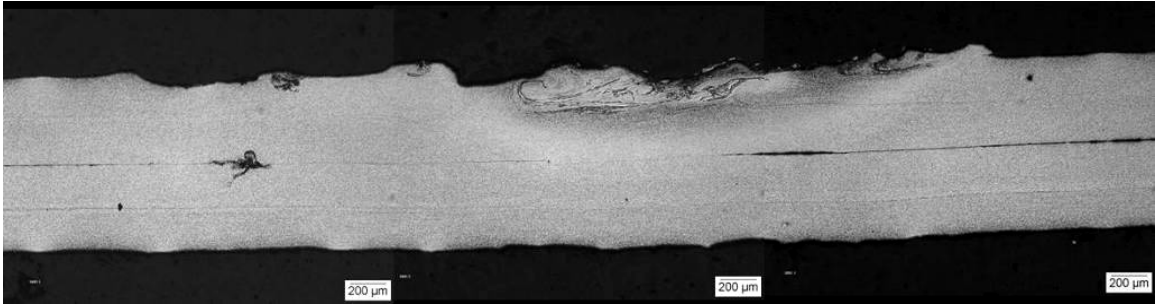


**Figure 68: Cross-section of SS410 Trial No. 5091 at 5X**

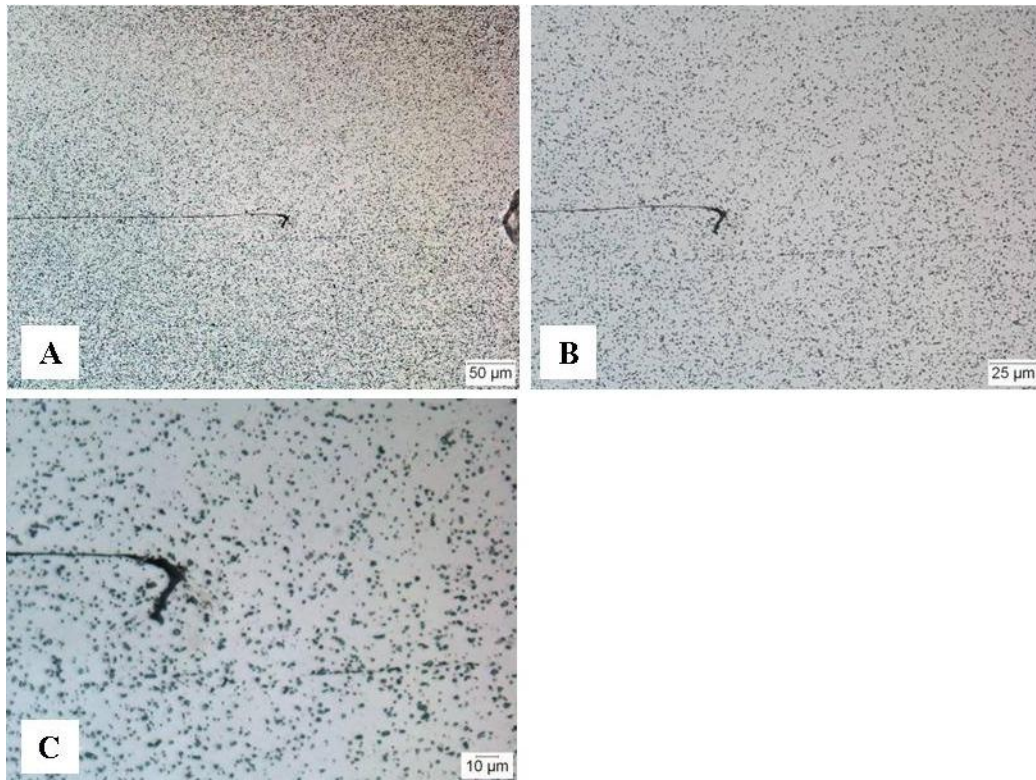


**Figure 69: SS410 Trial No. 5091 weld centerline; A – 20X, B – 40X, C – 100X.**

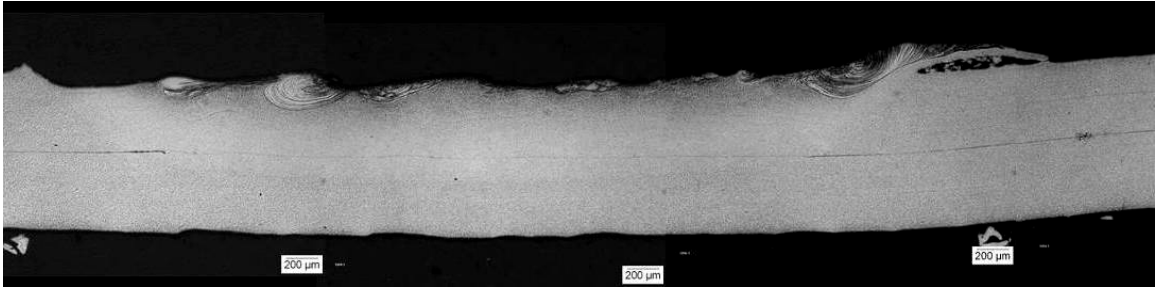


**Figure 70: Cross-section of SS410 trial No. 5094 at 5X**

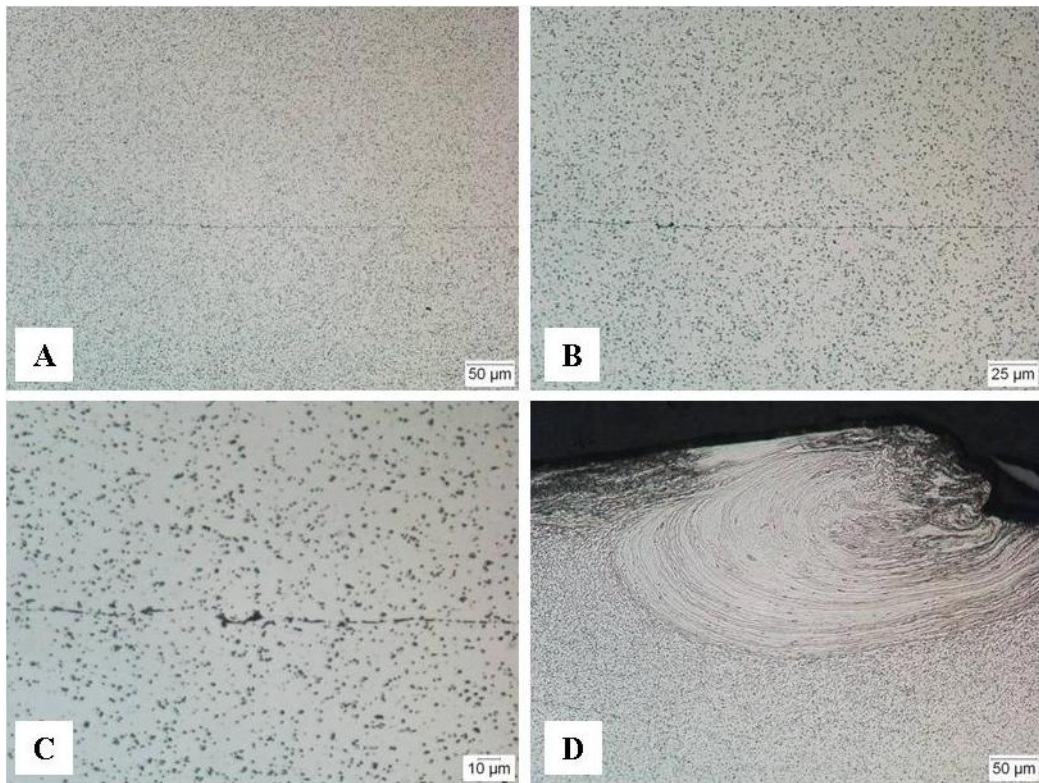


**Figure 71: SS410 Trial No. 5094 weld centerline; A – 20X, B – 40X, C – 100X; Tip Deformation at 20X**

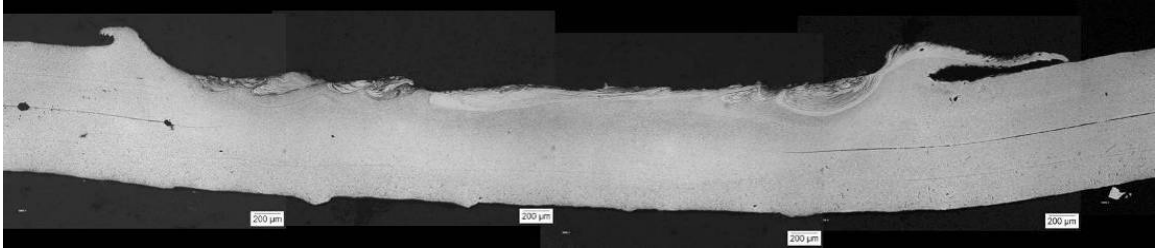


**Figure 72: Cross-section of SS410 Trial No. 5099**

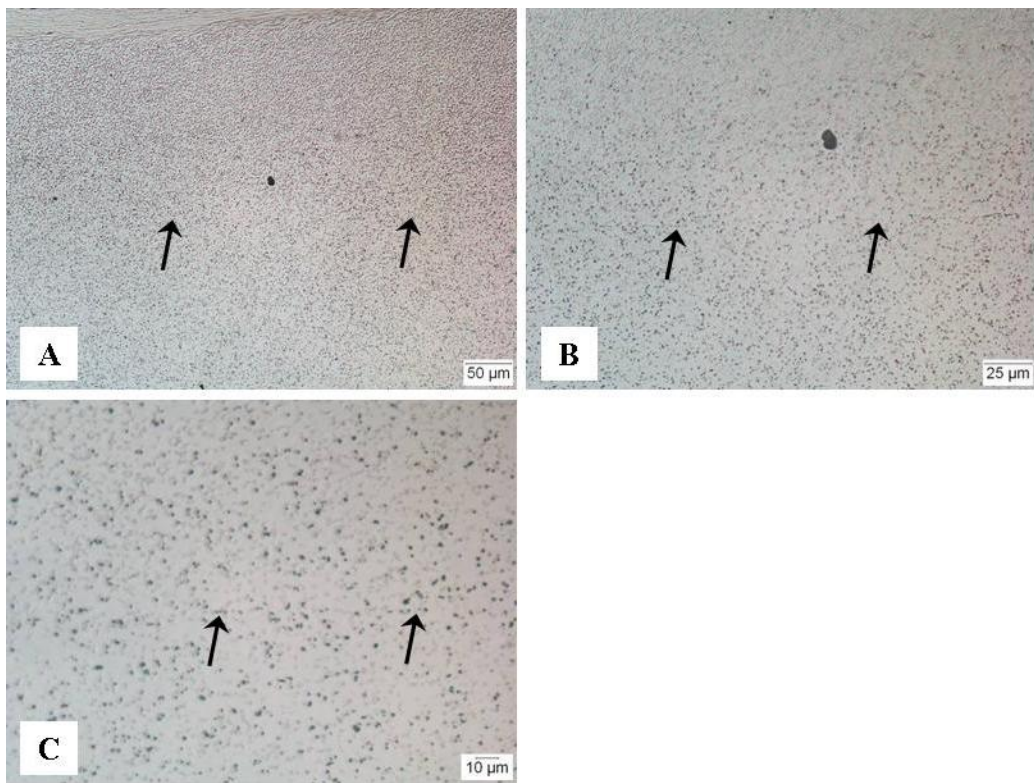


**Figure 73: SS410 Trial No. 5099 weld centerline; A – 20X, B – 40X, C – 100X**

### 6.1.3 C.P. TITANIUM

Figure 75 through Figure 85 are micrographs of several commercially-pure titanium weld trials. Most of the sections have an intermittent weld line that is difficult to observe. A high level of mechanical solid-state mixing and deformation has created high quality bonds. The C.P. titanium cross-sections have been created under various clamping forces and energy levels. In general, the quality of the bond increases with increasing energy and clamping force. However, during trial 2067, Figure 80, excessive weld energy forced the bondline down toward the anvil interface, decreasing the weld quality.

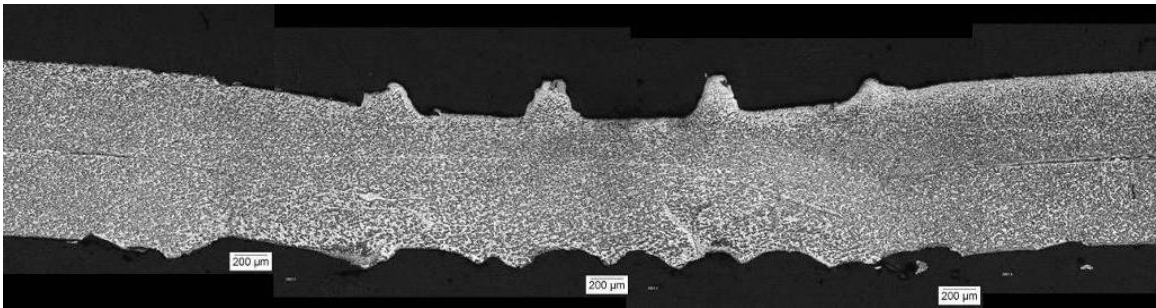


**Figure 74: Cross-section of C.P. Ti Weld Trial No. 2057**

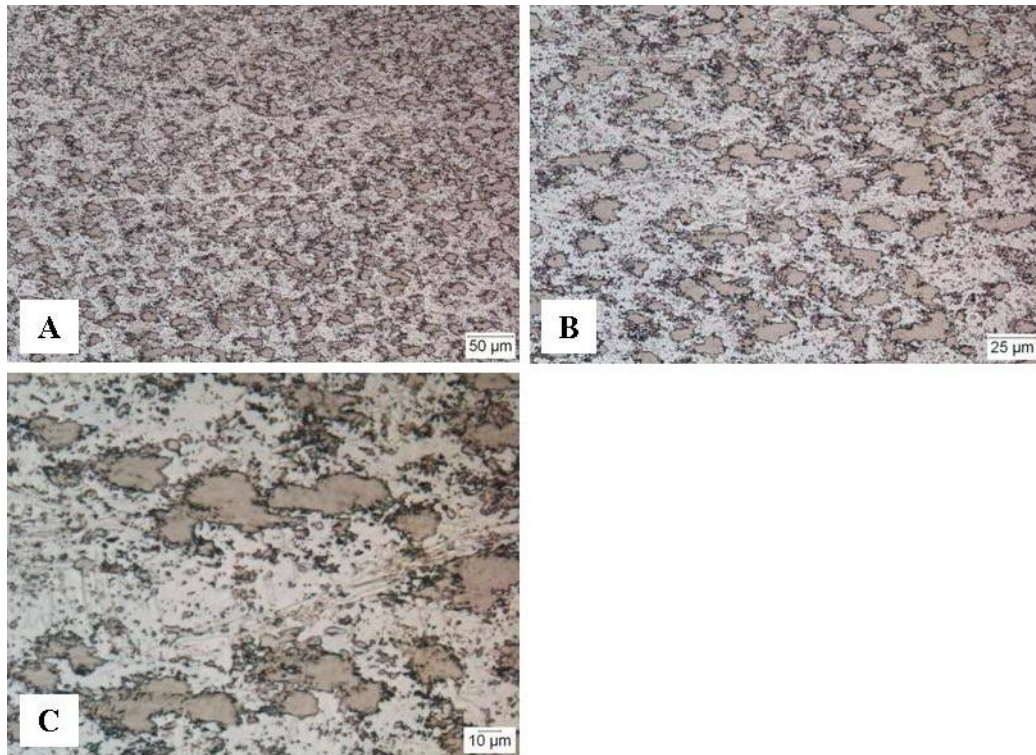


**Figure 75: C.P. Ti Trial No. 2057 weld centerline; A – 20X, B – 40X, C – 100X**

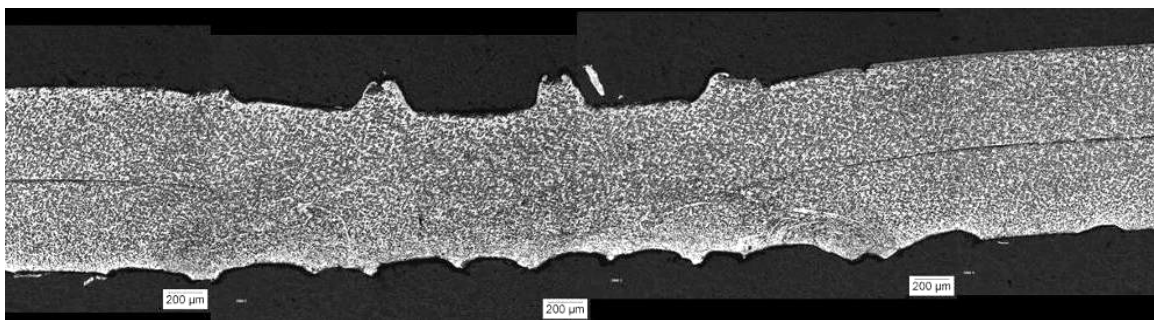


**Figure 76: Cross-section of C.P. Ti Weld trial No. 2060**

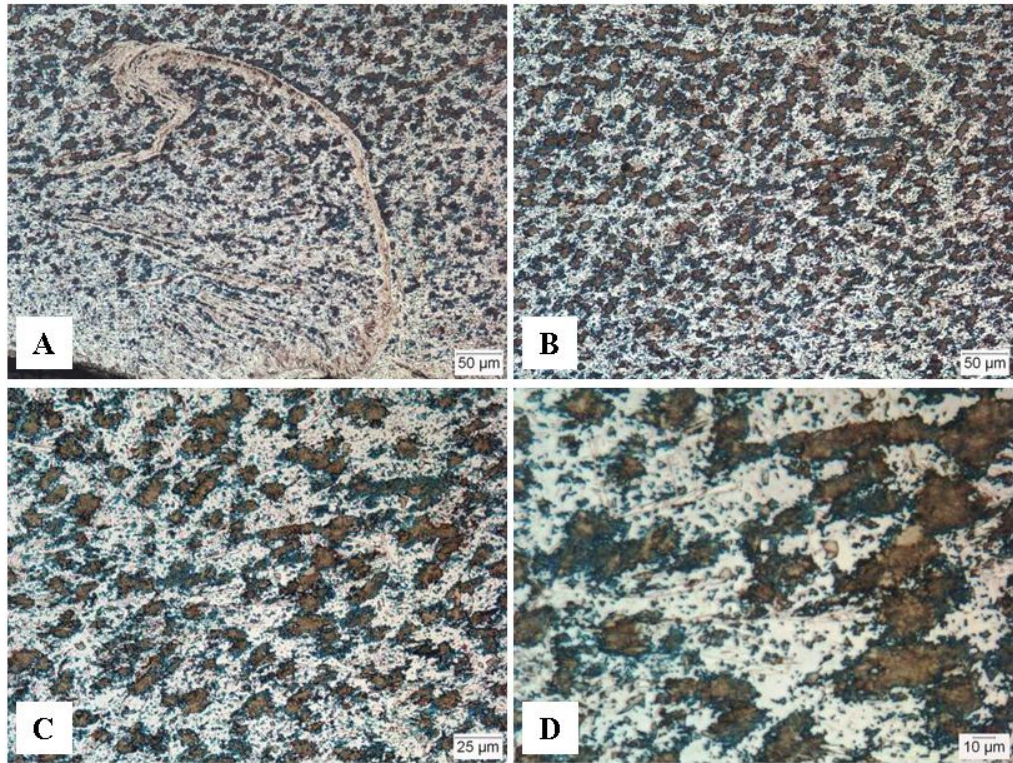


**Figure 77: C.P. Ti Trial No. 2060 left side at 20X, weld centerline; A – 20X, B – 40X, C – 100X**

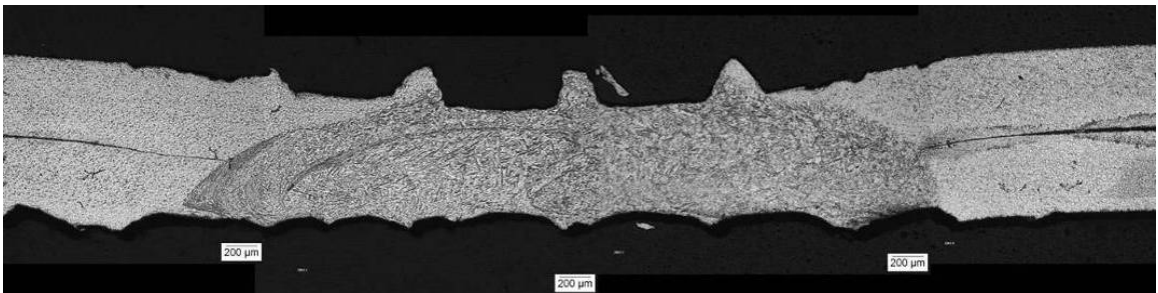


**Figure 78: Cross-section of C.P. Ti Weld Trial No. 2063**

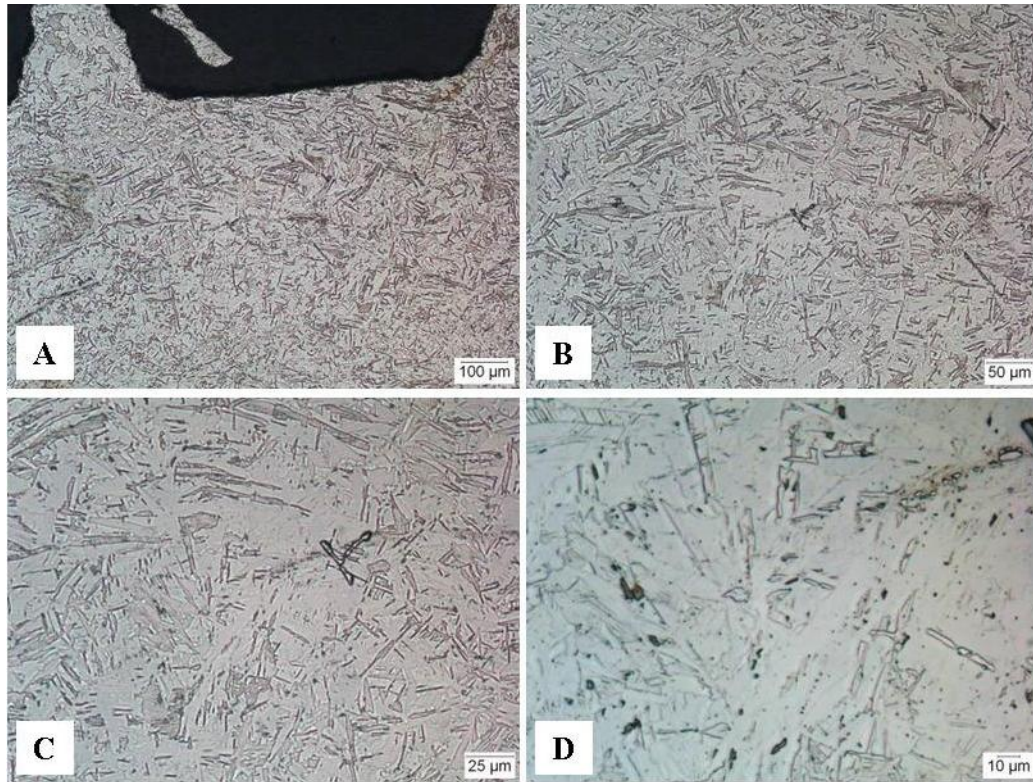


**Figure 79: C.P. Ti Trial No. 2063 weld centerline; A – 10X, B – 20X, C – 40X, D – 100X**

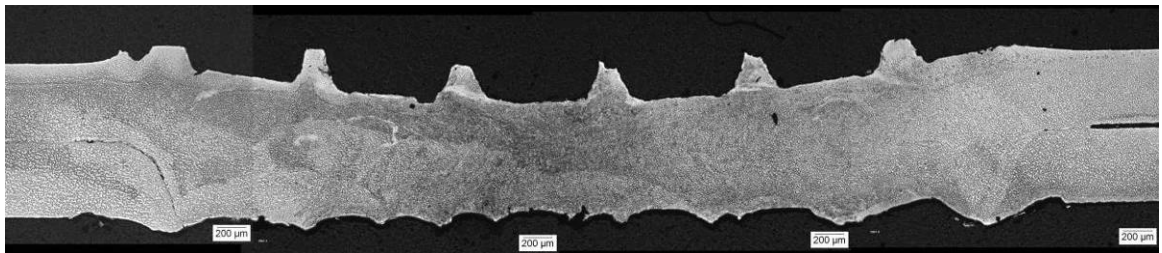


**Figure 80: Cross-section of C.P. Ti Weld Trial No. 2067**

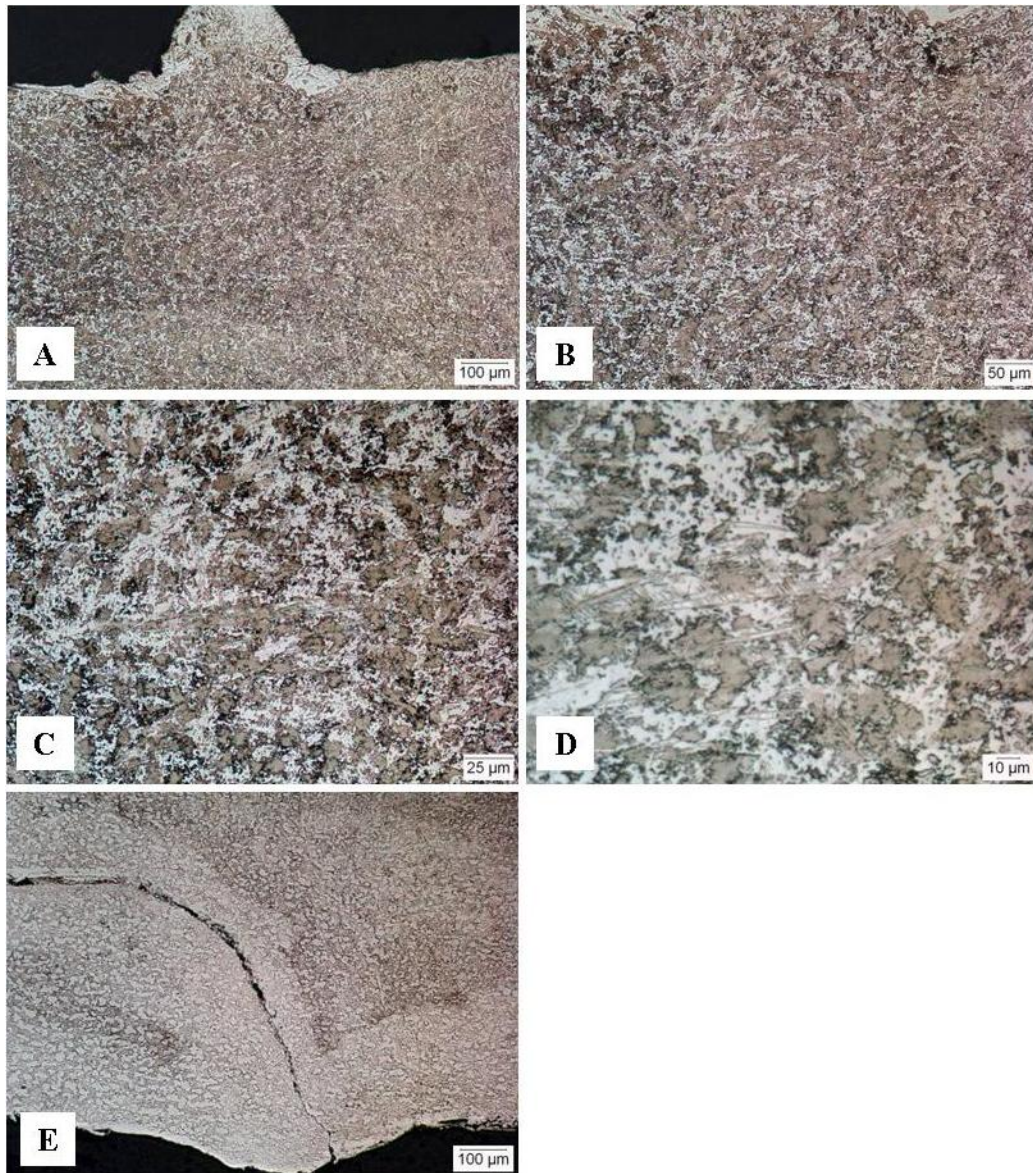


**Figure 81: C.P. Ti Trial No. 2067 weld centerline: A – 10X; B – 20X; C – 40X; D – 100X, E – left side at 10X.**

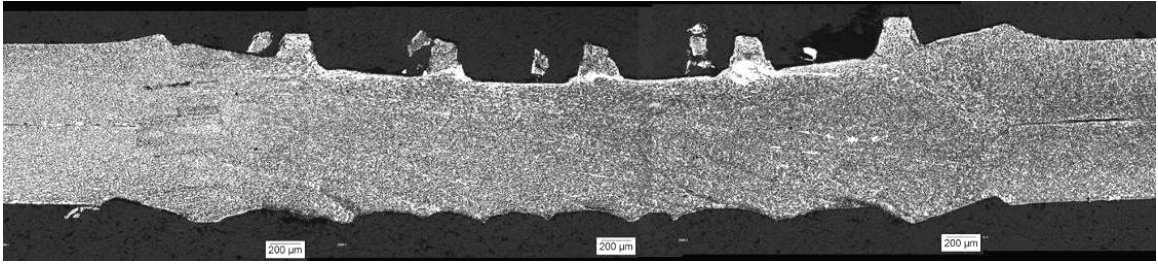


**Figure 82: Cross-section of C.P. Ti Weld Trial No. 2080.**

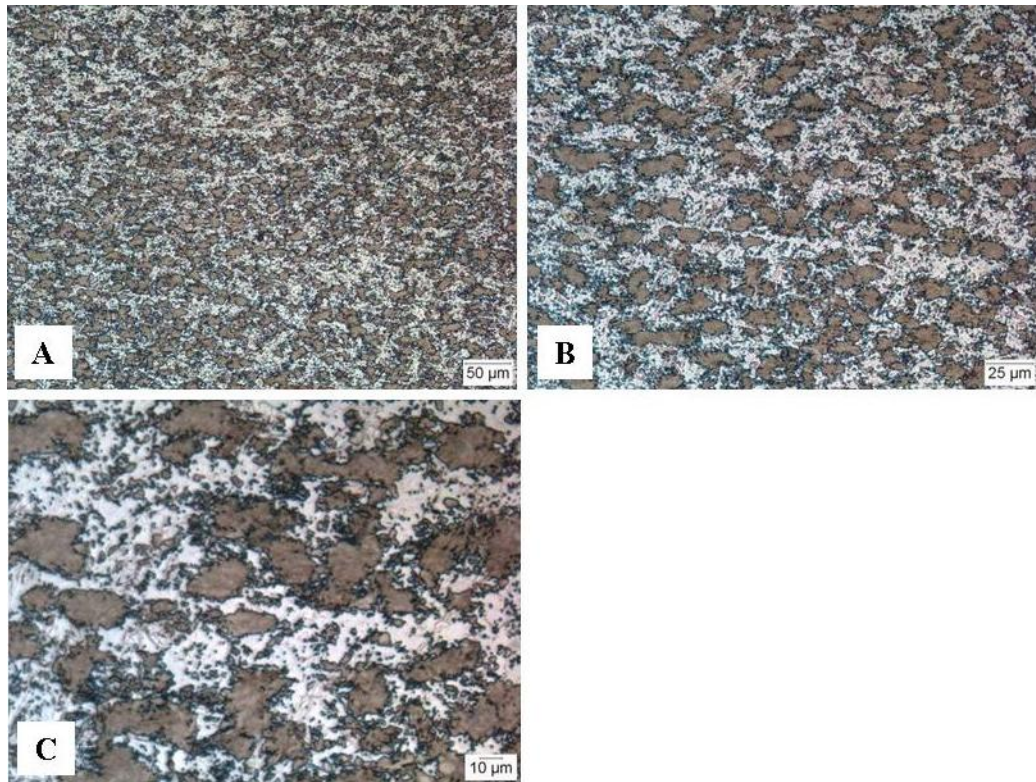


**Figure 83: C.P. Ti Trial No. 2080 weld centerline: A – 20X; B – 40X; C – 100X.**

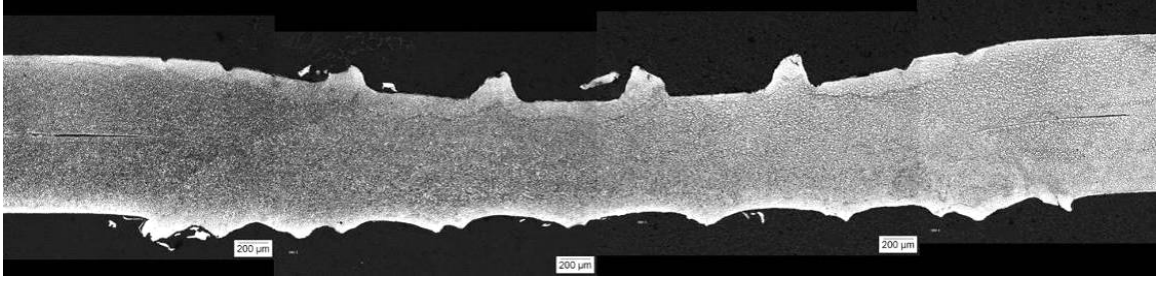


**Figure 84: Cross-section of C.P. Ti Weld Trial No. 2081**

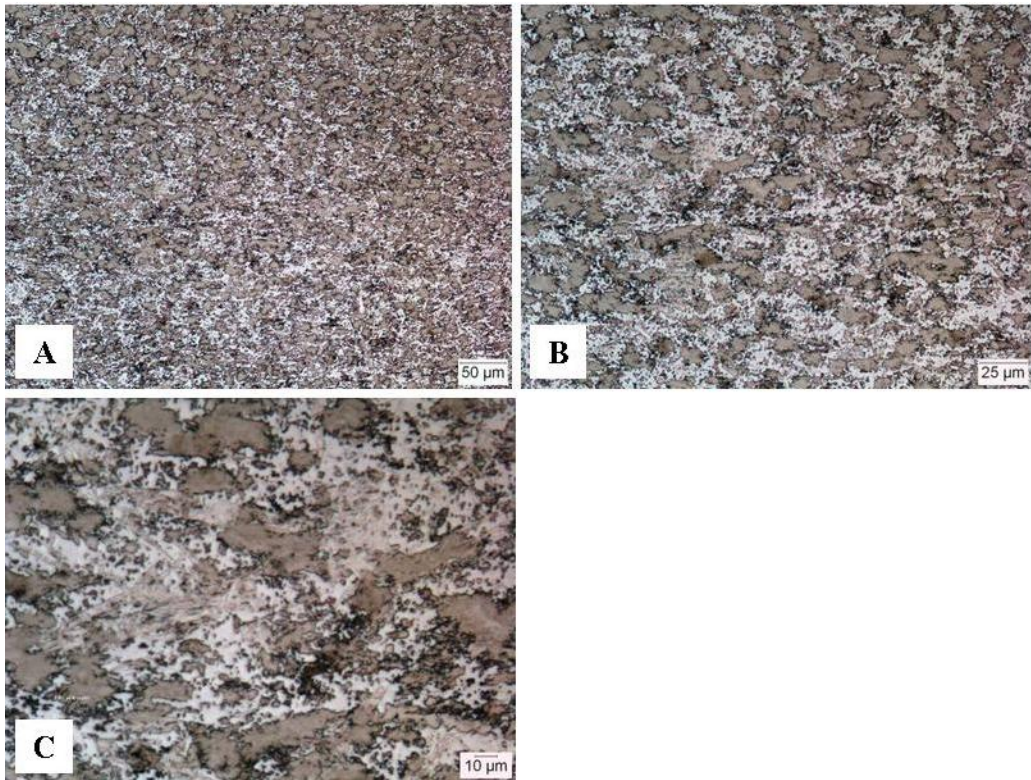


**Figure 85: C.P. Ti Trial No. 2081 weld centerline: A – 20X; B – 40X; C – 100X.**

#### 6.1.4 TITANIUM 6AL-4V

Figure 86 through Figure 95 are micrographs from Titanium 6Al-4V welds. The microstructures indicate the weld exceeded the beta transus temperature (970°C). Sections of welds with shorter times have fine beta grains and acicular alpha-plates restricted within single grains. The micrographs of trials 3026 and 3027, in Figure 90 and Figure 92, respectively, have what appear to be centerline stringers, but are more than likely lapping of the material due to mechanical deformation. Trial 3027, however, was made with higher energy, which caused shearing of the base metal. The micrographs in Figure 95 are of residual segregation from the original microstructure. The beta-phase did not have time to fully homogenize. Overall, the titanium sections reveal a very high quality weld due to high levels of mechanical deformation dissociations of oxides.

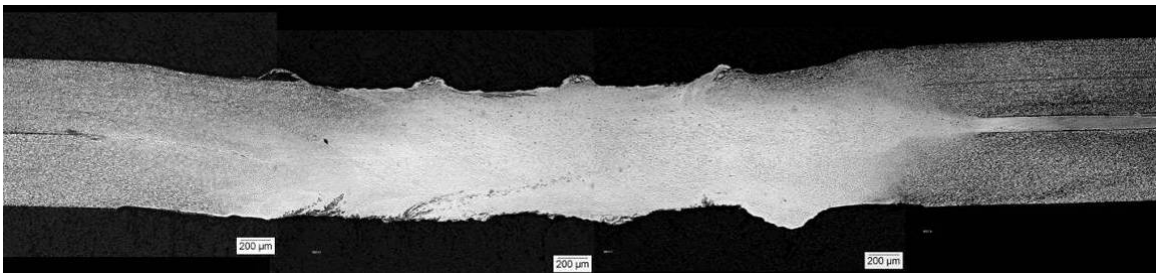


**Figure 86: Cross-section of Ti 6Al-4V Weld Trial No. 3023**

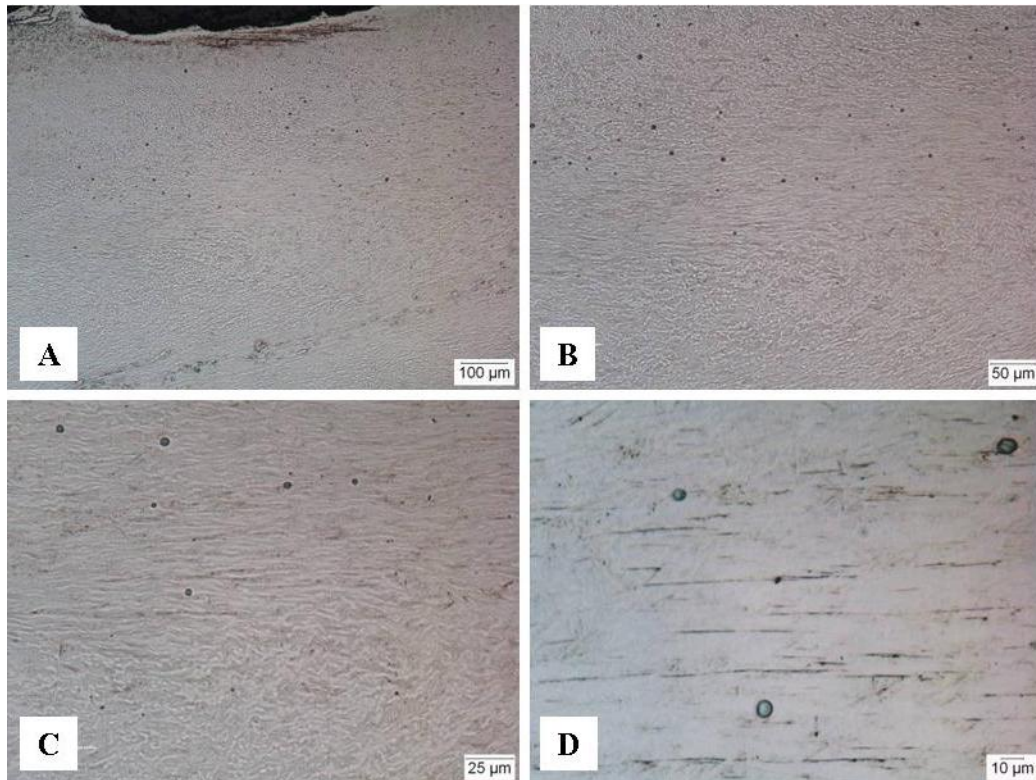


**Figure 87: Ti 6-4 Trial No. 3023 weld centerline: A – 10X; B – 20X; C – 40X; D – 100X.**

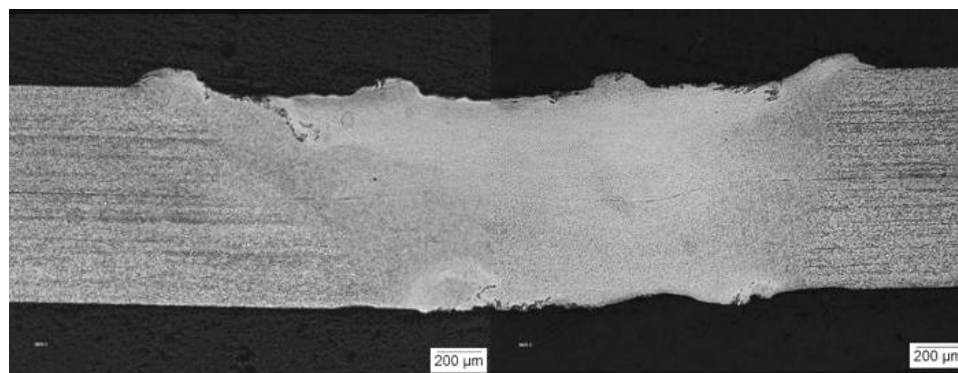


**Figure 88: Cross-section of Ti 6Al-4V Weld Trial No. 3025**

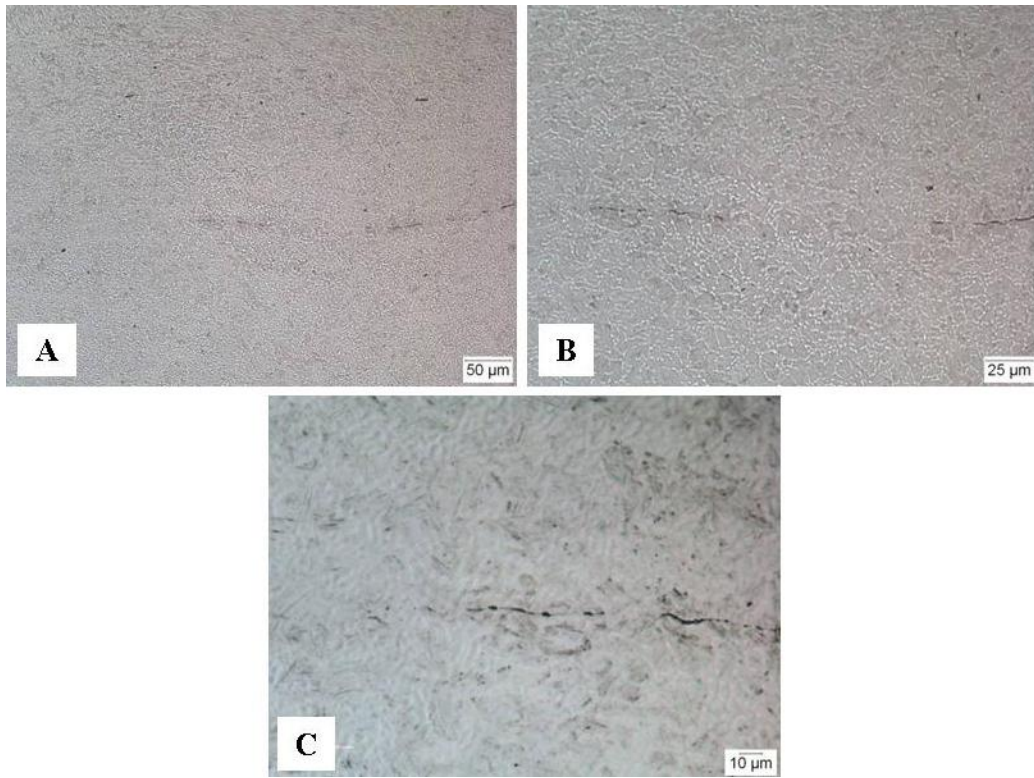


**Figure 89: Ti 6-4 Trial No. 3025 weld centerline: A – 20X; B – 40X; C – 100X**

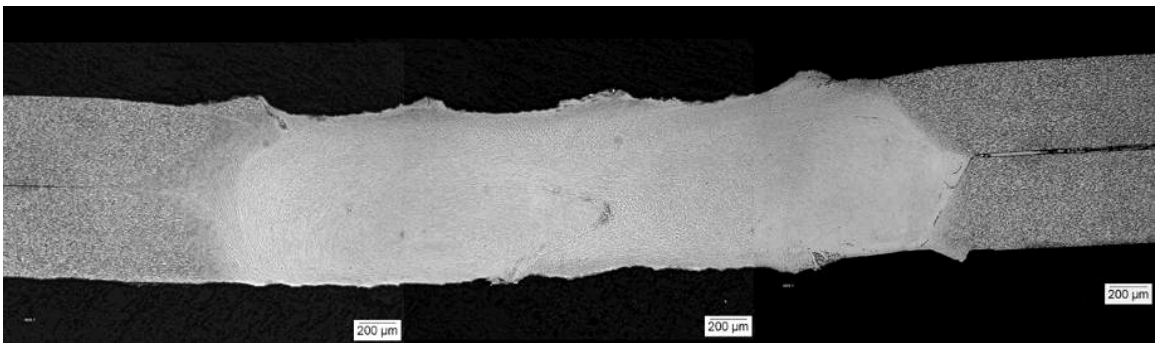


**Figure 90: Cross-section of Ti 6Al-4V Weld Trial No. 3026**

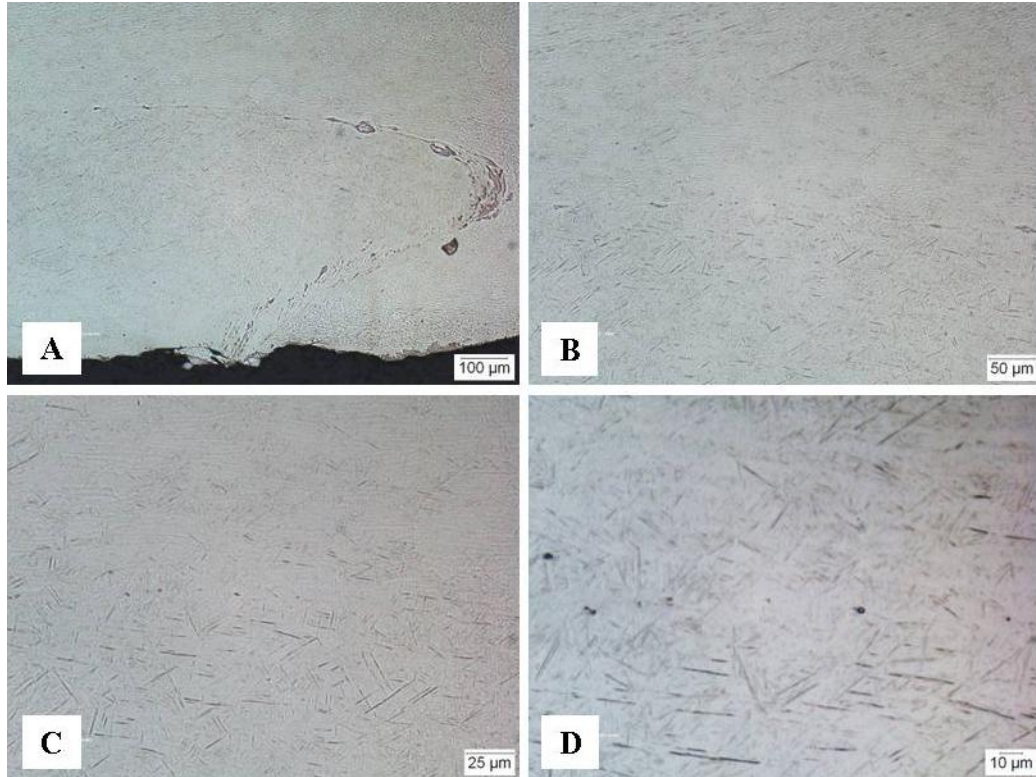


**Figure 91: Ti 6-4 Trial No. 3026 weld centerline: A – 10X; B – 20X; C – 40X; D – 100X.**

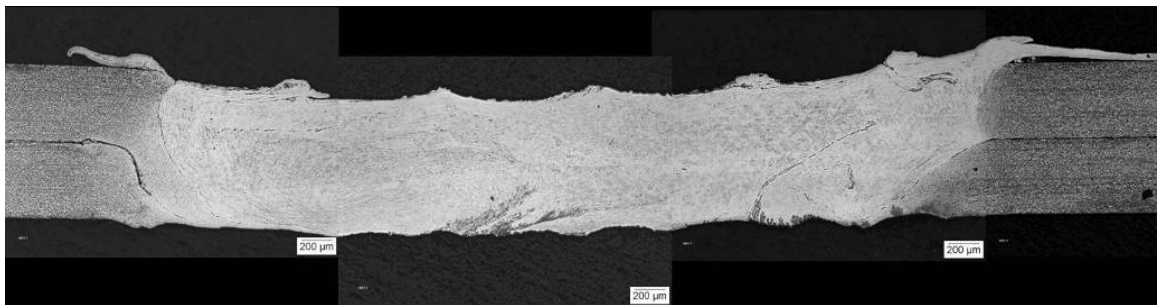


**Figure 92: Cross-section of Ti 6Al-4V Weld Trial No. 3027**

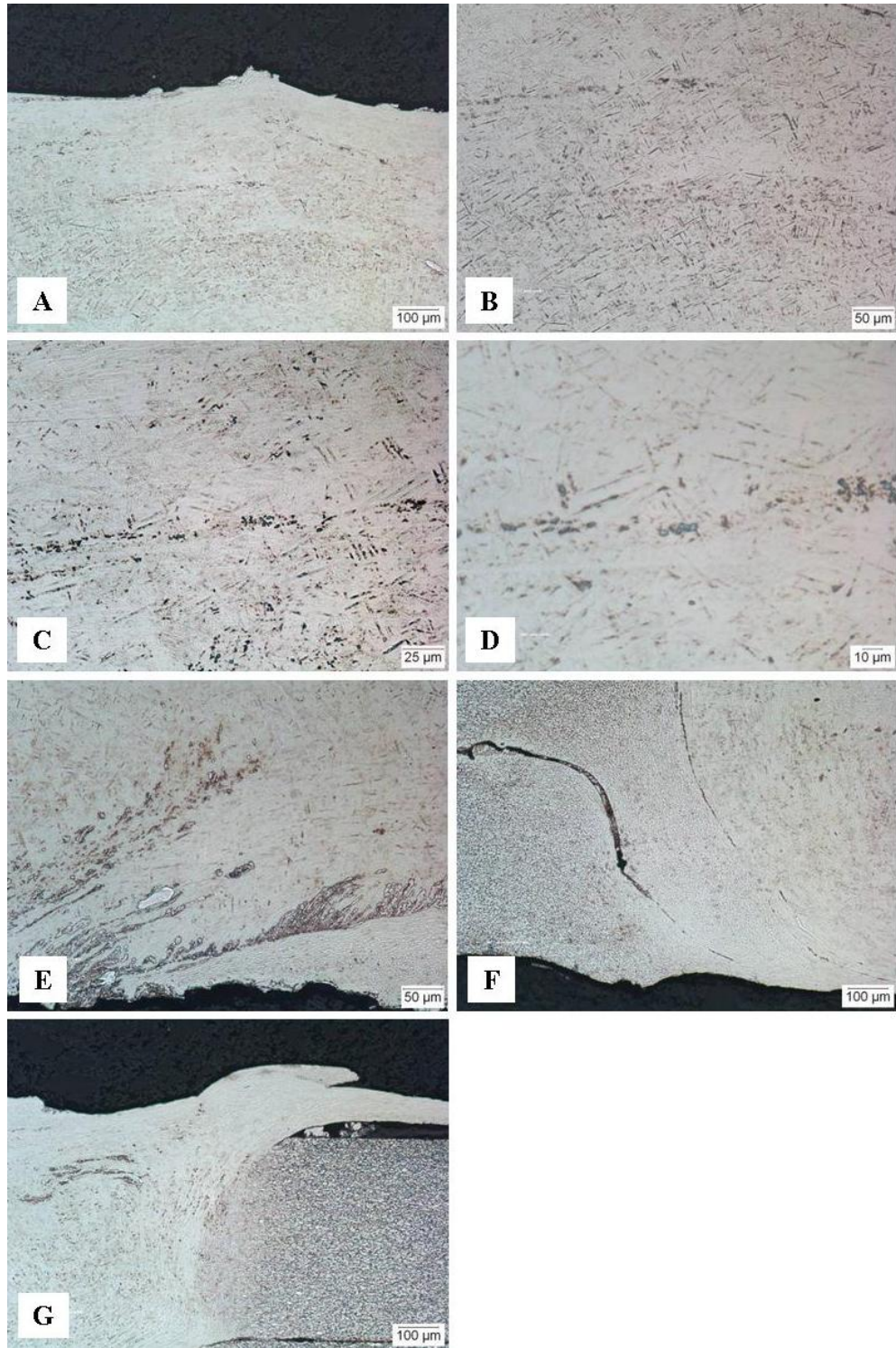


**Figure 93: Ti 6-4 Trial No. 3027 weld centerline: A – 10X; B – 20X; C – 40X; D – 100X, anvil interface: E – center at 20X; F – left side at 10X, G – left side tip interface at 10X.**

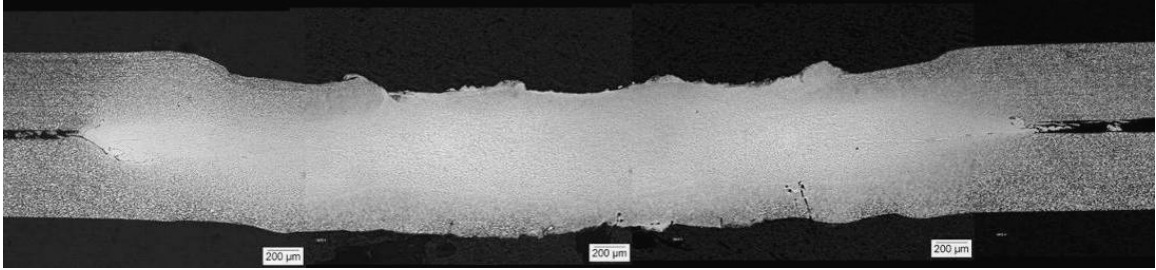


**Figure 94: Cross-section of Ti 6Al-4V Weld Trial No. 3029**

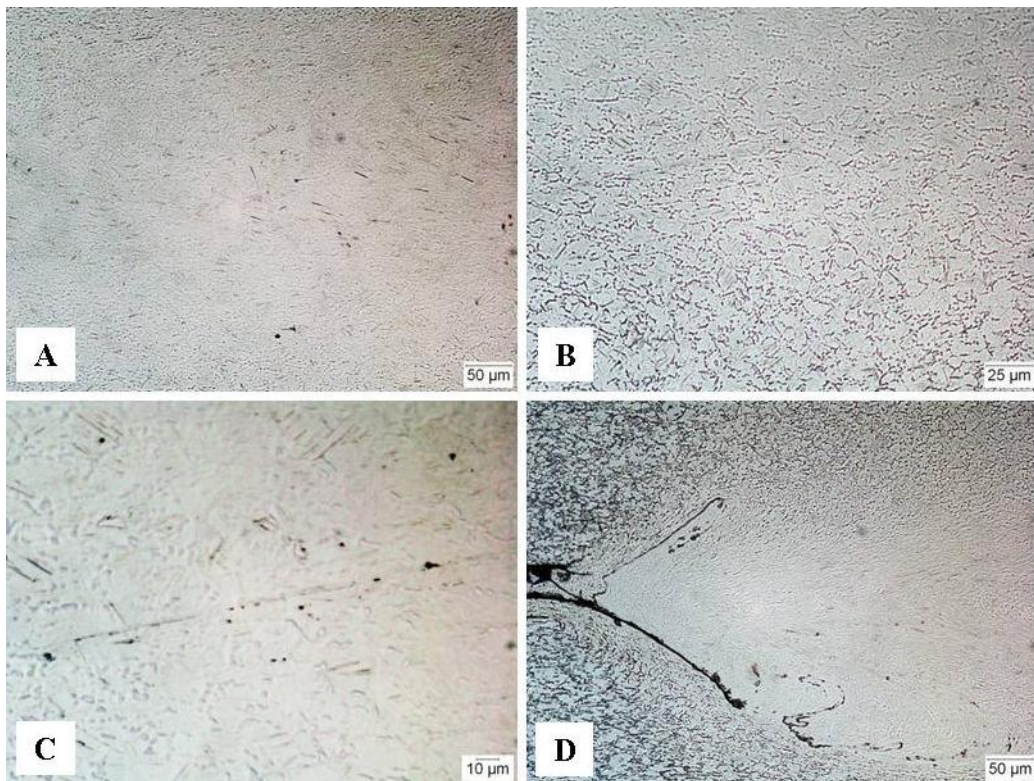


**Figure 95: Ti 6-4 Trial No. 3029 weld centerline: A – 20X; B – 40X; C – 100X, D – left side weld at 20X.**

### 6.1.5 NICKEL 625

Two Nickel Alloy 625 welds were sectioned. Figure 96 and Figure 97 is a section of trial 7000. Figure 98 and Figure 99 is a section of trial 7003. Trial 7003 was created with higher energy and clamping force than trial 7000, and is predicted to have a higher strength. The etched interfaces appear to have little evidence of a bond, but a similar weld recorded a peak tensile force approaching 800-lbf.

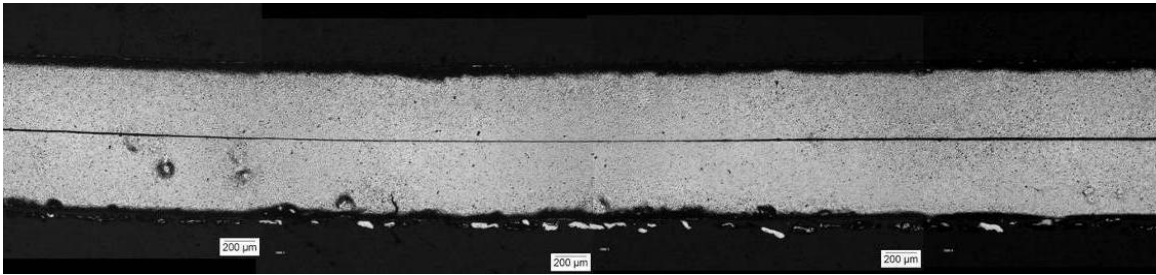


**Figure 96: Cross-section of Ni 625 Weld Trial No. 7000**

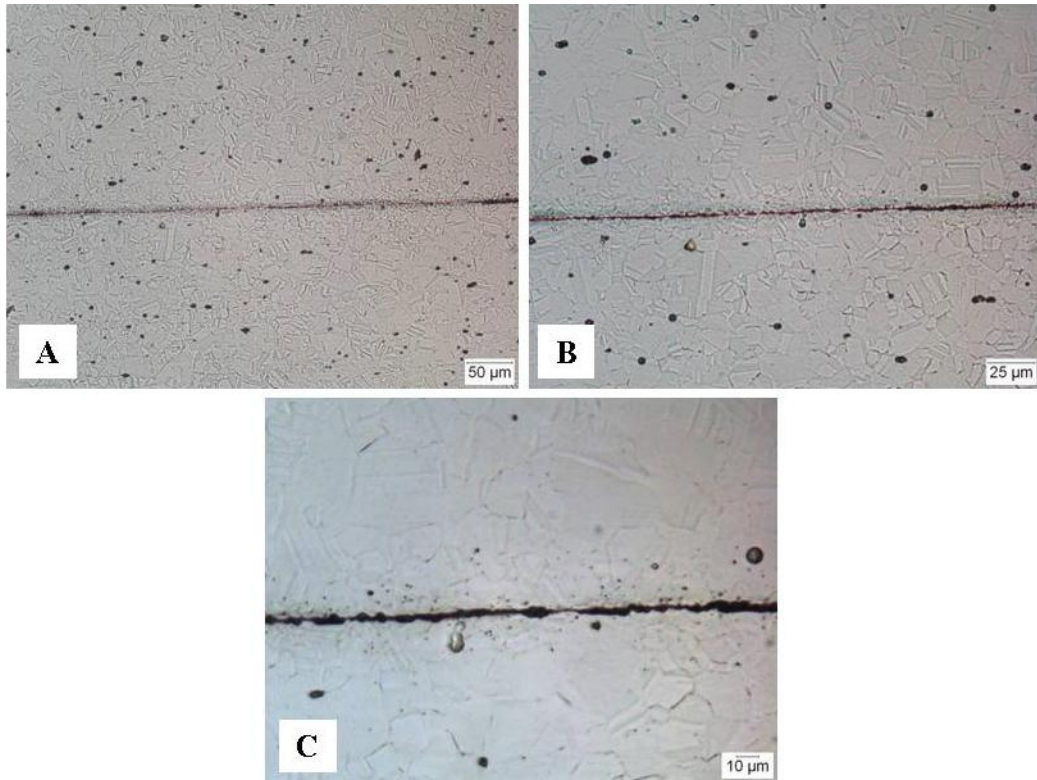


**Figure 97: Ni 625 Trial No. 7000 weld centerline: A – 20X; B – 40X; C – 100X.**

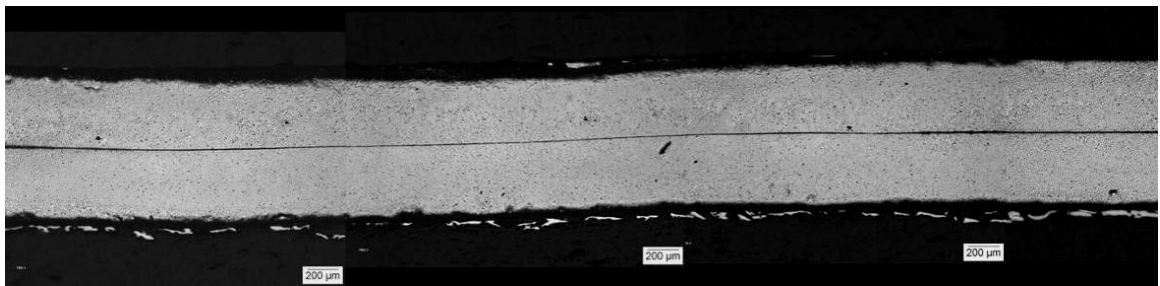


**Figure 98: Cross-section of Ni 625 Weld Trial No. 7003**

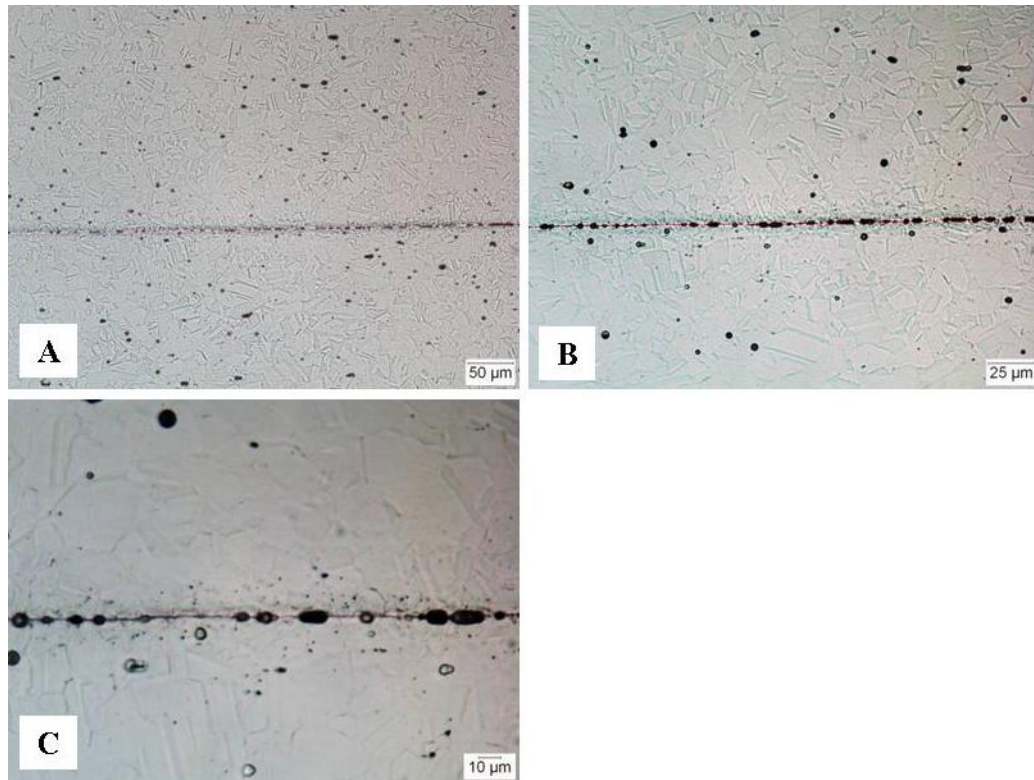


**Figure 99: Ni 625 Trial No. 7003 weld centerline: A – 20X; B – 40X; C – 100X.**

#### 6.1.6 NICKEL 718

The micrographs in Figure 100 and Figure 101 are of a Nickel 718 weld at high energy and clamping force. The bond is interfacial and has evidence of grain growth across the interface. At the tool interface, several areas have with slip lines indicative of the orientation of stresses.

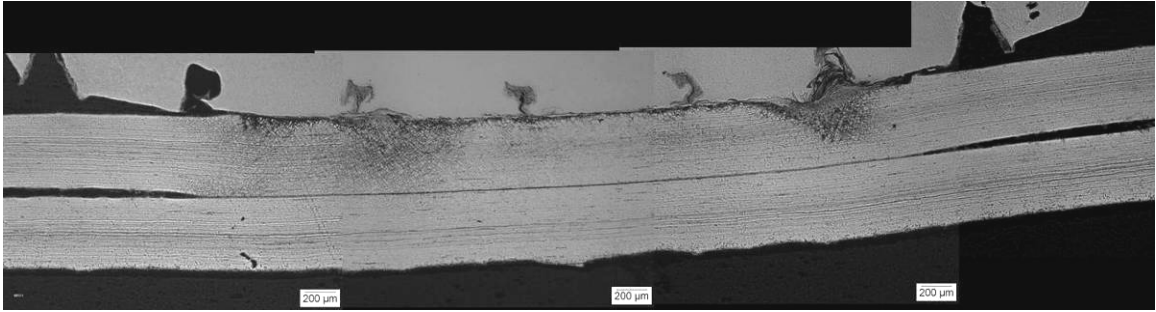


**Figure 100: Cross-section of Ni 718 Weld Trial No. 6013**

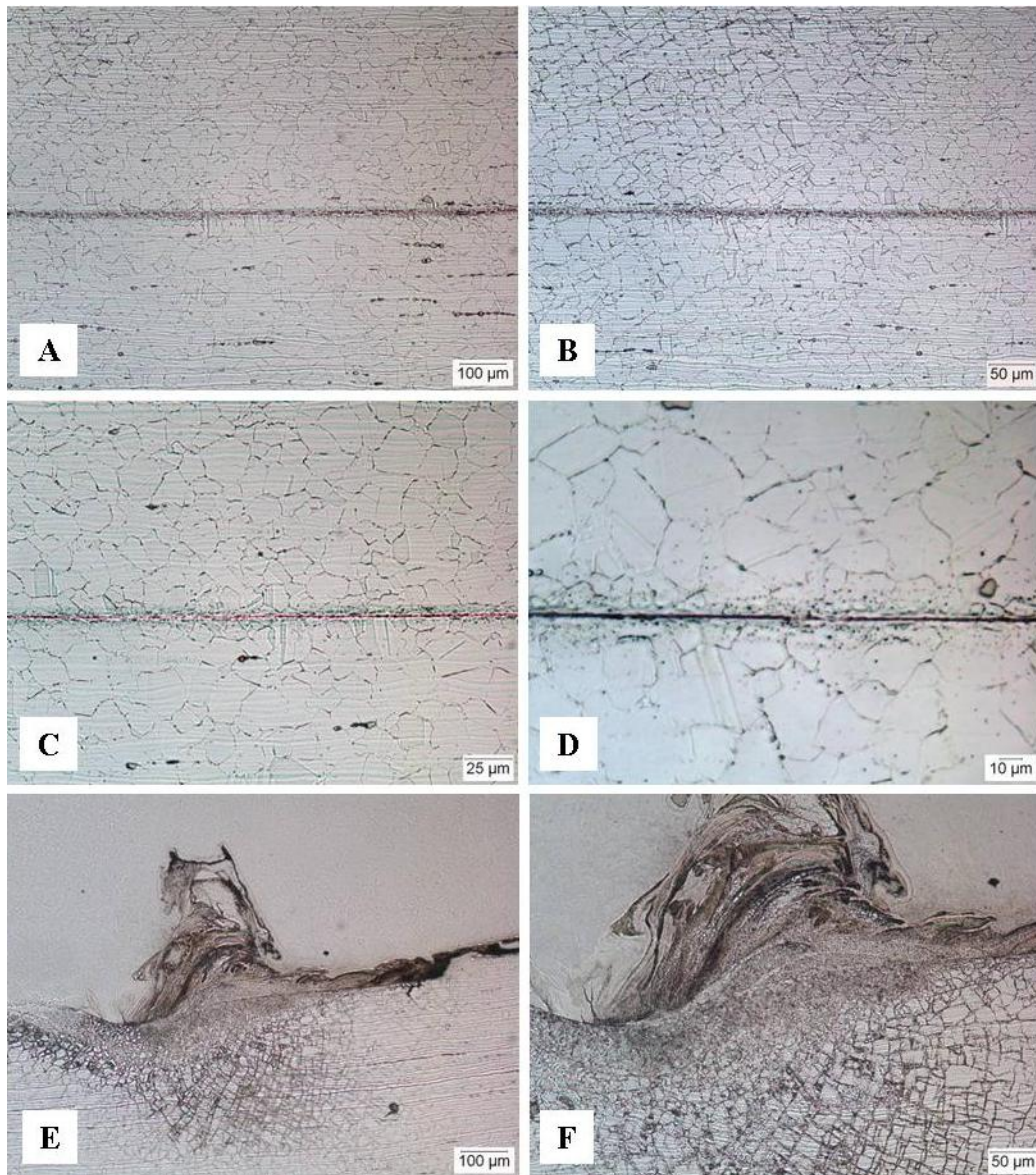


**Figure 101: Ni 718 Trial No. 6013 weld centerline: A – 10X; B – 20X; C – 40X; D – 100X, right side tip interface: E – 10X; F – 20X.**

## 6.2 FRACTOGRAPHY

A weld from each alloy with an interfacial-fracture surface was selected for fractography. The welding parameters for the six tensile tested weld fracture surfaces are listed in Table 10. Figure 102 is a picture of the samples prior to loading in the SEM. The characterization of the fracture surfaces depends on the exact location that is observed. With small differences in location, a large difference in the fracture surface was observed. For each alloy, a low-magnification picture (12-14X) was first taken so that the location of the high magnification images could be recorded.

Material	Trial	Actual Energy (J)	Clamping Force (lbf)	Time (s)	Power (W)	Tensile Force (lbf)	Extension (in)	Tooling Material	Comments
SS 304	<b>4062</b>	1203	177	0.46	3540	610	0.066	W-25Re	Sticking-to-tip, glow during welding
SS 410	<b>5086</b>	1507	177	0.60	3585	728	0.048	W-La	Long weld, glow orange-hot, sticking-to-tip
C.P. Ti	<b>2070</b>	214	374	0.15	3570	528	0.046	350M	Fast, sticking-to-anvil, small weld diameter
Ti 6-4	<b>3031</b>	565	242	0.26	3510	1176	0.055	Wrought-W	White sparks from tip interface, sticking-to-tip
Ni 625	<b>7002</b>	1001	571	1.08	1680	789	0.049	350M	New 350M tip and worn 350M anvil from Trial 7001 oxidized w/ an oxy-acetylene torch prior to weld, long weld, glow red-hot, no sticking-to-anvil, sticking-to-tip, larger diameter weld than Trial 7002
Ni 718	<b>6012</b>	601	440	0.72	1380	588	0.039	350M	New 350M tip, anvil from Trial 6011, glow red-hot, no sticking-to-anvil, strong sticking-to-tip, tip cut-off in order to further evaluate weld

**Table 10: Welding parameters for SEM fracture surfaces**

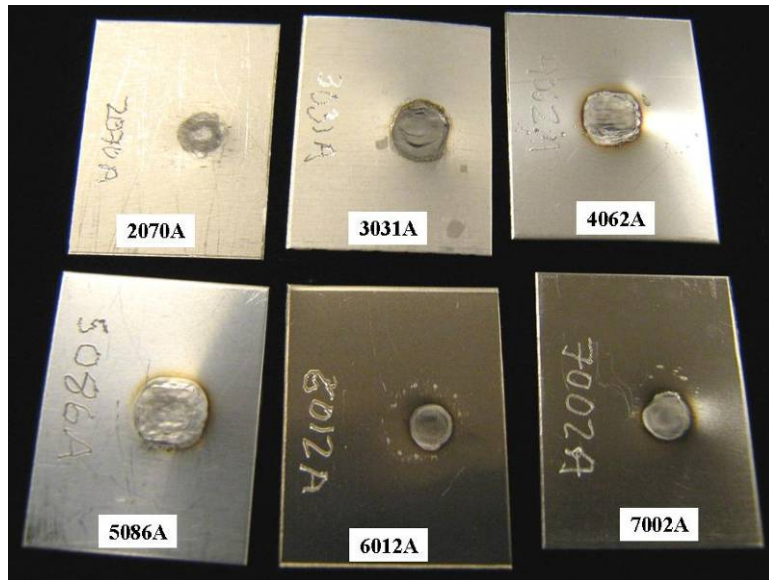


**Figure 102: Fracture surfaces for SEM, anvil/ lower coupon side of interface**

### 6.3 TYPE 304 STAINLESS STEEL

The 304 stainless steel fracture surfaces in Figure 103 and Figure 104 had a blurry-white appearance due to the presence of an oxide layer. Location '1' appears to be a non-bonded or mixed failure mode. Location '2' is a dimple-rupture failure mode.

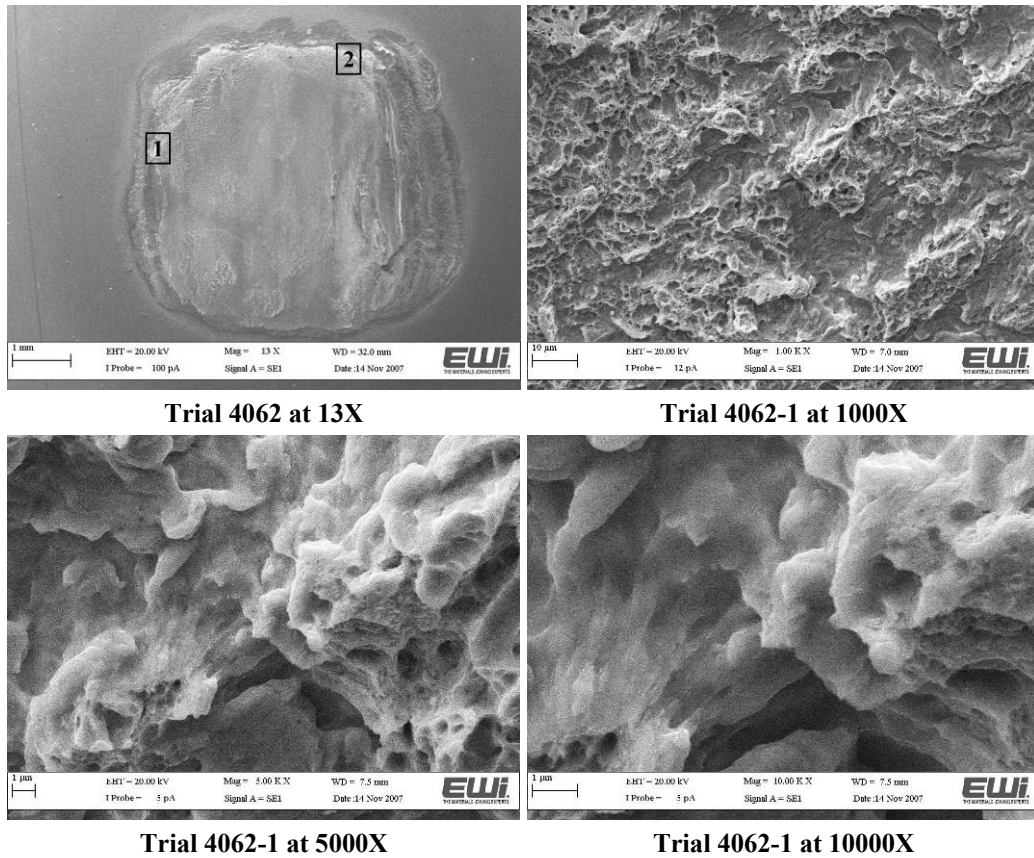
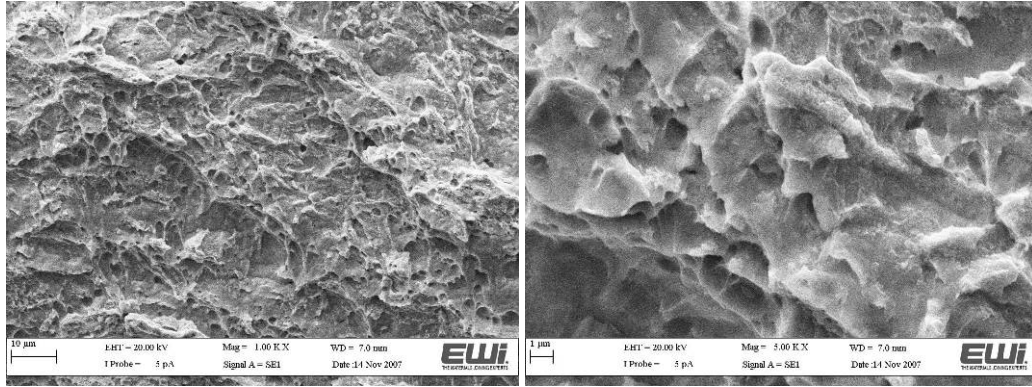
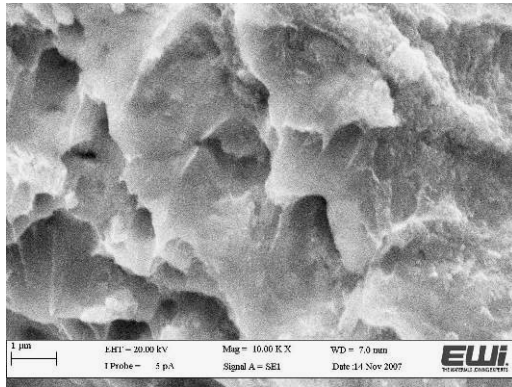


**Figure 103: SEM Fracture surface from SS304 trial 4062, location 1**



**Trial 4062-2 at 1000X**

**Trial 4062-2 at 5000X**

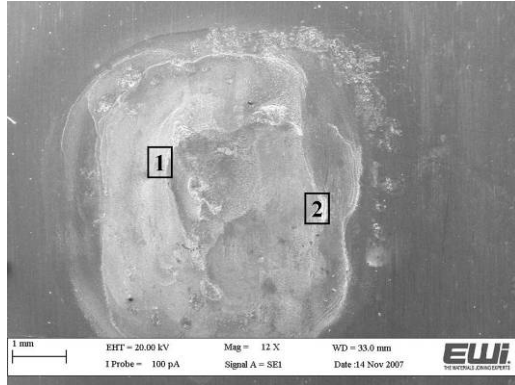


**Trial 4062-2 at 10000X**

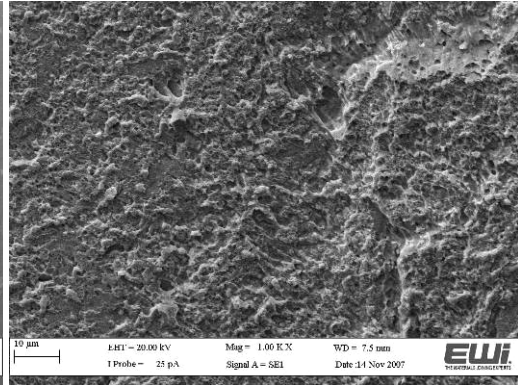
**Figure 104: SEM Fracture surface from SS304 trial 4062, location 2**

### 6.3.1 TYPE 410 STAINLESS STEEL

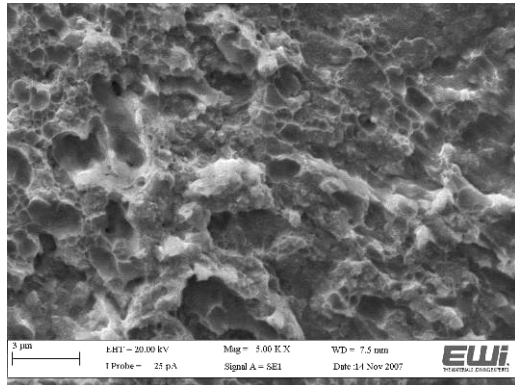
The 410 stainless steel fracture surfaces are arranged in Figure 105. Location ‘1’ appears to be a non-bonded surface that was subject to some amount of mechanical deformation. Location ‘2’ includes a mixed fracture surface, but is predominately dimple rupture.



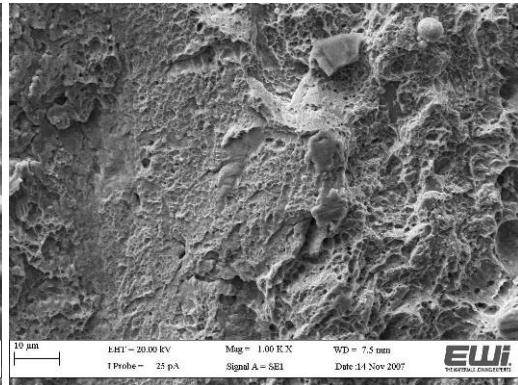
**Trial 5086 at 12X**



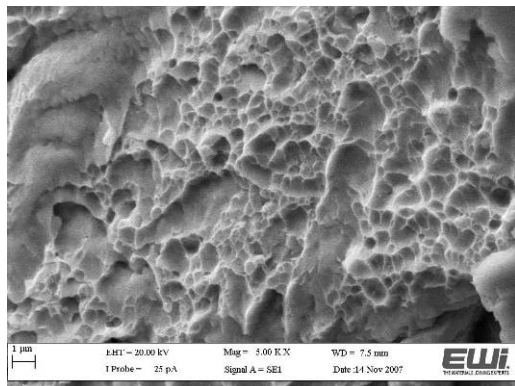
**Trial 5086-1 at 1000X**



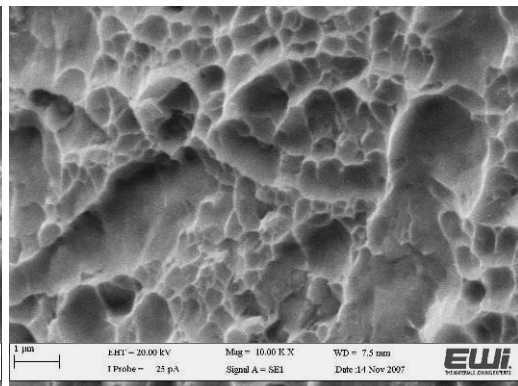
**Trial 5086-1 at 5000X**



**Trial 5086-2 at 1000X**



**Trial 5086-2 at 5000X**

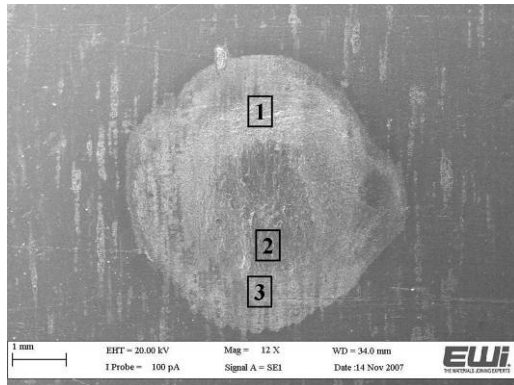


**Trial 5086-2 at 10000X**

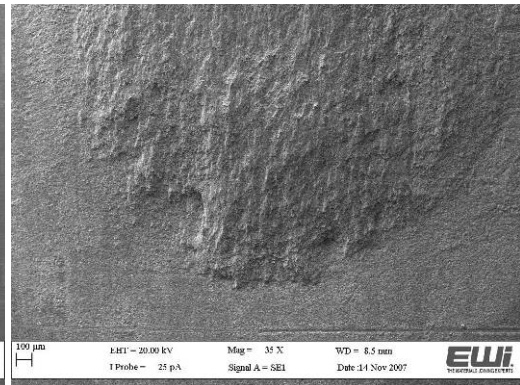
**Figure 105: SEM Fracture surface from SS410 trial 5086**

### 6.3.2 C.P. TITANIUM

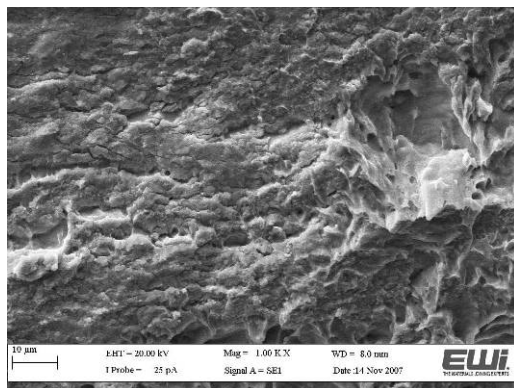
The commercially-pure titanium fracture surface is shown in Figure 106 and Figure 107. Location '1' and '3' are of a non-bonded or low-strength interface. The bright white spots are oxides that were not removed, which may help to support the conclusion that at these locations, the interface has been subject to mechanical scrubbing, but not enough to remove the oxide layers and begin the welding process. Location '2' is characteristic of the majority of the bonded surface. The entire center region of the weld consisted of a dimple-rupture failure mode.



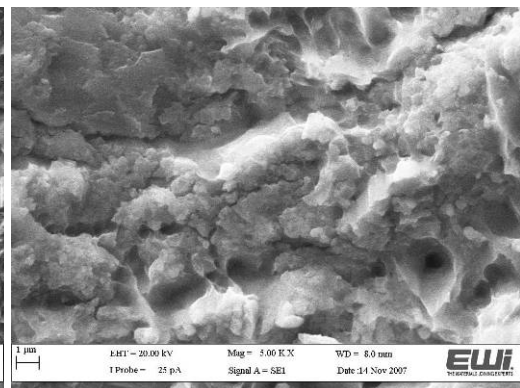
**Trial 2070 at 12X**



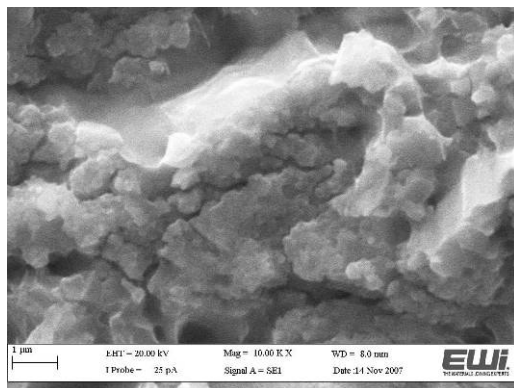
**Trial 2070 at 35X, Lower-half**



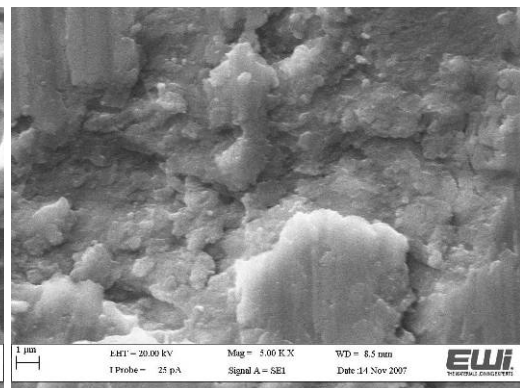
**Trial 2070-1 at 1000X**



**Trial 2070-1 at 5000X**



**Trial 2070-1 at 10000X**



**Trial 2070-3 at 5000X**

**Figure 106: SEM Fracture surface from CP Ti trial 2070, locations 1 & 3**

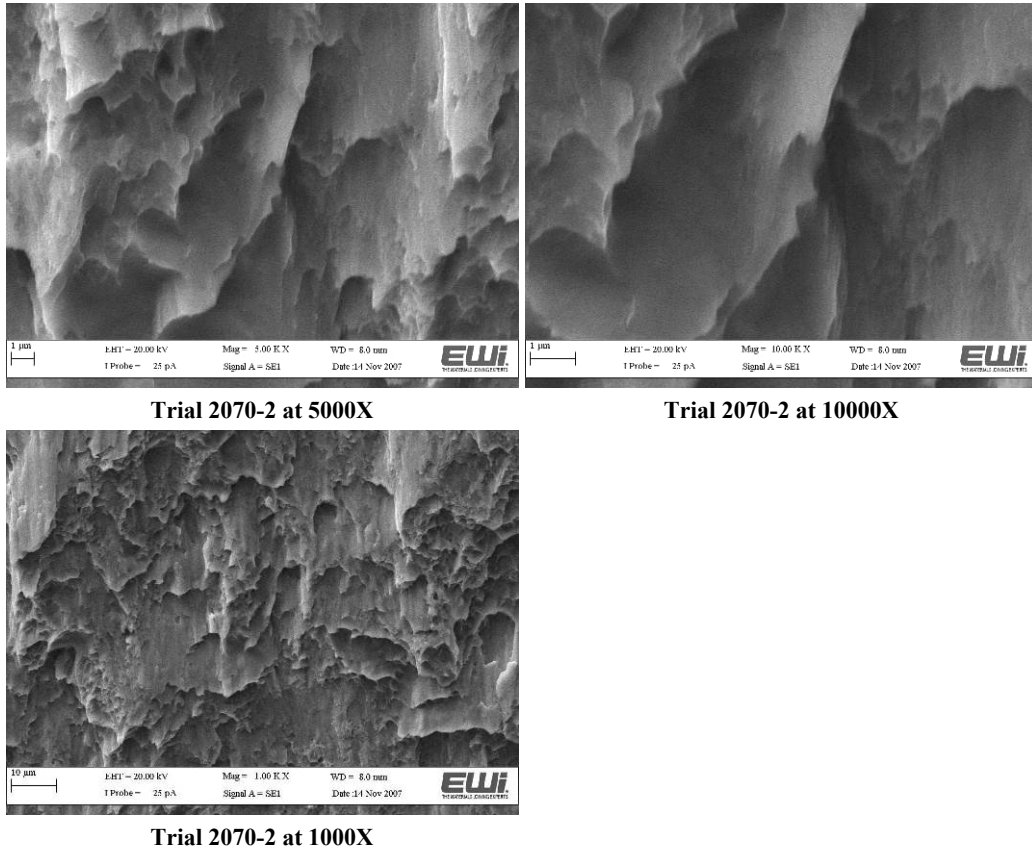
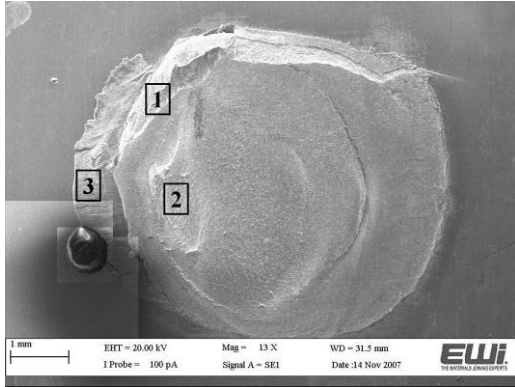


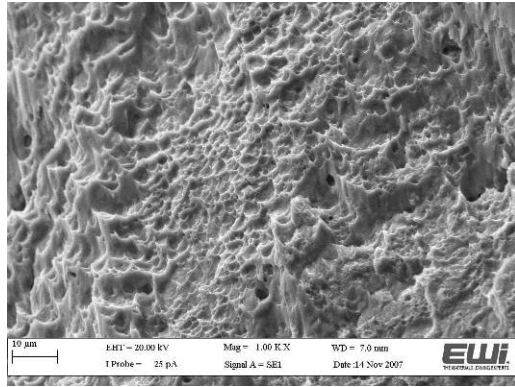
**Figure 107: SEM Fracture surface from CP Ti trial 2070, location 2**

### 6.3.3 TITANIUM 6AL-4V

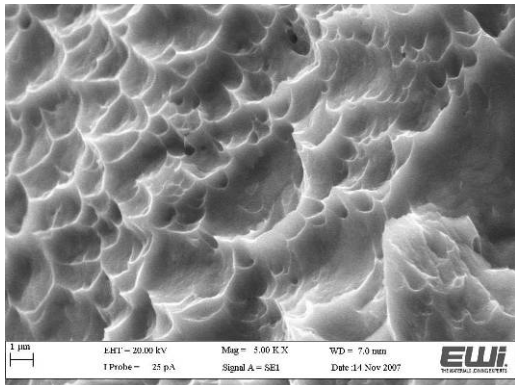
The titanium 6Al-4V images, shown in Figure 108, were taken at a number of locations across the fracture surface. In the low-resolution picture, the dark spot in the lower left-hand corner is due to the presence of a foreign contaminant, and should be ignored. Near the location ‘1’ and ‘2’, dimple rupture surfaces of different orientations and size were observed. This indicates the strain applied to the joint during testing was non-uniform, possibly due to a moment created during testing. Location ‘3’ is a non-bonded surface.



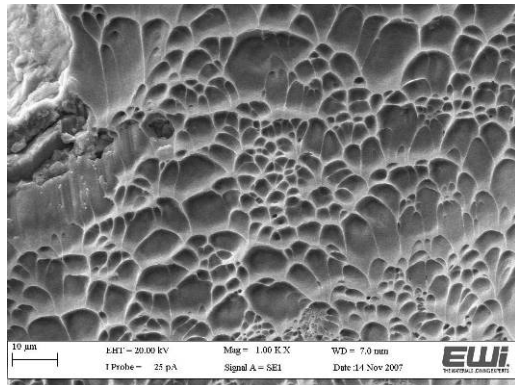
**Trial 3031 at 13X  
(foreign particle in lower left corner)**



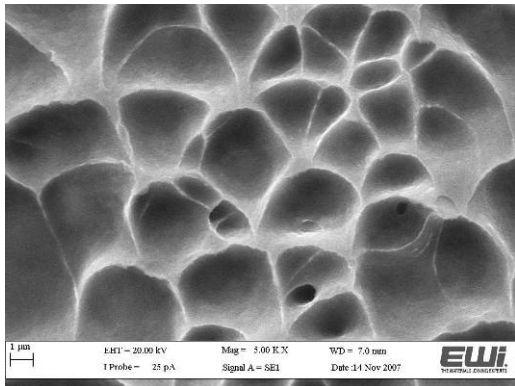
**Trial 3031-1 at 1000X**



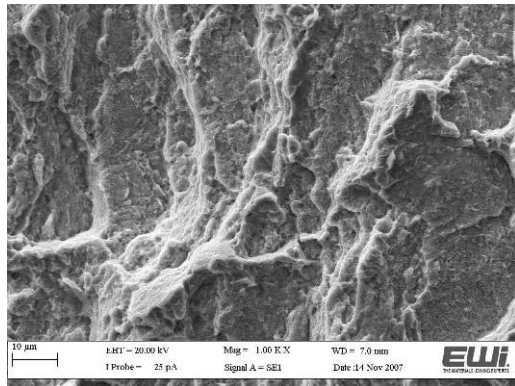
**Trial 3031-1 at 5000X**



**Trial 3031-2 at 1000X**



**Trial 3031-2 at 5000X**



**Trial 3031-3 at 1000X**

**Figure 108: Titanium 6Al-4V SEM Weld Fracture Surface Pictures**

### 6.3.4 NICKEL ALLOY 625

Figure 109 has fracture surfaces from a nickel 625 weld. The bond is only along the circumference of the welding area. Location '2' and '3' are of non-bonded areas or may be a variation of flutes. Location '1' is a mixed-failure mode, predominately dimple rupture.

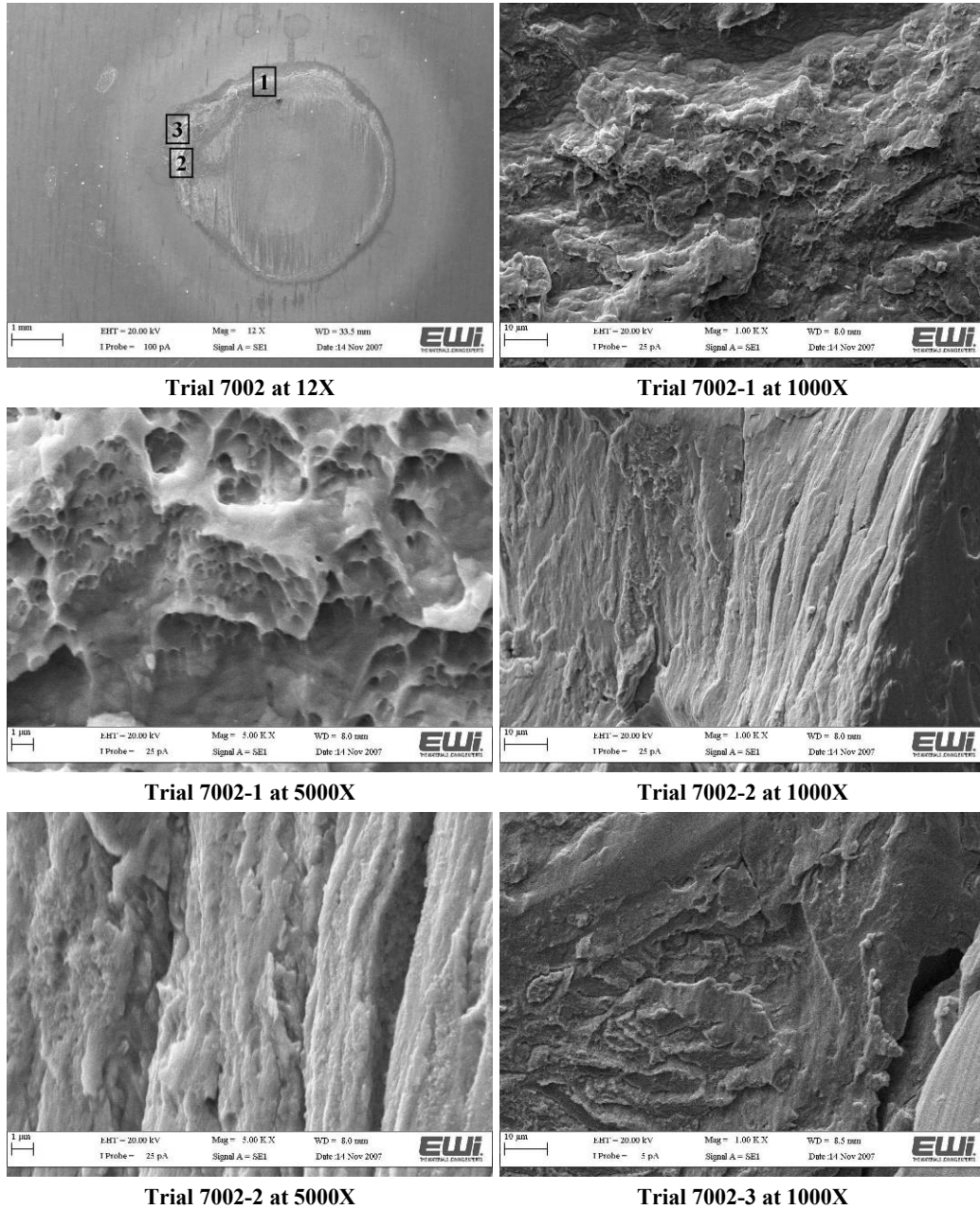
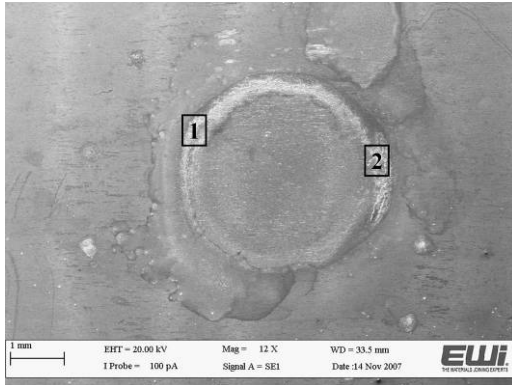


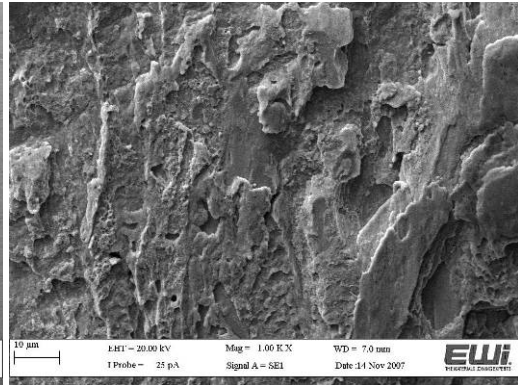
Figure 109: Nickel 625 SEM Weld Fracture Surface Pictures

### 6.3.5 NICKEL ALLOY 718

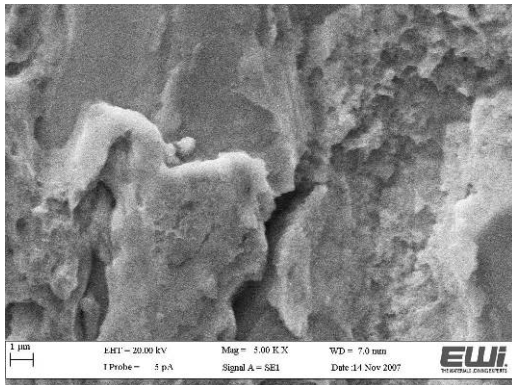
The fracture surface of a nickel 718 weld is shown in Figure 110. Similar to that seen with the nickel 625 fracture surface, location '1' includes a non-bonded surface with visible oxide layer. Location '2' is a dimple-rupture surface with different dimple sizes.



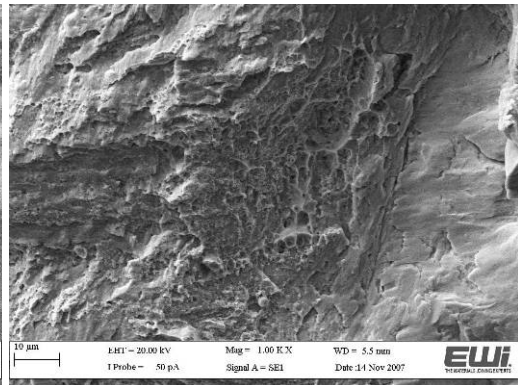
**Trial 6012 at 12X**



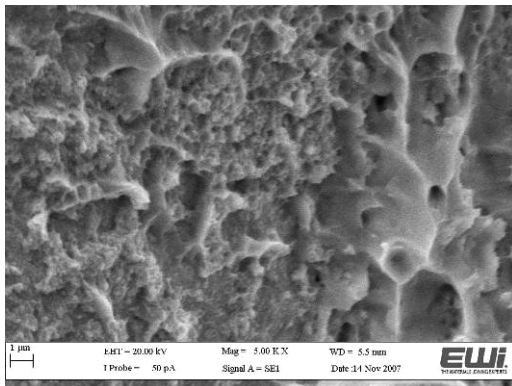
**Trial 6012-1 at 1000X**



**Trial 6012-1 at 5000X**



**Trial 6012-2 at 1000X**



**Trial 6012-2 at 5000X**

**Figure 110: Nickel 718 SEM Weld Fracture Surface Pictures**

## 6.4 SUMMARY

Micrographs of weld cross-sections have been reviewed. The titanium-alloy welds have excellent bond qualities, due to the reactivity at high temperature and the thin oxide layer. Sections of 304 stainless-steel welds had good deformation with a characteristic wavy ultrasonic interface. The ferritic (410) stainless steel, however, required very high energy levels to create a good weld section. Nickel 625 and 718 weld sections had little evidence of deformation, but interaction was visible across the interface at high magnification.

Interfacial weld fracture surfaces from each alloy were observed with the SEM at increasing magnifications. Dimple-rupture fracture surfaces were located in each weld, indicating ductile weld metal. No intermetallics were observed. Just outside the weld area, many of the samples had a non-bonded region that had been subject to mechanical deformation. The presence of oxides at these non-bonded areas supports the stages of the solid-state weld formation. In other words, due to the remaining oxides at some locations, the weld was not initiated.

The titanium alloys featured a uniform, ductile, weld area. The stainless-steel alloys were less uniform, having regions of bonded and non-bonded material throughout. The nickel-based alloys welds had a small circumferential weld area with mixed bonding modes.

## CHAPTER 7

### CONCLUSIONS

This experiment was able to successfully evaluate the weldability of stainless steel 304, stainless steel 410, commercially-pure titanium, and titanium 6Al-4V in detail. Nickel 625 and Nickel 718 were also evaluated, but to a lesser extent.

Tool materials and designs were evaluated. Welds were tensile tested, cross-sections and fracture surfaces evaluated. Energy curves for welding strengths at several clamping forces were developed from designed experiments. High energy and high clamping force welds were not possible due to equipment limitations, however; high-strength welds were still possible utilizing lower clamping forces and high energy. Unfortunately, these parameters generate excessive heat and tool wear, significantly reducing the life of the tools. Tooling and equipment problems created significant scatter in much of the data.

For each alloy in this study, the weld fracture surfaces observed with the SEM had areas of ductile dimple-rupture. Weld cross-sections had varied amounts of deformation and recrystallization, depending on the welding conditions.

A 12.7-mm spherical-radius welding tip with a laser-machined linear knurl, and a flat anvil with either a machined knurl (when possible) or a cross-hatched laser-machined knurl pattern were utilized during this investigation. Refractory-alloy welding tips required braze joints; the best joints were experienced using high-temperature nickel-based braze alloys.

The materials evaluated for ultrasonic tools include: AISI M2 high speed steel, AISI grade 18Ni (350M) Maraging steel, molybdenum TZM, CMW Elkon 100W tungsten, a higher-quality wrought tungsten, tungsten-25% rhenium, and a proprietary tungsten-lanthanum alloy. AISI M2 performs well with high-strength aluminum, but when welding more advance alloys, it fractures and bonds to the work. 350M performed well with the lower-strength metals. A TZM anvil faired well, but a TZM tip fractured after several weld cycles. The TZM anvil had a more ductile wear pattern than the tungsten-alloys. While the tungsten-based alloys outperformed the other tool materials, the different tungsten alloys had varied performance. Elkon 100W was too brittle for use as ultrasonic tooling. The wrought-tungsten and W-25Re wore heavily during the trials, but the wear was gradual and consistent. The wear occurred by fracturing-off small particles, which could be seen bonded to the weld coupon anvil interfaces. The W-La seemed to perform even better, with a more ductile wear than the other tungsten alloys.

In this investigation, titanium alloys were clearly the most weldable. It was common to pull buttons out during tensile testing, accompanied by high tensile strengths similar to the base material. C.P. Ti welds achieved tensile strengths above 800-lbf for 400 to 500-lbf clamping force and 600-J energy. Ti 6Al-4V welds made at 240 to 440-lbf clamping force and 500 to 700-J energy had the greatest strengths in the experiment, exceeding 1250-lbf.

SS 410 appears to be slightly more weldable than SS 304, but the statistical analysis is not good enough to do so with a high level of confidence. SS 410 welds strengths exceeded 800-lbf for 1500-J energy and 175-lbf clamping force. Similarly, SS 304 welds made with 1200-J energy and 175-lbf clamping force had strengths exceeding 700-lbf.

Nickel 625 and 718 were the most challenging materials to weld in this investigation. Weld strengths were comparable with the other alloys, but the actual weld only occurred along a small circumferential ring at the edge of the interface. The bond quality was not as great as the other alloys in this investigation. The nickel-based trials were detrimental to the tooling. It is

concluded that the weldability of a material is influenced by the yield strength, and the tenacity of the oxide layer. Titanium is an excellent material for UMW; titanium has a thin oxide that is easily removed by the ultrasonic process. In addition, it is very reactive at elevated temperature, enhancing the interaction at the weld interface. Nickel-based alloys, as well as stainless steels, have a tenacious chromium oxide layer that needs to be removed in order to initiate the weld.

During these welds, the tip and the top-coupon interface near the tip were observed to glow red-hot. With the titanium and stainless steel alloys, this indicates temperatures approaching 1000°C. At these temperatures, the yield strengths substantially decrease, allowing the formation of an ultrasonic weld. The nickel-based alloys, however, have exceptional high-temperature strengths, meaning the yield strength will not decrease with temperature like other alloys. This, in combination with the tenacious oxide layer, made nickel-based alloys the most difficult-to-weld metal in this study. Even with this said, a limited number of welds were possible with excessive tool wear or sticking to the tooling. Nickel alloy 625 reached almost 800-lbf at 575-lbf clamping force and 1000-J energy. Nickel alloy 718 reached almost 600-lbf peak tensile at 600-J energy and 450-lbf clamping force.

The weld trials in this investigation demonstrate the feasibility of ultrasonic metal welding for advanced alloys. Tool materials in these trials performed relatively good, especially when compared to the performance of more conventional tool materials.

## CHAPTER 8

### FUTURE WORK

The results of this work are very promising. A strong case for higher-powered ultrasonic equipment has been developed. While the depth of ultrasonic tooling research has been greatly expanded, it is believed that this may only be the start of the tooling experiments that are necessary to establish UMW for advanced alloys. The metallurgical evaluations in this investigation were relatively limited, and a more detailed metallurgical analysis is recommended.

The advancement of ultrasonic welding power levels is traditionally restricted to the amount of power the transducers can handle before failure. The equipment used in this study was limited to 3.6-kW. To date, 20-kHz transducers are available at power levels above 8-kW. This, combined with an “over-under” system, where ultrasonic vibrations are applied to both the tip and the anvil (out of phase), suggests that components are commercially available to manufacture a 16-kW UMW system. The power required to weld materials is not well defined because high weld energy welds can often take advantage of an otherwise incapable welding system. However, it is clear that a higher-powered ultrasonic system would allow welds in more advanced materials with thicker cross-sections.

This work made significant progress into ultrasonic tool development. The refractory-based alloys appear to be most promising. There are countless other tungsten-based alloys that may have significant potential for ultrasonic tooling that have not been evaluated. It is recommended that future investigations evaluate tool materials under identical welding conditions

to directly compare their relative performance. It is also recommended that alternative methods for evaluating tool materials are considered, such as a tapered fit joint, instead of a brazed joint, to allow the tips evaluated to be easily changed out.

This investigation has made significant developments concerning ultrasonic weldability and tooling. Investigations continuing this line of work should make-use of higher-powered equipment and continue to evaluate alternate tool materials.

## BIBLIOGRAPHY

1. Graff, K., et al., *Development of Advanced Joining Processes for AHSS and UHSS*. 2007, Edison Welding Institute (EWI): Columbus.
2. Graff, K., *Ultrasonic metal welding*, in *New developments in advanced welding*, N. Ahmed, Editor. 2005, Woodhead: Cambridge. p. 241-269.
3. Graff, K., *Introduction to High Power Ultrasonics*. 1999, Edison Welding Institute: Columbus. p. 91.
4. Mitskevich, A.M., *Ultrasonic Welding of Metals*, in *Physical Principles of Ultrasonic Technology*, L.D. Rozenberg, Editor. 1973, Plenum Press: Moscow. p. 101-238.
5. AWS, *Welding Processes: Ultrasonic Welding*, in *Welding Handbook*, R.L. O'Brien, Editor. 1991, American Welding Society: Miami. p. 783-812.
6. Greitmann, M.J., et al., *Present status and future prospects of special welding processes - Ultrasonic welding*. *Welding and Cutting*, 2003. **55**(5): p. 268-274.
7. deVries, E., *Mechanics and Mechanisms of Ultrasonic Metal Welding, Ph.D. Dissertation*, in *Welding Engineering*. 2004, The Ohio State University: Columbus. p. 253.
8. Wagner, J., U. Schlicker, and D. Eifler, *Bond formation during the ultrasonic welding of ceramic with metal*. *Schweissen und Schneiden (Germany)*, 1998. **50**(10): p. 636, 638, 640-642.
9. Kuprys, T., J. Janutėnienė, and R. Didžiokas, *Strength of copper wire connections welded by ultrasonic*. *Mechanika (Kaunas)*, 2007. **65**(3): p. 30-33.

10. Born, C., G. Wagner, and D. Eifler, *Ultrasonically Welded Aluminum foams/ Sheet Metal - Joints*. Advanced Engineering Materials, 2006. **8**(9): p. 816-820.
11. Tylecote, R.F., *The solid phase welding of metals*. 1968, New York: St. Martin's Press. 334.
12. Gould, J.E. *Mechanisms of bonding for solid-state welding processes*. in *Advances in Welding Technology, 11th Annual North American Welding Research Conference*. 1996. Columbus, OH 43212, USA: Edison Welding Institute.
13. Callister, W.D., Jr., *Dislocations and Strengthening Mechanisms*, in *Materials Science and Engineering an Introduction*. 2003, John Wiley & Sons, Inc. p. 163-191.
14. Dieter, G.E., *Mechanical Metallurgy*. SI Metric ed. 1988, London: McGraw-Hill Book Company. 751.
15. Brodyanski, A., C. Born, and M. Kopnarski, *Nm-scale resolution studies of the bond interface between ultrasonically welded Al-alloys by an analytical TEM: a path to comprehend bonding phenomena?*, in *13th Applied Surface Analysis Workshop (AOFA 13)*. 2005, Elsevier BV: Dresden, Germany.
16. Ren, W., K. Li, and Z. Feng, *Ultrasonic Welding Distribution Measured with Optical Rosette/ Ring-Core Method*. SAE Transactions: Journal of Materials & Manufacturing, 2005. **114**: p. 547-550.
17. Bay, N., *Mechanisms Producing Metallic Bonds in Cold Welding*. Welding Journal, 1983. **62**(5): p. 137s-142s.
18. Doumanidis, C. and Y. Gao, *Mechanical Modeling of Ultrasonic Welding*. Welding Journal, 2004. **83**(4): p. 140S-146S.
19. Gencsoy, H.T., J.A. Adams, and S. Shigeo, *On Some Fundamental Problems in Ultrasonic Welding of Dissimilar Metals*. Welding Journal, 1967. **46**(4): p. 145s-153s.
20. Lewis, W.J., et al., *Fundamental Studies on The Mechanism of Ultrasonic Welding*. 1960, Battelle Memorial Institute: Columbus. p. 34-43.
21. Weare, N.E. and R.E. Monroe, *Ultrasonic Welding of Heat- Resisting Metals*. Welding Journal, 1961: p. 351-357.

22. Weare, N.E., J.N. Antonevich, and R.E. Monroe, *Fundamental Studies of Ultrasonic Welding*. Welding Journal, 1960. **39**(8): p. 331s-341s.
23. Jahn, R., R. Cooper, and D. Wilkosz, *The Effect of Anvil Geometry and Welding Energy on Microstructures in Ultrasonic Spot Welds of AA6111-T4*. The Metallurgical and Materials Transactions, 2007. **38A**(3): p. 570-583.
24. Trapp, T., et al., EWI. Meeting, 15 June 2007.
25. Ely, K., *Ultrasonic Welding Development for Aluminum Automotive Structures*. 2000, Edison Welding Institute: Columbus.
26. Sorensen, C.D. *Progress in Friction Stir Welding of High Temperature Materials*. in *Proceedings of The Fourteenth (2004) International Offshore and Polar Engineering Conference (ISOPE)*. 2004. Toulon, France: International Society of Offshore and Polar Engineers, P.O. Box 189, Cupertino, CA, 95015-0189, USA.
27. *ASM Handbooks Online*. 2003, ASM International.
28. *MatWeb*. 2007, Automation Creations, Inc.
29. *Wesgo Metals Braze Alloy Selection Chart*. [Table] 2007 [cited 2007 10 September 2007]; Available from: <http://www.wesgometals.com/selec.html>.
30. *NICROBRAZ Technical Data Sheet*. 2005, Wall Colmonoy Corporation: Madison Heights, MI. p. Brazing Filler Metal Selection Chart.
31. Rabinkin, A., Metglas Inc. Telephone conversation, 7 September 2007.
32. Khan, H., C. Kramer, and J. Ocasio, *Ultrasonic Weldability of Aluminum 7075 and Stainless Steel 304*. 2007, The Ohio State University: Columbus.
33. AWS, *Refractory Metals*, in *Brazing Handbook*. 1991, American Welding Society: Miami, FL 33135, USA. p. 381-396.

APPENDIX A

WELD DATA TABLES

The welding parameters, testing results, tooling combinations tested, and comments for the entire series of weld trials are listed in Table 11. The columns are the parameters or variables and the rows are the trial numbers. It is necessary to explain the column labels. The columns for trial number, date, material, and comments are fairly self-explanatory. The other columns are organized into four groups: welding parameters, mechanical testing, regression analysis, and tooling.

Seven columns are dedicated to the welding parameters. Input energy is the desired energy programmed into the controller before the weld cycle. In many cases, due to equipment limitations, the input energy is not actually achieved. Actual energy is the true weld energy. Trigger pressure and weld pressure refer to the amount of pressure applied to the cylinder that generates the clamping force. Trigger pressure relates to the force that is applied prior to activating the ultrasonics during the weld cycle. Weld pressure relates to the amount of force that is applied during the weld cycle. Weld force is the amount of clamping force, and was measured with a spot weld force gauge for each weld pressure. The time is the duration of the weld cycle, excluding any hold times or after bursts. In the event of a weld overload or other system fault, the time is approximated from the power vs. time plot. Power is the peak power level achieved during the weld cycle.

The mechanical testing group includes results from tensile testing, if applicable. The peak force and extension were recorded by an Instron tensile tester. The failure mode is subjective; many welds had mixed failure modes that are not clearly categorized.

The regression analysis group is used to organize the welds for analysis. For the most part, the run order follows the trial numbers. Blocking was organized according to a short, continuous, series of weld trials in which the tooling was not removed and reinstalled, adjusted, modified, or heavily damaged. Some trials were justifiably excluded from analysis. After the regression analysis (based only on run order, actual energy, and welding force), the regression

equations were applied to the “equation for tensile force.” This allows the measured strengths of welds to be compared with the predicted strengths, or to predict the strengths of welds that were selected for metallurgy or otherwise not tested.

The tooling group includes several columns to indicate the design, texture, and material of the tip or anvil used for the weld trial. A key to several common terms and abbreviations used throughout Table 11 is listed in Table 12

Trial	Material	Welding Parameters							Mechanical Testing			Regression Analysis			Tooling				Comments
		Energy (J)	Actual Energy (J)	Trigger Pressure (psi)	Weld Pressure (psi)	Weld Force (lbf)	Time (s)	Power (W)	Peak Force (lbf)	Extension (in)	Failure Mode	Run Order	Blocking	Equation for Tensile Force	Tip Design/ Texture	Tip Material	Anvil Design/ Texture	Anvil Material	
1000	SS 304	400	400	60	60	440	0.33	2175	296	0.009	IF	-	-	-	TD1	TM1	AD1	AM1	Good appearance
1001	SS 304	600	603	60	60	440	0.34	3615	495	0.027	IF	-	-	-	TD1	TM1	AD1	AM1	CA, STA
1002	SS 304	600	607	80	80	571	0.34	3600	577	0.059	IF	-	-	-	TD1	TM1	AD1	AM1	STA, anvil broke, weld looked good
1003	CP Ti	600	616	55	55	403	0.34	3630	853	0.048	IF	-	-	-	TD1	TM1	AD1	AM1	Switched to new anvil, cycle alarm, STA, looks good, significant heat marks
1004	CP Ti	400	410	40	40	308	0.31	3570	699	0.045	B	-	-	-	TD1	TM1	AD1	AM1	STA, less heat marks, pulled button
1005	CP Ti	400	414	80	80	571	0.32	3510	695	0.043	B	-	-	-	TD1	TM1	AD1	AM1	Faster, less heat marks, less sticking, pulled button
1006	Ti 6-4	600	603	80	80	571	0.53	1620	291	0.010	IF	-	-	-	TD1	TM1	AD1	AM1	STT, little weld, very low power
1007	Ti 6-4	600	603	40	40	308	0.40	2520	1025	0.033	IF	-	-	-	TD1	TM1	AD1	AM1	More heat marks, no sticking, more thorough weld
1008	Ti 6-4	1000	1000	40	40	308	1.44	1080	0	0.000	IF	-	-	-	TD1	TM1	AD1	AM1	Very long weld, appearance similar to No. 1006, broke while loading into tensile tester
1009	Ti 6-4	400	401	40	40	308	0.73	720	0	0.000	IF	-	-	-	TD1	TM1	AD1	AM1	Shorter weld, similar to No. 1006 & 1008 in appearance, very low power, broke while loading into tensile tester
1010	Ni 625	600	609	60	60	440	0.52	2685	0	0.000	IF	-	-	-	TD1	TM1	AD1	AM1	Weld broke on removal, STA, broke anvil, welding tip has fatigue cracks across the knurl pattern, awkward power curve
1011	SS 410	400	410	60	60	440	0.21	3540	479	0.020	IF	-	-	-	TD1	TM1	AD1	AM2	STA, good appearance, pry-off anvil

Continued

Table 11: All Weld Data, by Trial Number

Table 11 continued

175

<b>1012</b> SS 410	400	404	60	60	440	0.25	2775	481	0.020	IF	-	-	-	TD1	TM1	AD1	AM2	No sticking, less strong
<b>1013</b> SS 410	600	604	60	60	440	0.26	3600	748	0.060	IF	-	-	-	TD1	TM1	AD1	AM2	Weld overload, STA, pry-off, deformed sample during pry-off
<b>1014</b> SS 410	600	443	60	60	440	0.18	3630	363	0.013	IF	-	-	-	TD1	TM1	AD1	AM2	To avoid STA, a piece of 0.002in Sn foil was placed on the anvil surface prior to weld, No. 1013 repeat, no STA, WO, tip knurl fractured
<b>1015</b> SS 410	600	371	60	60	440	0.16	3615	234	0.008	IF	-	-	-	TD2	TM1	AD1	AM2	Switched to new weld tip with less-aggressive texture, 0.002in Sn foil was placed on the anvil surface prior to weld, no STA, good tip imprint, WO, high power
<b>1016</b> SS 410	200	211	60	60	440	0.12	3570	129	0.004	IF	-	-	-	TD2	TM1	AD1	AM2	0.002in Sn foil was placed on the anvil surface prior to weld, less strong, no sticking, high power
<b>1017</b> SS 410	400	414	40	40	308	0.18	3585	543	0.025	IF	-	-	-	TD2	TM1	AD1	AM2	0.002in Sn foil was placed on the anvil surface prior to weld, slight STT, very different appearance; appears to have extruded material from knurl
<b>1018</b> SS 410	400	404	20	20	177	0.20	3150	401	0.019	IF	-	-	-	TD2	TM1	AD1	AM2	0.002in Sn foil was placed on the anvil surface prior to weld, slight STT, too low pressure; material extruded out knurl
<b>1019</b> SS 304	400	400	40	40	308	0.38	3570	328	0.013	IF	-	-	-	TD2	TM1	AD1	AM2	0.002in Sn foil was placed on the anvil surface prior to weld, braze joint on tip failed, tip stuck to material, had to be pried apart with pliers
<b>1020</b> Ni 718	400	401	40	40	308	0.21	3540	294	0.018	IF	-	-	-	TD2	TM1	AD1	AM2	STA, pry-off, broke 350M anvil
<b>1021</b> Ni 718	400	403	60	60	440	0.18	3630	0	0.000	B	-	-	-	TD2	TM1	AD1	AM2	STA, extreme pry-off, broke sample during removal, weld nugget stuck to anvil
<b>1022</b> SS 410	400	399	60	60	440	0.18	3615	768	0.067	IF	-	-	-	TD2	TM1	AD2	AM3	Switched to new 100W anvil, WO, slight STA, tungsten has broken apart on anvil surface, W-25Re weld tip shows evidence of deterioration
<b>1023</b> Ni 718	400	407	40	40	308	0.26	2940	0	0.000	IF	-	-	-	TD2	TM1	AD2	AM3	No weld
<b>1024</b> Ni 625	400	407	60	60	440	0.20	3585	0	0.000	IF	-	-	-	TD2	TM1	AD2	AM3	No weld, slight STT, tungsten fragments from tip stuck to nickel
<b>1025</b> CP Ti	400	399	60	60	440	0.18	3645	907	0.042	B	-	-	-	TD2	TM2	AD1	AM2	Switched to 350M tip and anvil, sample glowed red-hot, slight STA, WO

Continued

Table 11 continued

<b>1026</b> CP Ti	600	562	40	40	308	0.22	3615	895	0.040	B	-	-	-	TD2	TM2	AD1	AM2	Sample glowed red-hot, slight STA, WO, heat marks around weld impression
<b>1027</b> CP Ti	600	135	80	80	571	0.10	3570	191	0.007	IF	-	-	-	TD2	TM2	AD1	AM2	Short weld, much less strength, weld overload, slight STA
<b>1028</b> CP Ti	200	209	40	40	308	0.14	3600	770	0.036	B	-	-	-	TD2	TM2	AD1	AM2	Short weld, okay strength, slight STA
<b>1029</b> CP Ti	200	214	60	60	440	0.14	3630	811	0.080	B	-	-	-	TD2	TM2	AD1	AM2	WO, slight STA
<b>1030</b> CP Ti	200	212	80	80	571	0.14	3600	797	0.083	B	-	-	-	TD2	TM2	AD1	AM2	Very fast, similar appearance
<b>1031</b> CP Ti	600	421	60	60	440	0.22	3645	910	0.079	B	-	-	-	TD2	TM2	AD1	AM2	Close to No. 1003 in parameters, WO, white sparks from tip interface during weld, STA
<b>1032</b> CP Ti	400	408	40	40	308	0.19	3600	880	0.037	B	-	-	-	TD2	TM2	AD1	AM2	Okay, STT, same as No. 1004
<b>1033</b> CP Ti	400	399	80	80	571	0.18	3660	897	0.049	B	-	-	-	TD2	TM2	AD1	AM2	Same as No. 1005, STA, WO
<b>1034</b> CP Ti	200	208	20	20	177	0.17	2190	482	0.018	B	-	-	-	TD2	TM2	AD1	AM2	Sparks from tip interface, poor impression
<b>1035</b> Ti 6-4	200	201	40	40	308	0.36	1410	0	0.000	IF	-	-	-	TD2	TM2	AD1	AM2	Shower of white sparks from tip interface, no weld, STA & STT, material filled tip knurl pattern
<b>1036</b> Ti 6-4	200	201	60	60	440	0.32	1335	0	0.000	IF	-	-	-	TD2	TM2	AD1	AM2	Micro-grit-blasted tip prior to weld, sparks, no weld
<b>1037</b> Ti 6-4	200	203	80	80	571	0.25	2280	0	0.000	IF	-	-	-	TD2	TM2	AD1	AM2	Sparks, no weld
<b>1038</b> Ti 6-4	600	599	40	40	308	0.99	960	0	0.000	IF	-	-	-	TD2	TM2	AD1	AM2	Shower of sparks, no weld, heat marks, poor tip impression
<b>1039</b> Ti 6-4	600	602	40	40	308	0.55	1545	0	0.000	IF	-	-	-	TD2	TM2	AD1	AM2	Tip knurl was filled clean by hand prior to weld and micro-grit-blasted, no weld, sparks, STT & STA, tip is significantly worn after one weld, anvil is starting to wear
<b>1040</b> Ti 6-4	400	410	60	60	440	0.23	2775	0	0.000	IF	-	-	-	TD2	TM1	AD2	AM4	Switched to W-25Re tip and M2 anvil, no weld, no sparks
<b>1041</b> Ti 6-4	600	519	40	40	308	0.22	3630	1420	0.048	B	-	-	-	TD2	TM1	AD2	AM4	Glow red hot during weld, STA, CA, WO, high power
<b>1042</b> Ti 6-4	600	416	60	60	440	0.21	3660	0	0.000	IF	-	-	-	TD2	TM1	AD2	AM4	WO, no weld
<b>1043</b> Ti 6-4	600	545	40	60	440	0.22	3570	1061	0.035	B	-	-	-	TD2	TM1	AD2	AM4	Repeat of No. 1042 with a lower trigger force, glow red-hot & white sparks
<b>1044</b> Ti 6-4	600	266	40	80	571	0.15	3570	0	0.000	IF	-	-	-	TD2	TM1	AD2	AM4	No weld, WO

176

Continued

Table 11 continued

<b>1045</b>	Ti 6-4	400	414	40	40	308	0.20	3570	964	0.026	IF	-	-	-	TD2	TM1	AD2	AM4	Some sparks, STA
<b>1046</b>	Ti 6-4	400	402	40	60	440	0.20	3555	930	0.027	IF	-	-	-	TD2	TM1	AD2	AM4	Very fast, stronger STA
<b>1047</b>	SS 304	400	407	40	40	308	0.18	3615	544	0.024	IF	-	-	-	TD2	TM1	AD2	AM4	Switched to W-25Re anvil, WO, slight STA & STT, heat marks around tip
<b>1048</b>	SS 304	400	410	60	60	440	0.19	3630	537	0.021	IF	-	-	-	TD2	TM1	AD2	AM4	CA, pieces of anvil breaking-off/ stuck to coupon
<b>1049</b>	SS 304	600	462	60	60	440	0.18	3600	480	0.020	IF	-	-	-	TD2	TM1	AD2	AM4	WO, chunk of anvil broke of at crack, stuck to coupon
<b>1050</b>	SS 304	600	480	40	40	308	0.19	3615	394	0.015	IF	-	-	-	TD2	TM1	AD2	AM4	WO, heat marks around tip, some anvil fragments on bottom of coupon, STA
<b>1051</b>	SS 304	600	518	40	80	571	0.21	3585	496	0.015	IF	-	-	-	TD2	TM1	AD2	AM4	WO, STA, heat marks, anvil pieces stuck to coupon
<b>1052</b>	SS 304	200	209	40	40	308	0.12	3600	251	0.009	IF	-	-	-	TD2	TM1	AD2	AM4	Short weld, less heat marks, anvil fragments
<b>1053</b>	SS 304	200	207	60	60	440	0.13	3420	242	0.008	IF	-	-	-	TD2	TM1	AD2	AM4	No significant anvil pieces or heta marks, but 'looks' weaker
<b>1054</b>	SS 304	800	525	40	40	308	0.21	3600	417	0.014	IF	-	-	-	TD2	TM1	AD2	AM4	WO, heat marks, anvil fragments
<b>1055</b>	SS 304	600	604	20	20	177	0.28	3105	569	0.028	IF	-	-	-	TD2	TM1	AD2	AM4	Glow from tip interface, no STA, significant heat marks on anvil side
<b>1056</b>	SS 304	400	400	20	20	177	0.18	3405	456	0.018	IF	-	-	-	TD2	TM1	AD2	AM4	STT, 'looks' weaker
<b>1057</b>	SS 410	600	444	60	60	440	0.18	3630	734	0.036	IF	-	-	-	TD2	TM1	AD2	AM4	WO, STA
<b>1058</b>	SS 410	600	458	40	40	308	0.18	3660	688	0.026	B	-	-	-	TD2	TM1	AD2	AM4	WO, STA
<b>1059</b>	SS 410	600	606	20	20	177	0.25	3480	580	0.019	IF	-	-	-	TD2	TM1	AD2	AM4	Glow red at tip interface, STT, heat marks on anvil interface
<b>1060</b>	SS 410	400	406	60	60	440	0.18	3615	731	0.030	B	-	-	-	TD2	TM1	AD2	AM4	CA, STA
<b>1061</b>	SS 410	400	402	40	40	308	0.18	3630	656	0.030	IF	-	-	-	TD2	TM1	AD2	AM4	CA, STA
<b>1062</b>	SS 410	400	410	20	20	177	0.18	3540	401	0.018	IF	-	-	-	TD2	TM1	AD2	AM4	Glow red at tip interface, heat ring at anvil interface
<b>1063</b>	SS 410	200	216	60	60	440	0.13	3630	0	0.000	IF	-	-	-	TD2	TM1	AD2	AM4	CA, less STA than previous welds at 60psi, no heat marks, broke while loading into tensile tester
<b>1064</b>	SS 410	200	206	40	40	308	0.12	3585	311	0.017	IF	-	-	-	TD2	TM1	AD2	AM4	Weaker, STA
<b>1065</b>	CP Ti	400	404	40	40	308	0.18	3660	874	0.097	B	-	-	-	TD2	TM3	AD2	AM4	Switched to wrought-tungsten tip, repeat of No. 1032, STA, no STT, WO
<b>1066</b>	Ti 6-4	400	402	40	40	308	0.19	3615	707	0.031	B	-	-	-	TD2	TM3	AD2	AM4	Repeat of No. 1045, CA, STA

177

Continued

Table 11 continued

<b>1067</b>	SS 304	400	400	40	40	308	0.17	3645	528	0.025	IF	-	-	-	TD2	TM3	AD2	AM4	Repeat of No. 1047, CA, glow red hot around tip impression, heat marks around tip & anvil
<b>1068</b>	SS 410	400	393	40	40	308	0.16	3645	682	0.034	B	-	-	-	TD2	TM3	AD2	AM4	Repeat of No. 1061, WO, short weld
<b>1069</b>	SS 304	400	409	40	40	308	0.18	3630	783	0.065	B	-	-	-	TD2	TM3	AD2	AM5	Repeat of No. 1032 & 1065, No STA or STT, WO
<b>1070</b>	SS 410	400	405	40	40	308	0.21	3600	974	0.045	B	-	-	-	TD2	TM3	AD2	AM5	Repeat of No. 1045 & 1066, slight glow from tip interface, no STA, slight STT
<b>1071</b>	CP Ti	400	399	40	40	308	0.18	3630	503	0.022	IF	-	-	-	TD2	TM3	AD2	AM5	Repeat of No. 1047 & 1067, small heat marks, CA, slight STT
<b>1072</b>	Ti 6-4	400	402	40	40	308	0.18	3615	795	0.066	B	-	-	-	TD2	TM3	AD2	AM5	Repeat of No. 1061 & 1068, WO, STA, anvil shows similar ware to W-25Re anvil when viewed with stereoscope
<b>1073</b>	Ni 718	400	400	40	40	308	0.22	3420	328	0.015	IF	-	-	-	TD2	TM3	AD2	AM5	Small, short weld, STT, tip and anvil have significant ware
<b>1074</b>	Ni 625	400	408	40	40	308	0.22	3210	0	0.000	IF	-	-	-	TD2	TM3	AD2	AM5	No weld, tip and anvil worn even more
<b>1075</b>	CP Ti	800	810	20	20	177	0.36	3465	764	0.060	B	-	-	-	TD2	TM3	AD2	AM5	White sparks from tip interface, slight STT, heat marks on tip & anvil, material extruded at tip interface
<b>1076</b>	CP Ti	800	466	40	40	308	0.18	3615	797	0.070	B	-	-	-	TD2	TM3	AD2	AM5	WO, fast, slight STA, actual energy much lower, no heat marks
<b>1077</b>	CP Ti	800	436	60	60	440	0.18	3660	746	0.057	B	-	-	-	TD2	TM3	AD2	AM5	WO, slight STA, similar to previous
<b>1078</b>	CP Ti	800	812	20	40	308	0.34	3570	594	0.033	B	-	-	-	TD2	TM3	AD2	AM5	Slight STT, heat marks, similar to No. 1075
<b>1079</b>	CP Ti	800	590	20	60	440	0.24	3630	769	0.059	B	-	-	-	TD2	TM3	AD2	AM5	WO, weaker, no STT or STA
<b>1080</b>	SS 410	800	698	20	20	177	0.26	3600	750	0.059	B	-	-	-	TD2	TM3	AD2	AM5	WO, STT, some heat marks
<b>1081</b>	SS 410	800	437	40	40	308	0.17	3615	686	0.042	IF	-	-	-	TD2	TM3	AD2	AM5	WO, STA, small weld diameter
<b>1082</b>	SS 410	800	587	20	40	308	0.23	3630	761	0.052	IF	-	-	-	TD2	TM3	AD2	AM5	Stronger STT, similar to previous, WO
<b>1083</b>	Ti 6-4	200	202	20	20	177	0.15	2550	474	0.031	IF	-	-	-	TD2	TM3	AD2	AM5	Fast, small diameter weld, STT
<b>1084</b>	Ti 6-4	400	403	20	20	177	0.22	3240	644	0.031	IF	-	-	-	TD2	TM3	AD2	AM5	STT, white spark from tip interface
<b>1085</b>	Ti 6-4	600	607	20	20	177	0.31	2940	673	0.032	IF	-	-	-	TD2	TM3	AD2	AM5	Similar to previous, STT, more sparks
<b>1086</b>	Ti 6-4	800	814	20	20	177	0.33	3570	862	0.044	B	-	-	-	TD2	TM3	AD2	AM5	WO, STT, white sparks from tip interface
<b>1087</b>	Ti 6-4	1000	1003	20	20	177	0.65	2970	577	0.033	IF	-	-	-	TD2	TM3	AD2	AM5	Warm, STT, lots of white sparks, heat marks, oddly-shaped power vs. time plot

178

Continued

Table 11 continued

179

<b>1088</b>	Ti 6-4	1000	767	20	60	440	0.28	3540	1187	0.056	B	-	-	-	TD2	TM3	AD2	AM5	WO, STT, weaker, tip may be worn
<b>1089</b>	SS 304	1000	518	20	60	440	0.20	3600	348	0.020	IF	-	-	-	TD2	TM3	AD2	AM5	WO, fast, STT, some heat marks, tip imprint indicates tip is worn
<b>1090</b>	CP Ti	600	468	60	60	440	0.19	3645	646	0.052	B	-	-	-	TD2	TM3	AD2	AM5	WO, STA
<b>1091</b>	CP Ti	600	523	60	60	440	0.21	3615	651	0.047	B	-	-	-	TD2	TM3	AD2	AM5	WO, STA
<b>1092</b>	CP Ti	600	547	20	60	440	0.22	3600	678	0.040	B	-	-	-	TD2	TM3	AD2	AM5	Slightly higher energy, lower power, WO, STA
<b>1093</b>	CP Ti	600	599	20	60	440	0.25	3615	695	0.045	B	-	-	-	TD2	TM3	AD2	AM5	WO, STA, higher energy
<b>1094</b>	CP Ti	600	513	40	40	308	0.20	3615	674	0.047	B	-	-	-	TD2	TM3	AD2	AM5	WO, STA, lower energy
<b>1095</b>	CP Ti	600	496	40	60	440	0.19	3645	680	0.040	B	-	-	-	TD2	TM3	AD2	AM5	WO, STA, lower energy
<b>1096</b>	CP Ti	600	504	40	60	440	0.21	3600	685	0.045	B	-	-	-	TD2	TM3	AD2	AM5	WO, STA, lower energy
<b>1097</b>	CP Ti	600	446	60	60	440	0.18	3630	710	0.059	B	-	-	-	TD2	TM3	AD2	AM5	Tooling removed and reinstalled without modification prior to weld, WO
<b>1098</b>	CP Ti	446	445	60	60	440	0.19	3630	705	0.051	B	-	-	-	TD2	TM3	AD2	AM5	Energy set to actual energy of previous weld; No. 1097, WO, weld was almost identical to previous
<b>1099</b>	CP Ti	600	601	28	28	231	0.54	1335	446	0.038	B	-	-	-	TD2	TM4	AD2	AM6	Lots of white sparks, poor quality weld
<b>1100</b>	CP Ti	600	603	28	28	231	0.41	1860	484	0.043	B	-	-	-	TD2	TM4	AD2	AM6	Less white sparks, still poor quality weld, STT, braze joint failed, had to pry-off from weldment
<b>1101</b>	SS 304	400	415	40	40	308	0.19	3585	354	0.037	IF	-	-	-	TD2	TM2	AD2	AM2	Needed to "officially" try 350M tooling with SS 304, okay weld, some STT, welded substrate to anvil, had to pry off with pliers, anvil is significantly damaged, 350M is not a good tool material for SS 304
<b>2000</b>	CP Ti	350	360	50	50	374	0.21	3540	489	0.025	B	1	1	619	TD2	TM2	AD1	AM2	Started with new tooling; took stereoscope pictures of tooling prior to weld, first weld of central composite DOE block 2 (replicate 1), STA, okay
<b>2001</b>	CP Ti	350	358	71	71	513	0.19	3630	663	0.045	B	2	1	607	TD2	TM2	AD1	AM2	CA, STA
<b>2002</b>	CP Ti	200	200	35	35	275	0.15	3510	378	0.016	IF	3	1	427	TD2	TM2	AD1	AM2	Fast, STA
<b>2003</b>	CP Ti	350	354	50	50	374	0.19	3570	643	0.045	B	4	1	619	TD2	TM2	AD1	AM2	STA
<b>2004</b>	CP Ti	350	360	50	50	374	0.19	3570	670	0.036	B	5	1	619	TD2	TM2	AD1	AM2	Less STA
<b>2005</b>	CP Ti	200	212	65	65	472	0.15	3570	493	0.028	B	6	1	393	TD2	TM2	AD1	AM2	STA

Continued

Table 11 continued

<b>2006</b> CP Ti	350	353	50	50	374	0.19	3615	691	0.032	B	7	1	619	TD2	TM2	AD1	AM2	CA:P, STA
<b>2007</b> CP Ti	350	357	29	29	233	0.19	3510	569	0.034	B	8	1	618	TD2	TM2	AD1	AM2	STA
<b>2008</b> CP Ti	562	575	50	50	374	0.25	3570	801	0.082	B	9	1	776	TD2	TM2	AD1	AM2	STA, good
<b>2009</b> CP Ti	138	143	50	50	374	0.13	3540	344	0.014	IF	10	1	306	TD2	TM2	AD1	AM2	Fast, small diameter weld, STA
<b>2010</b> CP Ti	350	359	50	50	374	0.19	3615	666	0.052	B	11	1	619	TD2	TM2	AD1	AM2	CA:P
<b>2011</b> CP Ti	500	512	35	35	275	0.23	3600	715	0.047	B	12	1	733	TD2	TM2	AD1	AM2	STA
<b>2012</b> CP Ti	500	500	65	65	472	0.23	3585	775	0.076	B	13	1	752	TD2	TM2	AD1	AM2	STA
<b>2013</b> CP Ti	350	352	50	50	374	0.19	3660	636	0.053	B	14	2	619	TD2	TM2	AD1	AM2	Took stereoscope pictures of tooling prior to weld, first weld of central composite DOE block 1 (replicate 2), no tip wear, anvil knurl is rounded-off at weld center, CA:P, light STA
<b>2014</b> CP Ti	350	362	50	50	374	0.19	3585	637	0.045	B	15	2	619	TD2	TM2	AD1	AM2	More STA
<b>2015</b> CP Ti	562	574	50	50	374	0.28	3510	717	0.062	B	16	2	776	TD2	TM2	AD1	AM2	Less STA, good
<b>2016</b> CP Ti	200	202	65	65	472	0.16	3570	199	0.016	IF	17	2	393	TD2	TM2	AD1	AM2	Light STA, small diameter weld
<b>2017</b> CP Ti	138	146	50	50	374	0.12	3615	0	0.000	IF	18	2	306	TD2	TM2	AD1	AM2	CA:P, no weld
<b>2018</b> CP Ti	500	509	65	65	472	0.29	3600	580	0.040	B	19	2	752	TD2	TM2	AD1	AM2	STA
<b>2019</b> CP Ti	350	358	71	71	513	0.25	3520	349	0.016	IF	20	2	607	TD2	TM2	AD1	AM2	No STA, very small weld diameter, looks weak
<b>2020</b> CP Ti	200	215	35	35	275	0.15	3555	434	0.030	IF	21	2	427	TD2	TM2	AD1	AM2	Stronger STA, fast, small diameter weld
<b>2021</b> CP Ti	350	349	50	50	374	0.19	3630	637	0.038	B	22	2	619	TD2	TM2	AD1	AM2	CA:P, STA
<b>2022</b> CP Ti	350	360	29	29	235	0.22	2850	679	0.048	B	23	2	618	TD2	TM2	AD1	AM2	STT
<b>2023</b> CP Ti	350	364	50	50	374	0.19	3630	651	0.049	B	24	2	619	TD2	TM2	AD1	AM2	CA:P, STA
<b>2024</b> CP Ti	500	506	35	35	275	0.23	3570	697	0.044	B	25	2	733	TD2	TM2	AD1	AM2	STA
<b>2025</b> CP Ti	350	359	50	50	374	0.19	3570	629	0.053	B	26	2	619	TD2	TM2	AD1	AM2	STA
<b>2026</b> CP Ti	138	152	50	50	374	0.13	3450	274	0.021	IF	27	3	306	TD2	TM2	AD1	AM2	Took stereoscope pictures of tooling prior to weld, first weld of central composite DOE block 3 (replicate 3), no tip wear, anvil knurl is rounded-off at weld center, STA, small diameter weld
<b>2027</b> CP Ti	500	514	65	65	472	0.23	3630	761	0.084	B	28	3	752	TD2	TM2	AD1	AM2	CA:P, STA

Continued

Table 11 continued

2028	CP Ti	350	358	50	50	374	0.19	3585	654	0.055	B	29	3	619	TD2	TM2	AD1	AM2	STA
2029	CP Ti	350	359	50	50	374	0.19	3540	684	0.060	B	30	3	619	TD2	TM2	AD1	AM2	STA
2030	CP Ti	350	352	50	50	374	0.19	3615	667	0.048	B	31	3	619	TD2	TM2	AD1	AM2	CA:P, less STA
2031	CP Ti	350	359	50	50	374	0.19	3600	678	0.051	B	32	3	619	TD2	TM2	AD1	AM2	STA
2032	CP Ti	200	201	35	35	275	0.15	3300	332	0.020	IF	33	3	427	TD2	TM2	AD1	AM2	Smaller weld diameter, STA
2033	CP Ti	350	365	71	71	513	0.19	3585	710	0.064	B	34	3	607	TD2	TM2	AD1	AM2	STA
2034	CP Ti	562	563	50	50	374	0.25	3570	753	0.069	B	35	3	776	TD2	TM2	AD1	AM2	More STA, good
2035	CP Ti	350	361	29	29	235	0.21	3300	636	0.047	B	36	3	618	TD2	TM2	AD1	AM2	Smaller weld diameter, faster, STA
2036	CP Ti	350	362	50	50	374	0.19	3615	689	0.060	B	37	3	619	TD2	TM2	AD1	AM2	CA:P, STA
2037	CP Ti	260	214	65	65	472	0.14	3630	591	0.050	B	38	3	490	TD2	TM2	AD1	AM2	CA:P
2038	CP Ti	500	510	35	35	275	0.24	3495	735	0.062	B	39	3	733	TD2	TM2	AD1	AM2	More STA, fast, took stereoscope pictures of tooling following weld
2039	CP Ti	600	613	29	29	235	0.30	3390	751	0.053	B	40	4	755	TD2	TM2	AD1	AM2	First weld of central composite DOE No.2 (1 replicate), continued with tooling from DOE No.1, STA, okay
2040	CP Ti	500	511	65	65	472	0.22	3630	796	0.076	B	41	4	752	TD2	TM2	AD1	AM2	CA:P, stronger STA
2041	CP Ti	600	604	50	50	374	0.26	3630	773	0.068	B	42	4	787	TD2	TM2	AD1	AM2	CA:P, less STA
2042	CP Ti	600	610	50	50	374	0.26	3615	772	0.062	B	43	4	787	TD2	TM2	AD1	AM2	CA:P, STA
2043	CP Ti	459	464	50	50	374	0.22	3570	728	0.171	B	44	4	719	TD2	TM2	AD1	AM2	STA
2044	CP Ti	500	500	35	35	275	0.24	3480	674	0.171	B	45	4	733	TD2	TM2	AD1	AM2	Smaller weld diameter, STA
2045	CP Ti	600	605	50	50	374	0.26	3570	797	0.083	B	46	4	787	TD2	TM2	AD1	AM2	STA
2046	CP Ti	700	704	65	65	472	0.30	3600	803	0.078	B	47	4	817	TD2	TM2	AD1	AM2	Less STA, heavy tip indent
2047	CP Ti	600	608	50	50	374	0.26	3660	758	0.055	B	48	4	787	TD2	TM2	AD1	AM2	CA:P, STA
2048	CP Ti	600	604	71	71	513	0.27	3660	771	0.073	B	49	4	806	TD2	TM2	AD1	AM2	CA:P
2049	CP Ti	600	608	50	50	374	0.26	3585	760	0.066	B	50	4	787	TD2	TM2	AD1	AM2	STA
2050	CP Ti	741	753	40	40	308	0.31	3600	757	0.052	B	51	4	763	TD2	TM2	AD1	AM2	STA, but weld made with wrong pressure, so will repeat with correct pressure
2051	CP Ti	741	741	50	50	374	0.31	3615	800	0.076	B	52	4	785	TD2	TM2	AD1	AM2	CA:P, STA

181

Continued

Table 11 continued

2052	CP Ti	700	700	35	35	275	0.30	3480	731	0.052	B	53	4	763	TD2	TM2	AD1	AM2	STA, took pictures of tooling with stereoscope following weld
2053	CP Ti	741	751	29	29	235	0.38	2850	744	0.070	B	54	5	735	TD2	TM2	AD1	AM2	Additional welds for testing/ met-lab, STA, glow red-hot during weld
2054	CP Ti	741	752	71	71	513	0.31	3630	800	0.094	B	55	5	822	TD2	TM2	AD1	AM2	CA:P, STA, deep tip indent/ impression
2055	CP Ti	700	706	50	50	374	0.29	3615	747	0.073	B	56	5	793	TD2	TM2	AD1	AM2	CA:P, lighter STA
2056	CP Ti	600	608	50	50	374	0.26	3600	730	0.070	B	57	5	787	TD2	TM2	AD1	AM2	STA
2057	CP Ti	600	601	50	50	374	0.26	3630	NA	NA	NA	58	5	787	TD2	TM2	AD1	AM2	CA:P, STA, CS
2058	CP Ti	600	609	50	50	374	0.26	3645	756	0.062	B	59	5	787	TD2	TM2	AD1	AM2	CA:P, STA
2059	CP Ti	350	363	50	50	374	0.19	3645	663	0.063	B	60	5	619	TD2	TM2	AD1	AM2	CA:P, less STA
2060	CP Ti	350	363	50	50	374	0.19	3630	NA	NA	NA	61	5	619	TD2	TM2	AD1	AM2	CA:P, less STA, CS
2061	CP Ti	350	361	50	50	374	0.19	3615	651	0.050	B	62	5	619	TD2	TM2	AD1	AM2	CA:P, STA
2062	CP Ti	741	748	29	29	235	0.37	3120				63	5	735	TD2	TM2	AD1	AM2	STT, heat marks
2063	CP Ti	900	908	50	50	374	0.36	3630	NA	NA	NA	64	5	700	TD2	TM2	AD1	AM2	CA:P, red-hot during weld, CS
2064	CP Ti	1200	640	50	50	374	0.25	3585	717	0.059	B	65	5	298	TD2	TM2	AD1	AM2	WO
2065	CP Ti	900	632	50	50	374	0.24	3630	715	0.059	B	66	5	700	TD2	TM2	AD1	AM2	WO, low energy as compared with No.2063
2066	CP Ti	741	743	71	71	513	0.31	3630				67	5	822	TD2	TM2	AD1	AM2	CA:P
2067	CP Ti	900	903	29	29	235	0.42	3105	NA	NA	NA	68	5	630	TD2	TM2	AD1	AM2	Glow red-hot during weld, strong weld, heat marks, CS
2068	CP Ti	900	901	29	29	235	0.43	3030	654	0.044	B	69	5	630	TD2	TM2	AD1	AM2	Glow red-hot, strong STT
2069	CP Ti	900	903	71	71	513	0.36	3585				70	5	756	TD2	TM2	AD1	AM2	Wider weld, glow red-hot, STA, heat marks
2070	CP Ti	200	214	50	50	374	0.15	3570	528	0.046	IF	71	5	414	TD2	TM2	AD1	AM2	Fast, STA, small weld diameter, SEM fractography
2071	CP Ti	200	213	50	50	374	0.15	3600	513	0.046	B	72	5	414	TD2	TM2	AD1	AM2	Fast, STA, small weld diameter
2072	CP Ti	200	212	50	50	374	0.14	3585	502	0.041	IF	73	5	414	TD2	TM2	AD1	AM2	Fast, STA, small weld diameter
2073	CP Ti	350	354	29	29	235	0.24	2310	696	0.062	B	74	5	618	TD2	TM2	AD1	AM2	STT & STA, minor heat marks
2074	CP Ti	350	349	71	71	513	0.18	3630				75	5	607	TD2	TM2	AD1	AM2	CA:P, removed tooling & took pictures with stereoscope
2075	CP Ti	900	559	50	50	374	0.22	3615	784	0.066	B	76	6	700	TD2	TM2	AD1	AM2	Reinstalled & recalibrated tooling prior to weld, WO, slight STA

182

Continued

Table 11 continued

<b>2076</b>	CP Ti	900	556	71	71	513	0.23	3615	812	0.087	B	77	6	756	TD2	TM2	AD1	AM2	WO, slight STA
<b>2077</b>	CP Ti	900	901	29	29	235	0.42	2970				78	6	630	TD2	TM2	AD1	AM2	Glow red-hot during weld cycle, slight STS, heat marks
<b>2078</b>	CP Ti	350	351	29	29	235	0.20	3345	706	0.066	B	79	6	618	TD2	TM2	AD1	AM2	Fast, STA
<b>2079</b>	CP Ti	350	356	71	71	513	0.20	3630	760	0.082	B	80	6	607	TD2	TM2	AD1	AM2	CA:P, less STA
<b>2080</b>	CP Ti	600	609	29	29	235	0.32	3120	NA	NA	NA	81	6	755	TD2	TM2	AD1	AM2	STA & STT, heat marks, CS
<b>2081</b>	CP Ti	600	599	71	71	513	0.25	3615	NA	NA	NA	82	6	806	TD2	TM2	AD1	AM2	WO, STA, CS
<b>2082</b>	CP Ti	600	610	35	35	275	0.26	3600				83	6	766	TD2	TM2	AD1	AM2	Glow red-hot, STA & STT
<b>2083</b>	CP Ti	600	602	65	65	472	0.26	3630	974	0.110	M	84	6	802	TD2	TM2	AD1	AM2	CA:P, STA, clamped sample between two Teflon blocks during tensile test to minimize moment
<b>2084</b>	CP Ti	200	199	28	28	231	0.16	2685	467	0.037	IF	85	6	431	TD2	TM2	AD1	AM2	Small diameter weld, STT & STA, removed tooling & took pictures with stereoscope
<b>3000</b>	Ti 6-4	500	501	20	20	177	0.52	2370	397	0.030	IF	1	1	518	TD2	TM3	AD2	AM5	"New" wrought-W anvil surface, tip worn from preliminary trials, STT, white parks, bad power-time plot; may indicate braze joint issues
<b>3001</b>	Ti 6-4	500	508	40	40	308	0.22	3600	1250	0.064	B	2	1	997	TD2	TM3	AD2	AM5	Glow red-hot, looks good
<b>3002</b>	Ti 6-4	500	425	60	60	440	0.19	3615	879	0.051	B	3	1	882	TD2	TM3	AD2	AM5	WO, fast, weaker
<b>3003</b>	Ti 6-4	1000	1001	20	20	177	1.41	2490	418	0.041	IF	4	1	442	TD2	TM3	AD2	AM5	Strange power-time plot, STT, looks weak
<b>3004</b>	Ti 6-4	1000	540	40	40	308	0.21	3630	975	0.055	B	5	1	1053	TD2	TM3	AD2	AM5	WO, STT
<b>3005</b>	Ti 6-4	1000	423	60	60	440	0.23	3615	1026	0.053	B	6	1	878	TD2	TM3	AD2	AM5	WO, STA
<b>3006</b>	Ti 6-4	500	446	30	30	242	0.18	3600	980	0.059	B	7	1	955	TD2	TM3	AD2	AM5	Fast, WO
<b>3007</b>	Ti 6-4	1000	1002	30	30	242	0.92	3600	1014	0.050	B	8	1	1189	TD2	TM3	AD2	AM5	Lots of heat/ glow red-hot, strange power-time plot, looks strong, took pictures of tooling with stereoscope
<b>3008</b>	Ti 6-4	550	553	16	16	150	0.31	2745	780	0.047	B	1	2	717	TD2	TM3	AD2	AM5	First weld of Ti 6-4 DOE No.1, block 3, replicate 1, took pictures of tooling prior to weld, new wrought-tungsten tip weld surface (side 2), white sparks from tip interface, STT, partial button
<b>3009</b>	Ti 6-4	300	313	30	30	242	0.18	3360	808	0.046	B	2	2	756	TD2	TM3	AD2	AM5	Fast, small diameter weld, light STT
<b>3010</b>	Ti 6-4	300	299	30	30	242	0.18	3120	709	0.038	IF	3	2	608	TD2	TM3	AD2	AM5	Parameter mistake, repeat of previous trial, fast, small diameter weld, light STT

Continued

Table 11 continued

3011	Ti 6-4	196	199	30	30	242	0.15	2970	475	0.029	IF	4	2	484	TD2	TM3	AD2	AM5	Short, small diameter weld, STT
3012	Ti 6-4	550	554	30	30	242	0.26	3450	925	0.028	B	5	2	907	TD2	TM3	AD2	AM5	Okay, STT
3013	Ti 6-4	550	552	30	30	242	0.26	3450	708	0.043	B	6	2	906	TD2	TM3	AD2	AM5	Okay, STT, coupon moved during weld
3014	Ti 6-4	550	554	30	30	242	0.26	3420	896	0.046	B	7	2	888	TD2	TM3	AD2	AM5	Okay, STT
3015	Ti 6-4	800	803	20	20	177	0.35	3600	918	0.045	B	8	2	935	TD2	TM3	AD2	AM5	WO, long weld, white sparks from tip interface
3016	Ti 6-4	550	562	44	44	335	0.25	3600	1306	0.060	IF	9	2	1066	TD2	TM3	AD2	AM5	Good, STT, IF, but crack at edge of weld area in coupon
3017	Ti 6-4	800	698	40	40	308	0.28	3615	1318	0.061	IF	10	2	1190	TD2	TM3	AD2	AM5	WO, sparks from tip interface, STA, good weld, IF, but tear at weld of weld area in coupon
3018	Ti 6-4	550	554	30	30	242	0.26	3390	1043	0.050	B	11	2	869	TD2	TM3	AD2	AM5	Okay, STT
3019	Ti 6-4	550	552	30	30	242	0.26	3450	1086	0.055	B	12	2	906	TD2	TM3	AD2	AM5	Parameter mistake, repeat of previous trial, okay, STT
3020	Ti 6-4	300	302	40	40	308	0.17	3240	485	0.031	IF	13	2	495	TD2	TM3	AD2	AM5	Fast, small diameter weld, STT
3021	Ti 6-4	550	552	30	30	242	0.25	3630	866	0.047	B	14	2	1019	TD2	TM3	AD2	AM5	CA:P, glow red-hot, STT
3022	Ti 6-4	904	755	30	30	242	0.31	3540	1182	0.056	B	15	2	1046	TD2	TM3	AD2	AM5	WO, STT, end of block 1, replicate 1, stopped to tensile test
3023	Ti 6-4	800	736	40	40	308	0.29	3540	NA	NA	NA	16	3	1158	TD2	TM3	AD2	AM5	Repeated welds for additional testing and metallurgy, WO, STT, good appearance, CS
3024	Ti 6-4	550	559	44	44	335	0.24	3630				17	3	1092	TD2	TM3	AD2	AM5	CA:P, STA
3025	Ti 6-4	300	306	30	30	242	0.18	3060	NA	NA	NA	18	3	574	TD2	TM3	AD2	AM5	Fast, small diameter weld, STT, CS
3026	Ti 6-4	550	559	30	30	242	0.26	3540	NA	NA	NA	19	3	965	TD2	TM3	AD2	AM5	STT, okay, CS
3027	Ti 6-4	800	801	20	20	177	0.35	3555	NA	NA	NA	20	3	917	TD2	TM3	AD2	AM5	Reset light on PS, coupon around tip glow red-hot, STT, CS
3028	Ti 6-4	800	660	40	40	308	0.26	3630	727	0.046	B	21	3	1167	TD2	TM3	AD2	AM5	WO, STT
3029	Ti 6-4	550	567	44	44	335	0.25	3615	NA	NA	NA	22	3	1086	TD2	TM3	AD2	AM5	CA:P, STT, CS
3030	Ti 6-4	300	304	30	30	242	0.18	3120				23	3	609	TD2	TM3	AD2	AM5	Small diameter weld, STT
3031	Ti 6-4	550	565	30	30	242	0.26	3510	1176	0.055	IF	24	3	949	TD2	TM3	AD2	AM5	White sparks from tip interface, STT, SEM fractography
3032	Ti 6-4	800	808	20	20	177	0.34	3540				25	3	910	TD2	TM3	AD2	AM5	Reset light on PS, glow red-hot, STT, removed tooling and took pictures with stereoscope

Continued

Table 11 continued

3033	Ti 6-4	550	558	30	30	242	0.26	3540	1021	0.051	B	26	4	965	TD2	TM3	AD2	AM5	First weld of Ti 6-4 DOE No.1, block 2, replicate 2, okay, STT
3034	Ti 6-4	904	909	30	30	242	0.37	3405	952	0.051	B	27	4	1019	TD2	TM3	AD2	AM5	Ti-coupon glowing red-hot, STT, pulled button from both sides
3035	Ti 6-4	550	551	44	44	335	0.24	3630	675	0.039	B	28	4	1082	TD2	TM3	AD2	AM5	WO, strong STA, partial button
3036	Ti 6-4	800	790	40	40	308	0.32	3570	1132	0.057	B	29	4	1236	TD2	TM3	AD2	AM5	WO, glow red-hot, STT
3037	Ti 6-4	300	312	20	20	177	0.20	2820	818	0.048	IF	30	4	720	TD2	TM3	AD2	AM5	Short weld, STT
3038	Ti 6-4	800	806	20	20	177	0.35	3420	1013	0.055	B	31	4	862	TD2	TM3	AD2	AM5	Glow red-hot, STT
3039	Ti 6-4	550	562	30	30	242	0.25	3510	1069	0.056	B	32	4	948	TD2	TM3	AD2	AM5	Okay, STT
3040	Ti 6-4	550	564	30	30	242	0.25	3555	799	0.043	IF	33	4	977	TD2	TM3	AD2	AM5	Strong STA
3041	Ti 6-4	550	557	30	30	242	0.25	3435	931	0.039	B	34	4	899	TD2	TM3	AD2	AM5	STT
3042	Ti 6-4	300	300	40	40	308	0.16	3600	486	0.031	IF	35	4	800	TD2	TM3	AD2	AM5	Fast, strong STA
3043	Ti 6-4	550	560	30	30	242	0.25	3495	889	0.047	B	36	4	937	TD2	TM3	AD2	AM5	Strong STA
3044	Ti 6-4	196	201	30	30	242	0.14	3060	351	0.026	IF	37	4	537	TD2	TM3	AD2	AM5	STT, small diameter weld
3045	Ti 6-4	550	564	16	16	150	0.27	3300	855	0.047	B	38	4	861	TD2	TM3	AD2	AM5	Glow red-hot, STT
3046	Ti 6-4	550	551	60	60	440	0.23	3600	1248	0.059	IF	39	5	1113	TD2	TM3	AD2	AM5	Additional welds for testing/ met-lab, short weld, glow red-hot, STT, reset light on power supply
3047	Ti 6-4	550	559	60	60	440	0.23	3600				40	5	1129	TD2	TM3	AD2	AM5	Short weld, glow red-hot, STT, reset light on power supply
3048	Ti 6-4	550	484	60	60	440	0.18	3630	573	0.034	IF	41	5	1021	TD2	TM3	AD2	AM5	WO, strong STA, small diameter weld
3049	Ti 6-4	550	549	50	50	374	0.21	3615				42	5	1089	TD2	TM3	AD2	AM5	Short weld, WO, strong STA, small diameter weld
3050	Ti 6-4	550	531	50	50	374	0.20	3570	688	0.037	B	43	5	1012	TD2	TM3	AD2	AM5	WO, strong STA, small diameter weld, partial button
3051	Ti 6-4	1000	678	30	30	242	0.26	3585	708	0.039	B	44	5	1043	TD2	TM3	AD2	AM5	WO, heat marks, strong STA, small diameter weld, partial button
3052	Ti 6-4	1000	736	30	30	242	0.27	3555				45	5	1048	TD2	TM3	AD2	AM5	WO, no STA or STT, heat marks, small diameter weld
3053	Ti 6-4	550	551	30	30	242	0.24	3600	661	0.037	B	46	5	999	TD2	TM3	AD2	AM5	Reset light on power supply, strong STA, some of the tungsten from the anvil is transferred to the coupon

185

Continued

Table 11 continued

<b>3054</b>	Ti 6-4	550	566	30	30	242	0.24	3570				47	5	987	TD2	TM3	AD2	AM5	Reset light on power supply, strong STA, some of the tungsten from the anvil is transferred to the coupon, stopped and took pictures of tooling with stereoscope
<b>3055</b>	Ti 6-4	200	203	20	20	177	0.16	2565	595	0.040	IF	48	6	658	TD2	TM3	AD2	AM5	Additional welds to try and better define effect of pressure at low and high energy levels. Okay, weld location offset to the left
<b>3056</b>	Ti 6-4	1000	1001	20	20	177	0.89	2520	650	0.036	IF	49	6	455	TD2	TM3	AD2	AM5	Long weld, lots of white sparks, STT, heat marks on tip
<b>3057</b>	Ti 6-4	200	202	60	60	440	0.12	3405	1049	0.055	IF	50	6	152	TD2	TM3	AD2	AM5	Fast weld, STT
<b>3058</b>	Ti 6-4	1000	454	60	60	440	0.18	3645	1325	0.066	B	51	6	981	TD2	TM3	AD2	AM5	WO, STT
<b>3059</b>	Ti 6-4	200	211	25	25	210	0.14	2970	615	0.036	IF	52	6	639	TD2	TM3	AD2	AM5	STT
<b>3060</b>	Ti 6-4	1000	1002	25	25	210	0.94	3060	622	0.035	IF	53	6	753	TD2	TM3	AD2	AM5	Excessive weld time, STT
<b>3061</b>	Ti 6-4	200	205	16	16	150	0.19	1740	0	0.000	IF	54	6	639	TD2	TM3	AD2	AM5	STT, broke weld during removal
<b>3062</b>	Ti 6-4	1000	1000	16	16	150	1.28	2010	0	0.000	IF	55	6	292	TD2	TM3	AD2	AM5	STT, broke weld during removal
<b>3063</b>	Ti 6-4	200	210	30	30	242	0.13	3330	633	0.036	IF	56	6	698	TD2	TM3	AD2	AM5	STT, tip is starting to wear
<b>3064</b>	Ti 6-4	1000	1003	30	30	242	0.79	3450	1071	0.056	B	57	6	1087	TD2	TM3	AD2	AM5	Long weld, white sparks, STT, power-time curve may indicate braze joint failure, partial button
<b>3065</b>	Ti 6-4	200	202	35	35	275	0.15	2460	0	0.000	IF	58	6	-31	TD2	TM3	AD2	AM5	No weld, top coupon, STT
<b>3066</b>	Ti 6-4	1000	1003	35	35	275	0.84	2085	0	0.000	IF	59	6	103	TD2	TM3	AD2	AM5	No weld, tip glow red-hot, braze joint is failing
<b>4000</b>	SS 304	550	561	29	29	235	0.23	3540	526	0.039	IF	1	1	468	TD2	TM1	AD2	AM4	Started with new tooling; took stereoscope pictures of tooling prior to weld, first weld of central composite DOE block 2 (replicate 1), STT, heat marks, moved anvil slightly to avoid welding directly on CTE mismatch crack
<b>4001</b>	SS 304	400	403	65	65	472	0.20	3570	411	0.026	IF	2	1	323	TD2	TM1	AD2	AM4	Fast, slight STA, some tungsten transferred to coupon
<b>4002</b>	SS 304	338	352	50	50	374	0.17	3600	396	0.026	IF	3	1	362	TD2	TM1	AD2	AM4	Fast, some heat marks
<b>4003</b>	SS 304	700	549	35	35	275	0.22	3630	545	0.036	IF	4	1	466	TD2	TM1	AD2	AM4	WO, STA & STT, more heat marks
<b>4004</b>	SS 304	550	560	71	71	513	0.24	3645	435	0.030	IF	5	1	368	TD2	TM1	AD2	AM4	WO, light STA
<b>4005</b>	SS 304	550	549	50	50	374	0.23	3630	389	0.027	IF	6	1	447	TD2	TM1	AD2	AM4	WO, STA
<b>4006</b>	SS 304	550	550	50	50	374	0.23	3660	402	0.028	IF	7	1	447	TD2	TM1	AD2	AM4	WO, STA, anvil has signs of wear

Continued

Table 11 continued

4007	SS 304	550	550	50	50	374	0.23	3630	405	0.029	IF	8	1	447	TD2	TM1	AD2	AM4	WO, STA, anvil fractured outside of weld area (will not be a problem)
4008	SS 304	550	549	50	50	374	0.22	3600	405	0.026	IF	9	1	447	TD2	TM1	AD2	AM4	WO, less STA
4009	SS 304	400	411	35	35	275	0.18	3600	393	0.027	IF	10	1	415	TD2	TM1	AD2	AM4	Fast, anvil is significantly worn at weld location
4010	SS 304	700	610	65	65	472	0.25	3615	364	0.030	IF	11	1	423	TD2	TM1	AD2	AM4	WO, strong STA, lower energy than needed
4011	SS 304	762	567	50	50	374	0.23	3600	329	0.024	IF	12	1	454	TD2	TM1	AD2	AM4	WO, STA
4012	SS 304	550	549	50	50	374	0.23	3630	344	0.024	IF	13	1	447	TD2	TM1	AD2	AM4	Took pictures of tooling with stereoscope following weld, WO, STA
4013	SS 304	650	660	40	40	308	0.25	3570	566	0.036	IF	15	2	505	TD2	TM1	AD2	AM4	First weld of SS DOE No. 2, WO, glow red-hot, light STA, significant heat marks around tip impression
4014	SS 304	550	565	30	30	242	0.22	3630	399	0.032	IF	16	2	471	TD2	TM1	AD2	AM4	CA:P, STT, glow around tip, heat marks
4015	SS 304	650	661	20	20	177	0.27	3330	462	0.032	IF	17	2	486	TD2	TM1	AD2	AM4	More STT, glow around tip
4016	SS 304	550	557	30	30	242	0.22	3555	408	0.029	IF	18	2	468	TD2	TM1	AD2	AM4	STT, heat marks, glow around tip during weld
4017	SS 304	550	553	30	30	242	0.22	3540	468	0.035	IF	19	2	466	TD2	TM1	AD2	AM4	Less STT, heat marks, glow around tip
4018	SS 304	550	553	30	30	242	0.22	3630	416	0.027	IF	20	2	466	TD2	TM1	AD2	AM4	CA:P, less STT, heat marks
4019	SS 304	550	560	44	44	335	0.24	3480	579	0.037	IF	21	2	463	TD2	TM1	AD2	AM4	Light STT, heat marks
4020	SS 304	450	455	20	20	177	0.20	3495	422	0.029	IF	22	2	423	TD2	TM1	AD2	AM4	More STT, less heat marks
4021	SS 304	550	554	16	16	150	0.30	2865	526	0.038	IF	23	2	444	TD2	TM1	AD2	AM4	More STT, less heat marks
4022	SS 304	450	417	40	40	308	0.18	3630	379	0.026	IF	24	2	412	TD2	TM1	AD2	AM4	WO, STT, less heat marks on anvil side
4023	SS 304	550	488	30	30	242	0.21	3630	400	0.028	IF	25	2	444	TD2	TM1	AD2	AM4	WO, STT, heat marks
4024	SS 304	409	412	30	30	242	0.17	3630	337	0.025	IF	26	2	417	TD2	TM1	AD2	AM4	Fast, WO, more STT
4025	SS 304	691	702	30	30	242	0.27	3555	569	0.042	IF	27	2	517	TD2	TM1	AD2	AM4	Threw power supply reset light, STT, significant heat marks, end of DOE block "2," replicate "1"
4026	SS 304	200	200	20	20	177	0.12	3270	460	0.035	IF	28	3	340	TD2	TM1	AD2	AM4	Start of additional SS304 weld trials, small diameter weld, looks weak, STT
4027	SS 304	200	205	40	40	308	0.12	3615	516	0.033	IF	29	3	326	TD2	TM1	AD2	AM4	Fast, CA:P, STA
4028	SS 304	300	311	20	20	177	0.15	3300	459	0.033	IF	30	3	377	TD2	TM1	AD2	AM4	Fast, STT
4029	SS 304	300	307	40	40	308	0.15	3630	551	0.035	IF	31	3	368	TD2	TM1	AD2	AM4	Fast, CA:P, STA

187

Continued

Table 11 continued

4030	SS 304	1000	1000	16	16	150	0.51	2610	677	0.077	IF	32	3	566	TD2	TM1	AD2	AM4	Long weld, another piece of the anvil broke off near the CTE crack
4031	SS 304	1000	1000	40	40	308	0.25	3630	576	0.049	IF	33	3	628	TD2	TM1	AD2	AM4	WO, lower energy, STT & STA
4032	SS 304	1000	1008	20	20	177	0.40	3435	791	0.140	IF	34	3	585	TD2	TM1	AD2	AM4	Tear in center of weld in both coupons, glow red-hot, STT, significant heat marks
4033	SS 304	550	461	44	44	335	0.19	3615	557	0.033	IF	35	3	423	TD2	TM1	AD2	AM4	WO, anvil braze joint failed, repaired- see Furnace Run 50410-17, took pictures of tooling with stereoscope
4034	SS 304	550	519	44	44	335	0.22	3645	445	0.027	IF	36	4	446	TD2	TM1	AD2	AM4	Took pictures of repaired tooling prior to weld, STT, WO
4035	SS 304	1000	473	30	30	242	0.20	3615	490	0.032	IF	37	4	438	TD2	TM1	AD2	AM4	WO, STT
4036	SS 304	1000	1000	10	10	111	0.80	1770	430	0.030	IF	38	4	538	TD2	TM1	AD2	AM4	Glow red-hot, long weld, STT
4037	SS 304	1000	1004	20	20	177	0.42	3540	628	0.066	IF	39	4	584	TD2	TM1	AD2	AM4	Long weld, glow red-hot, STT, tip might be worn
4038	SS 304	1500	533	25	25	210	0.21	3615	0	0.000	B	40	4	455	TD2	TM1	AD2	AM4	WO, welded through coupon, nugget stuck to tip, took pictures of tip with stereoscope
4039	SS 304	550	541	29	29	235	0.21	3660	472	0.039	IF	14	1	462	TD2	TM1	AD2	AM4	DOE Run Order No.2, Repeat of No. 4000 with moved anvil, STT, WO
4040	SS 304	500	512	40	40	308	0.30	2700	NA	NA	B	-	-	449	TD2	TM1	AD2	AM4	To remove nugget (from No. 4038) from tip, welded a single SS 304 coupon, unfortunately a large piece of the W-25Re tip knurl broke off, stuck to the coupon, see pictures
4041	SS 304	342	347	20	20	177	0.19	3105	358	0.028	IF	41	5	388	TD2	TM1	AD2	AM4	Switched to new/unused side of welding tip, glow red-hot, STT
4042	SS 304	100	102	20	20	177	0.09	3300	349	0.024	IF	42	5	306	TD2	TM1	AD2	AM4	Fast, STT
4043	SS 304	800	806	20	20	177	0.37	3555	582	0.043	IF	43	5	529	TD2	TM1	AD2	AM4	Glow red-hot, STT, long weld
4044	SS 304	100	101	40	40	308	0.09	3540	399	0.028	IF	44	5	282	TD2	TM1	AD2	AM4	Very fast, low heat, weak
4045	SS 304	800	625	40	40	308	0.24	3600	518	0.039	IF	45	5	492	TD2	TM1	AD2	AM4	WO, STA & STT
4046	SS 304	100	111	30	30	242	0.10	3420	0	0.000	IF	46	5	305	TD2	TM1	AD2	AM4	Very fast, broke weld while removing from anvil; STA
4047	SS 304	800	719	30	30	242	0.27	3570	550	0.045	IF	47	5	523	TD2	TM1	AD2	AM4	WO, strong STA & STT
4048	SS 304	800	804	10	10	111	0.63	2085	494	0.035	IF	48	5	491	TD2	TM1	AD2	AM4	Long weld, glow red-hot

Continued

Table 11 continued

4049	SS 304	1200	1208	20	20	177	0.58	3555	604	0.055	IF	49	5	637	TD2	TM1	AD2	AM4	Long weld, glow red-hot, strong STT & STA
4050	SS 304	1200	1201	10	10	111	0.91	2145	515	0.037	IF	50	5	583	TD2	TM1	AD2	AM4	Very long weld, lots of heat, STT
4051	SS 304	100	101	60	60	440	0.10	3465	0	0.000	IF	51	5	200	TD2	TM1	AD2	AM4	Very fast, weak, broke during removal, light STA
4052	SS 304	200	211	60	60	440	0.13	3600	348	0.025	IF	52	5	254	TD2	TM1	AD2	AM4	Very fast, STA, weak, took pictures of tooling: tip knurl is filled with SS material
4053	SS 304	1000	1004	12	12	124	0.72	2130	470	0.035	IF	-	-	548	TD2	TM1	AD2	AM4	Switched to partially-worn W-25Re tip from preliminary weld trials, long weld, STT
4054	SS 304	1000	599	33	33	263	0.23	3615	350	0.027	IF	-	-	484	TD2	TM1	AD2	AM4	WO, STT, tip braze joint failed after "test" button pressed, had to pry tip apart from coupon with pliers
4055	SS 304	1000	1004	20	20	177	0.48	3000	591	0.049	IF	53	6	584	TD2	TM1	AD2	AM4	Switched-back to "hand-filled" W-25Re tip, STT & STA, glow during weld
4056	SS 304	550	549	44	44	335	0.21	3615	453	0.035	IF	54	6	458	TD2	TM1	AD2	AM4	WO
4057	SS 304	650	665	40	40	308	0.26	3540	NA	NA	NA	55	6	507	TD2	TM1	AD2	AM4	Fast, reset light on power supply, CS
4058	SS 304	1000	1007	20	20	177	0.43	3345	623	0.062	IF	56	6	585	TD2	TM1	AD2	AM4	STT & STA, glow during weld
4059	SS 304	1000	1007	20	20	177	0.42	3405				57	6	585	TD2	TM1	AD2	AM4	STT & STA, glow during weld
4060	SS 304	1200	1210	20	20	177	0.49	3480	694	0.079	B	58	6	638	TD2	TM1	AD2	AM4	More glow/ red-hot, no STT, STA
4061	SS 304	550	550	44	44	335	0.22	3600	NA	NA	NA	59	6	459	TD2	TM1	AD2	AM4	Reset light on power supply, stronger STA, CS
4062	SS 304	1200	1203	20	20	177	0.46	3540	610	0.066	IF	60	6	636	TD2	TM1	AD2	AM4	STT, glow during welding, SEM fractography
4063	SS 304	200	203	20	20	177	0.12	3510	0	0.000	IF	61	6	341	TD2	TM1	AD2	AM4	Fast, STT, weld failed after "test" button pressed to separate coupon and tip, need to repeat without "test" button
4064	SS 304	200	216	20	20	177	0.12	3540	NA	NA	NA	62	6	345	TD2	TM1	AD2	AM4	Fast, STT, CS
4065	SS 304	1000	647	20	20	177	0.25	3630	363	0.027	IF	63	6	482	TD2	TM1	AD2	AM4	WO, strong STT
4066	SS 304	1400	1400	20	20	177	0.52	3570	NA	NA	NA	64	6	685	TD2	TM1	AD2	AM4	Long, lots of heat input, strong STT, high deformation, CS
4067	SS 304	550	556	44	44	335	0.23	3570	379	0.032	IF	65	6	461	TD2	TM1	AD2	AM4	Fast, piece of anvil broke-off onto coupon, took pictures of tooling with stereoscope
4068	SS 304	1000	553	20	20	177	0.23	3600	615	0.059	IF	66	7	453	TD2	TM1	AD2	AM4	WO, lower energy
4069	SS 304	650	559	40	40	308	0.22	3570	598	0.059	IF	67	7	467	TD2	TM1	AD2	AM4	WO, lower energy

Table 11 continued

061

4070	SS 304	1400	775	20	20	177	0.29	3570	623	0.062	IF	68	7	520	TD2	TM1	AD2	AM4	WO, strong STA & STT
4071	SS 304	1000	1003	16	16	150	0.50	3135				69	7	567	TD2	TM1	AD2	AM4	Glow red-hot, strong STA & STT
4072	SS 304	200	203	20	20	177	0.12	3540	369	0.026	IF	70	7	341	TD2	TM1	AD2	AM4	Strong STA & STT, small diameter weld than previous at same settings, will re-align tip and anvil
4073	SS 304	1000	1010	20	20	177	0.40	3525	631	0.076	IF	71	7	585	TD2	TM1	AD2	AM4	Glow red-hot, strong STA & STT
4074	SS 304	550	403	44	44	335	0.17	3630	563	0.051	IF	72	7	399	TD2	TM1	AD2	AM4	WO, STA, anvil pieces stuck to coupon
4075	SS 304	1200	1199	20	20	177	0.45	3615	710	0.111	B	73	7	635	TD2	TM1	AD2	AM4	Glow red-hot, CA:P, strong STA & STA
4076	SS 304	200	207	20	20	177	0.12	3615	0	0.000	IF	74	7	342	TD2	TM1	AD2	AM4	CA:P, STT & STA, broke during removal
4077	SS 304	800	803	20	20	177	0.30	3600	636	0.062	IF	75	7	528	TD2	TM1	AD2	AM4	Glow red-hot, STA & STT
4078	SS 304	550	439	30	30	242	0.18	3630	446	0.040	IF	76	7	426	TD2	TM1	AD2	AM4	WO, anvil pieces stuck to coupon
4079	SS 304	1000	1004	16	16	150	0.44	3375	625	0.062	IF	77	7	567	TD2	TM1	AD2	AM4	Glow red-hot, strong STA & STT
4080	SS 304	100	108	40	40	308	0.10	3600	0	0.000	IF	78	7	285	TD2	TM1	AD2	AM4	Fast, weak, STA, broke weld while removing from anvil
4081	SS 304	1000	501	20	20	177	0.20	3600	435	0.033	IF	79	7	437	TD2	TM1	AD2	AM4	WO, STA & STT, poor anvil impression
4082	SS 304	550	553	30	30	242	0.22	3540	435	0.034	IF	80	7	466	TD2	TM1	AD2	AM4	Moved anvil slightly, welded scrap copper coupon prior to weld, STT
4083	SS 304	1000	1005	20	20	177	0.40	3360	597	0.055	IF	81	7	584	TD2	TM1	AD2	AM4	STT, glow red-hot
4084	SS 304	650	658	40	40	308	0.26	3540	446	0.044	IF	82	7	505	TD2	TM1	AD2	AM4	Welded scrap copper coupon prior to weld, STT
4085	SS 304	1000	820	40	40	308	0.31	3510	496	0.036	IF	83	7	565	TD2	TM1	AD2	AM4	WO, took pictures of tooling with stereoscope
4086	SS 304	1000	1007	20	20	177	0.50	3000				-	-	585	TD2	TM1	AD2	AM6	Re-using same tip, will try several welds with Molybdenum TZM anvil, no sticking to anvil, STT
4087	SS 304	650	495	40	40	308	0.18	3630	419	0.031	IF	-	-	442	TD2	TM1	AD2	AM6	WO, STT
4088	SS 304	1400	1403	20	20	177	0.73	2910	534	0.041	IF	-	-	685	TD2	TM1	AD2	AM6	Long weld, glow red-hot
4089	SS 304	550	497	44	44	335	0.20	3645	398	0.026	IF	-	-	437	TD2	TM1	AD2	AM6	WO, STT
4090	SS 304	200	200	20	20	177	0.12	3315	342	0.026	IF	-	-	340	TD2	TM1	AD2	AM6	STT, looks weak
4091	SS 304	1000	1006	20	20	177	0.55	3240	465	0.035	IF	-	-	584	TD2	TM1	AD2	AM6	STT, glow red-hot, braze-joint failed when pressing "test" button, took pictures of tooling with stereoscope, braze joint was full of porosity
5000	SS 410	1000	893	20	20	177	0.35	3495	608	0.045	IF	-	-	699	TD2	TM5	AD2	AM7	Using tip side 1, WO, STT

Continued

Table 11 continued

5001	SS 410	1000	450	60	60	440	0.19	3645	0	0.000	IF	-	-	38	TD2	TM5	AD2	AM7	WO, no weld
5002	SS 410	1000	496	30	30	242	0.20	3615	421	0.033	IF	-	-	473	TD2	TM5	AD2	AM7	WO, STT, small diameter weld
5003	SS 410	1000	393	40	40	308	0.17	3660	253	0.021	IF	-	-	371	TD2	TM5	AD2	AM7	WO, STT, small diameter weld
5004	SS 410	1000	1001	10	10	111	1.23	2235	576	0.039	IF	-	-	610	TD2	TM5	AD2	AM7	Long weld, piece of tip broke-off during weld; took pictures of tooling with stereoscope, irregular power-time curve
5005	SS 410	500	505	40	40	308	0.22	3300	0	0.000	IF	-	-	462	TD2	TM5	AD2	AM7	Fast, very small diameter weld, broke while loading into tensile tester
5006	SS 410	1000	598	50	50	374	0.23	3585	13	0.008	IF	-	-	373	TD2	TM5	AD2	AM7	Fast, WO, small diameter weld, no STT or STA
5007	SS 410	1000	1002	20	20	177	0.51	2655	0	0.000	IF	-	-	757	TD2	TM5	AD2	AM7	Lower power, no weld
5008	SS 410	1000	1004	15	15	144	0.64	2205	0	0.000	IF	-	-	700	TD2	TM5	AD2	AM7	Small diameter weld, more pieces of the tip broke off, it appears the tip braze joint has been moving and re-solidifying during the weld cycle
5009	SS 410	400	410	40	40	308	0.20	3420	0	0.000	IF	-	-	386	TD2	TM5	AD2	AM7	Switched to tip side 2, very weak, broke by hand with almost no force
5010	SS 410	600	613	60	60	440	0.29	3360	0	0.000	IF	-	-	104	TD2	TM5	AD2	AM7	Weak, no weld, problem noticed: 70% of system power required to fire sonics in free air, due to unbalanced weld tip, see pictures
5011	SS 410	1000	1002	20	20	177	0.92	2265	398	0.033	IF	-	-	757	TD2	TM5	AD2	AM7	Repaired braze tip side 1; see furnace run: 50410-18, rebuilt ultrasonic stack following AmTech instruction manual, long weld, white sparks, discolored tip around braze joint/ heat marks, power-time plot indicated braze joint failure, will need to re-braze both sides with higher temp/ strength braze alloy
5012	SS 410	495	501	20	20	177	0.38	2070	0	0.000	IF	-	-	375	TD2	TM2	AD2	AM7	Trying 350M tip w/ AE-6 anvil, STT, broke weld when hit test button, tip impression looks bad, tip knurl is destroyed

161

Continued

Table 11 continued

5013	SS 410	800	420	40	40	308	0.17	3630	749	0.066	B	-	-	394	TD3	TM2	AD2	AM7	Installed another 350M tip, this one w/ cross-hatch knurl pattern, WO, STT & STA, partial button/ tear in weld during testing
5014	SS 410	800	602	30	30	242	0.23	3600	590	0.038	IF	-	-	562	TD2	TM5	AD2	AM7	Glow red-hot, WO, stronger STA, impression indicates weld pressure was too-low; tip knurl destroyed
5015	SS 410	500	503	20	20	177	0.29	2280	490	0.032	IF	-	-	377	TD2	TM3	AD2	AM5	Switched to wrought-W tooling, WO, glow red-hot, STT
5016	SS 410	500	507	20	20	177	0.30	2175	0	0.000	IF	-	-	381	TD2	TM5	AD2	AM7	Repaired AE-6 tip braze joints w/ BNi-9; furnace run: 50410-20, fast, no weld, STT
5017	SS 410	1000	1006	40	40	308	0.38	3615	621	0.049	B	-	-	689	TD2	TM5	AD2	AM7	CA:P, STT, heat marks, okay, partial button
5018	SS 410	1000	196	60	60	440	0.10	3555	0	0.000	IF	-	-	-128	TD2	TM3	AD2	AM5	WO, no weld, STT
5019	SS 410	1000	423	40	40	308	0.17	3645	707	0.053	IF	-	-	397	TD2	TM5	AD2	AM7	WO, STT, low energy, tensile: tear in weld center
5020	SS 410	1000	1009	20	20	177	0.41	3180	692	0.050	IF	-	-	760	TD2	TM5	AD2	AM7	Glow red-hot, heat marks, okay, STT, partial button
5021	SS 410	500	500	20	20	177	0.25	2970	492	0.033	IF	-	-	374	TD2	TM3	AD2	AM5	More STT, less heat marks
5022	SS 410	1000	696	30	30	242	0.25	3570	707	0.053	B	-	-	631	TD2	TM5	AD2	AM7	WO, low energy
5023	SS 410	1000	1006	20	20	177	0.43	3030	572	0.034	IF	-	-	759	TD2	TM5	AD2	AM7	Glow red-hot, STT, tip is discolored around braze joint; took pictures, heat marks
5024	SS 410	550	432	44	44	335	0.18	3660	610	0.047	IF	1	1	367	TD2	TM3	AD2	AM5	1st weld of SS410 DOE No.1, block 1, replicate 1, WO, STT
5025	SS 410	800	406	40	40	308	0.17	3645	668	0.041	IF	2	1	382	TD2	TM5	AD2	AM7	WO, STT
5026	SS 410	300	317	40	40	308	0.14	3615	429	0.027	IF	3	1	301	TD2	TM5	AD2	AM7	CA:P, STT
5027	SS 410	550	515	30	30	242	0.20	3615	514	0.034	IF	4	1	490	TD2	TM3	AD2	AM5	WO, STT
5028	SS 410	550	554	16	16	150	0.32	2340	371	0.026	IF	5	1	356	TD2	TM5	AD2	AM7	STT
5029	SS 410	550	482	30	30	242	0.18	3600	502	0.033	IF	6	1	460	TD2	TM5	AD2	AM7	WO, STT
5030	SS 410	196	198	30	30	242	0.11	3540	129	0.019	IF	7	1	149	TD2	TM3	AD2	AM5	STT, poor tip impression
5031	SS 410	550	515	30	30	242	0.19	3600	461	0.034	IF	8	1	490	TD2	TM5	AD2	AM7	WO, STT
5032	SS 410	550	469	30	30	242	0.17	3630	400	0.028	IF	9	1	448	TD2	TM5	AD2	AM7	WO, STT
5033	SS 410	904	541	30	30	242	0.20	3600	275	0.024	IF	10	1	512	TD2	TM3	AD2	AM5	WO, STT
5034	SS 410	800	812	20	20	177	0.32	3405	650	0.045	IF	11	1	647	TD2	TM5	AD2	AM7	Glow red-hot, more STT
5035	SS 410	550	485	30	30	242	0.18	3660	375	0.028	IF	12	1	462	TD2	TM5	AD2	AM7	WO, STT

Continued

Table 11 continued

193

5036	SS 410	300	304	20	20	177	0.16	3120	0	0.000	IF	13	1	144	TD2	TM3	AD2	AM5	last weld of SS410 DOE No. 1, block 1, STT, weld broke on removal
5037	SS 410	800	802	20	20	177	0.33	3255				-	-	640	TD2	TM5	AD2	AM7	Extra welds for metallurgy, glow red-hot, strong STT
5038	SS 410	550	454	30	30	242	0.17	3630	0	0.000	IF	-	-	433	TD2	TM5	AD2	AM7	WO, STT, broke during removal, took pictures of tooling with stereoscope
5039	SS 410	200	200	40	40	308	0.11	3600	0	0.0	IF	1	2	180	TD2	TM5	AD2	AM7	1st weld of SS410 DOE No.2, block 1, replicate 1, cleaned tool surfaces with sandpaper followed by re-laser machined knurl, pictures taken with stereoscope, short weld, STT, adjusted tip following weld
5040	SS 410	300	317	30	30	242	0.15	3585	88	88.3	IF	2	2	291	TD2	TM5	AD2	AM7	uneven tip impression, STT, adjusted tip alignment following weld
5041	SS 410	300	307	16	16	150	0.18	2700	0	0.0	IF	3	2	59	TD2	TM5	AD2	AM7	STT, broke weld during removal
5042	SS 410	441	441	30	30	242	0.18	3570	464	464.4	IF	4	2	421	TD2	TM5	AD2	AM7	Threw power supply reset light, STT
5043	SS 410	159	162	30	30	242	0.11	3060	33	33.0	IF	5	2	103	TD2	TM5	AD2	AM7	Fast, STT, looks weak
5044	SS 410	400	412	20	20	177	0.20	3480	299	299.3	IF	6	2	276	TD2	TM5	AD2	AM7	Okay, STT
5045	SS 410	300	235	30	30	242	0.12	3420	0	0.0	IF	7	2	195	TD2	TM5	AD2	AM7	WO, STT, broke while loading into tensile tester
5046	SS 410	300	306	44	44	335	0.15	3615	128	127.5	IF	8	2	260	TD2	TM5	AD2	AM7	CA:P, STT
5047	SS 410	400	411	40	40	308	0.18	3540	203	202.7	IF	9	2	387	TD2	TM5	AD2	AM7	Threw power supply reset light, STT, good
5048	SS 410	300	309	30	30	242	0.16	3525	0	0.0	IF	10	2	282	TD2	TM5	AD2	AM7	STT, good appearance, broke while loading into tensile tester
5049	SS 410	300	308	30	30	242	0.15	3510	161	160.5	IF	11	2	281	TD2	TM5	AD2	AM7	Reset light on power supply, STT
5050	SS 410	200	205	20	20	177	0.13	3060	0	0.0	IF	12	2	11	TD2	TM5	AD2	AM7	Fast, no weld, STT
5051	SS 410	200	208	20	20	177	0.14	2655	0	0.0	IF	13	2	15	TD2	TM5	AD2	AM7	Parameter mistake (repeat of previous trial), no weld, STT
5052	SS 410	300	313	30	30	242	0.15	3450	183	182.6	IF	14	2	286	TD2	TM5	AD2	AM7	STT
5053	SS 410	441	445	30	30	242	0.20	3435				15	3	425	TD2	TM5	AD2	AM7	Will repeat a few welds for metallurgy, STT, good
5054	SS 410	300	311	30	30	242	0.15	3465	NA	NA	NA	16	3	284	TD2	TM5	AD2	AM7	STT, weaker, CS
5055	SS 410	550	555	30	30	242	0.25	3510				17	3	524	TD2	TM5	AD2	AM7	Fast, STT, good

Continued

Table 11 continued

5056	SS 410	800	813	20	20	177	0.40	3270				18	3	647	TD2	TM5	AD2	AM7	Glow red-hot, STT, removed tooling and took pictures with stereoscope
5057	SS 410	300	303	20	20	177	0.20	2670	197	0.020	IF	19	4	143	TD2	TM5	AD2	AM7	Additional welds for testing, inadequate pressure, poor tip alignment, adjust alignment prior to next weld
5058	SS 410	300	307	20	20	177	0.18	2820	310	0.026	IF	20	4	148	TD2	TM5	AD2	AM7	Better alignment, but still poor impression due to low pressure
5059	SS 410	300	304	30	30	242	0.16	3660	565	0.041	IF	21	4	276	TD2	TM5	AD2	AM7	CA:P, STT, small diameter weld
5060	SS 410	300	306	40	40	308	0.15	3615	100	0.016	IF	22	4	290	TD2	TM5	AD2	AM7	CA:P, STT, looks weaker
5061	SS 410	300	306	50	50	374	0.15	3615	164	0.018	IF	23	4	182	TD2	TM5	AD2	AM7	CA:P, STT, looks weaker
5062	SS 410	300	311	60	60	440	0.15	3615	0	0.000	IF	24	4	-44	TD2	TM5	AD2	AM7	CA:P, no weld
5063	SS 410	550	550	20	20	177	0.26	3030	599	0.045	IF	25	4	425	TD2	TM5	AD2	AM7	STT
5064	SS 410	550	513	30	30	242	0.21	3600	644	0.052	IF	26	4	488	TD2	TM5	AD2	AM7	WO, STT
5065	SS 410	550	460	40	40	308	0.19	3600	177	0.021	IF	27	4	427	TD2	TM5	AD2	AM7	WO, STT, looks weaker
5066	SS 410	550	461	50	50	374	0.19	3660	0	0.000	IF	28	4	296	TD2	TM5	AD2	AM7	WO, STA, looks weaker, broke while loading into tensile tester
5067	SS 410	550	521	60	60	440	0.20	3615	135	0.018	IF	29	4	70	TD2	TM5	AD2	AM7	WO, no STA or STT
5068	SS 410	800	800	20	20	177	0.36	3270	627	0.040	IF	30	4	638	TD2	TM5	AD2	AM7	STT, long weld, heat marks
5069	SS 410	800	498	30	30	242	0.19	3630	654	0.065	B	31	4	474	TD2	TM5	AD2	AM7	WO, STT, partial button
5070	SS 410	800	466	40	40	308	0.19	3615	256	0.021	IF	32	4	432	TD2	TM5	AD2	AM7	WO, no STT or STA, looks weak
5071	SS 410	1000	1004	20	20	177	0.44	3120	683	0.043	IF	33	4	758	TD2	TM5	AD2	AM7	Glow red-hot, STT
5072	SS 410	1000	477	30	30	242	0.19	3630	660	0.073	B	34	4	455	TD2	TM5	AD2	AM7	WO, STT, partial button, removed tooling and took pictures with stereoscope
5073	SS 410	441	444	30	30	242	0.18	3645	537	0.033	IF	35	5	424	TD2	TM5	AD2	AM7	Additional welds for repeatability and metallurgy, CA:P, STT, alignment needs to be re-adjusted
5074	SS 410	441	450	30	30	242	0.19	3630	706	0.049	B	36	5	429	TD2	TM5	AD2	AM7	Adjusted tool alignment, CA:P, STT, glow red-hot, partial button
5075	SS 410	441	454	30	30	242	0.19	3630	NA	NA	NA	37	5	433	TD2	TM5	AD2	AM7	CA:P, STT, glow red-hot, CS
5076	SS 410	441	455	30	30	242	0.19	3600				38	5	434	TD2	TM5	AD2	AM7	Reset light on power supply, STT
5077	SS 410	441	444	30	30	242	0.19	3615	715	0.051	B	39	5	424	TD2	TM5	AD2	AM7	CA:P, STT, partial button

Table 11 continued

5078	SS 410	1000	1003	20	20	177	0.41	3420	756	0.043	IF	40	5	758	TD2	TM5	AD2	AM7	Glow red-hot, long weld, STT
5079	SS 410	1000	1002	20	20	177	0.40	3390	644	0.038	IF	41	5	757	TD2	TM5	AD2	AM7	Glow red-hot, long weld, STT
5080	SS 410	1000	1003	20	20	177	0.39	3420				42	5	758	TD2	TM5	AD2	AM7	Glow red-hot, long weld, STT
5081	SS 410	1000	1000	20	20	177	0.39	3600	NA	NA	NA	43	5	756	TD2	TM5	AD2	AM7	Glow red-hot, long weld, STT, CS
5082	SS 410	1000	1010	20	20	177	0.38	3540	733	0.043	IF	44	5	761	TD2	TM5	AD2	AM7	Glow red-hot, long weld, STT
5083	SS 410	1500	1505	20	20	177	0.59	3540	821	0.051	IF	45	5	845	TD2	TM5	AD2	AM7	Long weld, glow orange-hot, STT
5084	SS 410	1500	1501	20	20	177	0.59	3495				46	5	846	TD2	TM5	AD2	AM7	Long weld, glow orange-hot, STT
5085	SS 410	1500	1503	20	20	177	0.61	3480	816	0.046	IF	47	5	845	TD2	TM5	AD2	AM7	Long weld, glow orange-hot, STT
5086	SS 410	1500	1507	20	20	177	0.60	3585	728	0.048	IF	48	5	845	TD2	TM5	AD2	AM7	Long weld, glow orange-hot, STT, SEM fractography
5087	SS 410	1500	1499	20	20	177	0.59	3555	791	0.046	IF	49	5	846	TD2	TM5	AD2	AM7	Long weld, glow orange-hot, STT
5088	SS 410	1000	543	25	25	210	0.20	3615	613	0.037	B	50	5	481	TD2	TM5	AD2	AM7	WO, short glow, stronger STT, partial button
5089	SS 410	1000	526	25	25	210	0.20	3600	658	0.049	B	51	5	465	TD2	TM5	AD2	AM7	WO, short glow, stronger STT, partial button
5090	SS 410	1000	610	25	25	210	0.23	3660	708	0.050	B	52	5	541	TD2	TM5	AD2	AM7	WO, short glow, stronger STT, partial button
5091	SS 410	1000	611	25	25	210	0.23	3600	NA	NA	NA	53	5	542	TD2	TM5	AD2	AM7	WO, short glow, stronger STT, CS
5092	SS 410	1000	549	25	25	210	0.22	3600				54	5	487	TD2	TM5	AD2	AM7	WO, short glow, stronger STT
5093	SS 410	1000	1000	15	15	144	0.44	3150	541	0.033	IF	55	5	698	TD2	TM5	AD2	AM7	Glow red-hot, long weld
5094	SS 410	1000	1002	15	15	144	0.41	3330	NA	NA	NA	56	5	699	TD2	TM5	AD2	AM7	Glow red-hot, long weld, CS
5095	SS 410	1000	1008	15	15	144	0.42	3270				57	5	702	TD2	TM5	AD2	AM7	Glow red-hot, long weld
5096	SS 410	1000	1006	15	15	144	0.41	3330	619	0.039	IF	58	5	701	TD2	TM5	AD2	AM7	Glow red-hot, long weld
5097	SS 410	1000	1011	15	15	144	0.42	3270	691	0.044	IF	59	5	704	TD2	TM5	AD2	AM7	Glow red-hot, long weld
5098	SS 410	2000	2005	20	20	177	0.82	3540	780	0.040	IF	60	5	639	TD2	TM5	AD2	AM7	Long weld, lots of glow-orange, STT
5099	SS 410	2000	2006	20	20	177	0.82	3585	NA	NA	NA	61	5	638	TD2	TM5	AD2	AM7	Long weld, lots of glow-orange, STT, threw sparks from tip-coupon interface, CS
5100	SS 410	2000	685	20	20	177	0.26	3600	683	0.041	B	62	5	549	TD2	TM5	AD2	AM7	WO, STT, partial button
5101	SS 410	2000	2002	20	20	177	0.80	3480				63	5	641	TD2	TM5	AD2	AM7	Glow red-hot, took picture during weld of glowing tip, STT
5102	SS 410	2000	670	20	20	177	0.26	3600	688	0.052	B	64	5	537	TD2	TM5	AD2	AM7	WO, short glow, STT, partial button, removed tooling and took pictures with stereoscope

Table 11 continued

<b>6000</b> Ni 718	600	601	40	40	308	1.04	810	0	0.000	IF	1	-	NA	TD2	TM2	AD2	AM2	0.004" Sn-foil at tip and anvil interface, long weld cycle, no weld formed, no STA, strong STT
<b>6001</b> Ni 718	600	601	60	60	440	0.98	780	0	0.000	IF	2	-	NA	TD2	TM2	AD2	AM2	0.004" Sn-foil at tip and anvil interface, long weld cycle, no weld formed, glow red-hot at tip interface, less sticking to tip, no STA, anvil doesn't seem to grip sample w/ the Sn-foil
<b>6002</b> Ni 718	600	601	60	60	440	0.77	1095	0	0.000	IF	3	-	NA	TD2	TM2	AD2	AM2	0.0005" Cu-foil at tip and anvil interface, long weld cycle, but no weld, shorter cycle and higher-power than w/ Sn-foil, stronger STT, no STA
<b>6003</b> Ni 718	600	599	60	60	440	0.62	1380	0	0.000	IF	4	-	NA	TD2	TM2	AD2	AM2	0.0005" Cu-foil at tip and anvil interface, 0.002" Nickel 201 foil at weld interface, weld STT, broke weld during removal, this approach is promising but is not in line with the focus of this study
<b>6004</b> Ni 718	1500	1062	60	60	440	2.01	765	0	0.000	IF	5	-	NA	TD2	TM2	AD2	AM2	0.004" Sn-foil at tip and anvil interface- very small pieces, long weld, CA:T, lots of heat input, glow red-hot during weld, tip heat marks, no STA, strong STT, no weld
<b>6005</b> Ni 718	1500	1290	80	80	571	2.01	750	0	0.000	IF	6	-	NA	TD2	TM2	AD2	AM2	0.004" Sn-foil at tip and anvil interface- very small pieces, no weld, long cycle, tip glowing red-hot, it appears all the energy goes into the tip and not the coupon interface, meaning the Sn-foil may be preventing the tip from properly gripping the coup
<b>6006</b> Ni 718	600	599	80	80	571	0.48	3510	0	0.000	IF	7	-	NA	TD2	TM2	AD2	AM2	0.004" Sn-foil at tip and anvil interface- very small pieces, better, glow red-hot, no STA, strong STT, broke weld during removal, but I.F. bond area is much improved
<b>6007</b> Ni 718	1500	523	80	80	571	0.22	3600	0	0.000	IF	8	-	NA	TD2	TM2	AD2	AM2	No foil insert, WO, low energy, no weld, less STT, strong STA, pry-off
<b>6008</b> Ni 718	1000	546	60	60	440	0.22	3615	0	0.000	IF	9	-	NA	TD2	TM2	AD2	AM2	WO, low energy, no weld, less STT, strong STA pry-off

Table 11 continued

6009	Ni 718	1000	1002	40	40	308	0.96	3510	0	0.000	IF	10	-	NA	TD2	TM2	AD2	AM2	Welded tip, coupon, and anvil together, broke weld during removal, welded nugget to tip, anvil knurl is destroyed
6010	Ni 718	600	601	40	40	308	0.85	1275	0	0.000	IF	11	-	NA	TD2	TM2	AD2	AM2	New 350M tip and worn 350M anvil were oxidized w/ an oxy-acetylene torch prior to weld, glow red-hot, longer weld, no STA, STT, broke weld during removal, took pictures of tooling w/ stereoscope- oxide was removed from surfaces
6011	Ni 718	600	602	40	40	308	0.74	2550	0	0.000	IF	12	-	NA	TD2	TM2	AD2	AM2	Re-installed tooling from Trial 6010, to repeat weld w/o oxide layer, glow red-hot, no STA, strong STT- weld nugget STT, broke during removal
6012	Ni 718	600	601	60	60	440	0.72	1380	588	0.039	IF	13	-	NA	TD2	TM2	AD2	AM2	New 350M tip, anvil from Trial 6011, glow red-hot, no STA, strong STT, tip cut-off in order to further evaluate weld, SEM fractography
6013	Ni 718	1000	1002	80	80	571	1.04	2940	NA	NA	NA	18	-	NA	TD2	TM2	AD2	AM2	Re-oxidized worn 350M tip and anvil from Trial 7003, glow red-hot, no STA, strong STT, tip cut-off in order to further evaluate weld, CS
7000	Ni 625	1000	1000	60	60	440	1.46	1560	NA	NA	NA	1	-	NA	TD2	TM2	AD2	AM2	New 350M tip and anvil oxidized w/ an oxy-acetylene torch prior to weld, long weld, glow red-hot, STT, no STA, CS
7001	Ni 625	1000	530	80	80	571	0.19	3660	0	0.000	IF	2	-	NA	TD2	TM2	AD2	AM2	Same 350M tip and anvil from Trial 7000 w/ oxide removed, no weld, WO, STT, strong STA, pry-off w/ pliers

197

Continued

Table 11 continued

<b>7002</b> Ni 625	100 0	100 1	80	80	571	1.08	1680	789	0.049	IF	3	-	NA	TD2	TM 2	AD2	AM 2	New 350M tip and worn 350M anvil from Trial 7001 oxidized w/ an oxy-acetylene torch prior to weld, long weld, glow red-hot, no STA, STT, larger diameter weld than Trial 7002, SEM fractography
<b>7003</b> Ni 625	150 0	130 9	80	80	571	2.01	2250	NA	NA	NA	4	-	NA	TD2	TM 2	AD2	AM 2	Re-oxidized worn 350M tip and anvil from Trial 7002, no STA, strong STT, pry-off, similar appearance to Trial 7002, CS

Column/ Location	Abbreviation	Definition
Mechanical Testing: Failure Mode	IF	Interfacial Failure
	B	Button
	M	Base Material
Comments	WO	Weld Overload
	CA / CA:P / CA:T	Cycle Alarm / Cycle Alarm: Power / Cycle Alarm: Time
	STT	Sticking-to-Tip
	STA	Sticking-to-Anvil
Tooling: Tip Design/ Texture	TD1	0.5in spherical radius, Aggressive laser-machined linear laser knurl
	TD2	0.5in spherical radius, laser-machined linear laser knurl; less depth and lines spaced further apart
	TD3	0.5in spherical radius, laser-machined cross-hatch laser knurl; less depth and lines spaced further apart
Tooling: Tip Material	TM1	W-25Re tips brazed to M2 base tool
	TM2	Heat-treated AISI Grade 18Ni Maraging Steel (350M)
	TM3	Wrought-tungsten tips brazed to AISI M2 base tool
	TM4	TZM tips brazed to AISI M2 base tool
	TM5	W-La alloy tips brazed to AISI M2 base tool
Tooling: Anvil Design/ Texture	AD1	Machined cross-hatch knurl, 0.025in spacing x 0.008in depth x 45° angle
	AD2	Laser-machined cross-hatch knurl pattern, same parameters as "lighter" tungsten-based tips
Tooling: Anvil Material	AM1	Heat-treated AISI M2 HSS
	AM2	Heat-treated AISI Grade 18Ni Maraging Steel (350M)
	AM3	CMW Elkon 100W pure tungsten
	AM4	W-25Re weld surface brazed to ground AISI M2 anvil
	AM5	Wrought-tungsten weld surface brazed to ground AISI M2 anvil
	AM6	TZM weld surface brazed to ground AISI M2 anvil
	AM7	W-La weld surface brazed to ground AISI M2 anvil

**Table 12: Terms and abbreviations used throughout Table 11.**

APPENDIX B

PICTURES OF TOOL WEAR

Several different tool materials were evaluated during the course of the welding trials. The tool performance has been discussed in Chapter 4 and 5. Periodically (ideally between DOE blocks) the welding tip and anvil were removed from the welder and pictures were taken using a stereomicroscope. During some of the experiments, braze joints failed or the tooling otherwise required replacement or modification. Pictures of failed joints and tools are also included. Figure 111 through Figure 142 are the pictures of the tooling, organized by weld trial, in two resolutions (nominally 1.8X and 5.0X unless indicated otherwise by the scale).

B.1 C. P. TITANIUM WELD TRIALS

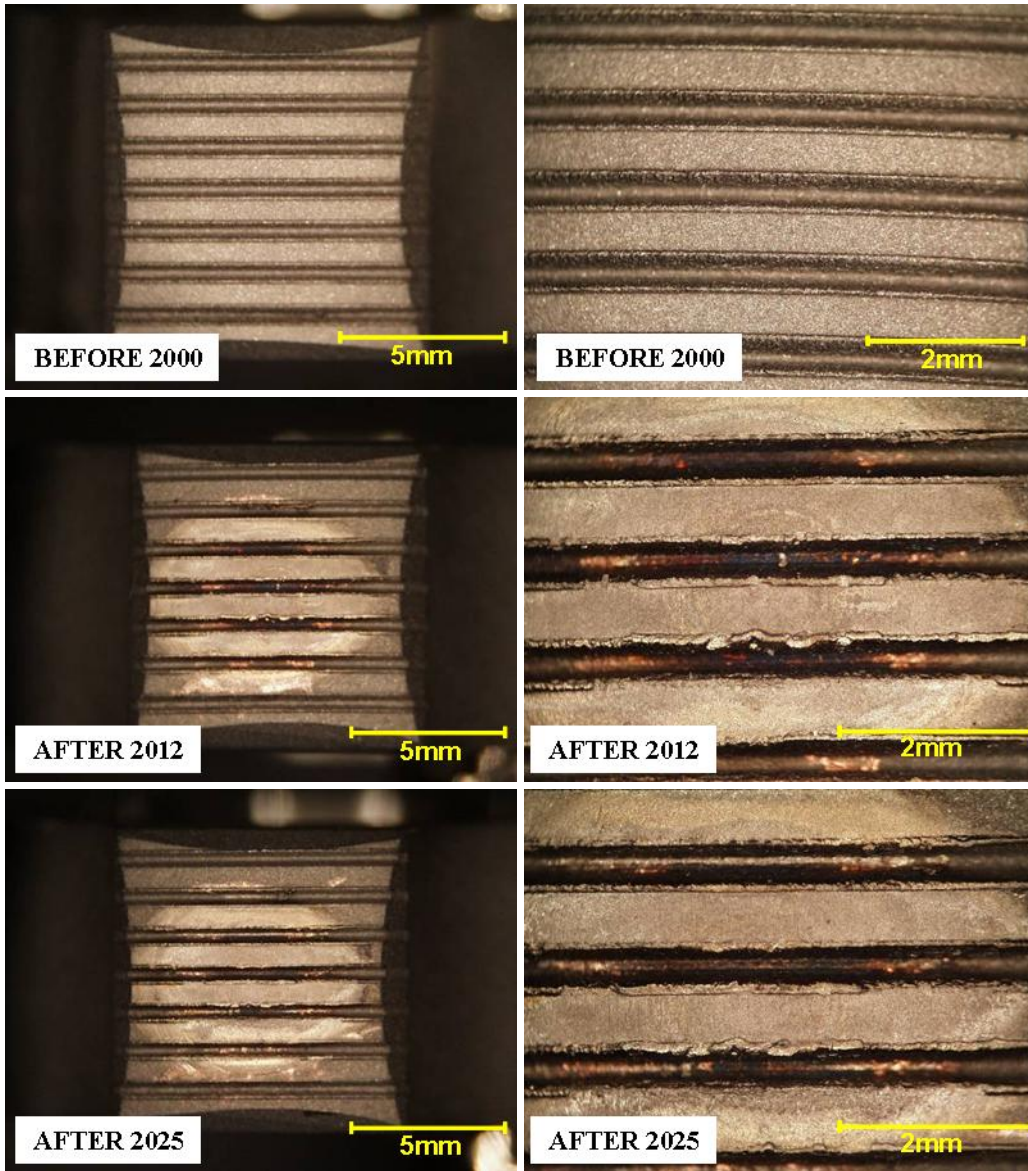


Figure 111: 350M weld tip during C.P. titanium weld trials 2000-2025

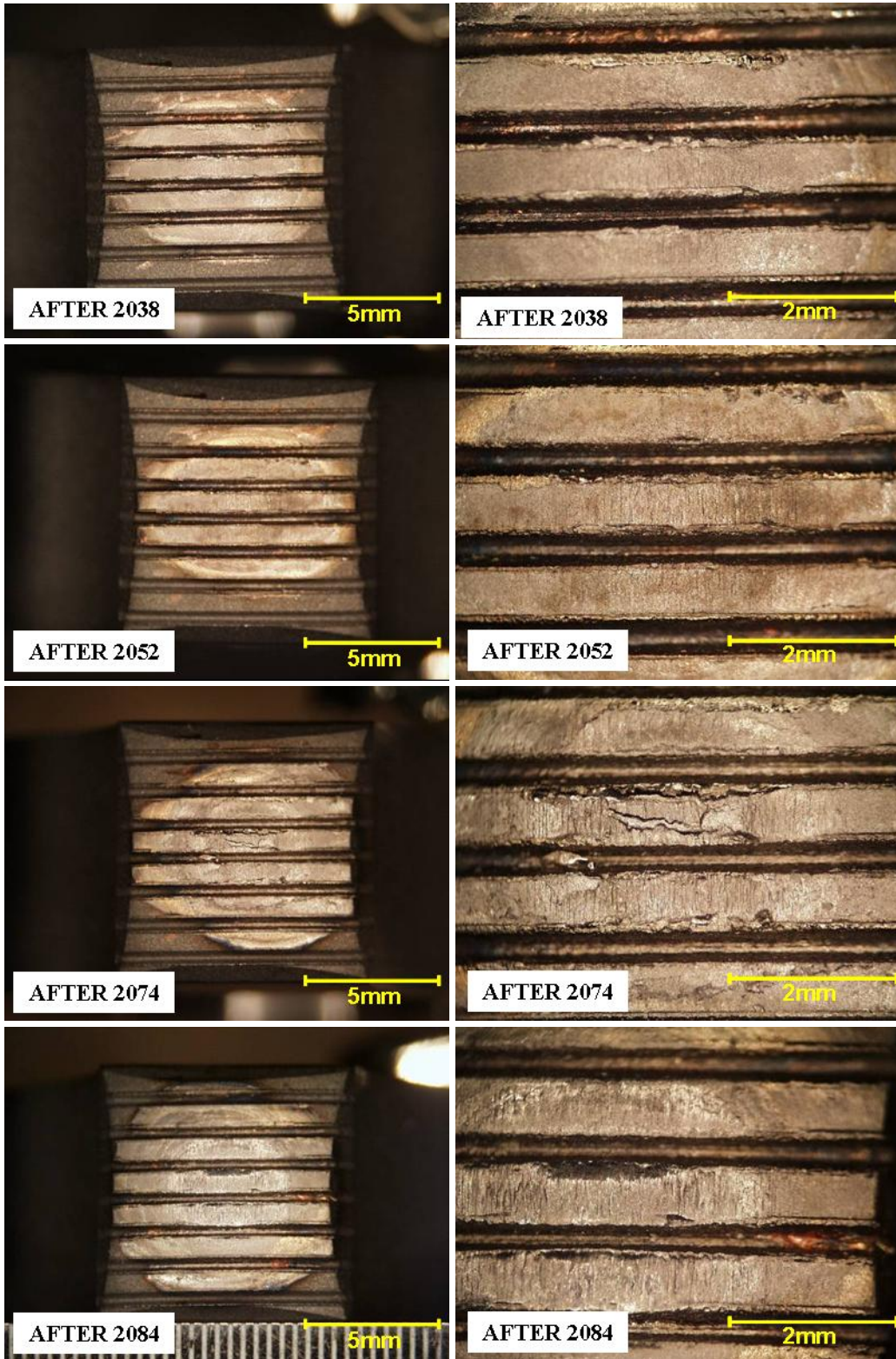


Figure 112: 350M weld tip after C.P. titanium weld trials 2026-2084

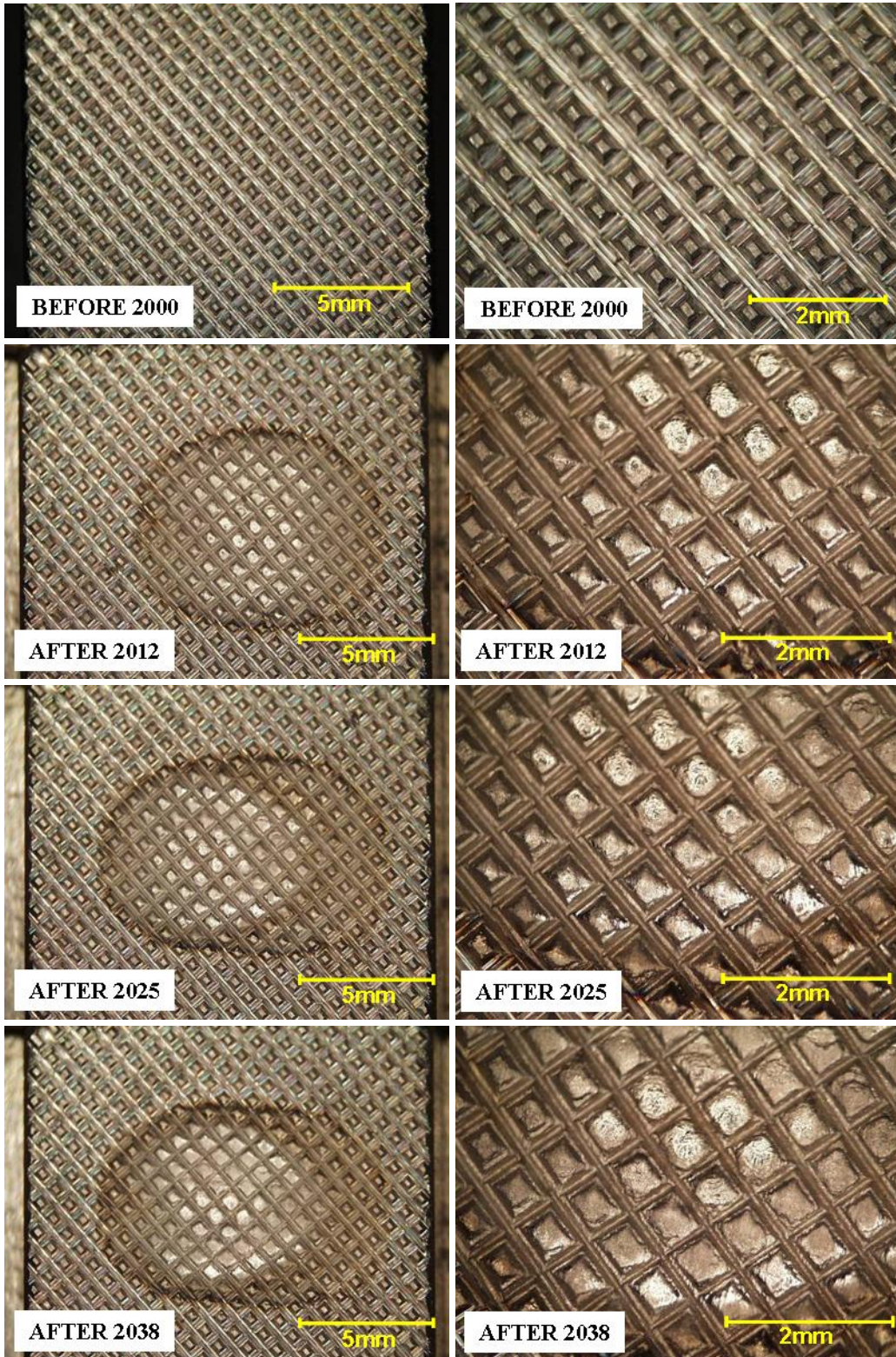


Figure 113: 350M anvil after C.P. titanium weld trials 2000-2038

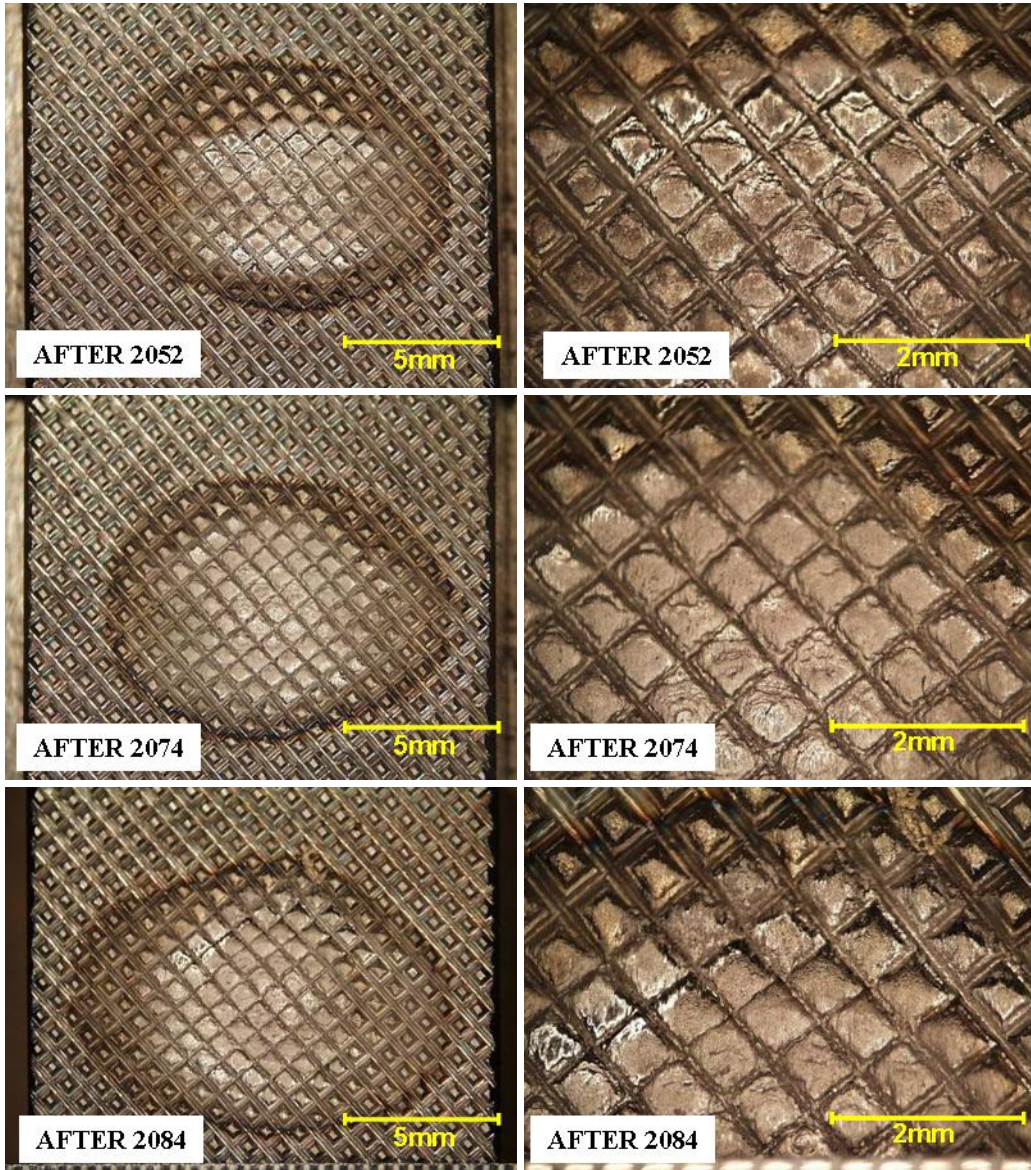


Figure 114: 350M anvil after C.P. titanium weld trials 2039-2084

B.2 TITANIUM 6AL-4V WELD TRIALS

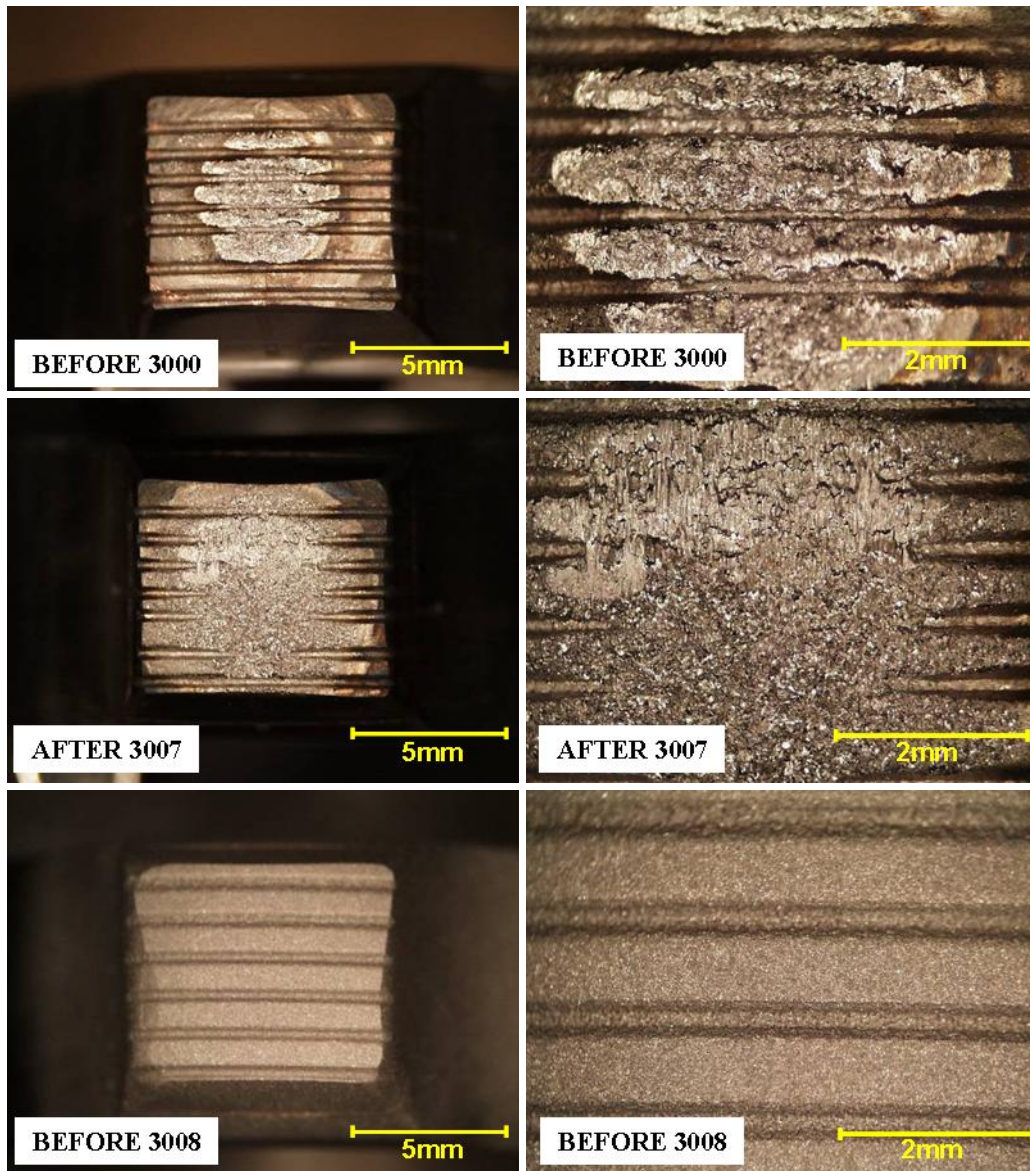


Figure 115: Wrought-tungsten tip during Titanium 6Al-4V weld trials 3000-3008

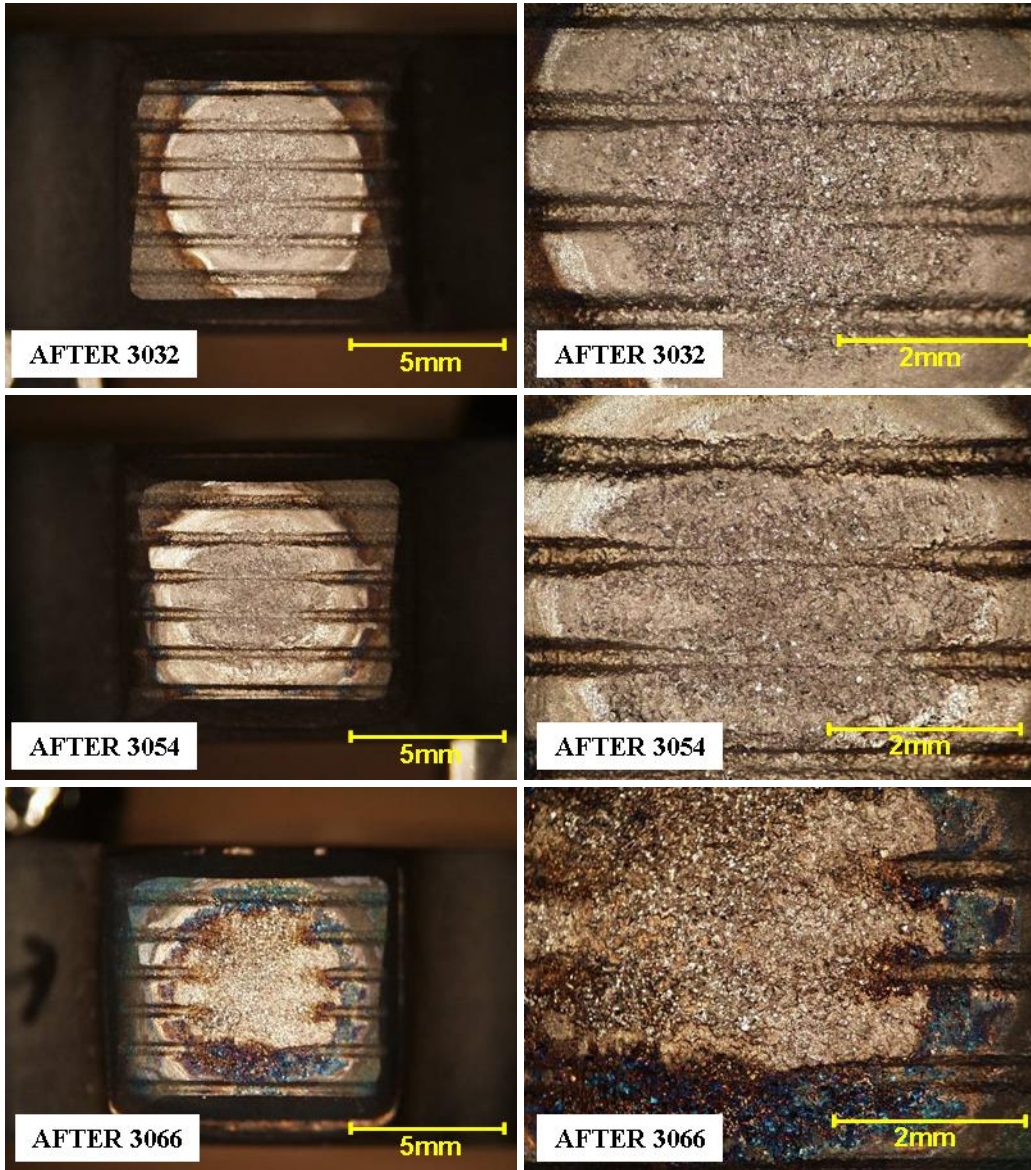


Figure 116: Wrought-tungsten tip after Titanium 6Al-4V weld trials 3008-3066

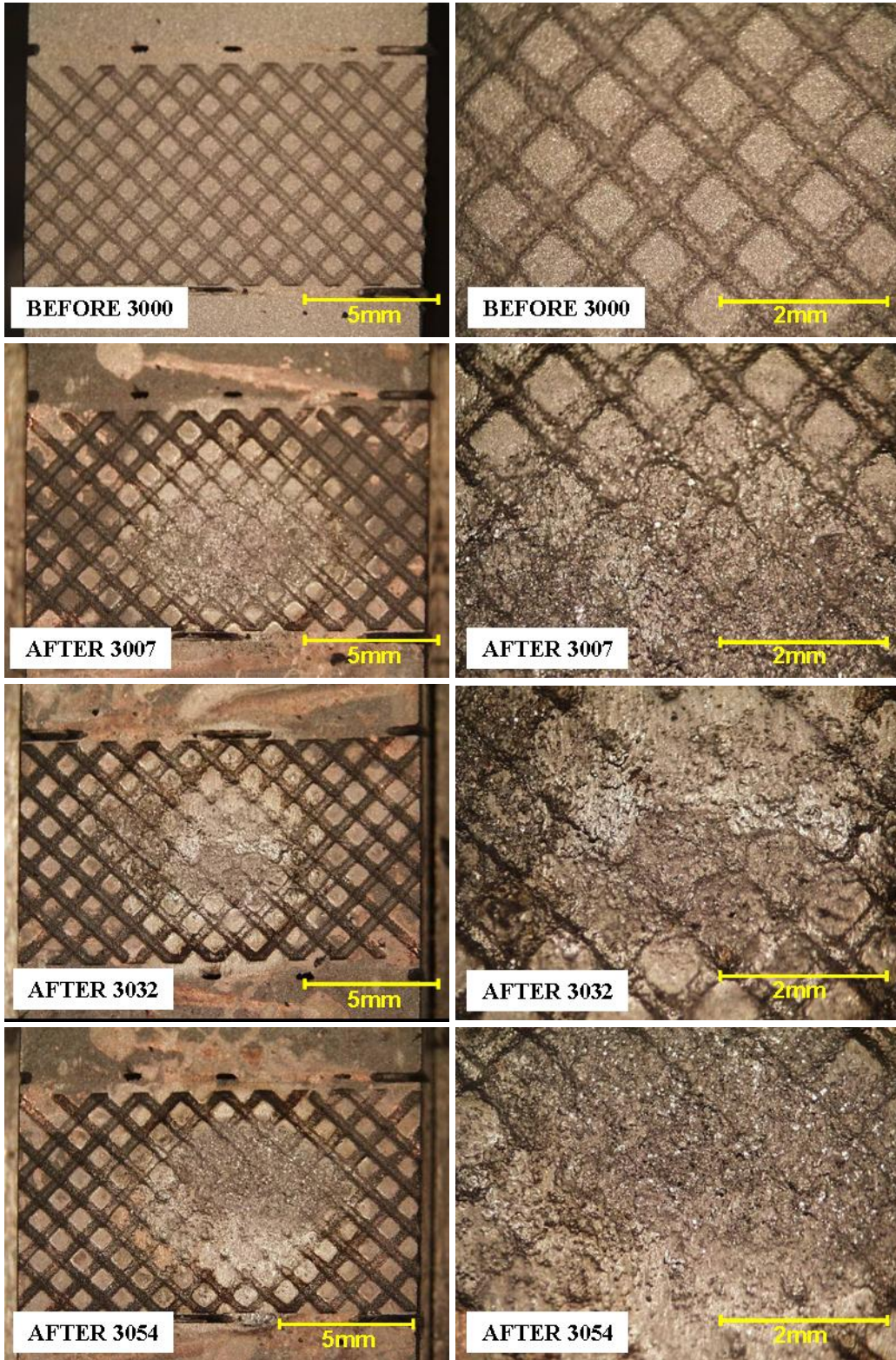
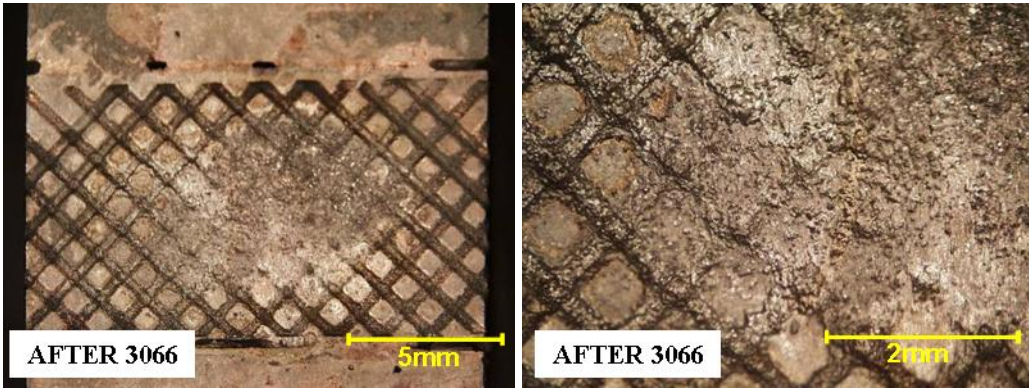


Figure 117: Wrought-tungsten anvil during Titanium 6Al-4V weld trials 3000-3054



**Figure 118: Wrought-tungsten anvil after Titanium 6Al-4V weld trials 3055-3066**

B.3 SS 304 WELD TRIALS

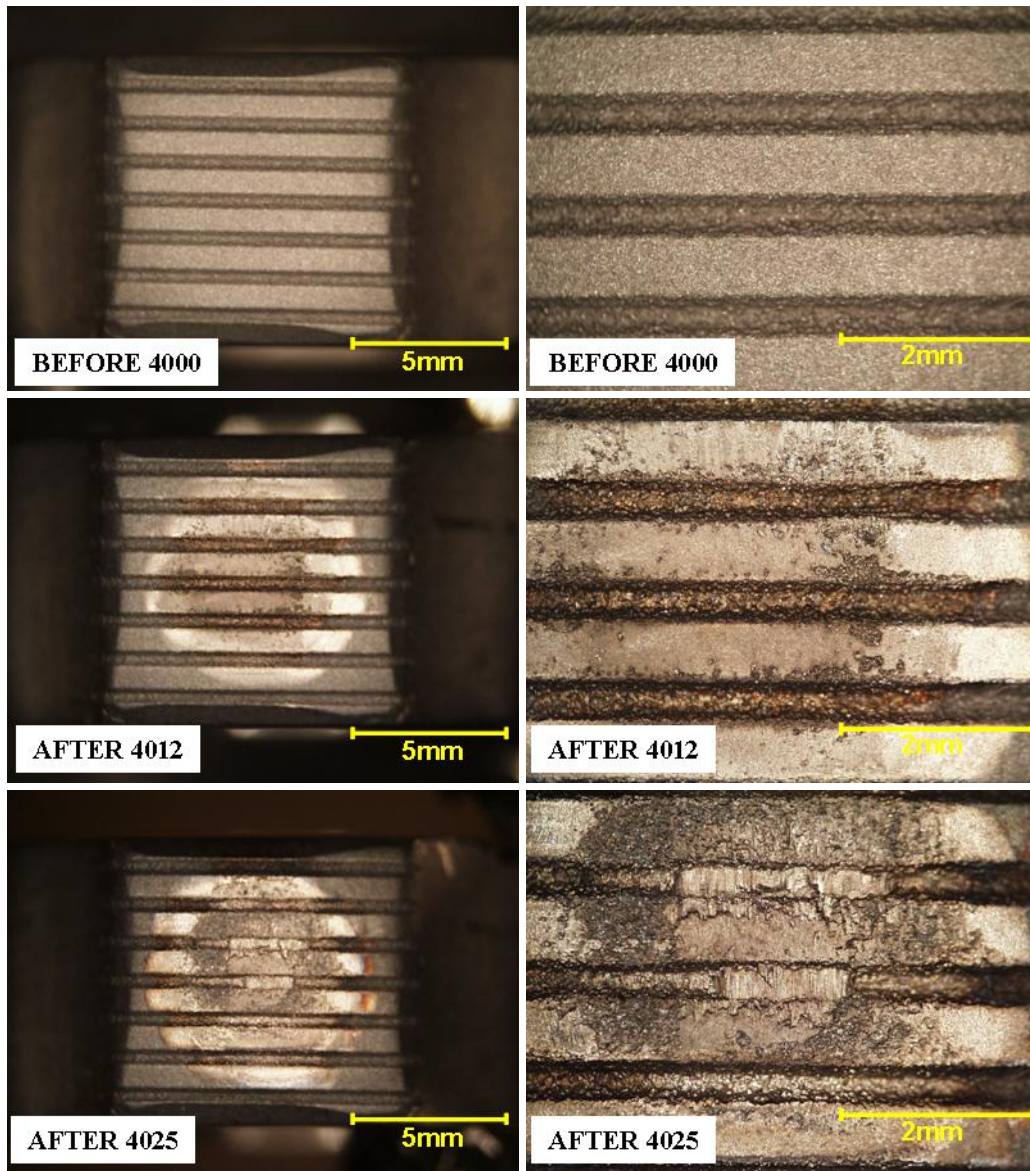


Figure 119: W-25Re tip after SS 304 weld trials 4000-4025

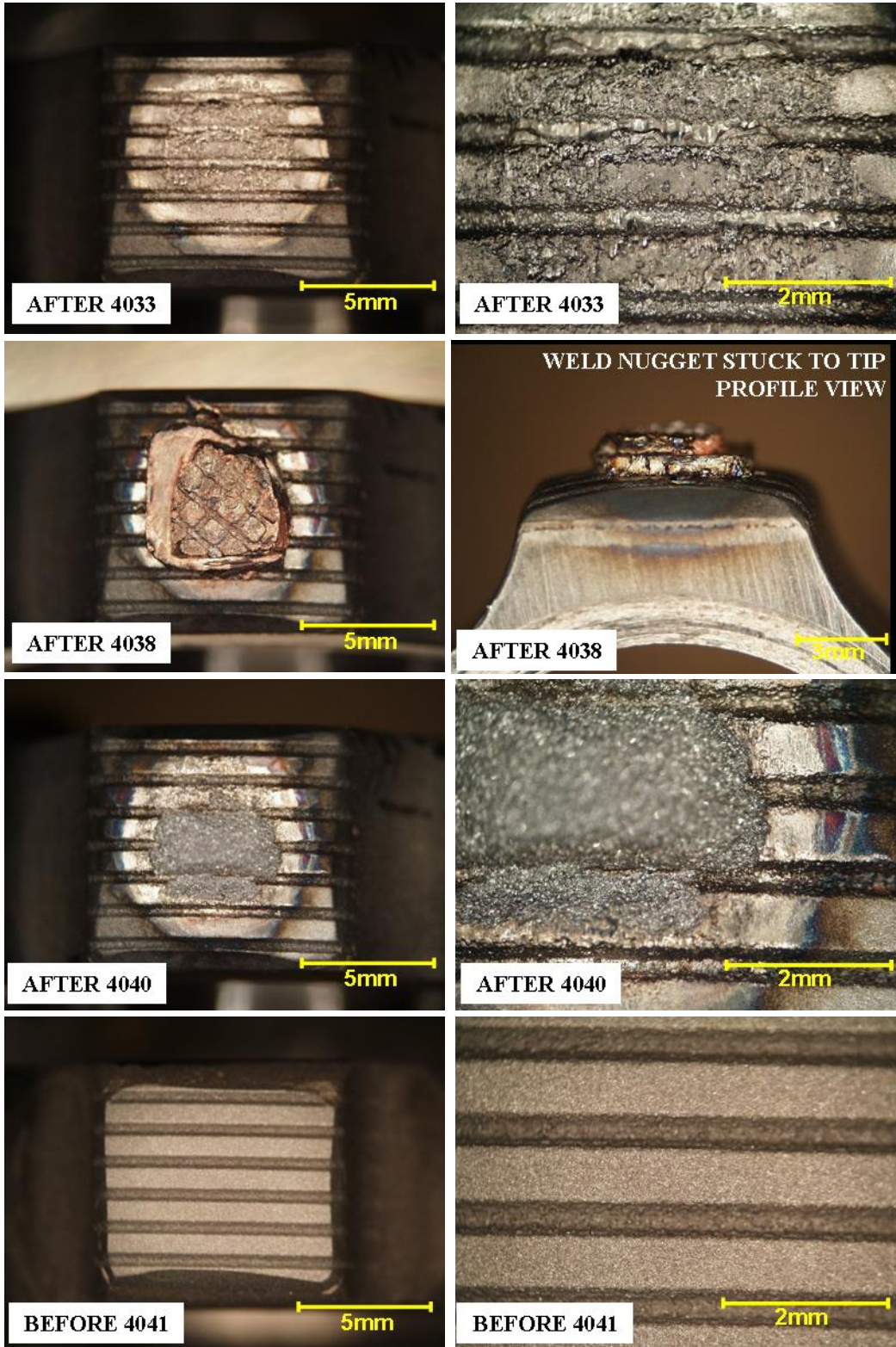


Figure 120: W-25Re tip during SS 304 weld trials 4033-4041

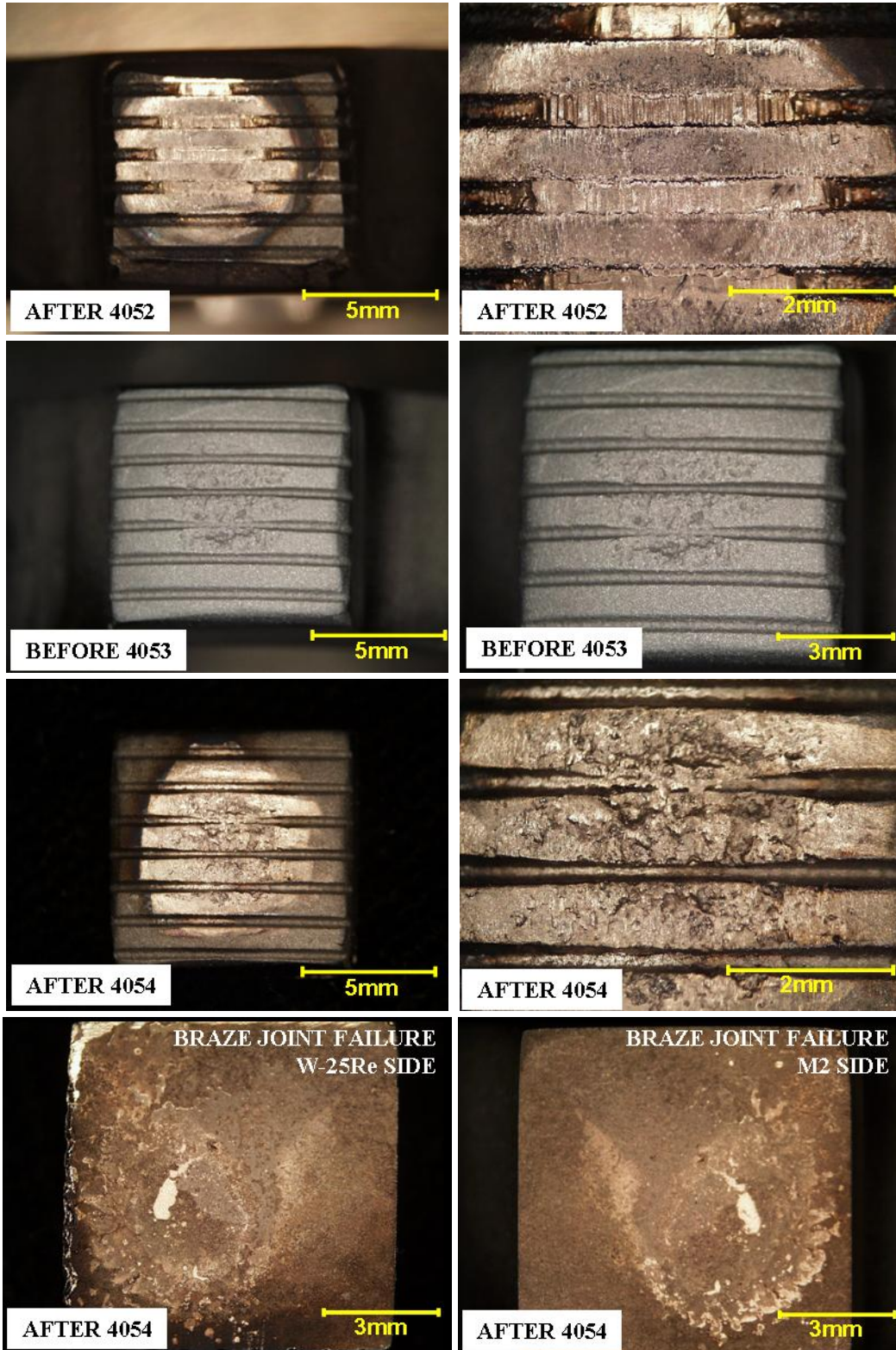


Figure 121: W-25Re tip after SS 304 weld trials 4042-4054

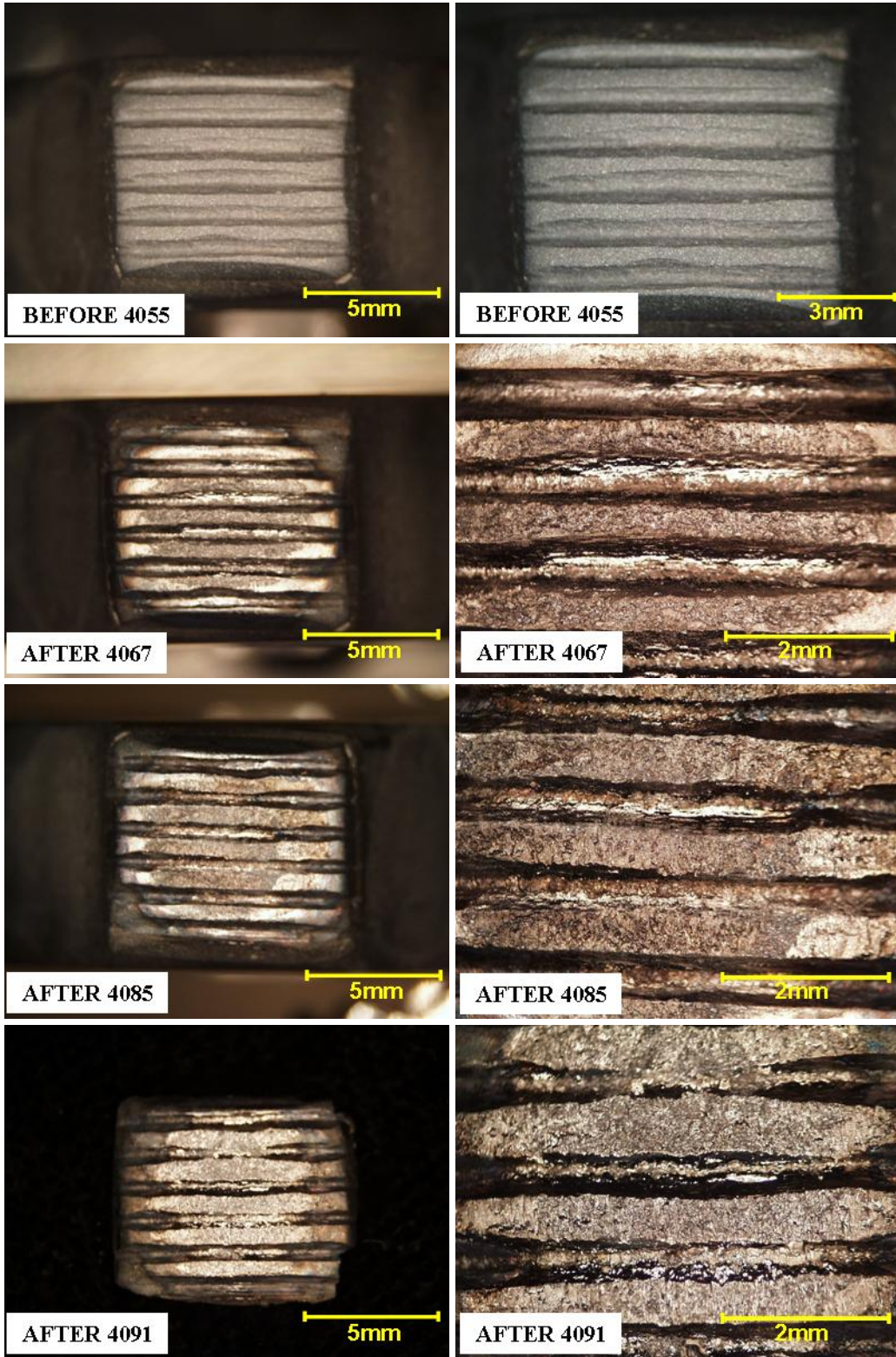


Figure 122: W-25Re tip during SS 304 weld trials 4055-4091

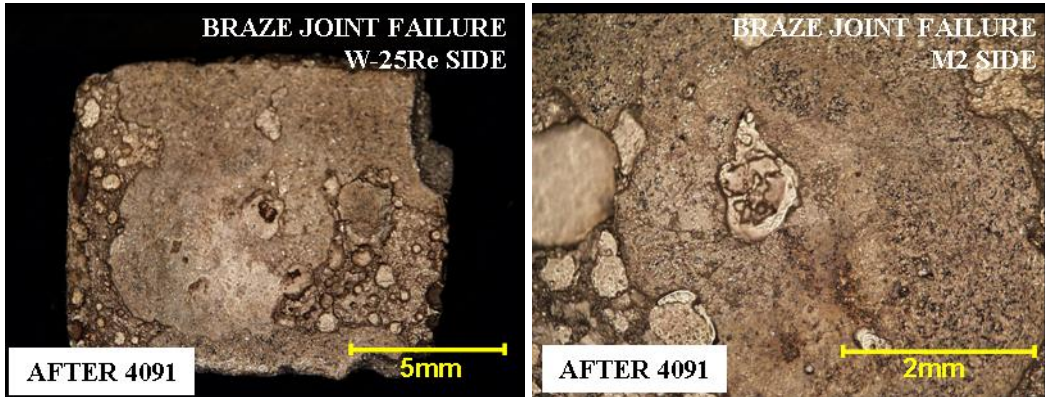


Figure 123: W-25Re tip braze joint failure after SS 304 weld trial 4091

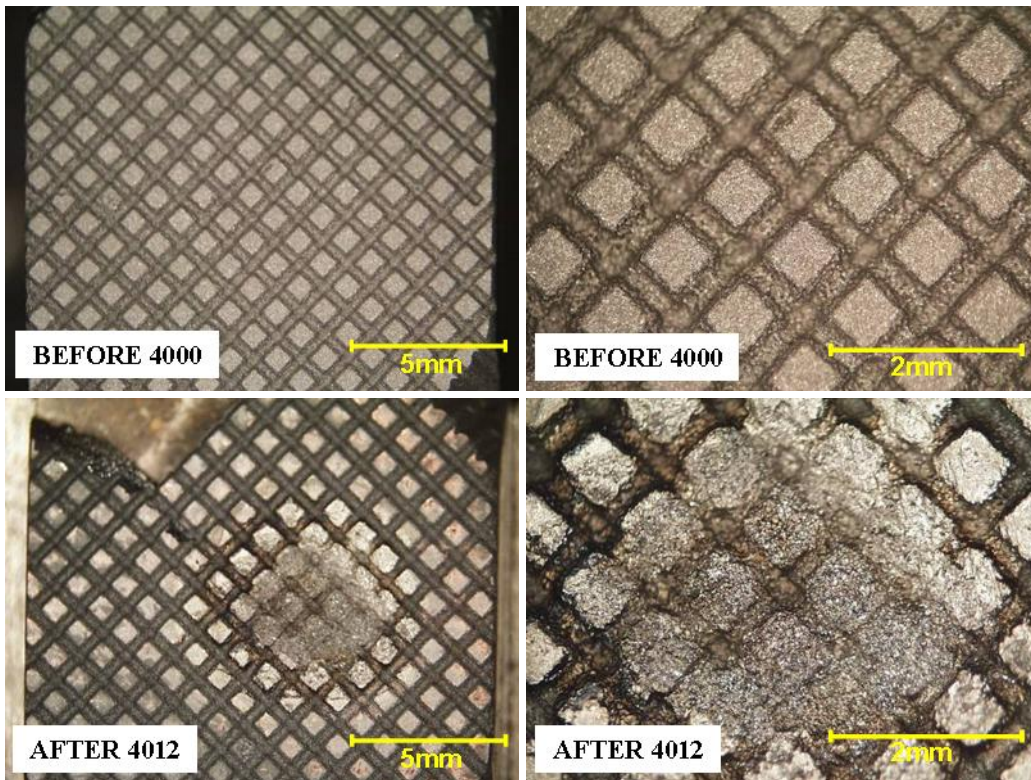


Figure 124: W-25Re anvil during SS 304 weld trials 4000-4012



Figure 125: W-25Re anvil during SS 304 weld trials 4025-4034

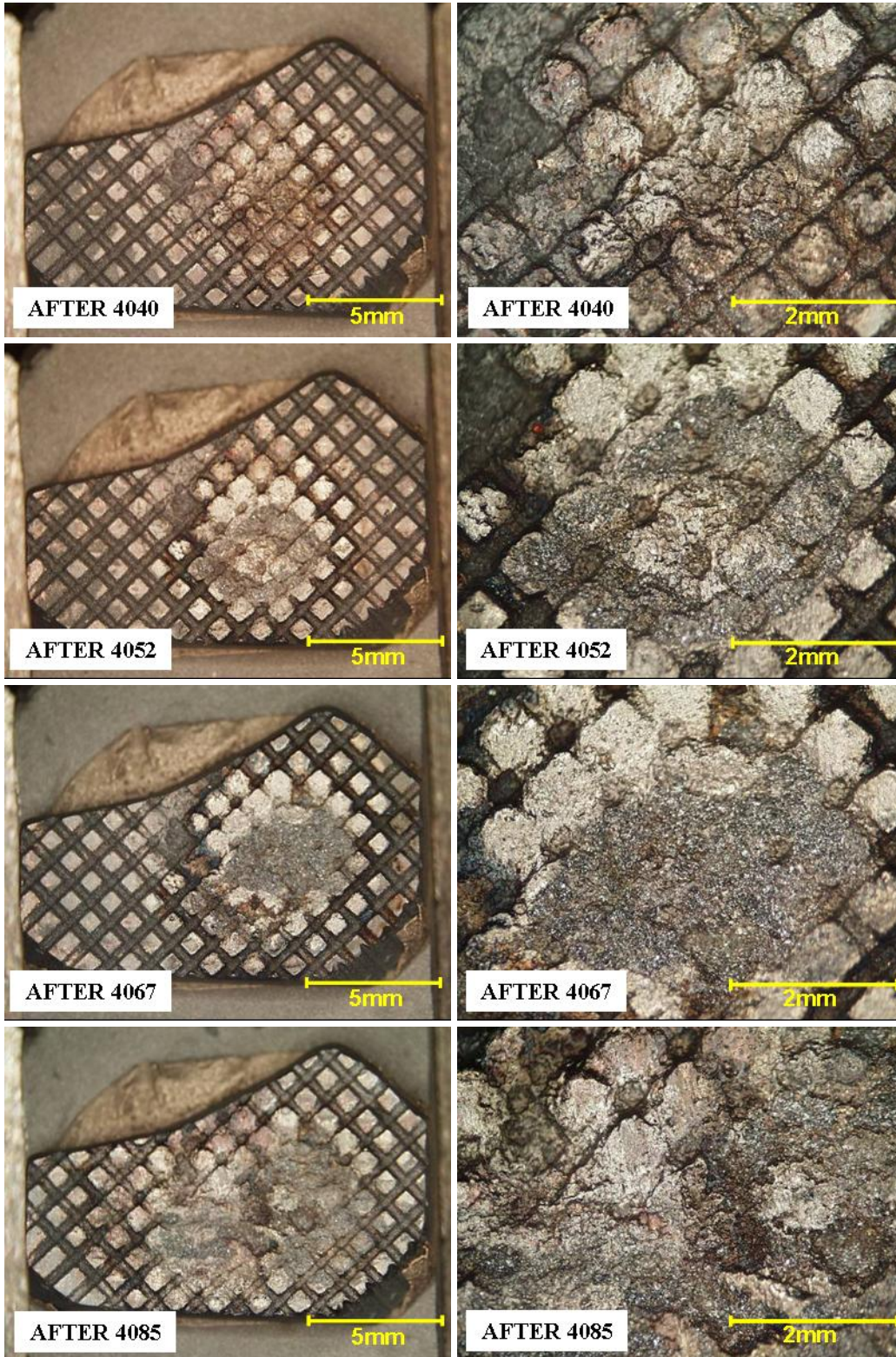


Figure 126: W-25Re anvil after SS 304 weld trials 4040-4085

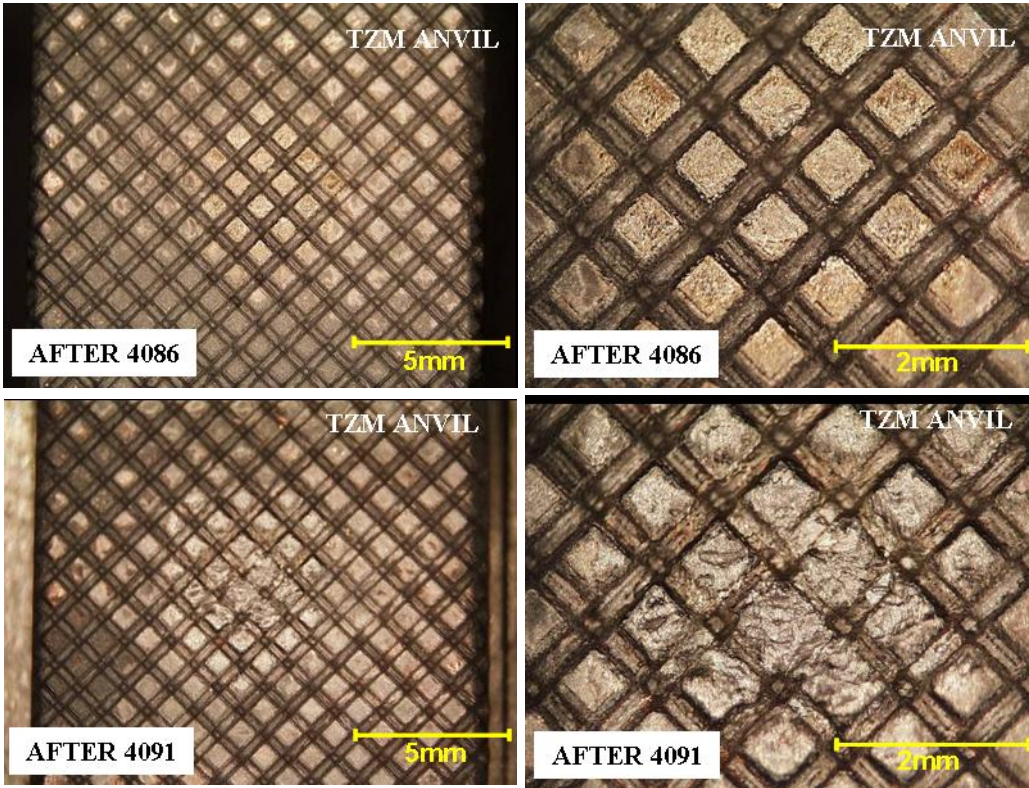


Figure 127: TZM anvil after SS 304 weld trials 4086-4091

B.4 SS 410 WELD TRIALS



Figure 128: W-La tip after SS 410 weld trials 5000-5008

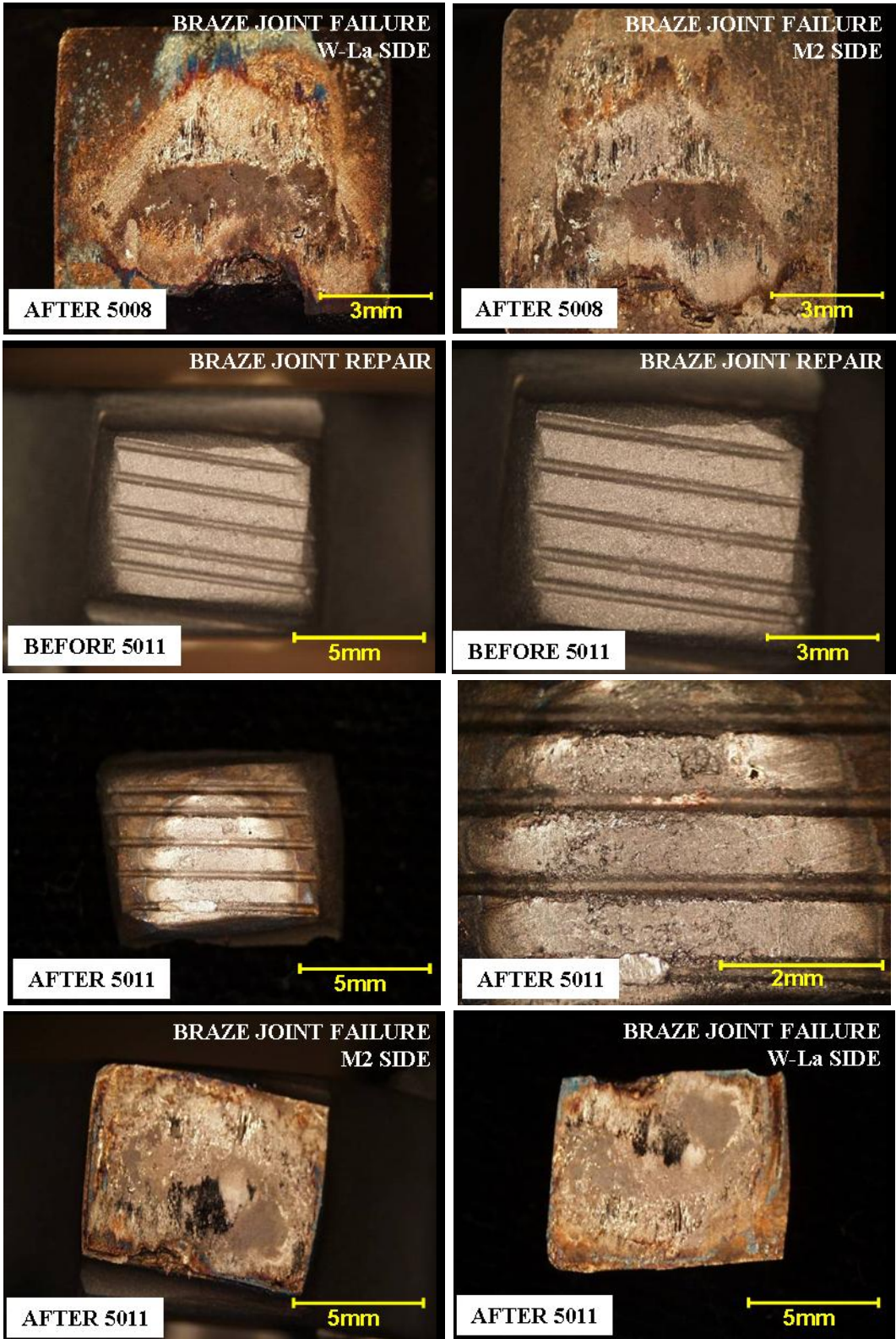


Figure 129: W-La tip after SS 410 weld trials 5008-5011

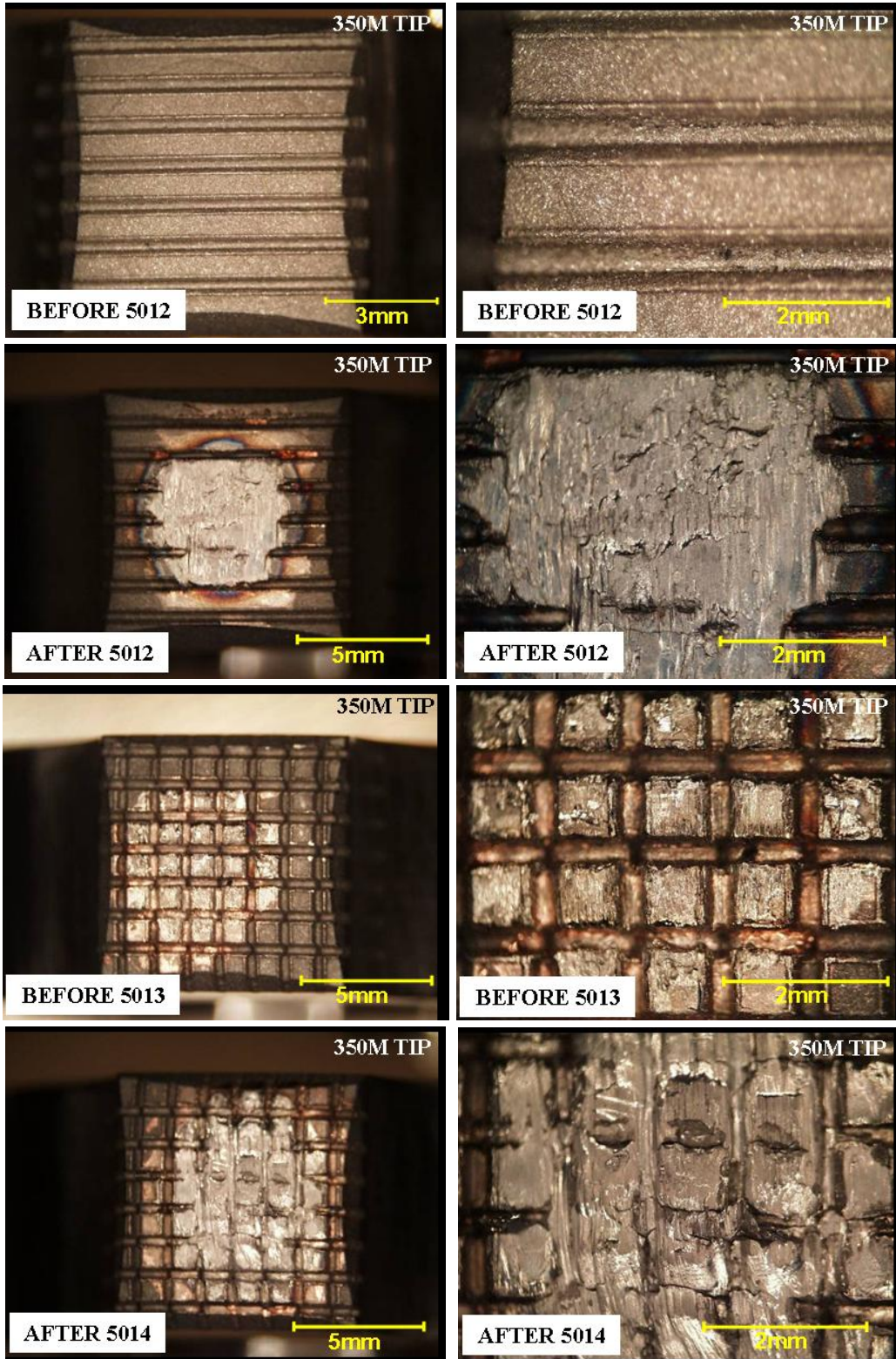


Figure 130: 350M tip before SS 410 weld trials 5012-5014

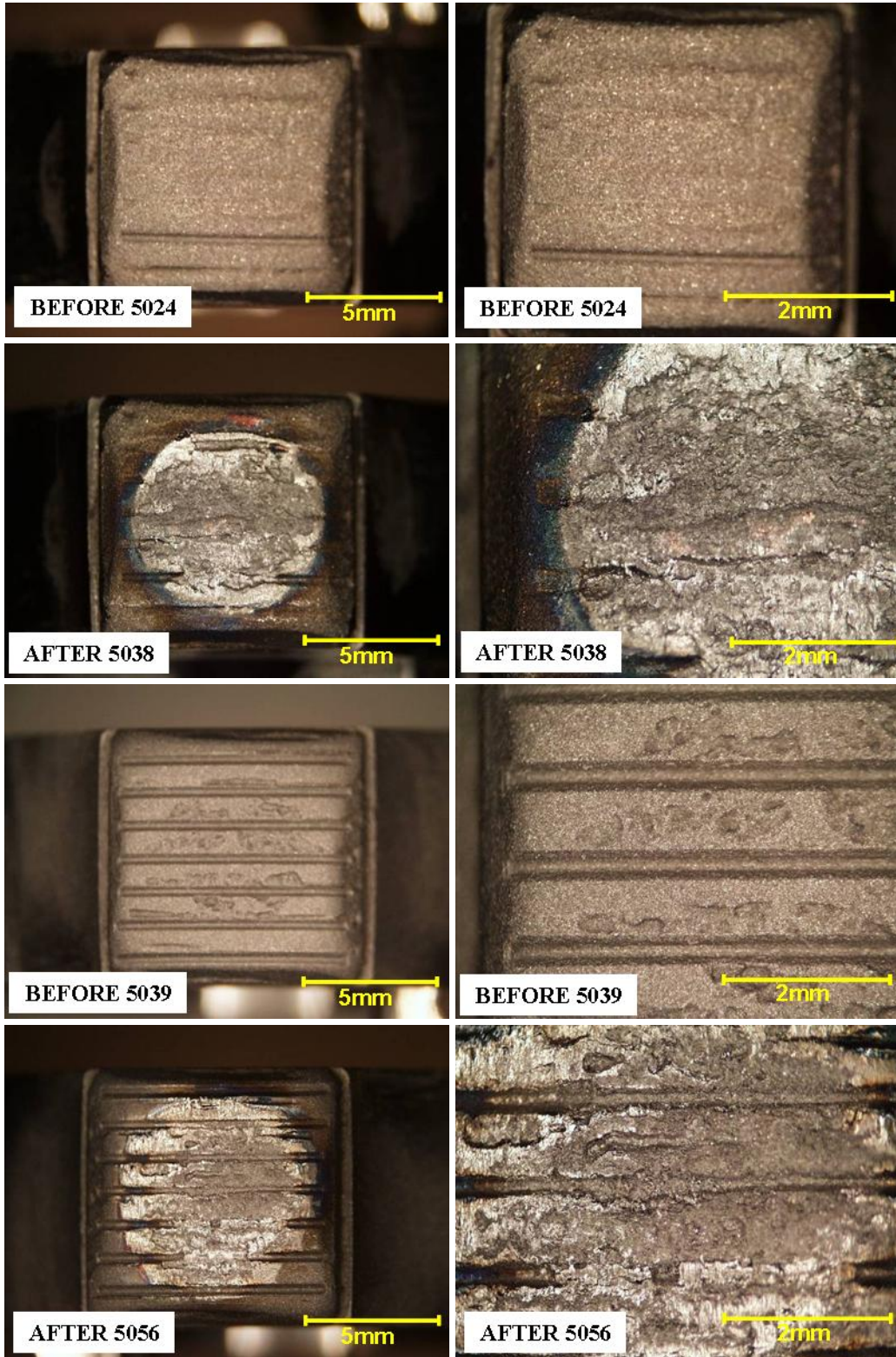


Figure 131: W-La tip during SS 410 weld trials 5024-5056

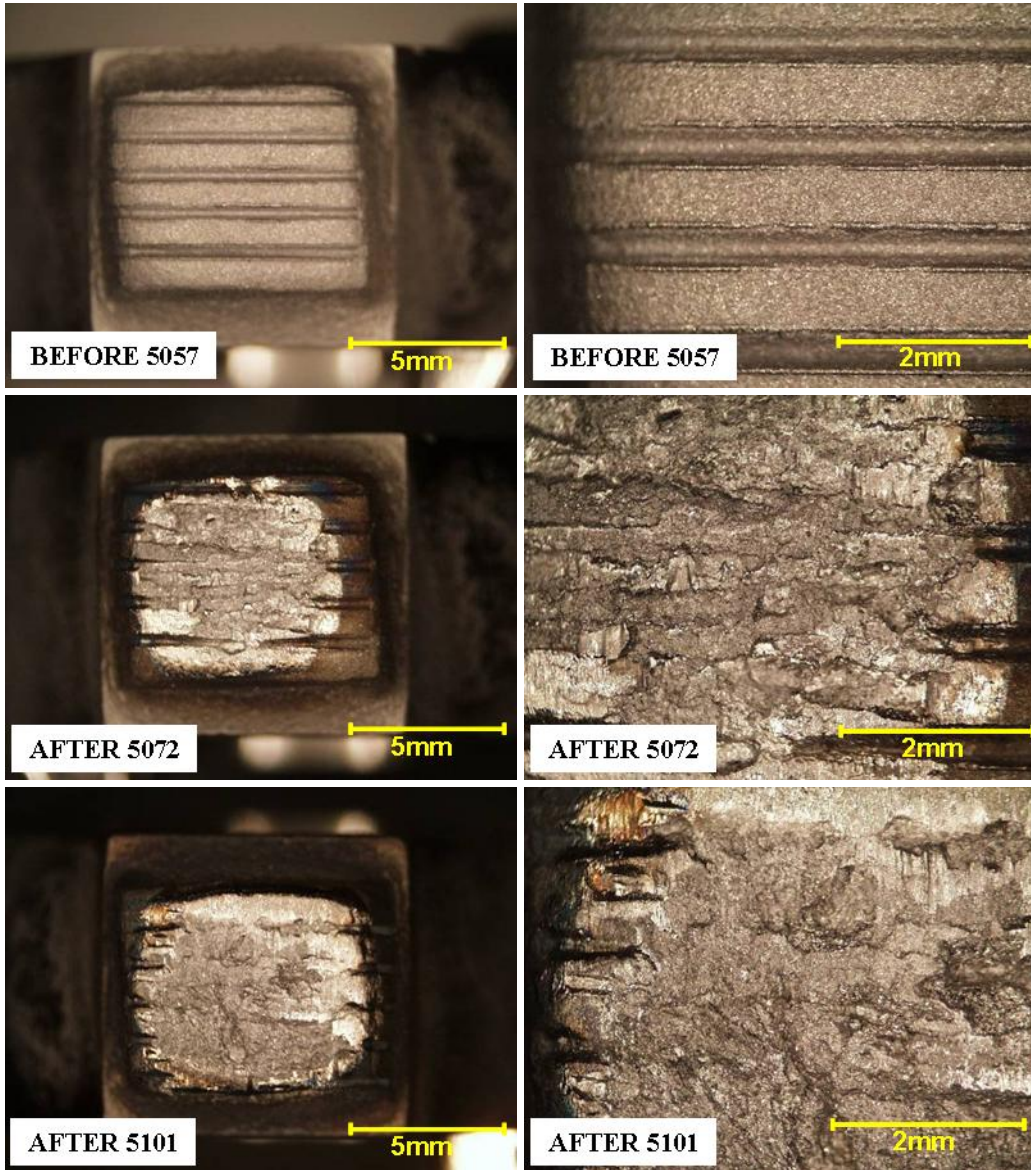


Figure 132: W-La tip after SS 410 weld trials 5057-5101

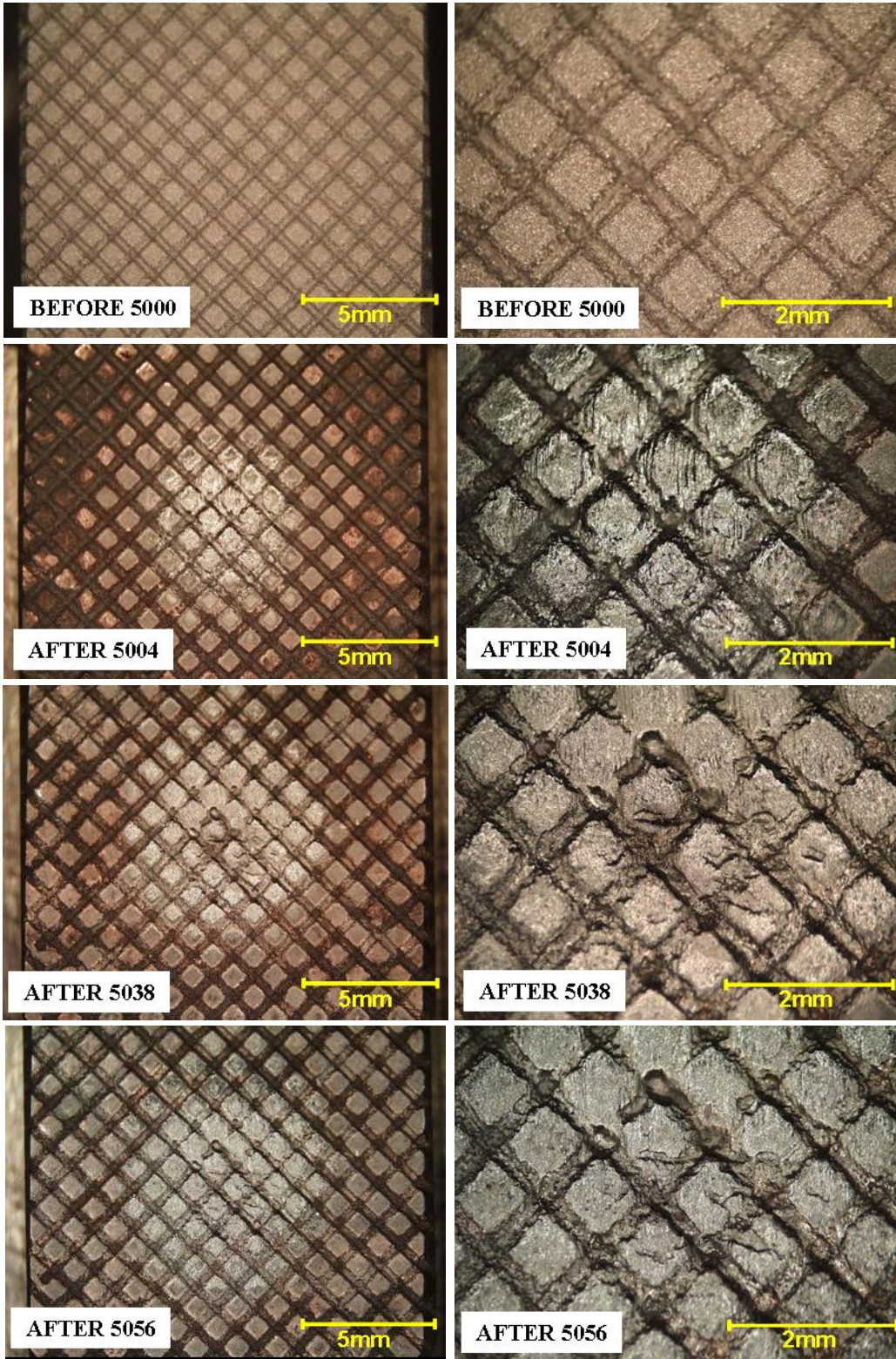


Figure 133: W-La anvil after SS 410 weld trials 5000-5056

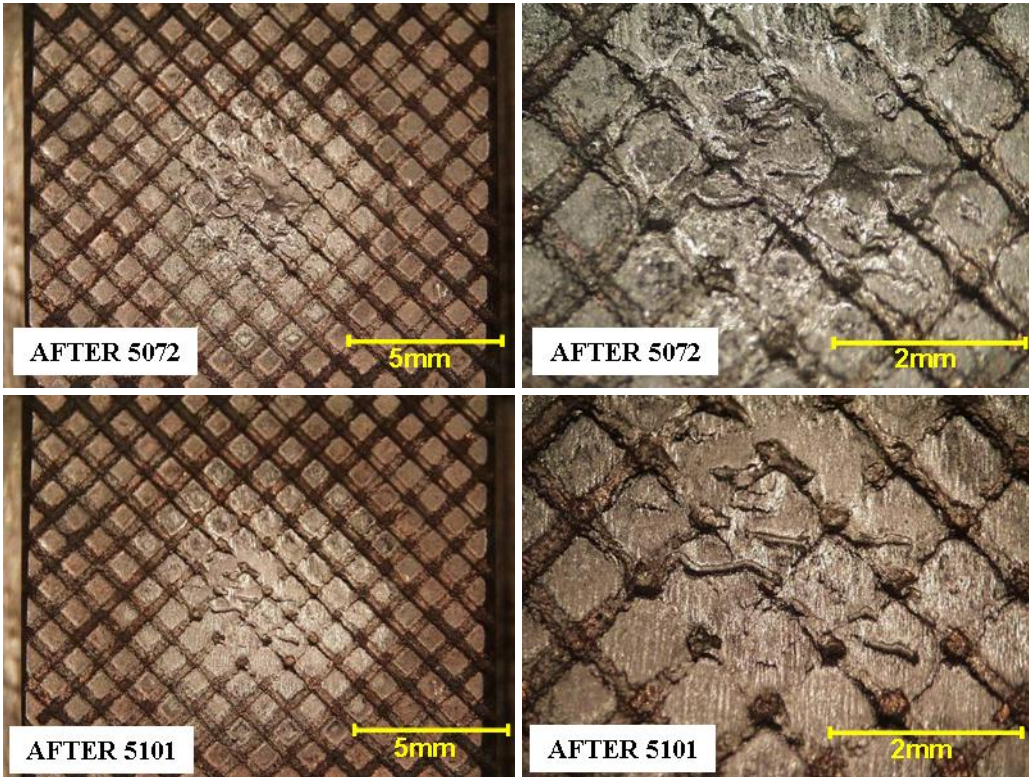


Figure 134: W-La anvil after SS 410 weld trials 5057-5101

B.5 NICKEL 718 WELD TRIALS

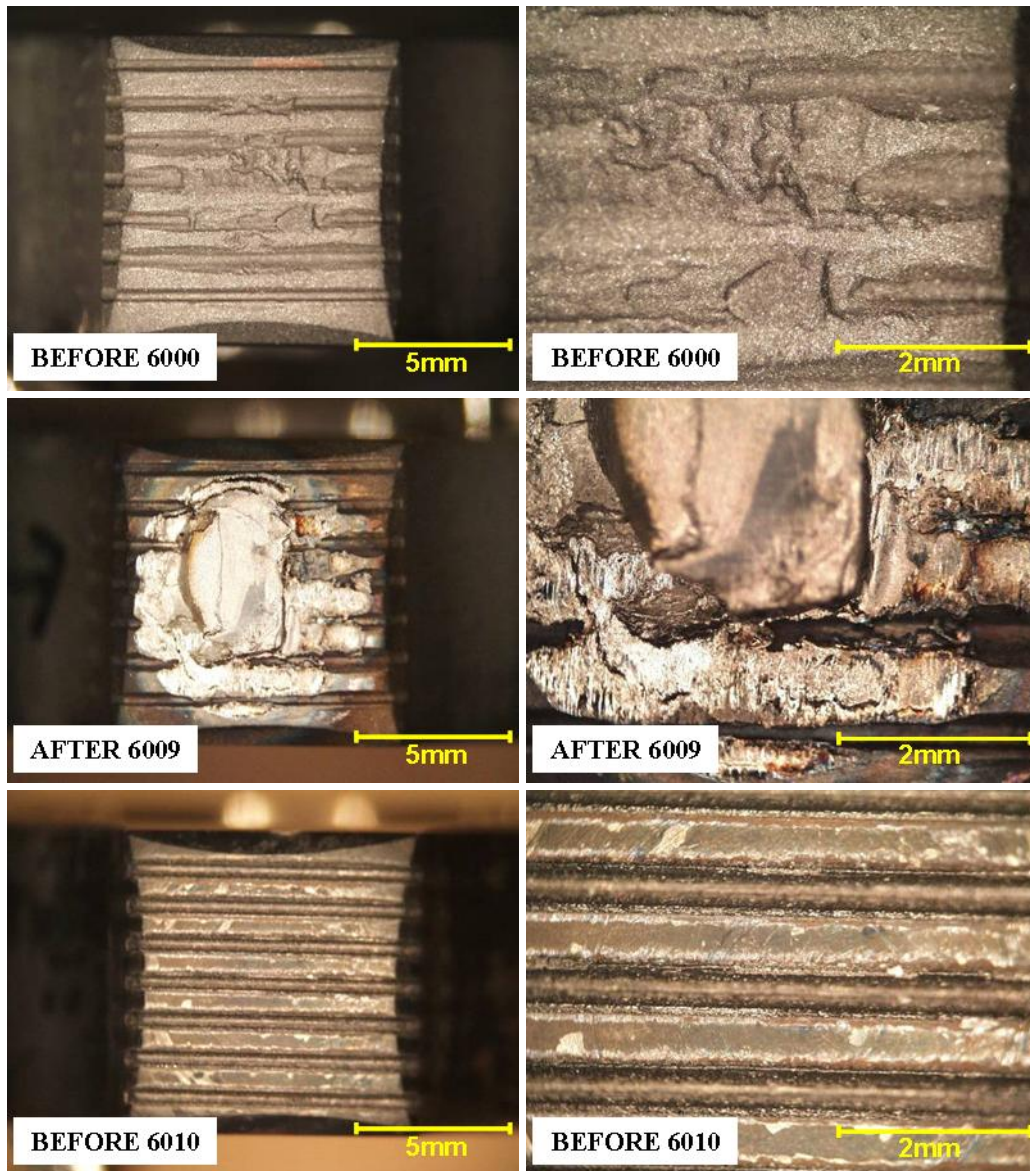


Figure 135: 350M tip during Ni 718 weld trials 6000-6010

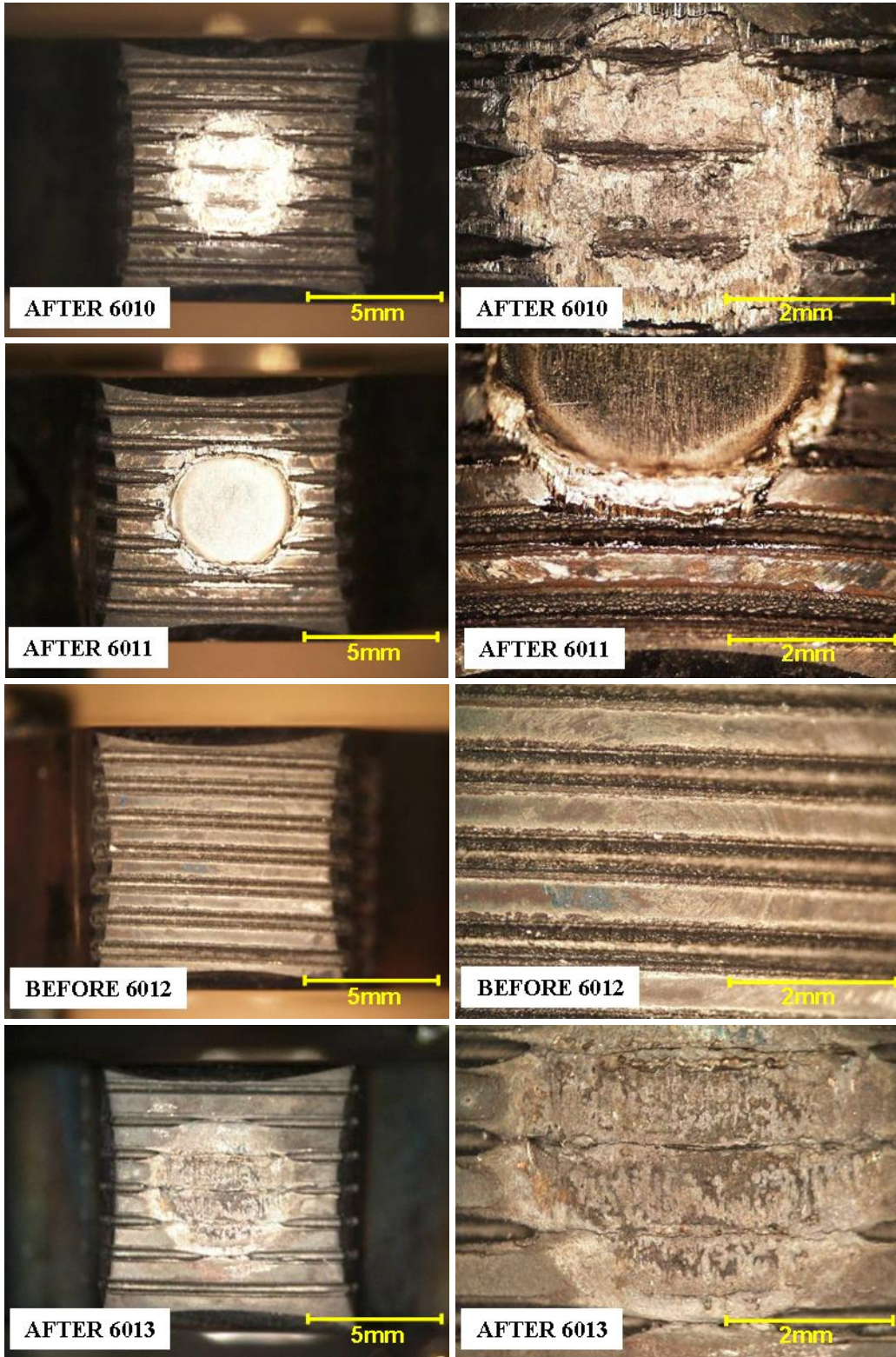


Figure 136: 350M tip after Ni 718 weld trials 6010-6013

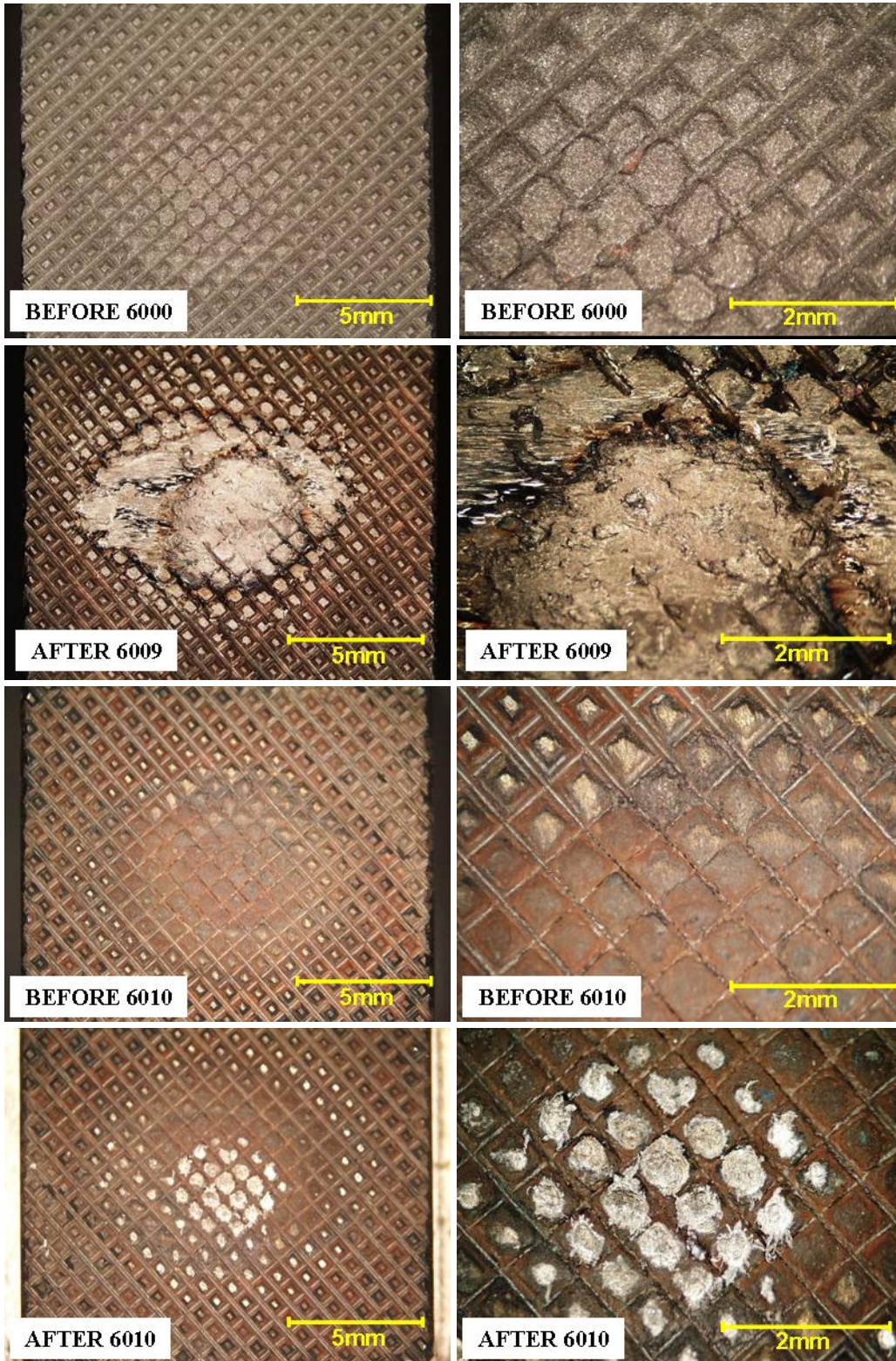


Figure 137: 350M anvil after Ni 718 weld trials 6000-6010

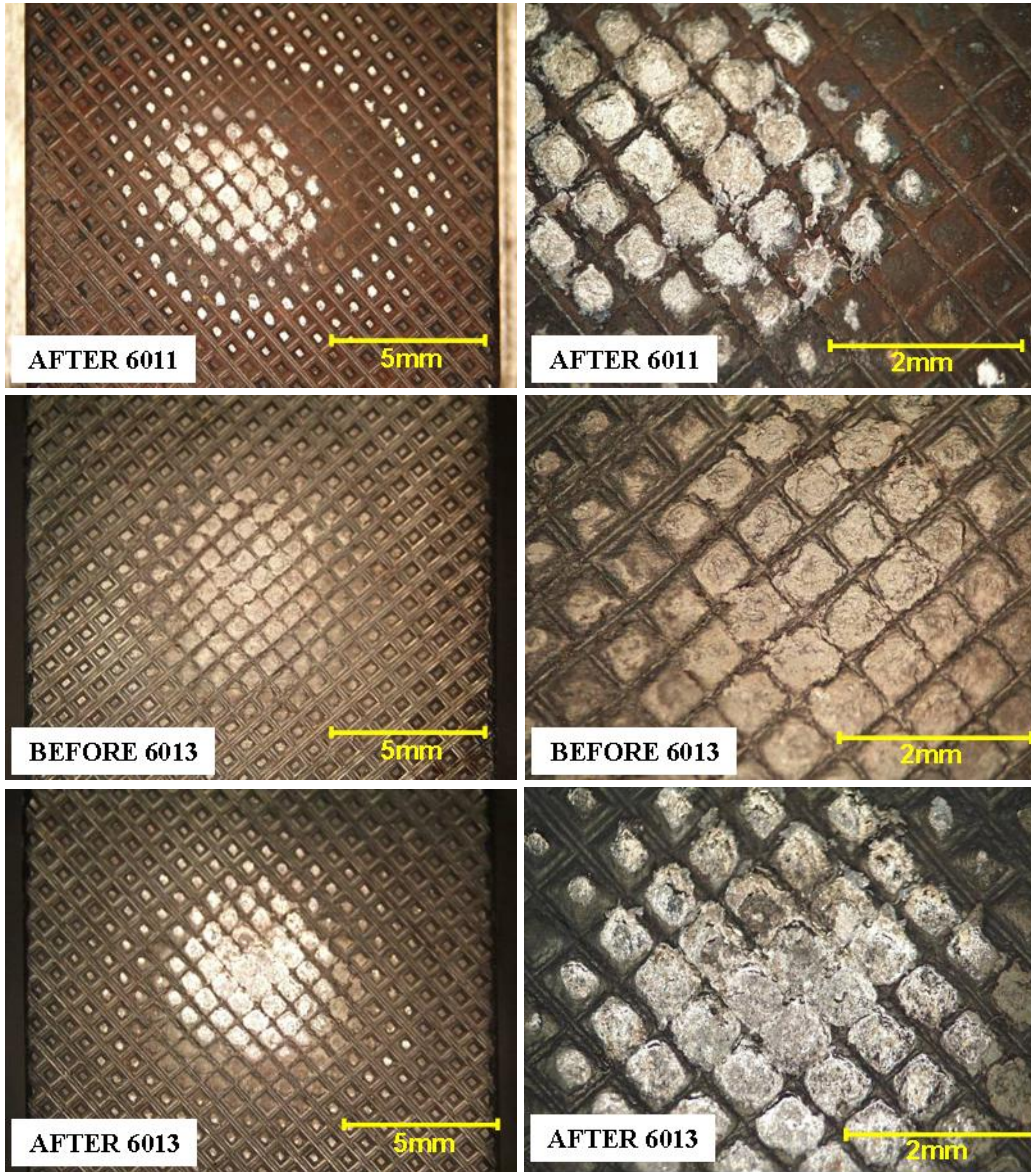


Figure 138: 350M anvil after Ni 718 weld trials 6011-6013

B.6 NICKEL 625 WELD TRIALS

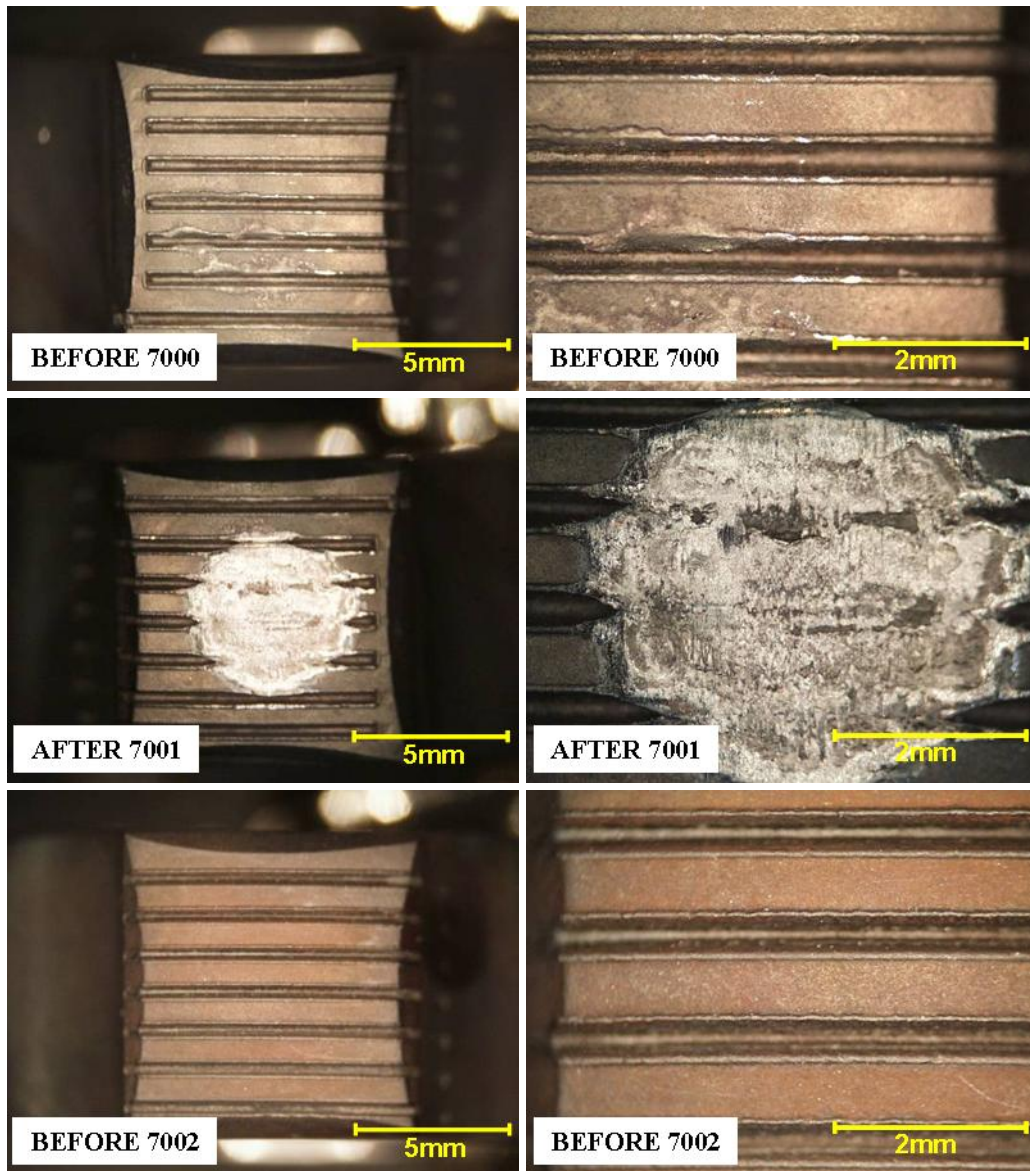


Figure 139: 350M tip during Ni 625 weld trials 7000-7002

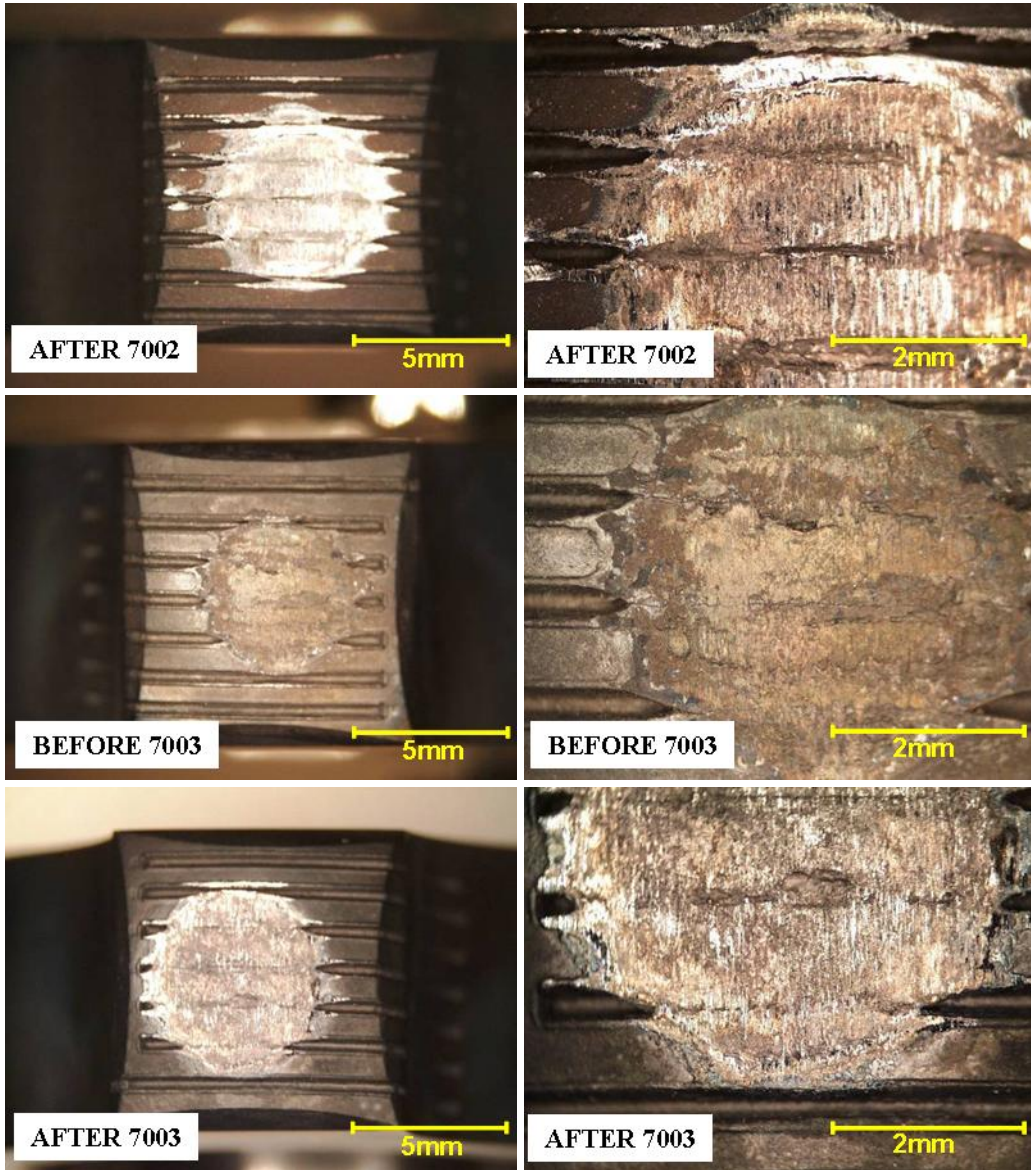


Figure 140: 350M tip after Ni 625 weld trials 7002-7003

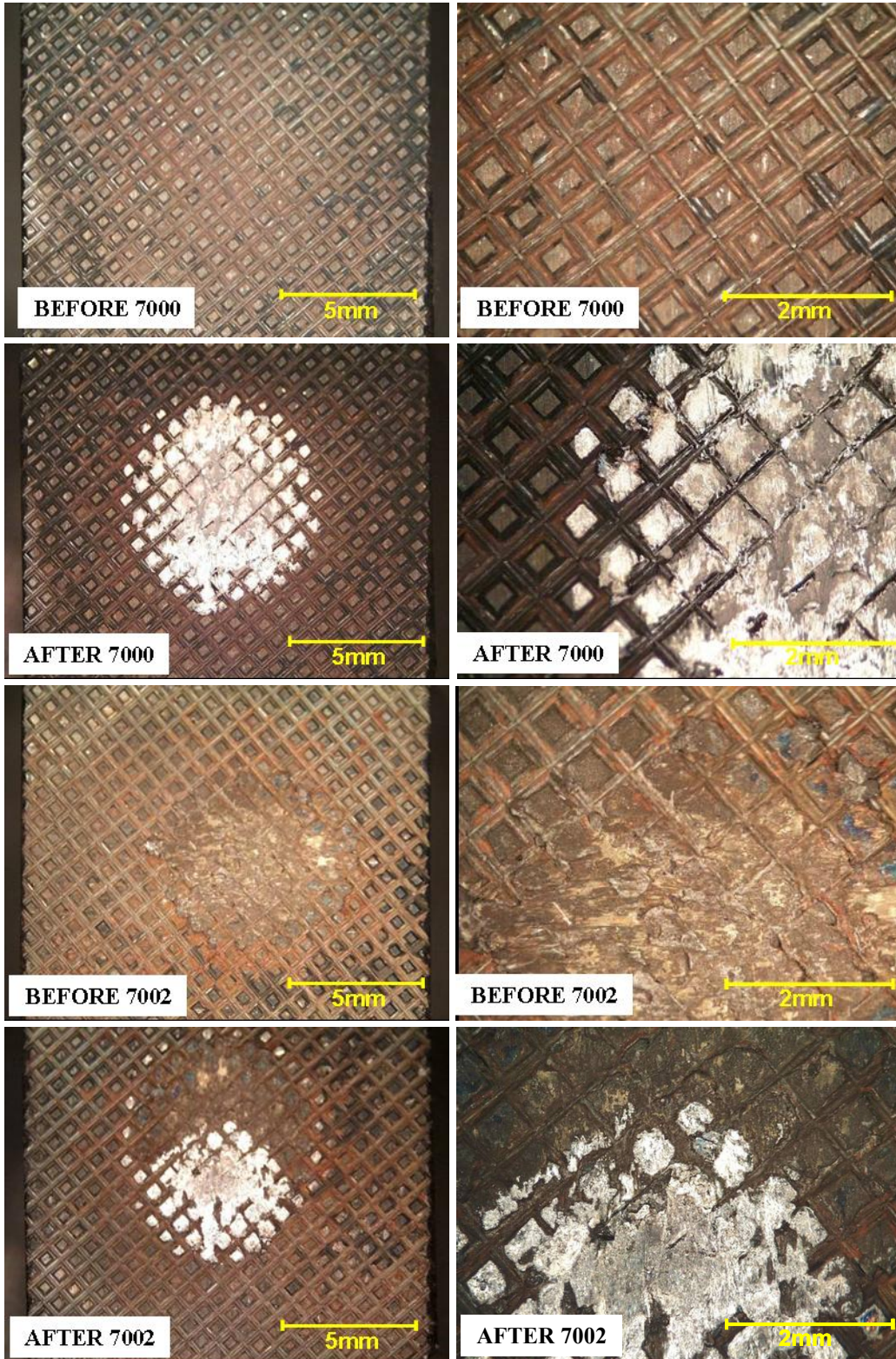


Figure 141: 350M anvil after Ni 625 weld trials 7000-7002

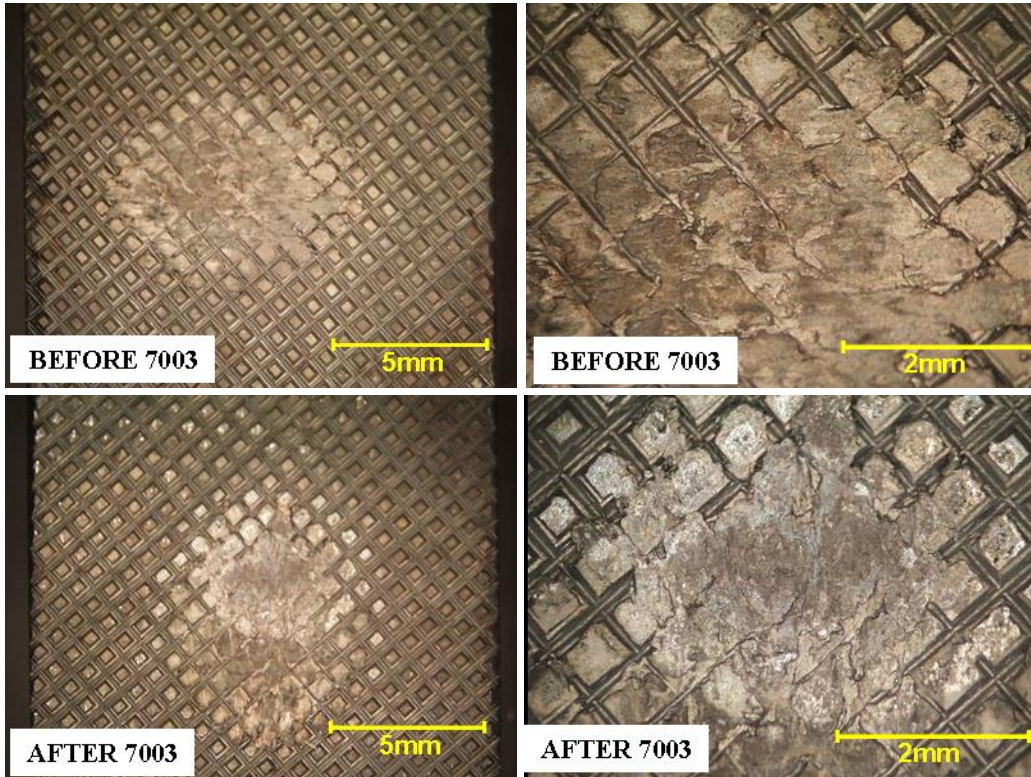


Figure 142: 350M anvil after Ni 625 weld trial 7003

APPENDIX C

TOOL DRAWINGS

Figure 143 and Figure 144 are detailed drawings of the welding tips. Figure 145 is a drawing of the anvil with the machined knurl pattern. The anvils with the brazed wear surfaces have the same specifications, but substitute a surface-ground face instead of the machined knurl pattern.

### C.1 TIP DESIGN

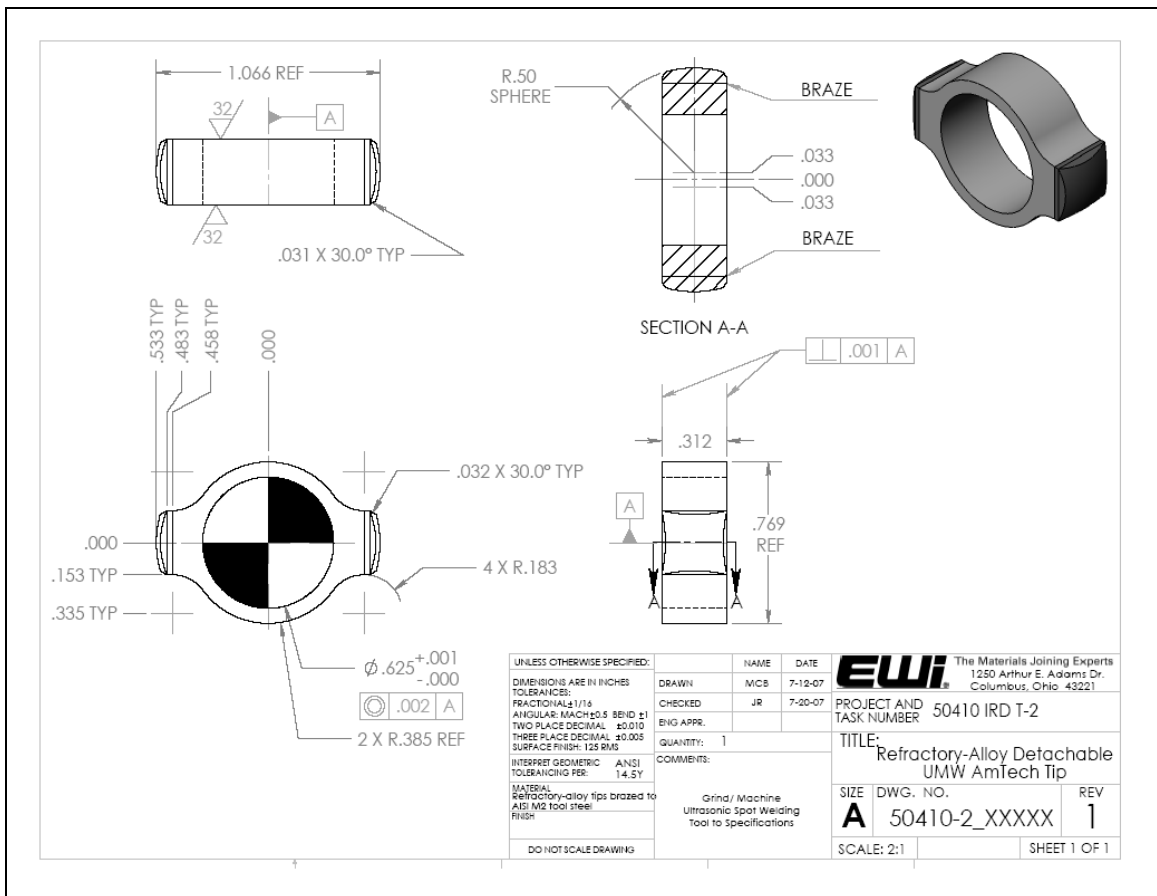


**Figure 143: W-25Re brazed to M2 UMW Tip Drawing**

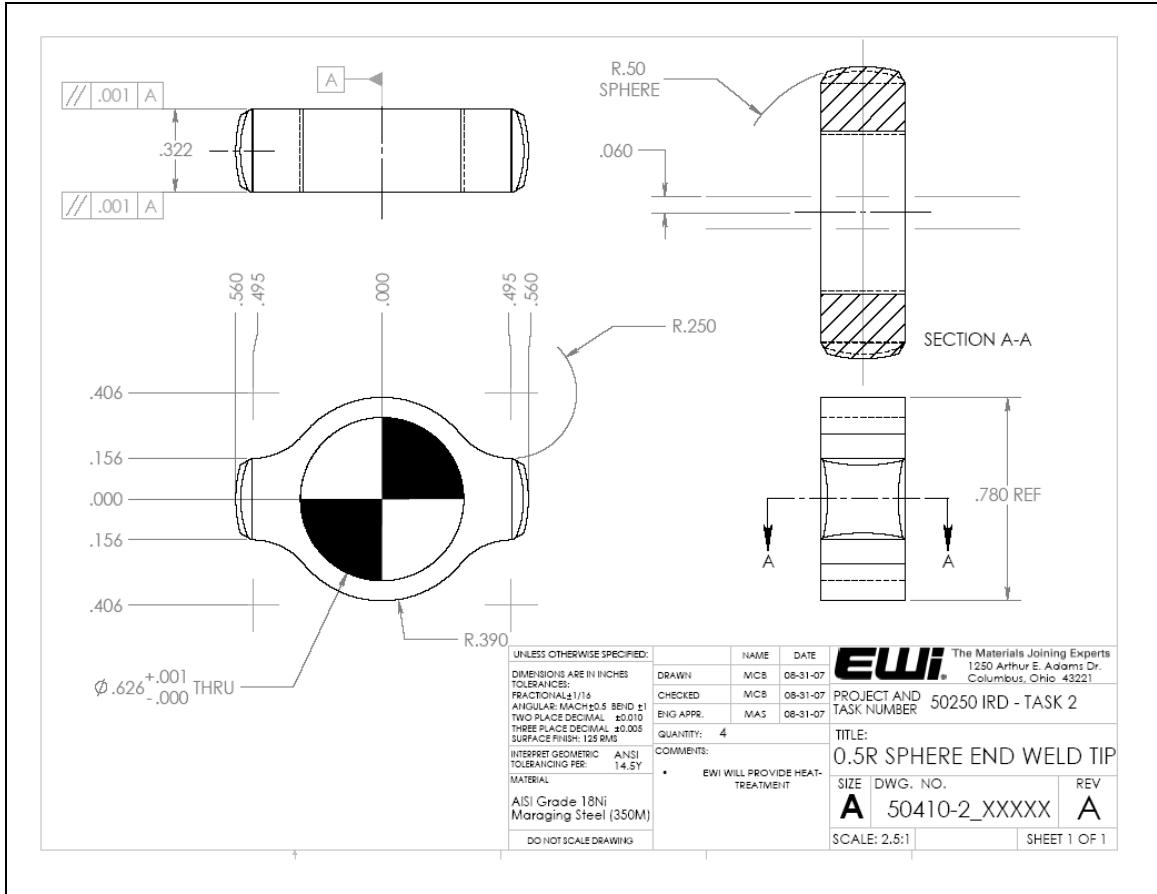


Figure 144: Solid tool-steel spherical weld tip

## C.2 ANVIL DESIGN

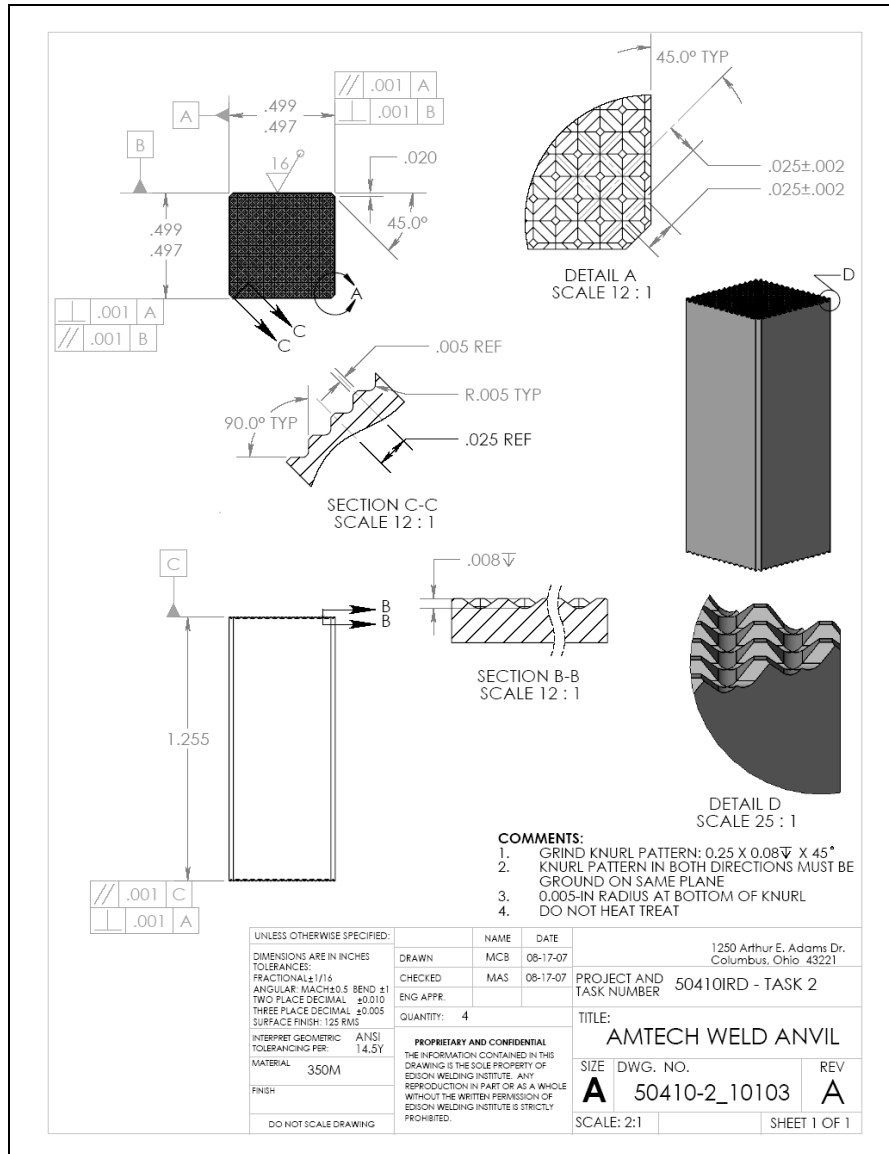


Figure 145: UMW Machined Anvil

APPENDIX D

MINITAB REGRESSION ANALYSIS

It was originally intended to use designed experiments for the weld trials and perform an in-depth data analysis. However, braze joint failures, excessive tool wear, non-repeatable tool alignment, equipment power limitations, and poor parameter windows prevented the use of a traditional designed experiment. Nevertheless, a basic regression analysis was performed using MiniTab 15 software to develop regression equations. This was not possible with Nickel 718 and Nickel 625 because of the limited number of weld trials. The regression analysis is not reviewed because of the significant scatter and poor repeatability in some cases., but the results are provided here for further interpretation. Figure 146 through Figure 149 are residual plots from the regression analysis, and provide a visual summary of the data quality.

#### D.1 SS 304 DOE REGRESSION ANALYSIS

**Regression Analysis: Tensile Forc versus Actual Energ, Clamping For, ...**

The regression equation is  
Tensile Force (lbf) = 209 + 0.396 Actual Energy (J) + 0.650 Clamping Force (lbf)  
+ 0.000301 Actual Energy\* Clamping Force  
- 0.000114 Actual Energy^2 - 0.00177 Clamping Force^2

Predictor	Coef	SE Coef	T	P
Constant	209.1	168.5	1.24	0.219
Actual Energy (J)	0.3956	0.2785	1.42	0.160
Clamping Force (lbf)	0.6496	0.8996	0.72	0.473
Actual Energy* Clamping Force	0.0003011	0.0006455	0.47	0.642
Actual Energy^2	-0.0001137	0.0001365	-0.83	0.408
Clamping Force^2	-0.001765	0.001223	-1.44	0.154

S = 92.7291    R-Sq = 54.3%    R-Sq(adj) = 50.8%

Analysis of Variance

Source	DF	SS	MS	F	P
Regression	5	683415	136683	15.90	0.000
Residual Error	67	576112	8599		
Total	72	1259527			

Source	DF	Seq SS
Actual Energy (J)	1	612497
Clamping Force (lbf)	1	19803
Actual Energy* Clamping Force	1	27075
Actual Energy^2	1	6134
Clamping Force^2	1	17905

Unusual Observations

Obs	Actual Energy (J)	Tensile Force (lbf)	Fit	SE Fit	Residual	St Resid
5	560	435.4	350.0	61.2	85.4	1.23 X
11	610	364.0	407.7	46.6	-43.7	-0.55 X
29	205	516.2	336.9	27.8	179.3	2.03R
34	1008	791.1	605.6	19.1	185.5	2.04R
41	102	349.0	313.3	49.4	35.7	0.45 X
45	111	0.0	313.4	36.3	-313.4	-3.67R
50	101	0.0	205.7	54.2	-205.7	-2.73RX

R denotes an observation with a large standardized residual.

X denotes an observation whose X value gives it large leverage.

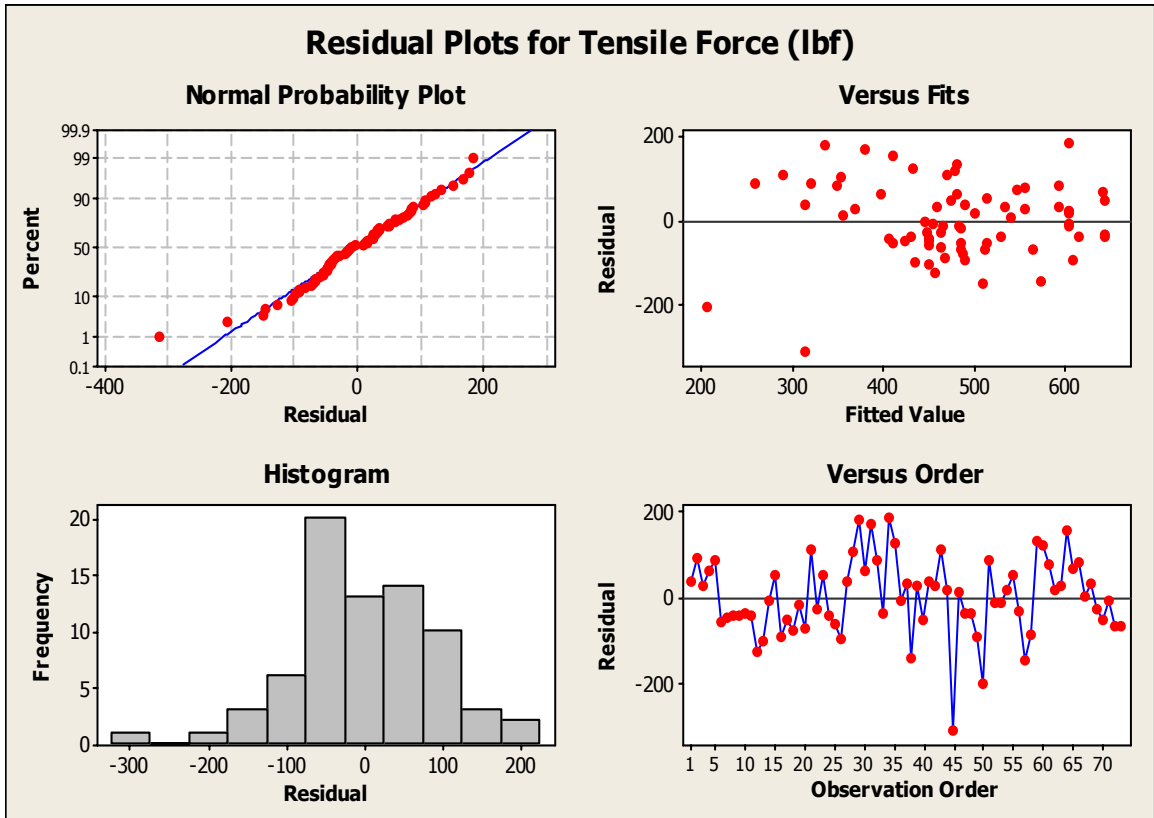


Figure 146: SS 304 Residual Plots for Tensile Force

## D.2 SS 410 DOE REGRESSION ANALYSIS

### Regression Analysis: Tensile Forc versus Actual Energy, Clamping For, ...

The regression equation is

$$\begin{aligned} \text{Tensile Force (lbf)} = & -1085 + 1.47 \text{ Actual Energy (J)} \\ & + 7.17 \text{ Clamping Force (lbf)} \\ & + 0.00060 \text{ Actual Energy} * \text{ Clamping Force} \\ & - 0.000566 \text{ Actual Energy}^2 - 0.0140 \text{ Clamping Force}^2 \end{aligned}$$

Predictor	Coef	SE Coef	T	P
Constant	-1084.9	394.4	-2.75	0.008
Actual Energy (J)	1.4733	0.5175	2.85	0.006
Clamping Force (lbf)	7.168	2.422	2.96	0.005
Actual Energy* Clamping Force	0.000595	0.002309	0.26	0.798
Actual Energy^2	-0.0005655	0.0001112	-5.09	0.000
Clamping Force^2	-0.013951	0.003535	-3.95	0.000

S = 154.628    R-Sq = 71.3%    R-Sq(adj) = 68.5%

#### Analysis of Variance

Source	DF	SS	MS	F	P
Regression	5	3088910	617782	25.84	0.000
Residual Error	52	1243311	23910		
Total	57	4332221			

Source	DF	Seq SS
Actual Energy (J)	1	2060960
Clamping Force (lbf)	1	91160
Actual Energy* Clamping Force	1	109209
Actual Energy^2	1	455208
Clamping Force^2	1	372373

#### Unusual Observations

Obs	Actual Energy (J)	Tensile Force (lbf)	Fit	SE Fit	Residual	St Resid
30	311	0.0	-144.7	106.5	144.7	1.29 X
34	461	0.0	306.6	54.6	-306.6	-2.12R
35	521	134.8	120.9	121.6	13.9	0.15 X
56	2005	779.9	637.9	125.4	142.0	1.57 X

R denotes an observation with a large standardized residual.

X denotes an observation whose X value gives it large leverage.

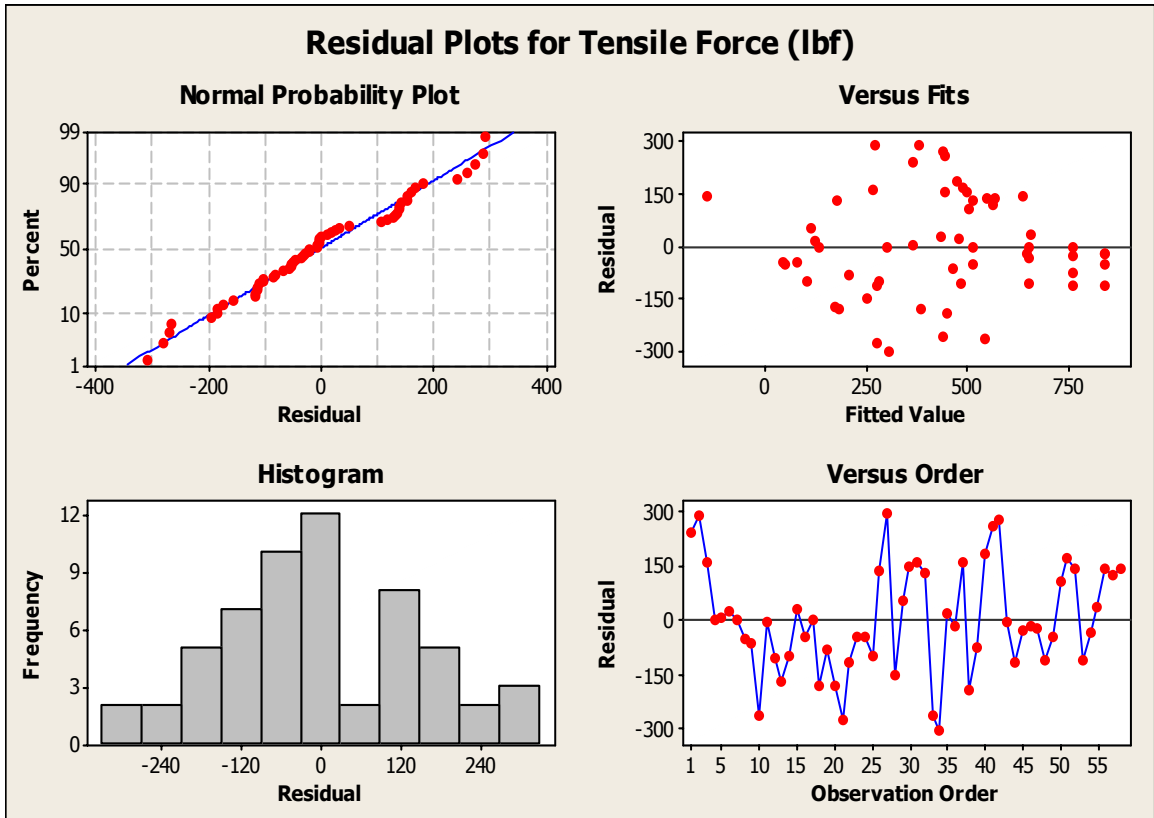


Figure 147: SS 410 Residual Plots for Tensile Force

### D.3 C.P. TI DOE REGRESSION ANALYSIS

Regression Analysis: Tensile Forc versus Actual Energ, Clamping For, ...						
The regression equation is						
Tensile Force (lbf) = 108 + 2.40 Actual Energy (J) - 0.579 Clamping Force (lbf)						
+ 0.000522 Actual Energy*Clamping Force						
- 0.00206 Actual Energy^2 + 0.00053 Clamping Force^2						
Predictor		Coef	SE Coef	T	P	
Constant		107.6	209.0	0.51	0.608	
Actual Energy (J)		2.3963	0.4204	5.70	0.000	
Clamping Force (lbf)		-0.5786	0.9675	-0.60	0.552	
Actual Energy*Clamping Force		0.0005218	0.0006811	0.77	0.446	
Actual Energy^2		-0.0020593	0.0003013	-6.83	0.000	
Clamping Force^2		0.000526	0.001253	0.42	0.676	
S = 83.3273 R-Sq = 74.8% R-Sq(adj) = 72.9%						
Analysis of Variance						
Source	DF	SS	MS	F	P	
Regression	5	1380083	276017	39.75	0.000	
Residual Error	67	465211	6943			
Total	72	1845294				
Source	DF	Seq SS				
Actual Energy (J)	1	986482				
Clamping Force (lbf)	1	18513				
Actual Energy*Clamping Force	1	50288				
Actual Energy^2	1	323578				
Clamping Force^2	1	1222				
Obs	Actual Energy (J)	Tensile Force (lbf)	Fit	SE Fit	Residual	St Resid
1	360	489.40	630.73	14.45	-141.33	-1.72
2	358	662.60	638.85	30.06	23.75	0.31
3	200	378.00	413.73	28.23	-35.73	-0.46
4	354	642.70	624.00	14.42	18.70	0.23
5	360	669.80	630.73	14.45	39.07	0.48
6	212	492.90	419.25	29.25	73.65	0.94
7	353	691.00	622.87	14.42	68.13	0.83
8	357	568.90	637.77	27.73	-68.87	-0.88
9	575	801.10	773.90	15.69	27.20	0.33
10	143	344.20	293.18	30.26	51.02	0.66
11	359	665.50	629.62	14.45	35.88	0.44
12	512	714.90	748.74	19.80	-33.84	-0.42
13	500	774.80	758.09	18.06	16.71	0.21
14	352	636.20	621.73	14.42	14.47	0.18
15	362	636.50	632.94	14.47	3.56	0.04
16	574	717.00	773.67	15.68	-56.67	-0.69

17	202	198.70	401.35	30.33	-202.65	-2.61R
18	146	0.00	299.17	29.76	-299.17	-3.84R
19	509	580.40	763.18	18.13	-182.78	-2.25R
20	358	349.30	638.85	30.06	-289.55	-3.73R
21	215	433.80	439.01	26.30	-5.21	-0.07
22	349	636.50	618.28	14.41	18.22	0.22
23	360	679.20	640.61	27.13	38.59	0.49
24	364	651.00	635.13	14.48	15.87	0.19
25	506	696.60	746.07	19.74	-49.47	-0.61
26	359	629.00	629.62	14.45	-0.62	-0.01
27	152	273.60	311.04	28.77	-37.44	-0.48
28	514	761.30	765.86	18.18	-4.56	-0.06
29	358	654.00	628.50	14.44	25.50	0.31
30	359	684.30	629.62	14.45	54.68	0.67
31	352	666.60	621.73	14.42	44.87	0.55
32	359	678.10	629.62	14.45	48.48	0.59
33	201	331.80	415.45	28.10	-83.65	-1.07
34	365	709.80	647.08	29.78	62.72	0.81
35	563	752.80	770.92	15.59	-18.12	-0.22
36	361	636.00	641.64	27.12	-5.64	-0.07
37	362	688.60	632.94	14.47	55.66	0.68
38	214	591.40	422.78	29.04	168.62	2.16R
39	510	735.00	747.86	19.78	-12.86	-0.16
40	613	750.60	770.90	30.17	-20.30	-0.26
41	511	796.20	764.26	18.15	31.94	0.39
42	604	773.40	778.64	16.14	-5.24	-0.06
43	610	772.10	779.19	16.29	-7.09	-0.09
44	464	727.50	723.75	15.34	3.75	0.05
45	500	673.60	743.26	19.69	-69.66	-0.86
46	605	796.80	778.74	16.17	18.06	0.22
47	704	802.70	791.42	32.11	11.28	0.15
48	608	758.40	779.02	16.24	-20.62	-0.25
49	604	770.50	806.86	30.81	-36.36	-0.47
50	608	759.70	779.02	16.24	-19.32	-0.24
51	753	757.00	737.03	26.18	19.97	0.25
52	741	800.30	754.20	26.58	46.10	0.58
53	700	730.70	757.02	24.20	-26.32	-0.33
54	751	743.90	730.86	37.33	13.04	0.18
55	752	800.00	787.86	49.41	12.14	0.18 X
56	706	746.60	767.79	22.36	-21.19	-0.26
57	608	729.90	779.02	16.24	-49.12	-0.60
58	609	756.20	779.11	16.26	-22.91	-0.28
59	363	663.40	634.04	14.47	29.36	0.36
60	361	651.30	631.83	14.46	19.47	0.24
61	640	716.50	779.70	17.38	-63.20	-0.78
62	632	714.60	779.93	17.03	-65.33	-0.80
63	901	653.70	598.37	59.49	55.33	0.95 X
64	214	527.70	424.97	20.40	102.73	1.27
65	213	513.30	423.26	20.50	90.04	1.11
66	212	502.00	421.54	20.61	80.46	1.00
67	354	695.80	634.32	27.19	61.48	0.78
68	559	784.20	769.80	15.57	14.40	0.18
69	556	812.30	793.65	28.34	18.65	0.24
70	351	705.50	631.12	27.23	74.38	0.94
71	356	760.30	636.47	30.15	123.83	1.59
72	602	974.00	796.18	21.37	177.82	2.21R
73	199	466.60	421.34	38.43	45.26	0.61

R denotes an observation with a large standardized residual.  
X denotes an observation whose X value gives it large leverage.

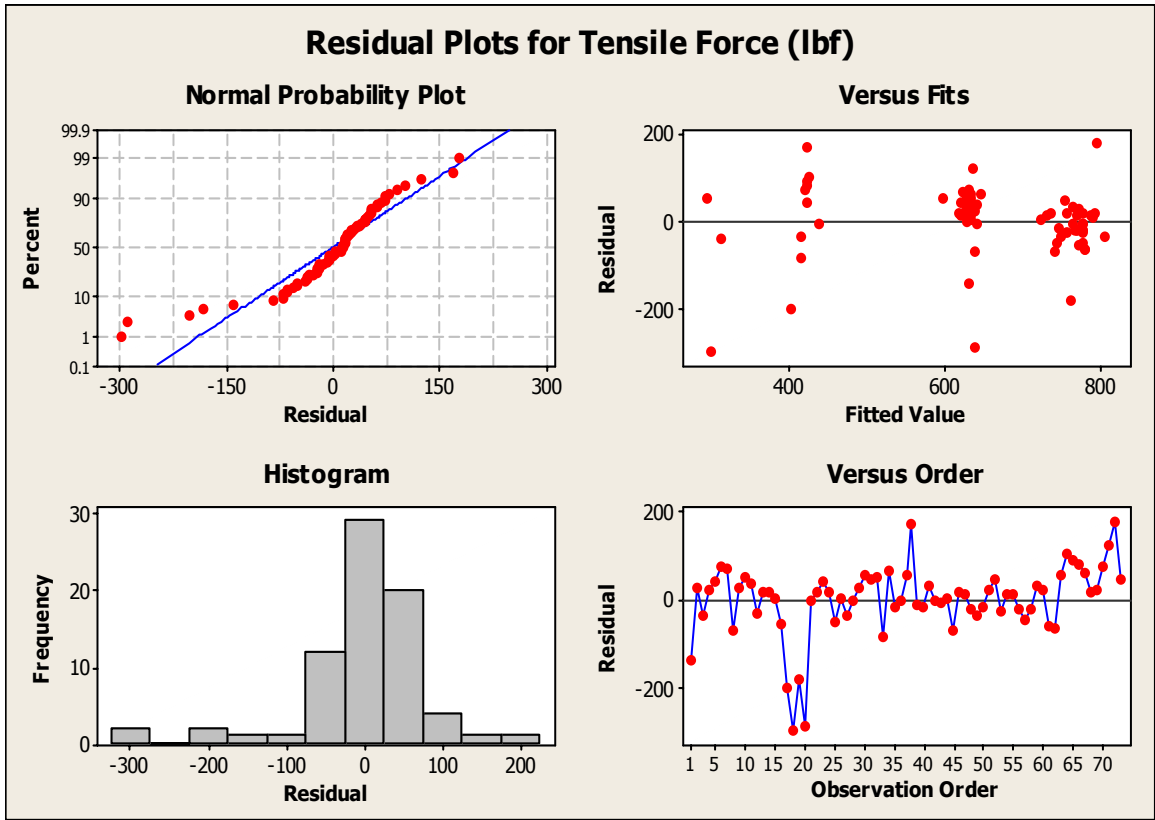


Figure 148: C.P. Ti Residual Plots for Tensile Force

## D.4 TI 6AL-4V DOE REGRESSION ANALYSIS

### Regression Analysis: Tensile Forc versus Actual Energy, Clamping For, ...

The regression equation is  
 Tensile Force (lbf) = - 385 + 2.08 Actual Energy (J) + 3.07 Clamping Force (lbf)  
 + 0.00162 Actual Energy\* Clamping Force  
 - 0.00177 Actual Energy^2 - 0.00438 Clamping Force^2

Predictor	Coef	SE Coef	T	P
Constant	-384.9	605.0	-0.64	0.528
Actual Energy (J)	2.082	1.038	2.01	0.051
Clamping Force (lbf)	3.068	3.522	0.87	0.388
Actual Energy* Clamping Force	0.001615	0.002668	0.61	0.548
Actual Energy^2	-0.0017746	0.0005713	-3.11	0.003
Clamping Force^2	-0.004377	0.004723	-0.93	0.359

S = 234.841 R-Sq = 43.2% R-Sq(adj) = 37.0%

#### Analysis of Variance

Source	DF	SS	MS	F	P
Regression	5	1925586	385117	6.98	0.000
Residual Error	46	2536903	55150		
Total	51	4462489			

Source	DF	Seq SS
Actual Energy (J)	1	135117
Clamping Force (lbf)	1	859254
Actual Energy* Clamping Force	1	313907
Actual Energy^2	1	569945
Clamping Force^2	1	47363

Obs	Actual Energy (J)	Tensile Force (lbf)	Fit	SE Fit	Residual	St Resid
1	508	1250.0	997.3	52.2	252.7	1.10
2	425	878.9	983.9	92.7	-105.0	-0.49
3	1001	418.0	612.2	96.2	-194.2	-0.91
4	540	974.5	1020.3	52.0	-45.8	-0.20
5	423	1026.1	981.3	92.7	44.8	0.21
6	446	979.9	851.8	47.9	128.1	0.56
7	1002	1014.0	798.2	106.4	215.8	1.03
8	553	780.4	718.9	105.4	61.5	0.29
9	313	807.8	702.0	56.1	105.8	0.46
10	299	708.7	682.5	58.5	26.2	0.12
11	199	475.4	523.6	85.4	-48.2	-0.22
12	554	924.6	927.2	48.9	-2.6	-0.01
13	552	707.9	926.2	48.9	-218.3	-0.95
14	554	896.1	927.2	48.9	-31.1	-0.14
15	803	918.1	777.3	74.9	140.8	0.63

16	562	1306.0	1065.2	55.1	240.8	1.05
17	698	1318.0	1080.7	66.2	237.3	1.05
18	554	1043.0	927.2	48.9	115.8	0.50
19	552	1086.0	926.2	48.9	159.8	0.70
20	302	484.8	762.0	78.6	-277.2	-1.25
21	552	865.5	926.2	48.9	-60.7	-0.26
22	755	1182.0	957.5	48.9	224.5	0.98
23	660	727.2	1074.3	60.3	-347.1	-1.53
24	565	1176.0	932.6	48.9	243.4	1.06
25	558	1021.0	929.2	48.9	91.8	0.40
26	909	951.9	883.6	72.6	68.3	0.31
27	551	675.2	1058.1	54.3	-382.9	-1.68
28	790	1132.0	1075.1	87.5	56.9	0.26
29	312	817.7	586.5	81.1	231.2	1.05
30	806	1013.0	775.9	74.9	237.1	1.07
31	562	1069.0	931.2	48.9	137.8	0.60
32	564	798.7	932.1	48.9	-133.4	-0.58
33	557	931.0	928.7	48.9	2.3	0.01
34	300	485.6	759.0	79.1	-273.4	-1.24
35	560	889.1	930.2	48.9	-41.1	-0.18
36	201	351.4	527.1	84.7	-175.7	-0.80
37	564	855.0	722.7	105.5	132.3	0.63
38	551	1248.0	1117.4	115.2	130.6	0.64
39	484	573.4	1053.4	97.5	-480.0	-2.25R
40	531	687.5	1075.9	60.0	-388.4	-1.71
41	678	708.2	962.8	48.1	-254.6	-1.11
42	551	661.2	925.7	48.9	-264.5	-1.15
43	203	594.6	428.1	107.9	166.5	0.80
44	1001	649.7	612.2	96.2	37.5	0.18
45	202	1049.0	609.5	161.1	439.5	2.57RX
46	454	1325.0	1019.6	93.6	305.4	1.42
47	211	614.8	497.6	82.5	117.2	0.53
48	1002	622.3	709.3	89.5	-87.0	-0.40
49	205	0.0	378.4	141.0	-378.4	-2.01RX
50	1000	0.0	525.7	120.2	-525.7	-2.61R
51	210	632.8	542.8	81.6	90.0	0.41
52	1003	1071.0	797.2	106.8	273.8	1.31

R denotes an observation with a large standardized residual.  
X denotes an observation whose X value gives it large leverage.

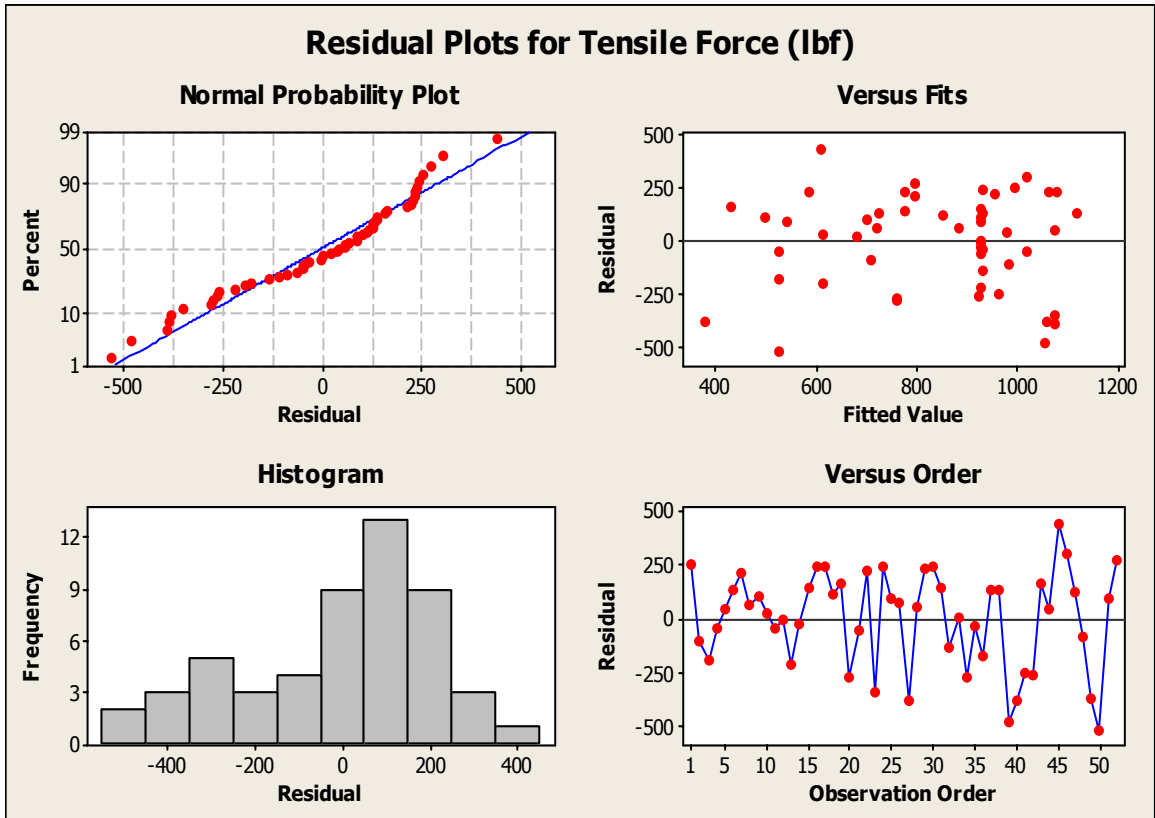


Figure 149: Ti 6Al-4V Residual Plots for Tensile Force